A detailed study of drift chambers

R. Browell

A DETAILED STUDY OF DRIFT CHAMBERS

by

R. BROWELL, B.Sc.

A thesis submitted to the University of Durham for the Degree of Doctor of Philosophy.

Being an account of work carried out at the University of Durham during the period September, 1972 to August, 1975.

ABSTRACT

This thesis describes a study made at Durham University of a new type of particle detector, the drift chamber. The device is a development of the multiwire proportional chamber but has a superior spatial resolution and requires less electronic channels per detecting area.

Two types of drift chamber have been built for investigating various operating characteristics, and the specific design and constructional details of each is described.

The main part of the work deals with an investigation into the behaviour of a specific gas mixture, argon + 10% methane, with regard to its suitability for drift chamber application. Measurements have been made of output pulses, detection efficiency, spatial resolution and electron drift velocity, and their variation with operating conditions, including the angle of the particle trajectory to the chamber normal.

Particular emphasis has been placed on the behaviour of chambers in strong magnetic fields, as this represents a common practical operating condition. Test chambers with this gas mixture have been successfully operated using a simple compensation technique, on an accelerator beam at Daresbury Laboratories, at magnetic fields up to 13.5kG.

Comparisons with other gas mixtures are made, using data obtained during this work and the experimental and theoretical results of other workers.

The results have indicated that argon + 10% methane is entirely applicable to practical drift chamber use and its behaviour is well described by simple theories. As an example of a practical application, the design, construction and testing of a third type of chamber for use in a high energy physics experiment involving non-uniform magnetic fields, is described.

CONTENTS

CHAPTER ONE

INTRODUCTION

There are many areas of scientific study in which the detection of elementary charged particles or ionising radiation forms one of the major sources of experimental data available. This is particularly true in high energy nuclear physics and cosmic ray studies, but it also applies to certain branches of astronomy and medical physics. Thus the particle detector represents a powerful and versatile experimental technique, and those detectors which depend on a process of electron multiplication in a gas for their mode of operation constitute one of the largest groups of such devices.

The subject of this thesis, the drift chamber, is a recent addition to this group, and it will be helpful here to discuss the development of the device in the context of other detectors within the group.

1.1 Classification of Gaseous Detectors

There are many possible subdivisions of devices within this group but probably the most basic is that between the primary, or continuously sensitive detectors such as the Gieger-Muller counter and the proportional counter; and the secondary or triggerable detector such as the spark chamber and the streamer chamber, in which the operating voltage is applied in the form of a pulse only when triggered by the passage of a particle. All detectors within this group have the same basic mechanism however in that a charged particle incident on the sensitive volume causes ionisation of the gas of the detector. The resulting electrons are accelerated in an electric field until they have sufficient energy to cause further ionisation within the gas and hence multiplication of the original

electrons occurs. It is from this stage that the differences between the processes in various detectors occur. In the primary detectors the applied electric gradients are kept relatively low so that the electron avalanche only occurs very close to a cathode wire, where the field becomes locally very large, and is detected electronically in the form of a pulse on that wire. (In an ionisation chamber the field does not become large enough to induce any multiplication so that the final pulse is simply due to the initial ionisation). In secondary detectors the applied gradients are much larger, (and hence one reason for them being pulsed is to avoid spurious breakdown), causing avalanching to occur very close to the initial ionisation and resulting in a visible discharge.

Thus in general the secondary detectors give information on the position of a particle as it passes through the sensitive volume, (the exception being the flash tube, in which the discharge is allowed to spread throughout the detector volume and many closely packed tubes are required to define position). This ability to locate the particle's position within the detector is extremely desirable in many instances, for example in plotting trajectories, determining beam profiles, and combined with magnetic fields, in giving a measure of particle type and energy. Furthermore, in many applications, particularly for energy measurements, the information obtained is dependant on the positional accuracy of the device, so that much of detector development has been directed towards improving this aspect of their operation.

Up until 1968 this provision of positional data separated the secondary detectors from the continuously sensitive devices, which were used almost entirely in a 'counting' mode, with positional accuracy merely the dimensions of the detector, and were thus unsuitable for many experimental applications.

1.2 The Multiwire Proportional Chamber

The first major step towards producing a continuously sensitive device which would also provide accurate positional information, was made in 1968 with the publication by Charpak et al (1) of a paper describing the operation of a detector having the basic principles of the proportional counter, but consisting of a plane of sense wires between two plane electrodes instead of the more usual cylindrical arrangement. This was to be known as the multiwire proportional chamber (M.W.P.C.) and a cross-section of such a chamber is shown in Figure 1.1. The cathode plane is either a grid of wires or a metal foil and typical dimensions are L = 5mm, S = 2mm, the sense wire diameter for such spacing being 25 μm. The equipotentials in such a chamber are shown in Figure 1.2 and it can be seen that the region around the sense wire is similar to the conditions in a cylindrical counter, and standard proportional counter behaviour can be achieved. That is electrons from the ionisation caused by the incident particle are accelerated towards the nearest sense wire until the field becomes sufficiently high to cause Townsend avalanche to occur. The applied voltage is kept to such a value that the avalanche does not saturate, so that the final number of ions produced (and hence the pulse height) is proportional to the number originally formed by the incident particle.

The novel feature of this chamber however is that each sense wire is independent and has its own amplifier. Thus when a particle passes through the chamber orthogonal to the sense wire plane, only the nearest wire will produce a pulse and the particle's position will be known to an accuracy of $\pm$ S/2 (i.e. typically $\pm$ 1mm). These chambers soon began to displace secondary detectors (particularly

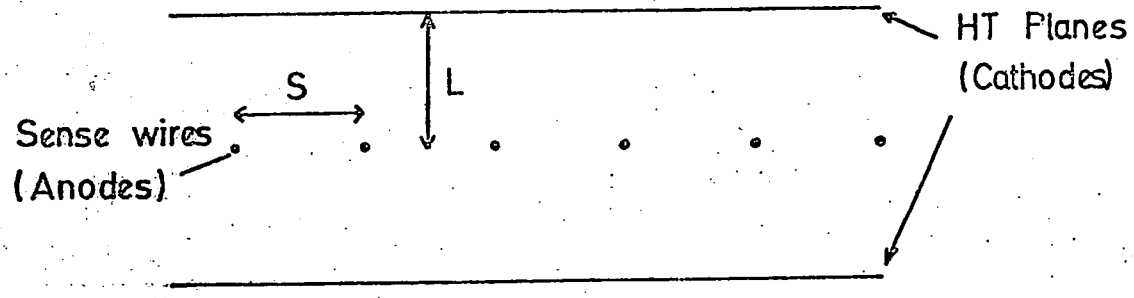

FIG 1.1 Section through M.W.P.C.

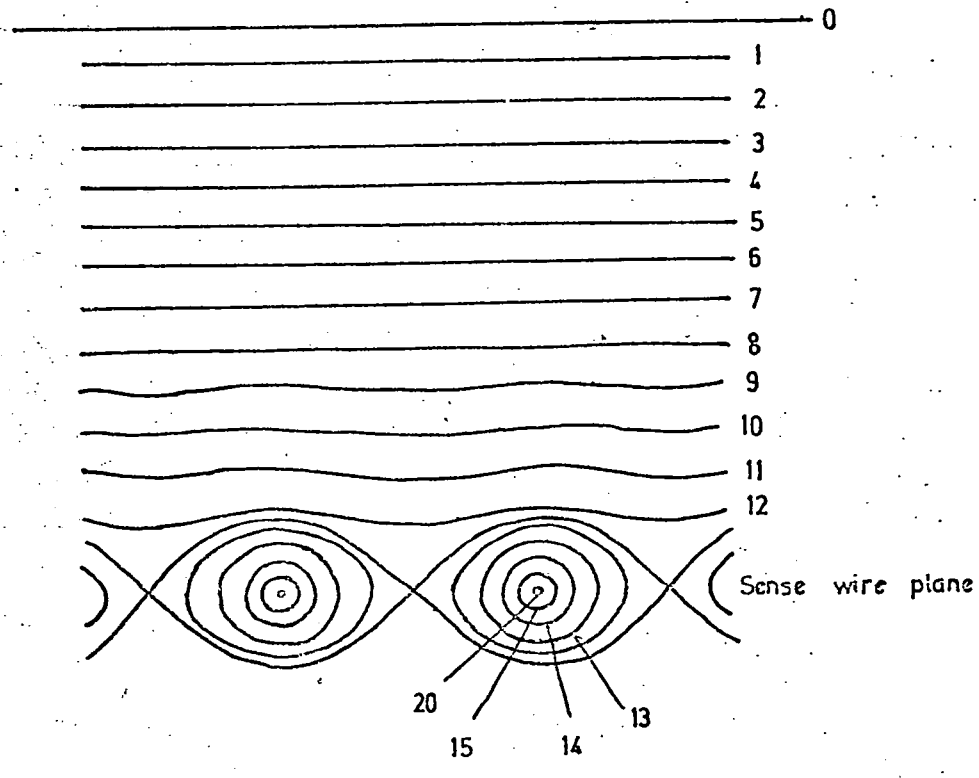

FIG 1.2 Relative equipotentials in a M.W.P.C. (from ref. 3.)

spark chambers) as particle locating devices, since as well as providing positional information they also had several operational advantages, three important ones being:-

i) The lack of intrinsic recovery time results in unimpaired operation at high counting rates (10^5 pulses/wire/sec (1)), or in high background environments.

ii) The device is continuously sensitive, and so the need for fast triggers and high voltage pulsing circuitry is removed.

iii) The output pulse height can be proportional to the energy deposited in the chamber by the initial particle.

The spark chamber however still retained the advantage of superior spatial resolution, a typical figure for wire chambers being 0.3mm, (depending on angle of incidence of the initial particle (2)), and for solid electrode or 'plate' chambers, accuracies of better than 0.1mm were quoted (3). In order to compete with spark chambers in this aspect, attempts were made to increase the accuracy of M.W.P.C's, mainly by reducing the sense wire spacing. Chambers with 1mm wire spacing have been built and tested at N.A.L.(4), C.E.R.N. (5), and by the author at Durham, whilst a 'scaled' chamber has been built (6), with a wire spacing of 0.5mm and all other dimensions scaled down from the standard 2mm chamber, even the mean free path of the gas molecules in the detector. Although such chambers do have resolutions approaching those of spark chambers, there are constructional problems involved in producing small sense

wire spacings, and the fact that each sense wire requires its own amplifier and associated electronics makes the cost of covering even moderate areas prohibitive. With reference to this latter problem, methods of reducing the numbers of electronic channels have been investigated (7),(8), involving the use of delay lines.

Other methods of improving the resolution of M.W.P.C.'s have included the following techniques:-

i) The application of the delay line principle to determine the coordinate along the anode wire (9)

ii) The use of electronegative gases to restrict the sensitive volume of the detectors to a region close to each sense wire (10), (11).

iii) The fact that the initial electrons formed take a finite time to reach the sense wire depending on how far they have travelled.

It is this third technique which forms the basic principle of the drift chamber.

1.3 The Drift Chamber.

It was noted in the original work on M.W.P.C's (1), that the time of arrival of an avalanche at the sense wire varied with the distance of the initial ionisation from that wire. This was referred to as time jitter, and was largely considered merely as the factor which limited the time resolution of the device. Even at this stage however, it was realised that this effect might be of some value; to quote from Charpak's paper (1) 'The variation in the delay with the distance from the wire may be exploited to give the

position of the particles between the wires'

This led to the development of a chamber which depended on this variation in time (the electron drift time) for its operation, and the first such chamber was described by Bressani et al (12), and later by Charpak et al (13). Figure 1.3 shows a section of the chamber, this being a standard M.W.P.C. to which a drift region has been added. A particle passing through the system causes a zero time pulse from the scintillator S, and produces ionisation along its path. The resulting electrons drift in the electric field maintained by the anode A_3, pass through the grid A_2, and are then detected in the M.W.P.C. region in the normal manner. The time between the zero time pulse and the pulse from the M.W.P.C. is measured and from this the position of the initial particle may be calculated, assuming that the drift velocity of electrons is known for the appropriate conditions. The gas used in this first chamber was 97% Argon - 3% Propane, and spatial resolutions of between $\pm$ 0.1mm and $\pm$ 0.2mm were quoted.

Although this type of design was utilised in some experimental detectors (see Chapter 8), a different basic design was developed by a group from Heidelburg (14) which has had more widespread application. In this design the structure of a standard M.W.P.C. is retained (see figure 1.1) but the separation of the sense wires is increased by a large factor (usually >10), thus reducing the number of electronic channels required to cover a given area. The location of a particle as it passes through the chamber is determined from the drift time of the ionisation electrons to the nearest sense wire, and the address of that wire. Gases used in preliminary tests were 90% Argon-10% Methane, and pure ethylene, resolutions of 0.2mm being quoted.

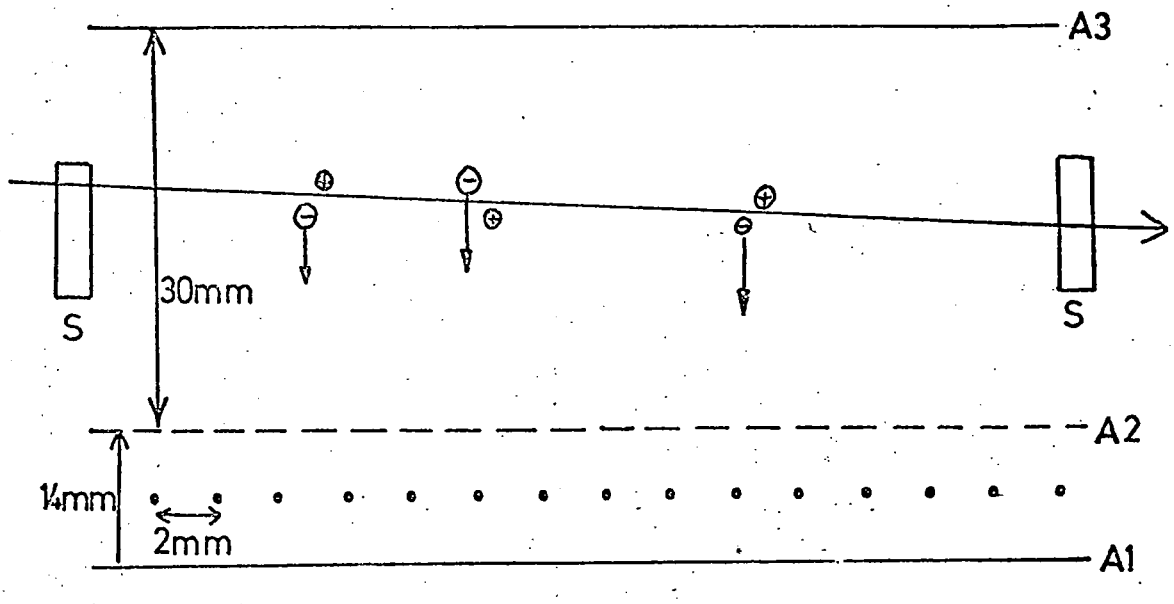

FIG 1.3 Section through first drift chamber

Such chambers as these however, have a major disadvantage in that the electric field in which the electrons drift is non-uniform, and is in fact zero midway between adjacent sense wires. Curve A on figure 1.4 shows the relative field for a hypothetical chamber with S = 48mm, and L = 6mm. Since the drift velocity of electrons is in general a function of the electric field, particularly at low field values, this would seriously complicate the performance of the detector, and to rectify this the Heidelburg group introduced a 'potential wire' midway between the sense wires and maintained at the cathode voltage. This produces the field shown by curve B on figure. 1.4, from which it can be seen that whilst the zero field region has been suppressed, there still exists and extensive non-uniform field region. Methods for compensating for this region involved either careful choice of gas, application of non-linear electronic timing systems (15), or modifications in the data analysis (16).

In order to increase the drift field uniformity further, a chamber was designed at C.E.R.N. (17) in which the cathode plane consisted of wires parallel to the sense wire plane and held at increasing negative potentials out from the sense wire to a maximum above the potential wire. A section through such a chamber is shown in figure 1.5 and the system results in a controllable, relatively uniform field, as shown by curve C on figure 1.4. The effect of removing the potential wire is shown by curve D. It should be noted here that the curves of figure 1.4 are intended to indicate general effects rather than precise field values, as they were obtained by assuming unrealistic H.T. values, (17), and more accurate values for fields in drift chambers will be calculated in chapter 4.

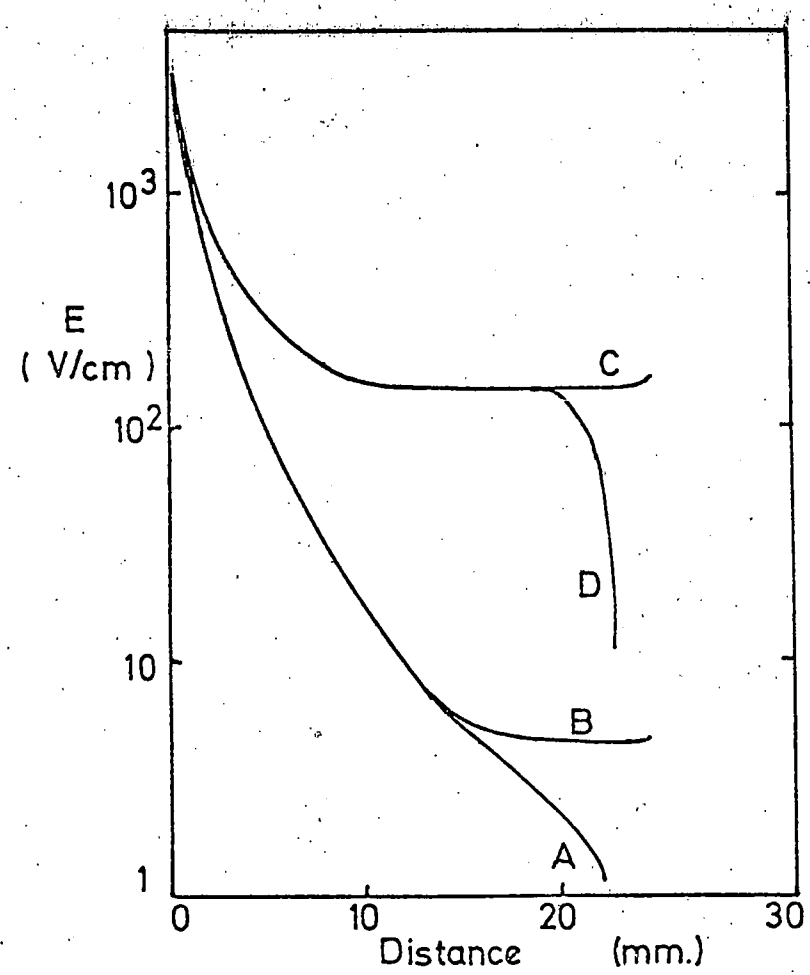

A Extended M.W.P.C.
B 'Heidelburg' chamber
C A.F. D.C.
D A F D C (no potential wire)

FIG 1.4 Form of electric field variation for different chamber types

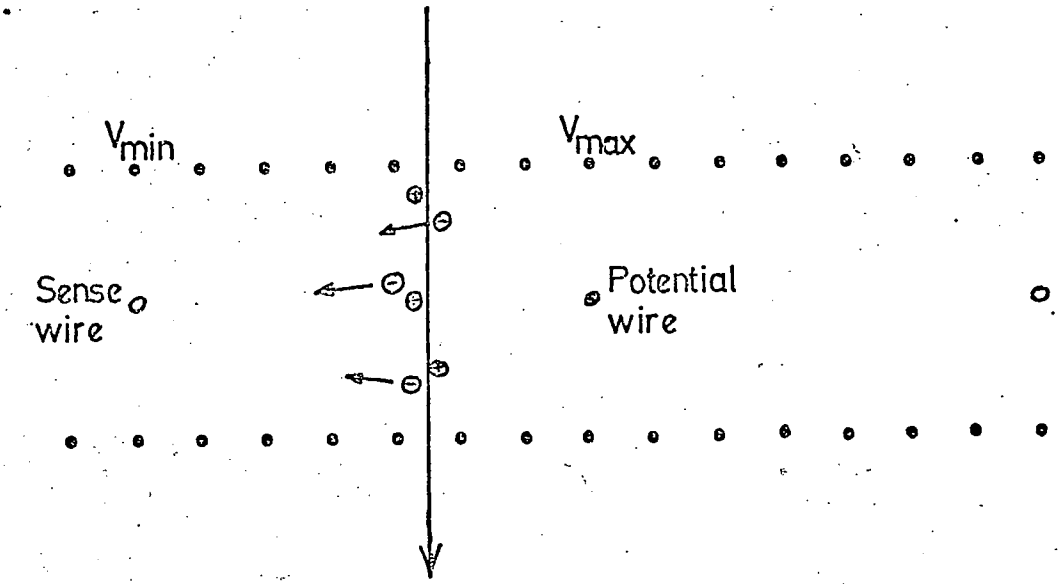

FIG 1.5 Section through A.F.D.C.

These adjustable field drift chambers (A.F.D.C.) have recently been extensively developed, particularly at C.E.R.N. and here at Durham, because of their potentially high spatial resolution, their constructional similarity with standard M.W.P.C's, and their versatility, the basic design allowing for variation of drift field, sense wire separation and a simple method of compensating for the effects of strong magnetic fields. It is this type of chamber which provides the subject of study for this thesis.

1.4 Present Work

The present study of drift chambers was instigated for several reasons. At the time of starting the work, although many drift chambers had already been built and even used in experiments, there was a lack of detailed results or theories concerning the various processes which were involved in their operation. It was felt that research in this area was needed both for the understanding of existing detectors, and to aid the development of future devices. Also at this time Durham University were asked to provide some specialised drift chambers to be used in an experiment at C.E.R.N., and although the specific development of these chambers is the subject of another work (18) it was realised that a simultaneous study of more general drift chamber properties would be of benefit to such development. Finally it was thought that any data on the behaviour of electrons in gases under the influence of electric and magnetic fields such as would be obtained in this study, would be of general interest to many workers not necessarily connected with drift chamber development. For example, a study of drift chambers appears to be one of the most accurate methods of determining the drift velocity of electrons, which is relevant to many branches of physics.

At the beginning of this investigation it was decided that a suitable gas would have to be chosen for the major part of the study, although the effects of various gases would be examined at some stage, and it was clear from the literature available at that time that many factors were important in determining the suitability of any gas. These factors will be discussed in greater detail in appropriate chapters, but some of the more basic will be listed briefly here in the context of necessary requirements for a drift chamber gas.

i) The gas must fulfil the normal proportional chamber requirements so as to give adequate output pulses on the sense wire (19).

ii) The attachment coefficient must be small enough to allow a small number of electrons to drift over the required drift length.

iii) Electron drift velocity should be high enough to avoid long resolution times, and low enough to avoid prohibitively fast electronic timing systems.

iv) A drift velocity that is largely independent of electric field, particularly at high fields, is an advantage in that it results in a linear drift time/drift distance relationship over the whole chamber.

v) The ratio of electron diffusion coefficient to drift velocity should be small, as this governs the spatial resolution of the device due to diffusion of the original drifting electrons.

vi) The effect of magnetic fields on the above parameters should be a minimum.

From this list it was realised that the choice of any particular gas would involve some compromise, but it became apparent that the mixture of a noble gas (usually argon) with certain molecular gases (such as ethylene, methane, isobutane) possessed many advantages. One of the earliest such mixtures recommended was argon + 10% methane (14), and investigation showed that this mixture was available in England ready mixed and at a very low cost. Those properties of this mixture that were already known seemed to indicate its possible suitability, and it was decided to study in detail chambers containing this gas even if other more sophisticated mixtures were shown elsewhere to be superior, since if its properties could be shown to be satisfactory, then its simplicity of use and price would make it an attractive choice in many applications.

Since the start of this work however, other detailed drift chamber studies have been undertaken, notably at C.E.R.N. under Professor Charpak, but their work has been concerned primarilly with chambers using argon-isobutane gas mixtures. Two important features of this present study then may be considered as the investigation of argon/methane as a suitable drift chamber gas, and the comparison of the operating characteristics of such chambers with those using other mixtures.

In order to do this, all the results presented here have been grouped under general headings of: basic properties including output pulses and chamber efficiency; spatial resolution; drift velocity measurements; effects of magnetic fields. This has however resulted in data being presented out of temporal sequence, and in fact data from the same series of tests being presented

in separate chapters, although of course the conditions under which any particular set of data was obtained will always be described.

CHAPTER 1 - References

1. G. Charpak, R. Bouclier, T. Bressani, J. Favier and C. Zupancic, Nuc. Inst. Meth 62 (1968) 262

2. J.G. Rutherglen and J.M. Patterson, Rev. Sci. Inst 32 (1961) 522.

3. P. Astbury, Nuc. Inst. Meth. 46 (1967) 61.

4. M. Atac and J. Lach, Nuc. Inst. Meth. 86 (1970) 173

5. B. Makowski and B. Sadoulet, Nuc. Inst. Meth. 3 (1973) 561

6. P.A. Souder, J. Sandweiss and A.A. Disco, Nuc. Inst. Meth. 109 (1973) 237

7. R. Grove, K. Lee, V. Perez-Mendez and J. Sperinde, Nuc. Inst. Meth. 89 (1970) 257

8. D.M. Lee, S.E. Sobottka and H.A. Thiessen, Nuc. Inst. Meth. 104 (1972) 179

9. P. Christie, K.D. Evans, J. Griffiths, E. Mathieson, P. Murphy Nuc. Inst. Meth. 130 (1975) 279. This contains references to earlier related work.

10. G. Grunberg, L. Cohen and L. Mathieu, Nuc. Inst. Meth. 78 (1970) 102

11. B. Meckel, Nuc. Inst. Meth 94 (1971) 573

12. T. Bressani, G. Charpak, D. Rahm and C. Zupancic, Proc. Int. Sem. Filmless spark and streamer chambers, Dubna, (1969)

13. G. Charpak, D. Rahm and H. Steiner, Nuc. Inst. Meth. 80 (1970) 13

14. A.H. Walenta, J. Heintze and B. Scharlein, Nuc. Inst. Meth. 92 (1971) 373

15. B. Schurlein, W. Farr, H.W. Siebert and A.H. Walenta, Nuc. Inst. Meth. 114 (1974) 587

16. J. Heintze and A.H. Walenta, Nuc. Inst. Meth. 111 (1973) 461

17. G. Charpak, F. Sauli and W. Duinker, Nuc. Inst. Meth. 108 (1973) 413

18. K.A. Short, Ph.D. Thesis, University of Durham (1976)

19. Such requirements are extensively reported. See for instance P. Rice-Evans, Spark, streamer, proportional and drift chambers, Richlieu Press, London (1974), Chapter 7.

CHAPTER TWO

CONSTRUCTION AND OPERATION OF DRIFT CHAMBERS

2.1 Introduction

As a preliminary to examining the results obtained from the operation of drift chambers it will be useful in this chapter to describe some of the mechanical and electrical properties of the chambers used in the tests. This will include general design considerations of our chambers and a discussion of the electric field within the active volume, as this is one of the principal factors influencing drift chamber operation.

A brief description will also be given of the methods of processing the basic information from the chambers i.e. measurement of the delay time of the pulse on the sense wire.

The information in this chapter then should provide a comprehensive background to the analysis of the operational results presented in later chapters.

2.2 Chamber Design

As stated in section 1.3 it was decided to study the Adjustable Field type of drift chamber as described by Charpak et al (1), largely because of its close constructional similarity with the M.W.P.C. which had already been extensively studied at Durham (2), and in fact the first drift chambers built at Durham were merely converted M.W.P.C.'s. It soon became apparent that there were some practical problems involved (3), and that such a technique did not represent the best possible design for drift chambers. It was decided therefore to design chambers specifically as drift chambers, and furthermore to standardise on those dimensions which would affect the performance of the devices so that results from various chambers

could be easily correlated.

Thus during the course of this study, several different chambers were used in various tests, the differences however being basically only in the design of the support structures or in methods of making electrical connections, necessary to meet any specific spatial requirements, and in all chambers the actual configuration of the wire planes was the same.

2.2.1 Wire plane configuration.

Figure 2.1 shows a section through part of the wire planes of one of the Durham chambers. The two outer wire planes are of 120 μm diameter copper beryllium wires which act as the H.T. or cathode planes providing both the electron amplification field around the sense wire and the lateral drift field throughout the rest of the chamber. The sense wires are 20 μm tungsten, gold plated to facilitate soldering, and in the same plane, symmetrically between them, are the potential wires (120 μm Cu/Be) which maintain the uniformity of the drift field. The volume between two adjacent potential wires is defined as a unit cell of the chamber, and variations in the width of this cell (distance between potential wires) constituted the only difference in wire configuration between the various chambers used. Thus two of the chamber designs used comprised a single unit cell of width 56 mm, and therefore a maximum drift length for electrons of 28 mm, whilst another was made up of many adjacent cells (i.e. having alternate sense and potential wires in the central plane) with each cell being 28 mm wide. For most of the laboratory tests, the single cell types of chamber were used, these having only one sense wire and therefore requiring only one channel of timing electronics. The multi-cell chambers were the prototypes of the experimental detectors required for the g-2 experiment at C.E.R.N. and were used mainly for

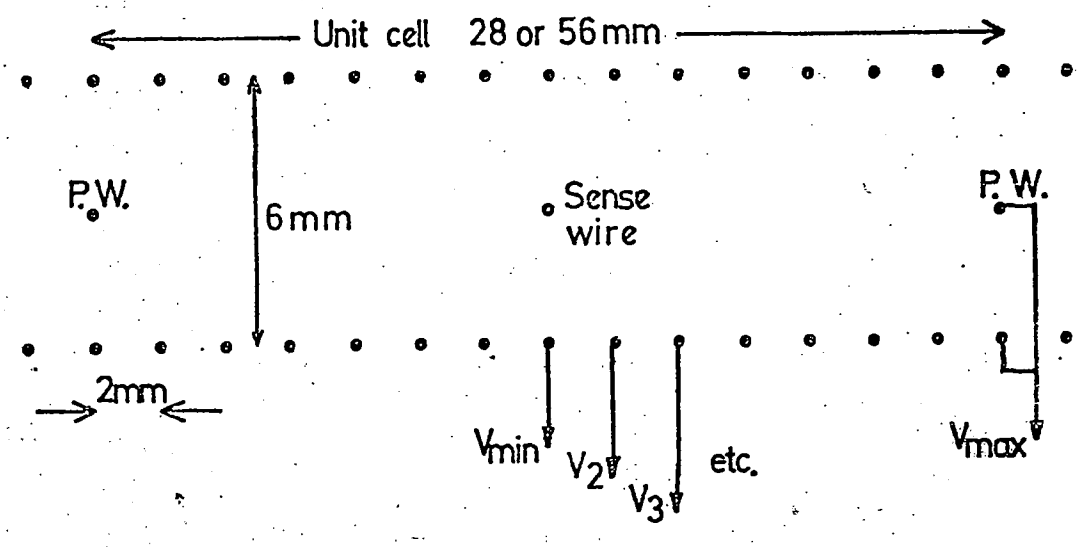

FIG 2.1 Section through wire planes of Durham drift chamber

some of the tests in the accelerator beam at the Daresbury Laboratory. The specific design of these latter chambers will be described more fully in Chapter 8.

Probably the most critical dimension in the chamber, apart from the actual positioning of the sense wires is the spacing between sense wire and cathode plane, as this determines the applied voltage necessary to provide a suitable electron multiplication field around the sense wire. As this dimension is reduced, the voltage required to give a fixed multiplication is also reduced, with obvious advantages as regards spurious electrical breakdown. At the same time however, the active thickness of the chamber is also reduced, with corresponding decrease in the average number of ionising collisions made by a high energy particle traversing the chamber. Since the actual number of collisions is statistical in nature, such a reduction in thickness could even affect the detection efficiency of the device. The chosen value of 3 mm was considered a suitable compromise, resulting in an operating voltage (V_{min}) of about 1.5 kV (for argon 90%, methane 10%), whilst maintaining a theoretical detection efficiency of $\sim$ 100% (see section 3.3), and allowing a high packing density of chambers along a particle trajectory.

It is also important that the sense wires are positioned exactly midway between the cathode planes, and that the cathode separation is accurately maintained in order to have uniform electric fields throughout the chamber. This will be more difficult to achieve for smaller values of cathode separation.

The importance of this effect was illustrated when difficulty was experienced operating chambers in which the sense wire - cathode plane distances were 2.8 mm and 3.2 mm (due to faulty construction) because internal electrical breakdown occurred around the sense wire at voltages lower than the required operating voltages.

2.2.2 Mechanical Construction

For the laboratory tests at Durham, generally using radioactive sources, and not requiring operation between the pole pieces of a magnet, a 56 mm cell width, single cell chamber was designed and constructed to fulfill certain requirements.

The overall thickness of the chamber was kept down to 25 mm to allow the positioning of the source (or collimator exit) and zero time counters as close as possible to the wire planes. This was desirable in view of the range and scattering properties of the radioactive decay particles.

The main frame of the chamber was machined from a single piece of 'Perspex' so as to minimise the possibility of air leaking into the chamber, this having a detrimental effect on the drifting and avalanching of the electrons. Also for this reason a large flat area of frame was made available for the window sealing surface. The windows themselves were made of 'Melinex' sheet (in most cases aluminised Melinex was used as it has useful electrical shielding properties) and in order to keep the amount of scattering material in the particle path to a minimum it was necessary to find the minimum practical thickness of Melinex for this application. This was found to be 120 μm, thinner material tending to crinkle along the seal as the windows bowed out on filling the chamber with gas. A more complex sealing system may have solved this problem but it was considered important that the chambers be simply demountable to gain access to the wire planes. The windows were sealed down to the frame using 3M's double-sided pressure sensitive tape, 120 μm thick, and this system was found to be leak-tight to within the sensitivity of the gas flow monitors (2%) whilst still permitting relatively simple removal.

The wire planes were positioned so as to allow quick access to any plane for repair purposes, and to facilitate external connections. These connections were made using specially etched copper clad printed circuit boards and figure 2.2 shows a section through the chamber frame illustrating the design used. As these chambers were not to operate in magnetic fields and thus did not require the slanting of the electric field described in Chapter 7, opposite wires in the top and bottom cathode planes were connected together (figure 2.2), as were wires equidistant from the sense wire in each half cell. These latter connections were made externally by means of a ribbon cable and this is seen in figure 2.3. which shows a view of the complete chamber.

Also shown in figure 2.3 are the 14 resistors of the H.T. distribution network connected directly between the H.T. wire contacts; the socket (centre) connecting to the sense wire; the socket (left) for the H.T. supply; the earthed, shielded window; and the two gas ports.

The position of the cathode wires was fixed by reference to the printed circuit connection board. This was manufactured to have 1 mm copper strips with 2 mm pitch. The cathode wires were then soldered to the centre of each strip, as judged by eye. Any slight variation in position would only marginally affect the drift field. The position of the sense wires however must be known to a much greater accuracy (better than 0.1 mm) with respect to some external reference line, as this directly affects the spatial resolution of the device. In our chambers this was done by trial and error, the position of each sense wire being checked with a travelling microscope and relocated if necessary until the required accuracy was achieved.

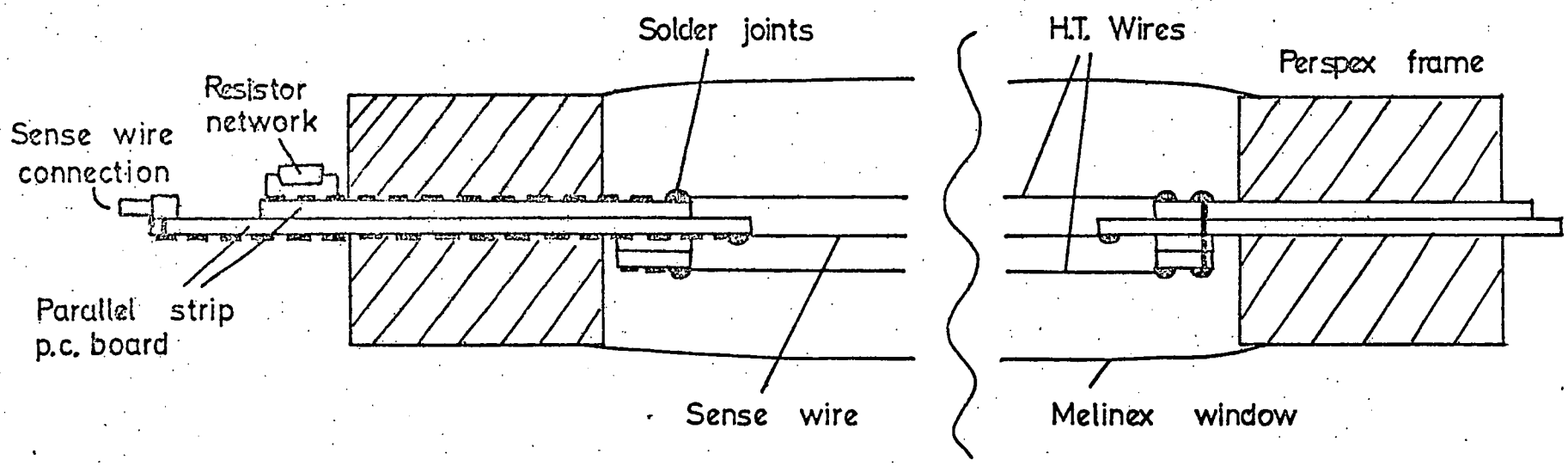

FIG 2.2. Section through 56 mm cell test chamber

Figure 2.3 - Single cell drift chamber for general laboratory tests.

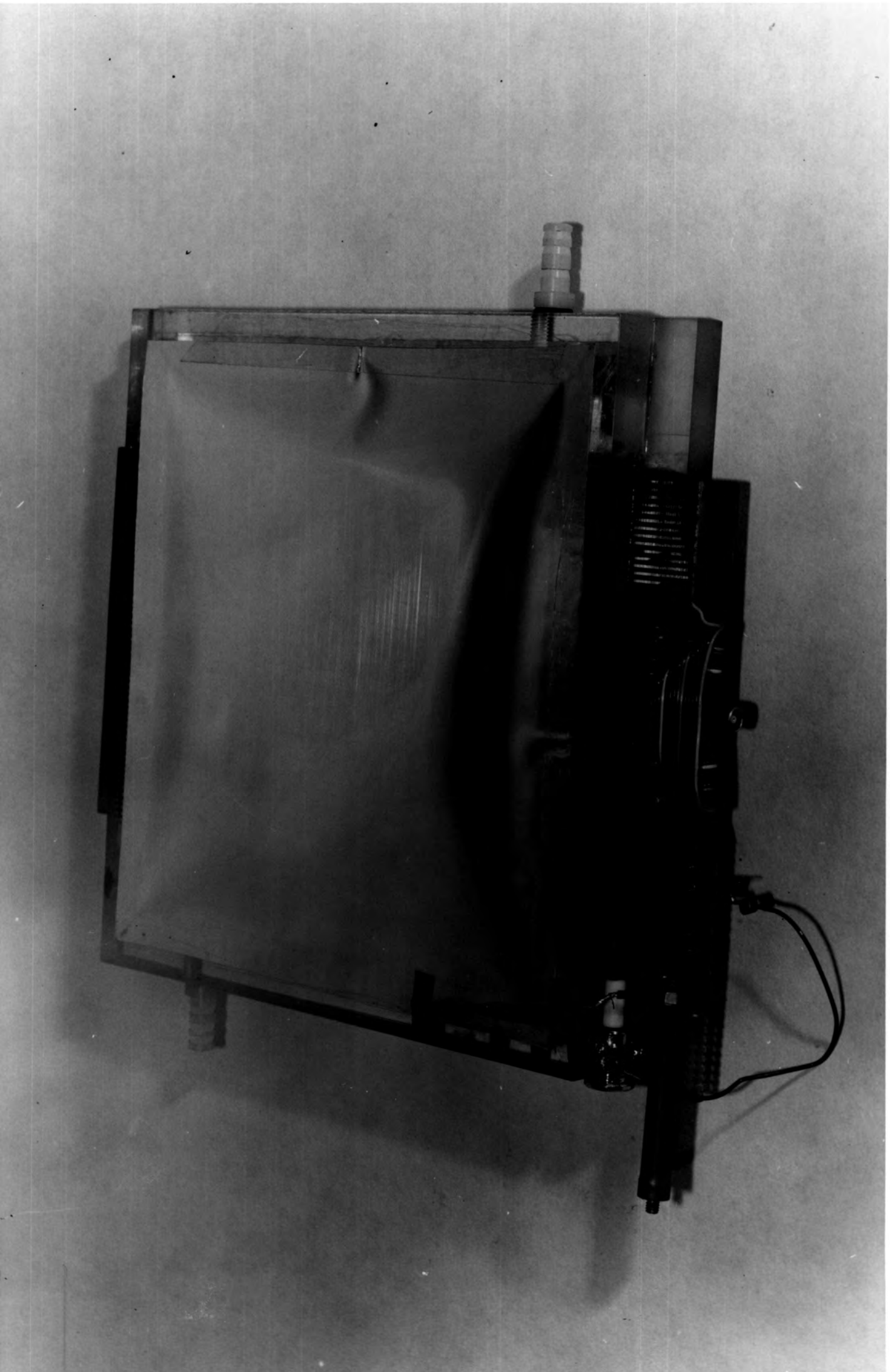

2.3 Application of Drift Field.

Figure 2.4 shows the method used to maintain the drift field within the chambers, which was achieved with a single H.T. power supply and a resistor network. Using this system the applied voltage gradient, and hence drift field, is varied by altering the final resistance to earth (R_E) of the network and then adjusting the supply voltage V_S so that V_{min}, which determines the field around the sense wire is kept at a suitable value. At C.E.R.N. (4) two supplies are used for this purpose. V_{min} is earth potential, one supply fixes a positive voltage on the sense wire and hence controls the amplification field, and the other maintains V_{max} and hence the drift field. This disposes of the need to vary any resistance values in order to change the drift field and results in lower absolute values of V_{max}, although we have always found the single supply — variable resistor method simple and effective.

In practice the value of R_E was varied by moving the earth connection along a resistor chain (seen to the left of figure 2.3) although it may have been better to have a calibrated potentiometer to fulfil this function. All the chambers described here had resistor networks with R_S = 10MΩ, R_N = 3.3MΩ and table 2.1 shows some of the voltage gradients obtained with various values of V_S and R_E such that V_{min} is maintained at approximately 1.5kV.

R_E MΩ	V_S kV	V_{max} kV	V_{min} kV	Voltage Gradient V/cm
25	4.9	4.3	1.51	995
45	3.4	3.1	1.51	555
75	2.6	2.4	1.49	326
175	2.0	1.9	1.51	144

TABLE 2.1

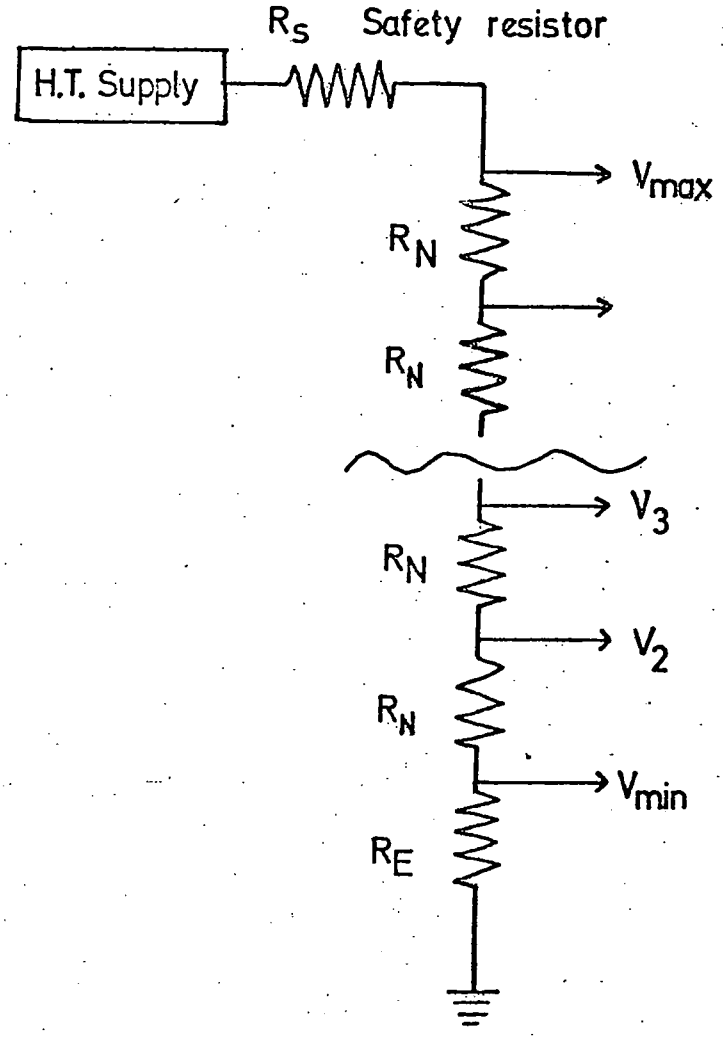

FIG 2.4 Method of applying drift field

It will be shown later however, (section 3.3) that the optimum operating voltage V_{min} depends on the magnitude of the applied drift field, and hence V_S must be set with reference to efficient operation of the chambers. It should also be noted that the calculated voltage gradient will not represent the value of the drift field throughout the whole chamber. For instance figure 2.5 shows the equipotential lines for half of one cell of a chamber, calculated by a numerical relaxation method, for an applied voltage gradient of 500 V/cm, and figure 2.6 shows the value of the electric field along the central plane of the chamber. From these it can be seen that the drift field is equivalent to the voltage gradient over much of the chamber, but rises in the region of the sense wire due to the effect of the multiplication field around it. It will also be shown later (section 4.3) that the extent of this non-uniformily increases as the applied voltage gradient is reduced.

Other factors may affect the drift field, for example the proximity of an earthed plane to the H.T. wires. This occurred during many of the tests, when earthed, metallised windows were used to avoid external electrical interference producing spurious pulses. Such variations in drift field have been investigated theoretically (5), and figure 2.7 from this reference shows the variation in field with d, the distance of an earthed plane from the H.T. wires for a cell of half width 25 mm. In our chambers d = 9 mm and it can be seen that this results in a reduction in field of about 2% from the value of the voltage gradient with no earthed plane.

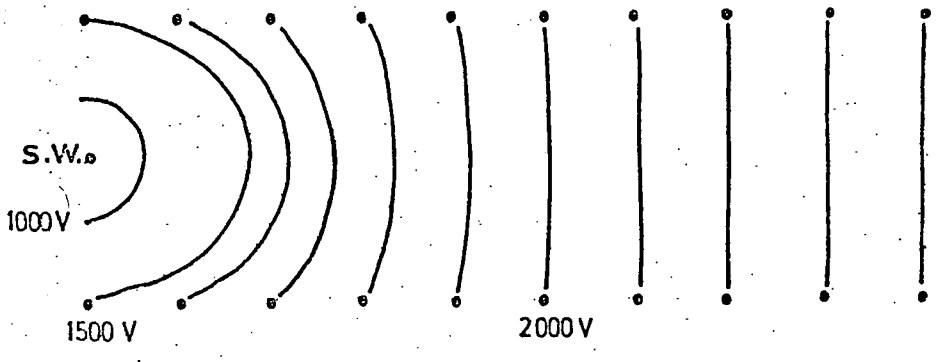

FIG 2.5 Simplified plot of equipotentials for an applied field of 500 V/cm

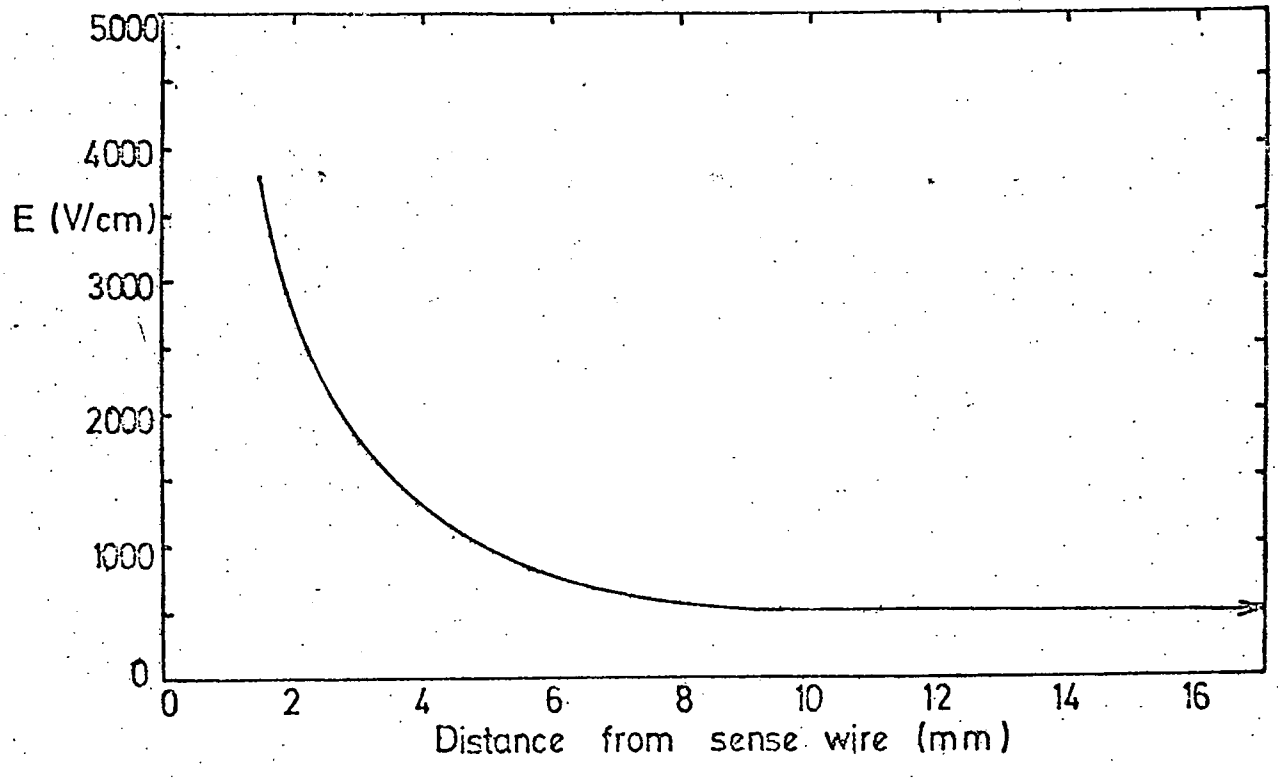

FIG 2.6 Electric field along sense wire plane, from figure 2.5

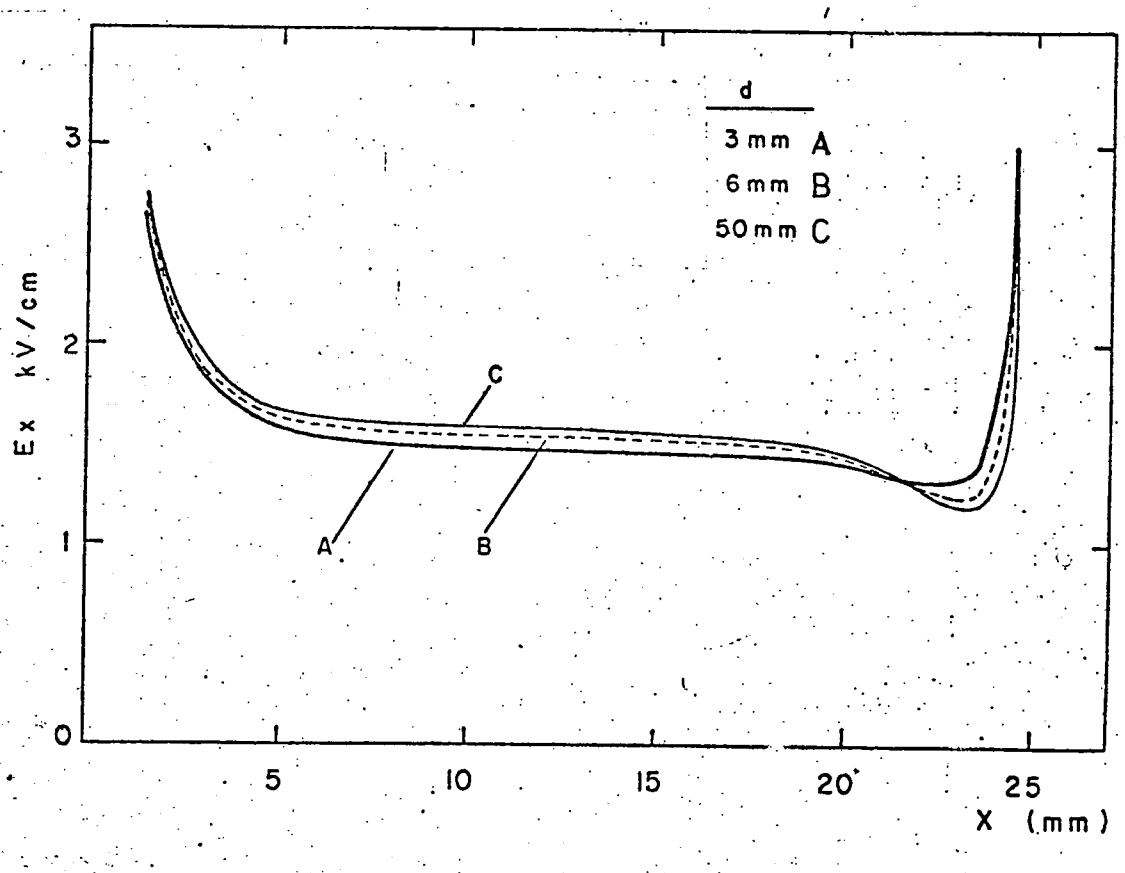

FIG 2.7 Variation in drift field Ex, for earthed planes at distance d from the H.T. planes.

2.4 Drift time measurement

In order to achieve the potential optimum resolution of drift chambers it is necessary to be able to measure the drift time of the electrons to a correspondingly high accuracy. Aiming at a possible resolution of 100 μm and assuming an electron drift velocity in the region of 30 - 50 mm/μsec. requires timing resolutions better than 2 or 3 nsec. The techniques available for making such measurements can be divided into 2 main types.

2.4.1 Analogue Techniques

In this method the drift time is converted to a corresponding voltage amplitude, using a commercially available module, the time-to-amplitude converter (T.A.C.). The T.A.C. works on the principle of charging a capacitor from a highly stable current source during the time interval between the start and stop pulse. The resulting voltage on the capacitor is amplified, shaped and presented at an output socket. This is then recorded using an analogue to digital converter (A.D.C.), which for many of the tests was in the form of a pulse height analyser (P.H.A).

The resolution of the T.A.C. is quoted as better than 500psec with a differential nonlinearity of less than 0.5%, whilst the resolution of the P.H.A. depends on the number of channels and the renge being examined. (e.g. 2 nsec for a 512 channel analyser looking at 1024 nsec or approx. 40 mm drift distance).

The disadvantages of the T.A.C. - A.D.C. system are that the use of a P.H.A. virtually restricts its use to one sense wire at a time (although the A.D.C. need not be in the form of a P.H.A.), and the long processing time (several microseconds) needed to convert the analogue signal. However, the advantages of simplicity, versatility, independance from computer interfacing, and the visual

presentation of the data in the form of a time distribution histogram make it extremely attractive, particularly for laboratory tests using radioactive sources and single chambers.

The analogue system can be compressed into a single component, a time-to-digital converter (.T.D.C.) such as the CAMAC T.D.C. manufactured in various forms by LeCroy Electronics Ltd. Multi-channel T.D.C. modules are manufactured so that events resulting in output from several chambers can be readily analysed. Long conversion times are still a disadvantage and a computer interface is now required to read out the data presented by the T.D.C's. Nevertheless this system was used successfully for tests on arrays of chambers using the accelerator beam at Daresbury Laboratory where CAMAC, small computers, and T.D.C. modules were more readily available.

The analogue system is not restricted to the testing of chambers however, a T.A.C. - A.D.C. set-up having been used in an operational environment at Saclay to localise high energy particles (6).

2.4.2 Digital Techniques

Probably the most suitable method of measuring drift times in operational chambers is one in which, in its simplest form, the zero-time (or start) pulse starts a fast clock, the pulse from the chamber (or stop pulse) stops it, and the number of clock pulses is recorded via a scaler.

To achieve the necessary resolution of about 2 nsec however, requires the clock frequency to be 500 MHz, and whilst such systems hove been successfully tested (7), they are likely to be expensive and difficult to achieve. In view of this, two methods have been devised to allow the same resolution with lower clock rates.

One of these is 'time stretching' (8, 9) in which the drift time is expanded by a known factor before measuring it by a digital method. This is done by discharging a capacitor for a time equal to the drift time, at a high current i_1, then allowing it to charge back up to its original value at a low current i_2. The charge time is then i_1/i_2 times the drift time and can be measured using slower electronics.

The other method is a vernier technique (7), in which the start and stop pulses are synchronised with the clock pulses by routing through various delays, thus effectively subdividing the time between two clock pulses.

An additional advantage of the digital method is that variations of drift velocity across the chamber may be compensated for by using a 'non linear clock', as described by Schurlein et al (10). This is a technique in which the time separation of the clock pulses is directly linked to the drift velocity. Thus if the drift velocity decreases with distance then the frequency of the clock is reduced with time so that the number of clock pulses counted remains proportional to the distance drifted by the electrons, rather than to the drift time.

2.4.3 Operational Systems

It is often necessary to have, in addition to the basic time measuring system, a supporting data handling system, in order to realise the full operational potential of a drift chamber array containing many sense wires.

As an example of a practical drift chamber data system, figure 2.8 shows the principle of a 'Digitron' scheme (11), also more fully described by Verweij(7), which handles all the data from a set of sense wires (8 in this example). The system records the

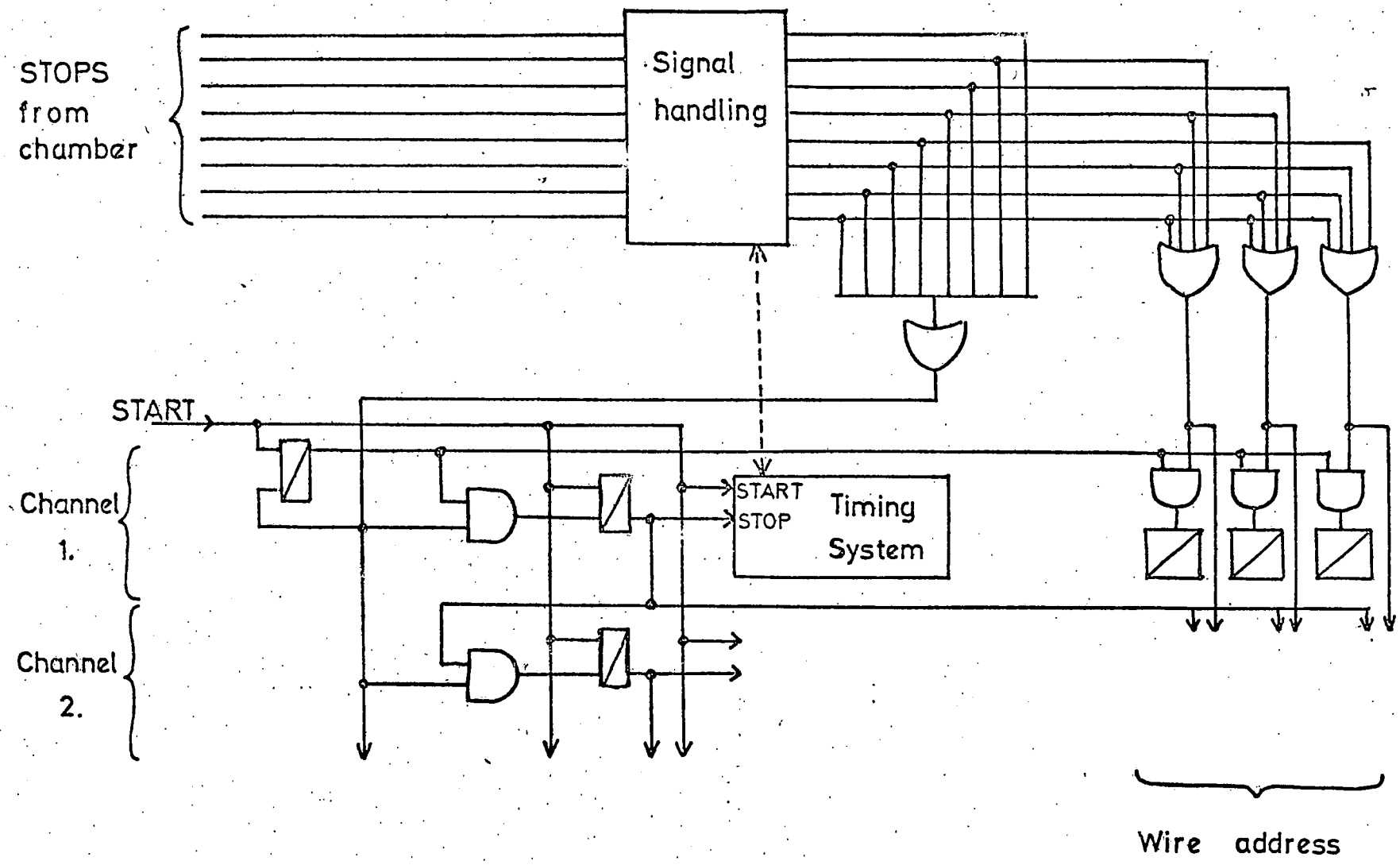

FIG 2.8 Principle of 'Digitron' system for handling drift chamber data

drift time and wire address corresponding to a particular event and is capable of recording multiple events within a chamber. The basic operation of the system is as follows.

The start pulse activates all the time measuring systems (e.g. starts scalers counting clock pulses) and also enables the first channel stop line and wire number indicator. The first stop pulse from the chamber then, after being amplified, shaped, and if necessary synchronised to the clock pulses, stops the first channel of the measuring system, producing the drift time, and in parallel sets the wire number indicator to record the appropriate wire. At the same time it enables the second channel stop line and wire number indicator ready for any second stop signal. Thus the number of channels required is equal to the maximum expected multiplicity, so that there may well be less timing channels than the number of sense wires, with obvious savings in cost. At very high event rates however it may be advantageous to have a system with separate measuring channels on each wire. The actual time measuring system used in these schemes may be either clock and scaler, T.A.C. and A.D.C., or T.D.C., and the resulting data may be read into an independant buffer or via CAMAC into a computer.

In a short review, Sauli (12) has examined the respective merits of various systems, including those described above, in terms of accuracy, efficiency, and ability to deal with multiple events. In particular he has compared the potential resolution obtainable with analogue and digital methods. Assuming the timing error with an analogue system is a fraction p of the time t, and standard deviation for a digital system is $\sigma = 0.46\ T$, where T is the clock period, we have the overall accuracy for analogue systems given by

$$\sigma_a^2(t) = \sigma_e^2(t) + (pt)^2$$

and for digital systems by:

$$\sigma_d^2(t) = \sigma_e^2(t) + (0.46T)^2$$

where $\sigma_e(t)$ is the intrinsic standard deviation associated with the electron drifting process. Figure 2.9 shows values of σ_a and σ_d plotted for various conditions, with σ_e being calculated from experimentally measured accuracies (obtained from ref. 1). From this figure it can be seen that digital systems offer more uniform accuracies, with obvious advantages for long drift times, and also that a 4 nsec digital system offers approximately the same performance as a 0.5% analogue system.

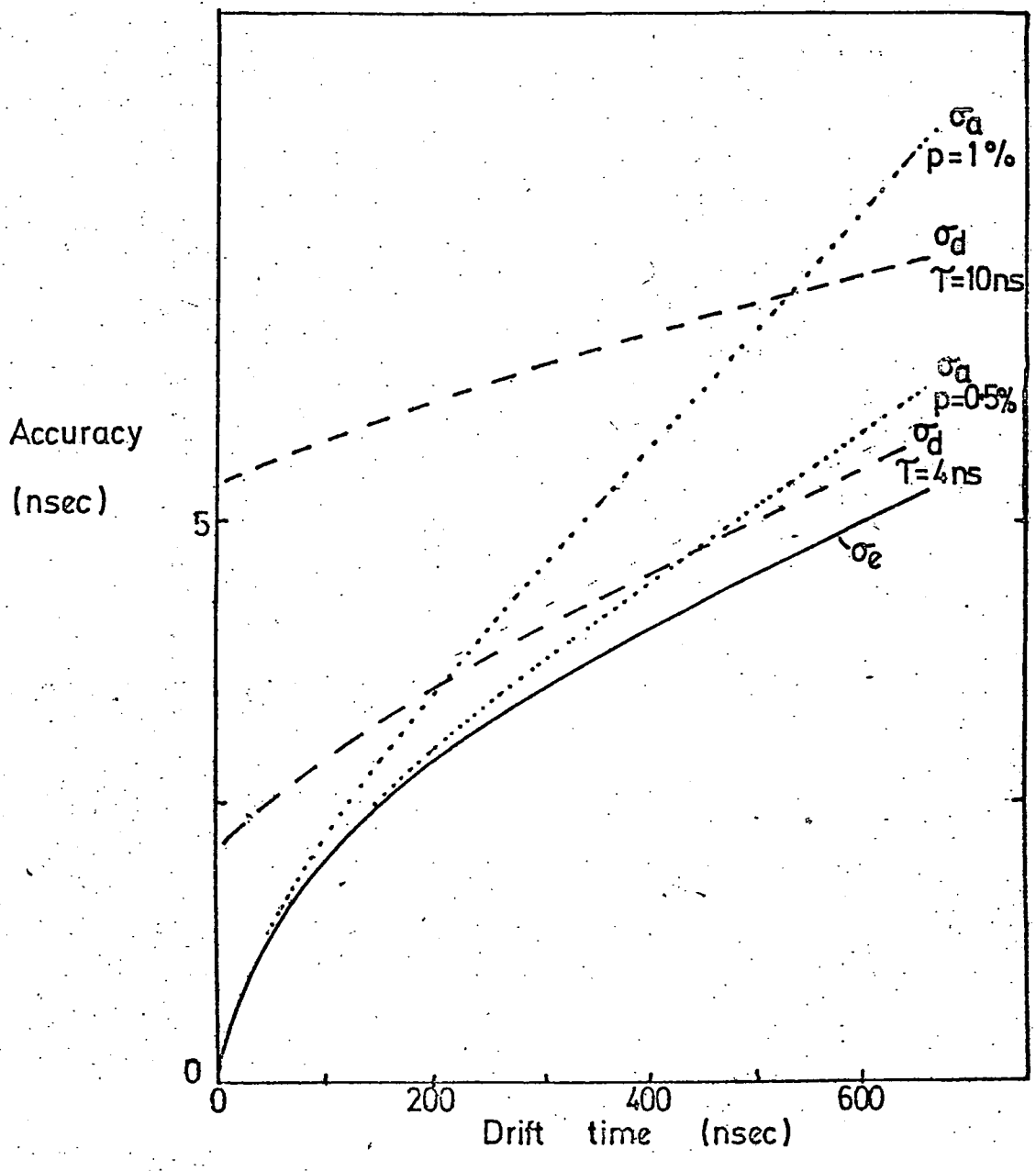

FIG 2.9 Effect of time-measuring electronics on chamber accuracy (from ref. 12)

CHAPTER 2 References

1. G. Charpak, F. Sauli and W. Duinker, Nuc. Inst. Meth. 108 (1973) 413

2. G.C. Smith, Ph.D. Thesis, University of Durham (1973)

3. K.A. Short, University of Durham Internal Report NI-73-4 (1973)

4. A. Breskin, G. Charpak, B. Gabioud, F. Sauli, N. Trautner, W. Duinker and G. Schultz, Nuc. Inst. Meth. 119 (1974) 9

5. A. Wylie, CERN NP Division Internal Report 74-7 (1974)

6. J. Saudinos, J.C. Duchazeaubeneix, C. Laspalles and R. Chaminade, Nuc. Inst. Meth. 111 (1973) 77.

7. H. Verweij, Proc. Int. Conf. Instrumentation for High Energy Physiks, Frascati (1973)

8. C. Rubbia, CERN NP Division Internal Report 73-1 (1973)

9. D.C. Cheng, W.A. Kozanecki, R.L. Piccioni, C. Rubbia, L.R. Sulak, H.J. Weedon and J. Whittaker, Nuc. Inst. Meth. 117 (1974) 157

10. B. Schurlein, W. Farr, H.W. Siebert and A.H. Walenta Nuc. Inst. Meth. 114 (1974) 587

11. R.A. Lundy, Rev. Sci. Inst. 34 (1963) 146

12. F. Sauli, CERN NP Division Internal Report 73-12 (1973).

CHAPTER THREE

SOME GENERAL PROPERTIES OF DRIFT CHAMBERS

3.1 Introduction

It is intended in this chapter to examine those aspects of the behaviour of drift chambers not specifically connected with the electron drift process. In particular it includes a study of chamber output pulses and efficiency, and their dependence on various operating parameters, from both a theoretical and experimental viewpoint.

A knowledge of this behaviour is of importance in setting up operating conditions such that optimum performance of the chambers can be realised. It is also essential that the more general chamber properties are understood before attempting to interpret results pertaining to the electron drift mechanism.

It may be noted here that from a study of the equipotential lines in a drift chamber (see for instance figure 2.5), the region around the sense wire more closely resembles a cylindrical proportional counter than a M.W.P.C. Thus a general description of the processes which occur in this region may be found in any of the literature concerning proportional counters (1).

3.2 Pulse Formation

The output pulse size from a drift chamber, as in a proportional chamber or counter, is largely determined by the final amount of charge produced by the electron avalanche process around the sense wire, and this in turn is determined by the number of electrons incident at the avalanche region, and the subsequent degree of multiplication which occurs. Furthermore, the first of these factors will be given by the number of electrons resulting from the initial ionisation caused by the incident particle.

3.2.1 Initial Ionisation

The total number of ions formed by the passage of a charged particle (for a fixed distance in a given gas) is related to the energy lost by the particle in collisions with atomic electrons of the gas, which in turn is related to the type of particle and its energy. The theory of this energy loss has been extensively reviewed, for instance by Rossi (2) and Bethe and Ashkin (3), and leads to the following expressions for the rate of energy loss for various particles having velocity βc in material of atomic number Z, mass number A.

$$-\frac{dE}{dx} = \frac{2\,Dmc^2}{\beta^2}\left[\ln \frac{\pi^2(mc^2)^2}{(1-\beta^2)^{3/2}\,I^2(z)} - a\right] \qquad (3.1)$$

for positrons and electrons, and

$$-\frac{dE}{dx} = \frac{2\,Dmc^2z^2}{\beta^2}\left[\ln \frac{4(mc^2)^2\,\beta^2}{(1-\beta^2)^2\,I^2(z)} - 2\beta^2\right] \qquad (3.2)$$

for other heavier particles of charge z

In these expressions m is the electron mass, a is 2.9 for electrons and 3.6 for positrons. D is related to the electron density of the particular gas by the expression

$$D = 0.15\ Z/A \quad g^{-1}cm^2 \qquad (3.3)$$

Because of the difficulty in dealing separately with all the possible energy losses for the various processes which could occur on collision, these have been combined in a single term I(Z), the average of all ionisation and excitation potentials, which is then determined experimentally or expressed empirically (4).

The rise in energy loss for very high β particles (shown by the $1-\beta^2$ term) does not continue indefinitely however, due to the density of atoms restricting the influence of the expanding field associated with particles of increasing β.

Figure 3.1 shows the energy loss against particle energy calculated from the above expressions, for electrons and muons in argon (from Dimcovski (5)). Also shown is a curve for electrons in methane, drawn by assuming a similar relationship and using a value of energy loss of 1.5 KeV per cm for 1.3 MeV electrons (6). Thus the energy deposited in one of our 6 mm, argon-methane chambers is expected to be about 1.5 KeV for 1 or 2 MeV electrons (e.g. from a Sr_{90} source) and about 2.5 KeV for 1 or 2 GeV electrons and positrons (e.g. from the accelerator beam at the Daresbury Laboratories).

This energy loss may be used to give the total number of ion pairs (Np) produced by a particle by introducing Ep, the mean energy required to create an ion pair. Experimental values of Ep are quoted by Palladino and Sadoulet (7) and Jesse and Sadaukis (8) and from these we have a value of about 26 eV per ion pair for argon + 10% methane, giving values for Np of 55 and 95 for the two cases mentioned above.

The energy loss (and hence the total number of ion pairs created) is however statistical in nature, due mainly to the probability of a close collision emitting a highly ionising atomic electron (delta ray). Several distributions have been derived to describe the energy loss process the first and most famous being by Landau (9) in 1944. Figure 3.2 shows a Landau distribution compared to a Poisson distribution for the same number of events with the same most probable value. Under certain conditions it has been suggested (10) and demonstrated (11) that the actual distribution obtained will be even wider.

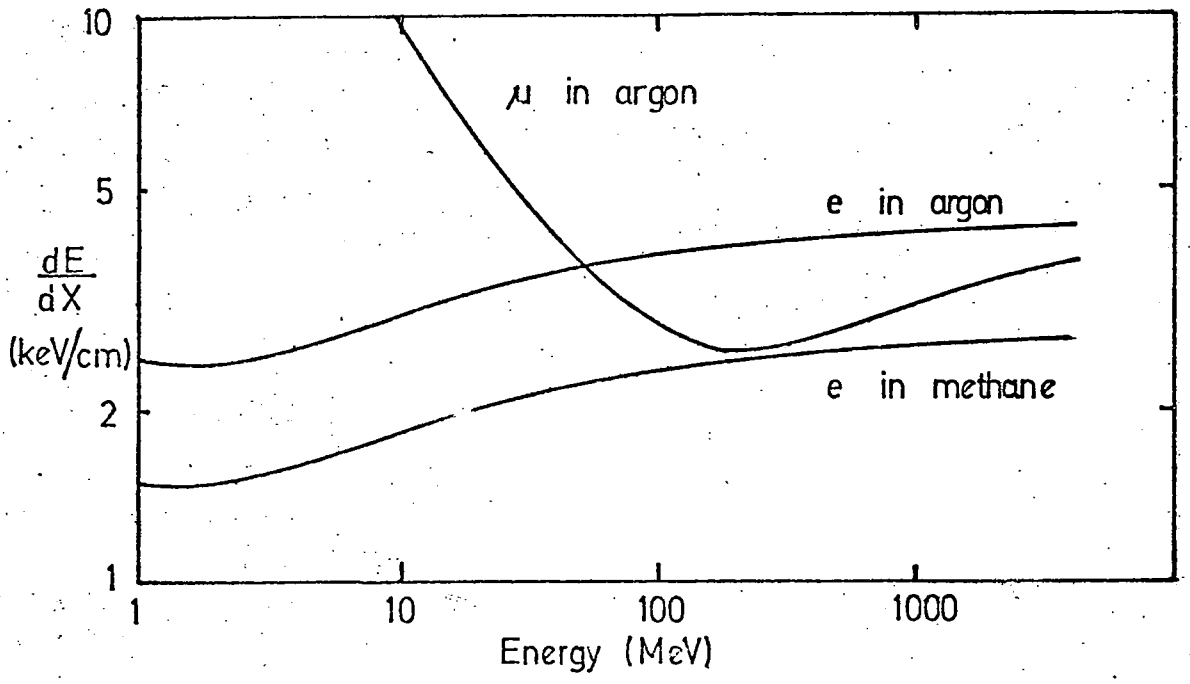

FIG 3.1 Variation in energy loss by collision, with particle energy.

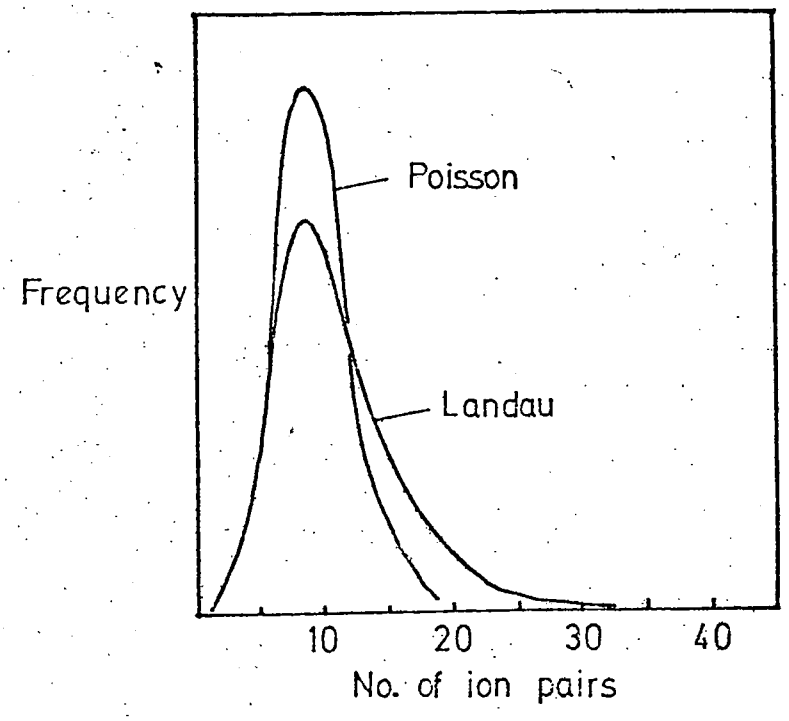

FIG 3.2 Distribution of total ionisation as predicted by Poisson and Landau statistics.

The number of collisions made by the incident particle on traversing the chamber (this is much less than the final number of ions produced, Np, as the electrons from each collision often have sufficient energy to cause further ionisation) is subject to simple Poisson statistics, thus allowing the inherent detection inefficiency to be calculated. Values of the mean number of collisions (or primary ions) are again given in reference (7) and give a minimum value of approximately 16 for our standard chambers. Thus the inefficiency of the chamber as given by the probability of no collisions occurring in the chamber, is given by exp(-16), and is obviously insignificant. There will however be a more significant probability of having a reduced number of collisions (eg $\sim 2\%$ for 8 or less collisions) and the resulting reduced pulse heights may be the cause of chamber inefficiency.

3.2.2 Avalanche Mechanism.

Assuming no loss of electrons during the drift process, the electrons from the initial ionisation are accelerated by the electric field near the sense wire until they gain sufficient energy to cause further ionisation of the gas. Successive ionisations result in an electron multiplication process, described by the parameter known as Townsend's first coefficient α. This is defined as the fractional increase in the number of electrons occurring during a 1 cm movement in the direction of a uniform field E, hence

$$\frac{dn}{n} = \alpha dx \qquad (3.4)$$

and the multiplication factor or gain (n_1/n_0) after a distance x is given by

$$\frac{n_1}{n_o} = \exp(\alpha x) \qquad (3.5)$$

In a drift chamber however, the multiplication takes place only in the high field region close to the sense wire where the equipotentials are concentric, and thus the electric field E is not constant but varies as 1/x, the distance from the centre of the sense wire. Now the gain in going from x_o to x_1 must be given by

$$\frac{n_1}{n_o} = \exp\left[\int_{x_o}^{x_1} \alpha\,(x)\,dx\right] \qquad (3.6)$$

where α varies with E and hence x.

Fortunately it has been shown by Palladino and Sadoulet (7) that even though E varies so strongly with x that equilibrium of the avalanche may not be achieved, it is still approximately correct to use the values of α for various values of E as obtained under constant field, equilibrium conditions.

Thus figure 3.3. shows the experimental variation of α with E for 90% argon 10% methane (12) obtained with constant E. The variation of E with x in our chambers was evaluated by assuming the region around the sense wire (up to a radius of the cathode sense wire spacing, 3 mm) approximated to the space inside a cylindrical proportional counter operating at voltage V_{min}, and using the expression

$$E = \frac{V}{x\ \mathrm{In}(r_2/r_1)} \qquad (3.7)$$

where r_1 is the sense wire radius and r_2 is 3 mm.

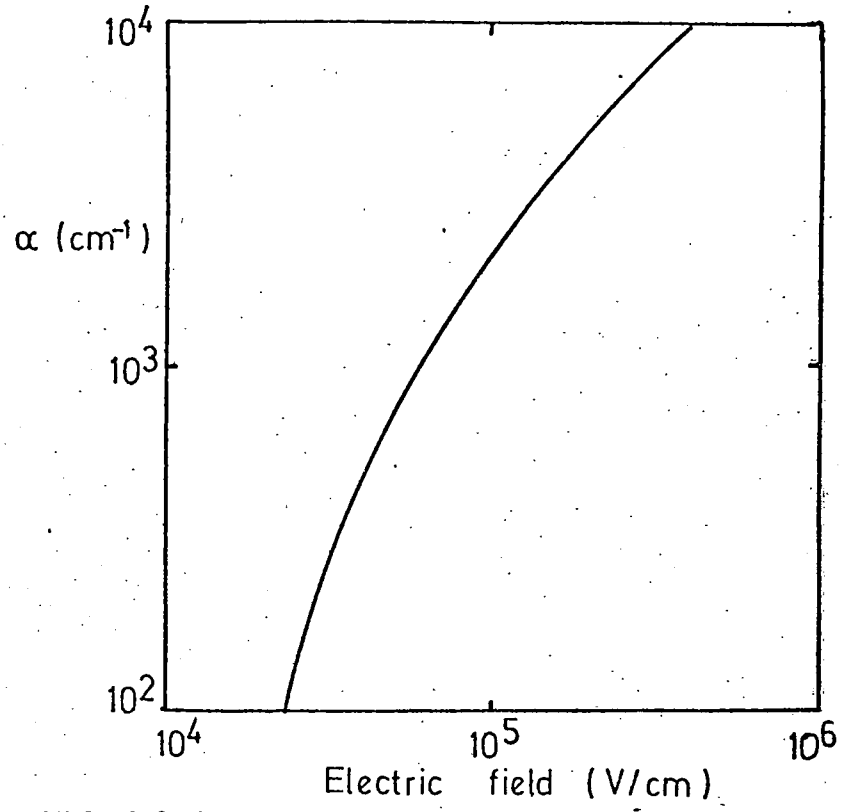

FIG 3.3 Variation of α with electric field, in argon + 10% methane.

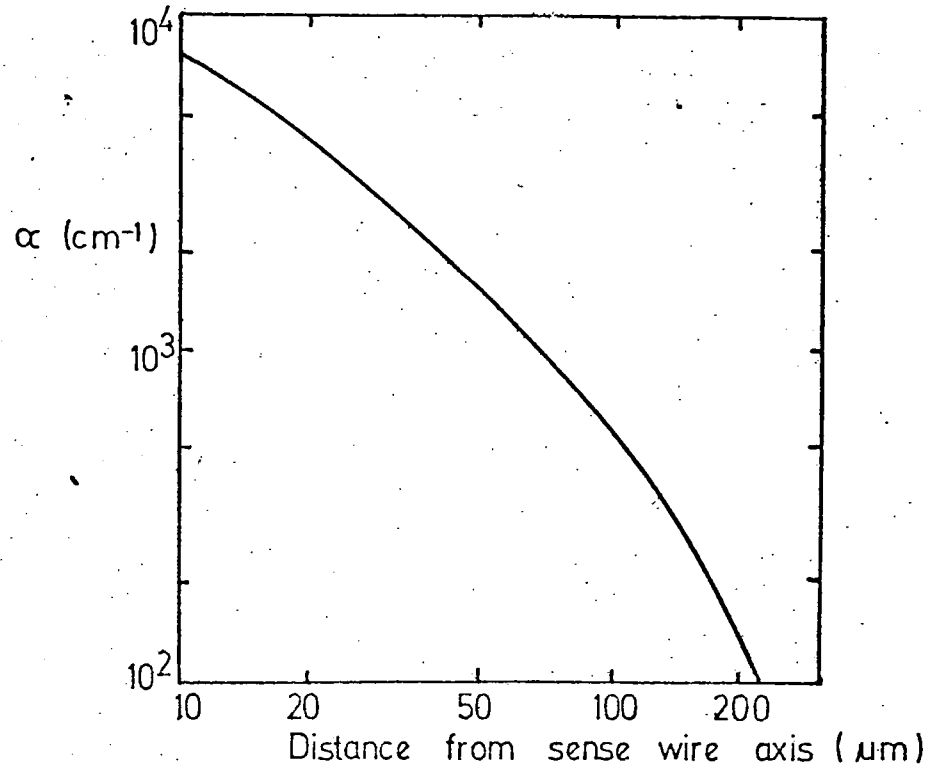

FIG 3.4 Variation of α with position in chamber.

Combining this data, for a V_{min} of 1.5 kV, and the data from figure 3.3, figure 3.4 was plotted showing the variation of α with x. Integrating numerically from the onset of significant multiplication to the sense wire surface (x = 10μm), and substituting the result in equation 3.6, gives a value of 10^7 for the electronic multiplication. This value of gain will depend on the value of V_{min} used (and also as will be shown later on the variations in the amplifying field as a result of the applied drift field) and although many expressions have been derived to describe the gain for proportional counters, (as reviewed in (7) and (12)) it seems generally accepted that the main variation is with exp (V_{min}).

The gain does not increase indefinitely however, as at higher gains the density of charges in the avalanche may become sufficiently high to cause significant space charge effects. Another effect is the tendency due to modification of the charge density on the sense wire, for the pulse heights to saturate, an effect noticed by many workers with proportional chambers (see for instance (6) and (13)). Using the criterion that this effects is significant when the number of charges in the avalanche is of the same order as the charge density on the sense wire, it has been shown (7) that the effect should be seen when there are about 2×10^8 ion pairs in the avalanche.

The electrons and ions formed in the avalanche immediately begin to move in their respective directions in the electric field, and it is this motion through the field which induces a pulse on the sense wire. As most of the ionisation takes place within a few microns of the sense wire, the highly mobile electrons are rapidly collected, giving the pulse a sharp rising edge, whilst the slower positive ions moving back through almost all of the field, contribute to the bulk of the pulse, which may extend for several microseconds as shown in figure 3.5. The time development of output pulses has been studied by Wilkinson (1) for

cylindrical counters and Charpak et al (6) for multi-wire chambers. As the usual practice is however to observe the output pulses using a differentiating circuit of some sort, only the first fast rising part of the pulse is used (i.e. mainly the electronic component). The form of the output pulse after differentiation is also shown in figure 3.5.

3.3 Pulse Height Measurements.

3.3.1 Variation with Voltage

The first attempts to examine the pulses from drift chambers consisted simply of connecting the sense wire of a 56 mm single cell chamber (as described in section 2.2.2) to the input of a vertical section of a fast oscilloscope (Tektronix 7704). Argon-methane, supplied premixed, from British Oxygen Company was continuously passed through the chamber which was irradiated using a collimated 10 mCi strontium 90 source. Unfortunately the β rays from the source were accompanied by a considerable flux of γ-rays produced by Bremstrahlung losses as the β rays passed through the material of the source and holder. Enclosing the source in a low z container (Perspex) did reduce the γ ray flux but a significant number of the chamber pulses were still resulting from γ ray conversion.

In order to observe only the β ray pulses, the system shown in figure 3.6 was used. The delay was adjusted to compensate for the drift time of the electrons in the chamber so that output pulses from any particular part of the chamber could be displayed with a very fast time-base. Due to the spread and scattering of the β rays however there was always a range of drift times for any source position and the pulses were displayed at varying times after the oscilloscope had been triggered. This is seen in figure 3.7 which shows the displayed output pulses for various chamber operating voltages (V_{min}) ranging from 1.42 kV to 1.58 kV for an applied drift field of approximately 550 V/cm and a mean drift distance of 10 mm.

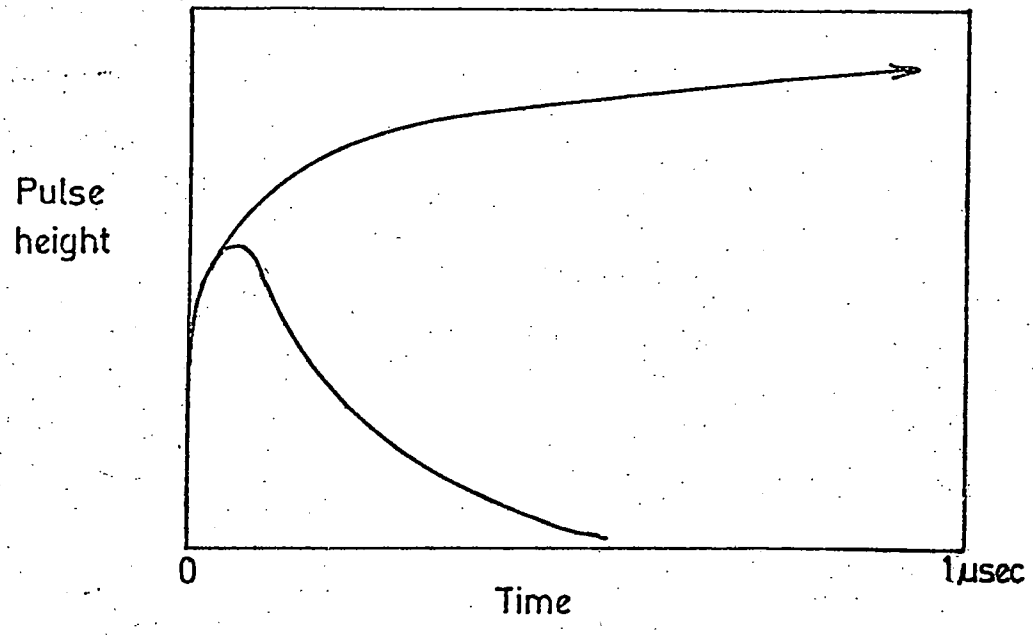

FIG 3·5 Time development of output pulses with and without differentiation.

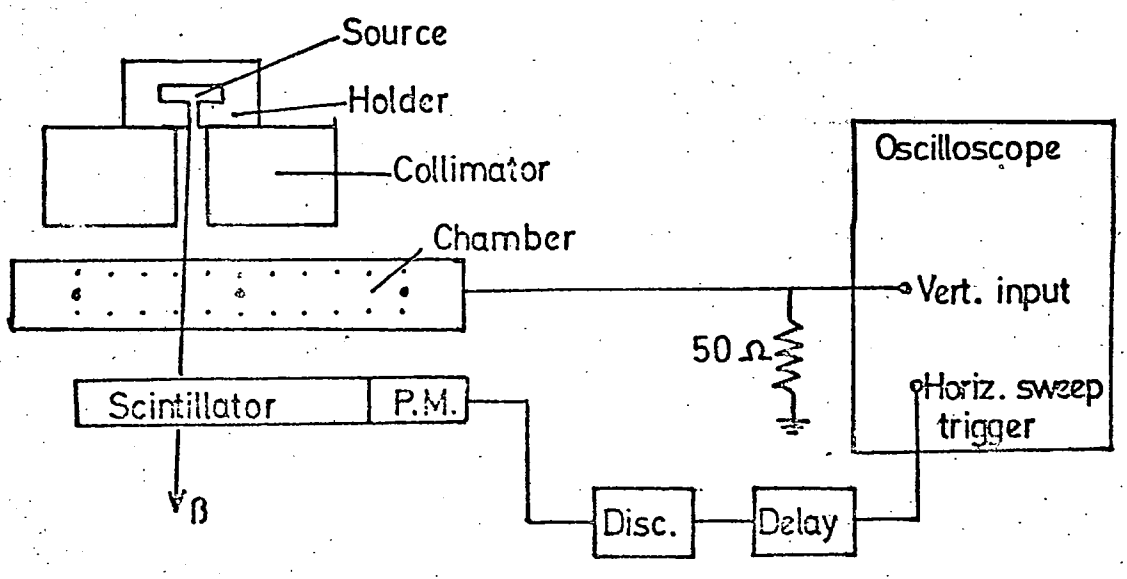

FIG 3.6 System for displaying output pulses due to β particles

Figure 3.7 - Drift chamber output pulses (into 50Ω) for various operating voltages.

(a) 1.42 kV.

(b) 1.47 kV.

(c) 1.51 kV

(d) 1.54 kV

(e) 1.56 kV

(f) 1.58 kV

Calibration for all traces:-

Vertical - 5 mv/div

Horizontal - 20 nsec/div

(a)

(b)

(c)

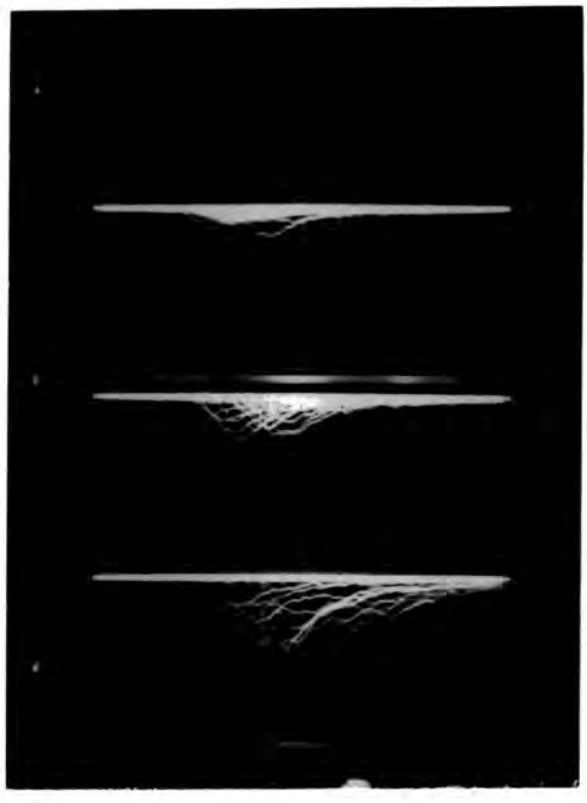

(d)

(e)

(f)

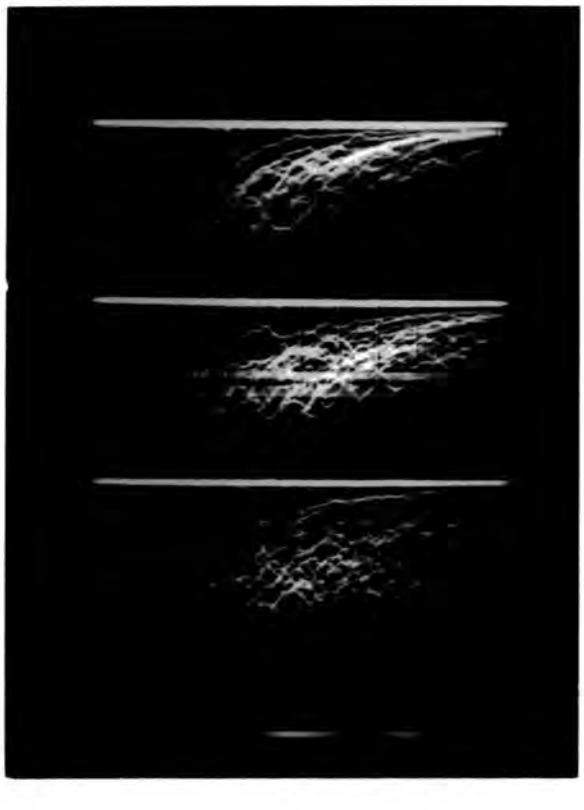

There will be an intrinsic range of pulse heights for the same conditions, due to the range of β ray energies emitted from the source and the statistical nature of the energy loss and avalanche mechanisms. Figure 3.8 shows a typical pulse height distribution from these tests obtained with a P.H.A. after linear amplification of the pulses, and the heights quoted in this chapter are estimated as being the most probable, from an examination of the oscilloscope traces and P.H.A. outputs.

The variation in pulse height with V_{min} is shown graphically in figure 3.9 for three different values of drift field and there are three features to note:

i) The chambers operated at all times without electrical breakdown up to the values of voltage shown by the extent of the curves shown in figure 3.9. The actual point at which breakdown began is not included however, as this varied considerably, particularly between different chambers.

ii) The shape of the graphs (exponential rise of pulse heights, flattening out for higher voltages) is in agreement with the theory and results mentioned in section 3.2.2.

iii) The value of the applied drift field has a marked effect on the pulse heights. For example there is an order of magnitude difference between the pulse heights obtained with the same operating voltage for applied fields of 930 V/cm and 140 V/cm. The explanation can be seen by realising that in this design of chamber the accelerating field around the sense wire, and the drift field in the rest of the chamber are not independent, each causing a distortion of the other. (This is separate from the slight interdependence due to using a common supply to provide both fields).

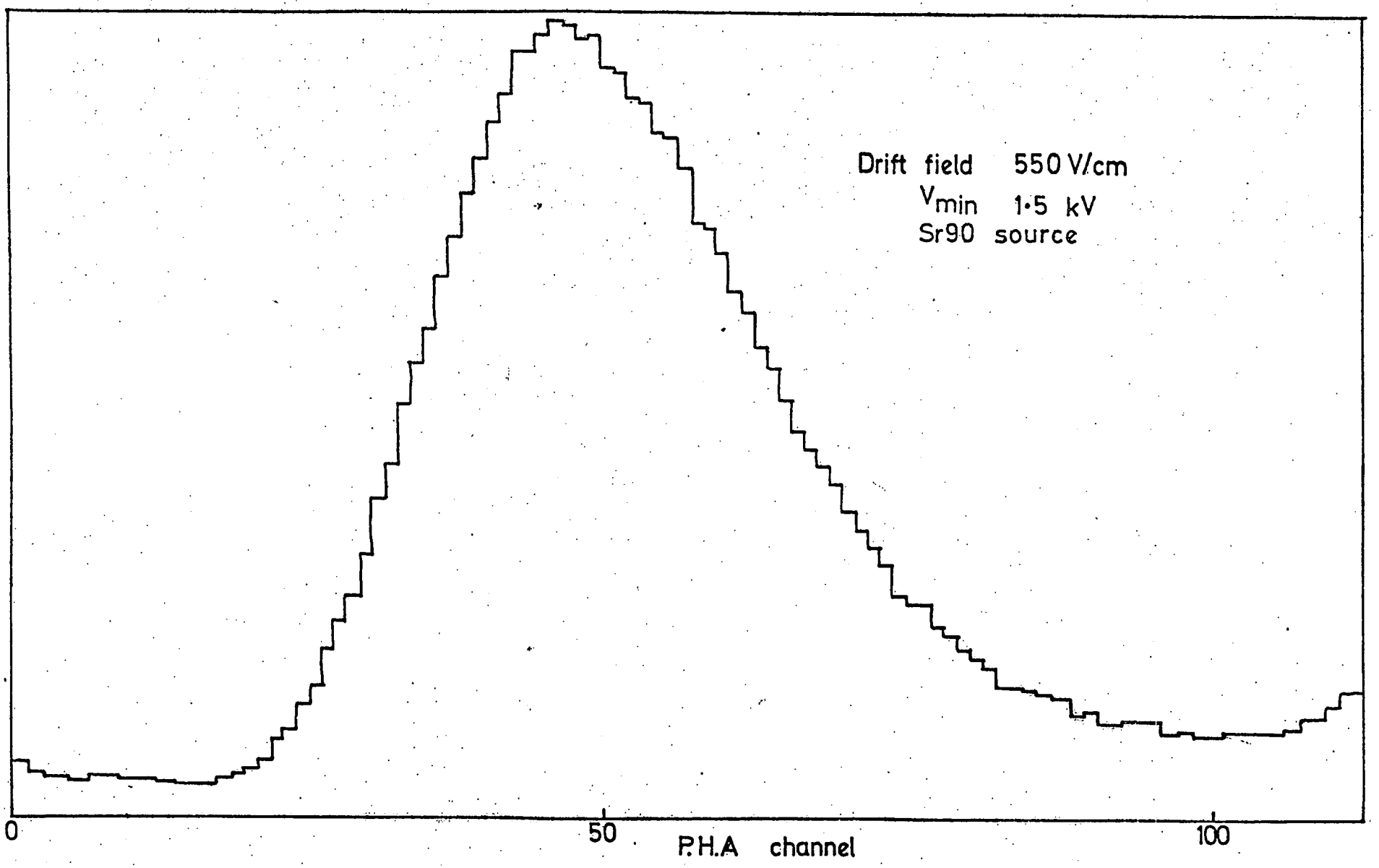

FIG 3.8 Pulse height spectrum for ß particles

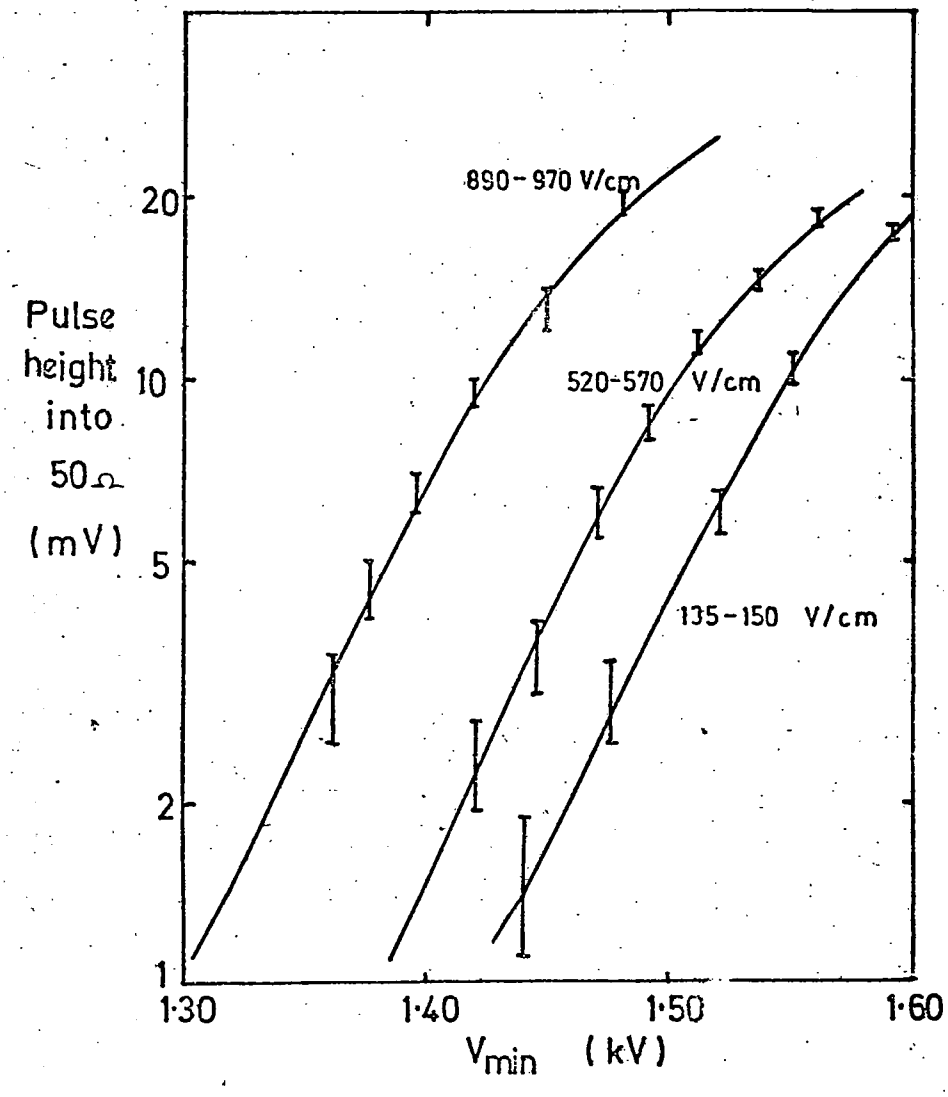

FIG 3.9 Pulse height versus operating voltage for various drift fields

Thus figure 3.10 shows the equipotential lines in the region of the sense wire for three applied drift fields and the same V_{min} of 1.5 kV. The data is calculated by the method mentioned in chapter 2, and small distortions around the cathode wires are ignored. From these diagrams it can be seen that although V_{min} fixes the multiplication field in the z direction, the field experienced by the drift electrons (i.e. in the x direction) is strongly affected by the drift field. To illustrate this figure 3.11 shows the value of the electric potential at a point 3 mm from the sense wire in the x plane. Thus the drifting electrons experience a multiplication field which rises approximately linearly with drift field and hence the variation of pulse height with drift field for constant V_{min} (as shown in figure 3.12 for V_{min} = 1.42 kV) is similar to the pulse height against V_{min} relationship of figure 3.9, with 600 V/cm change in drift field has the same effect on the pulse height as a 100 V change in V_{min}.

Note that from figure 3.11, a drift field of about 700 V/cm produces the most symmetrical multiplication field for a V_{min} of 1.5 kV, i.e. the closest approximation to cylindrical chamber conditions.

3.2.2 Variation with drift distance.

It was noticed during the tests described above that the pulse heights from the chamber varied with the position of the source above the chamber. To study this effect, the collimated source was moved across the chamber in measured steps and the resulting pulse heights recorded, after amplification, on a P.H.A. The amplifier used for these and all subsequent tests (unless specified) was designed at C.E.R.N. by H. Verweij, having an input impedance of 20Ω and a gain of 10 mV/μA (or X500).

The effect of this amplifier can be seen in figure 3.13 which shows some typical output pulse after amplification and which can be

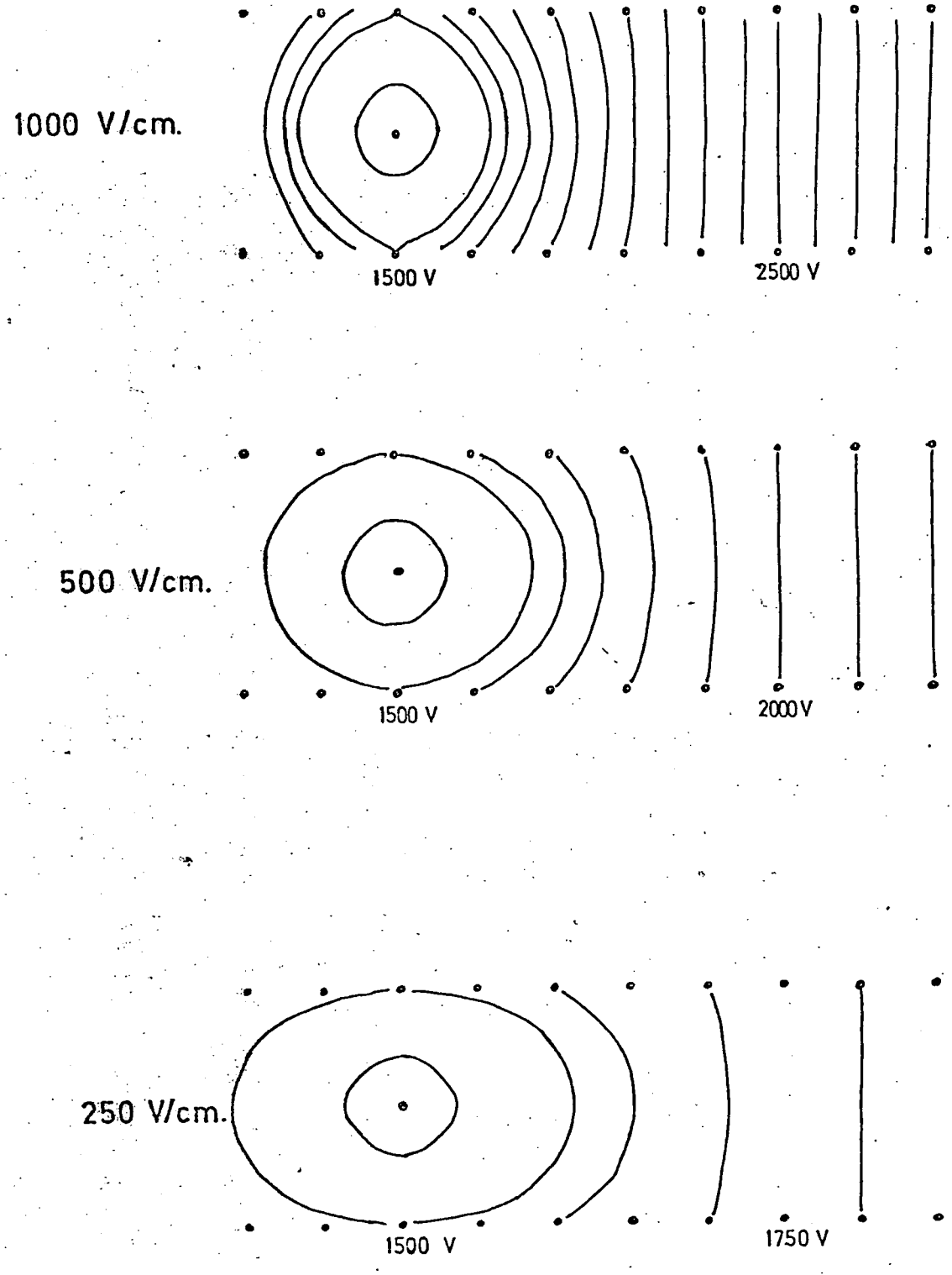

FIG 3.10 Simplified plot of equipotential lines in a chamber for various drift fields and constant Vmin

Lines at 1000V and at 100V intervals above 1500V

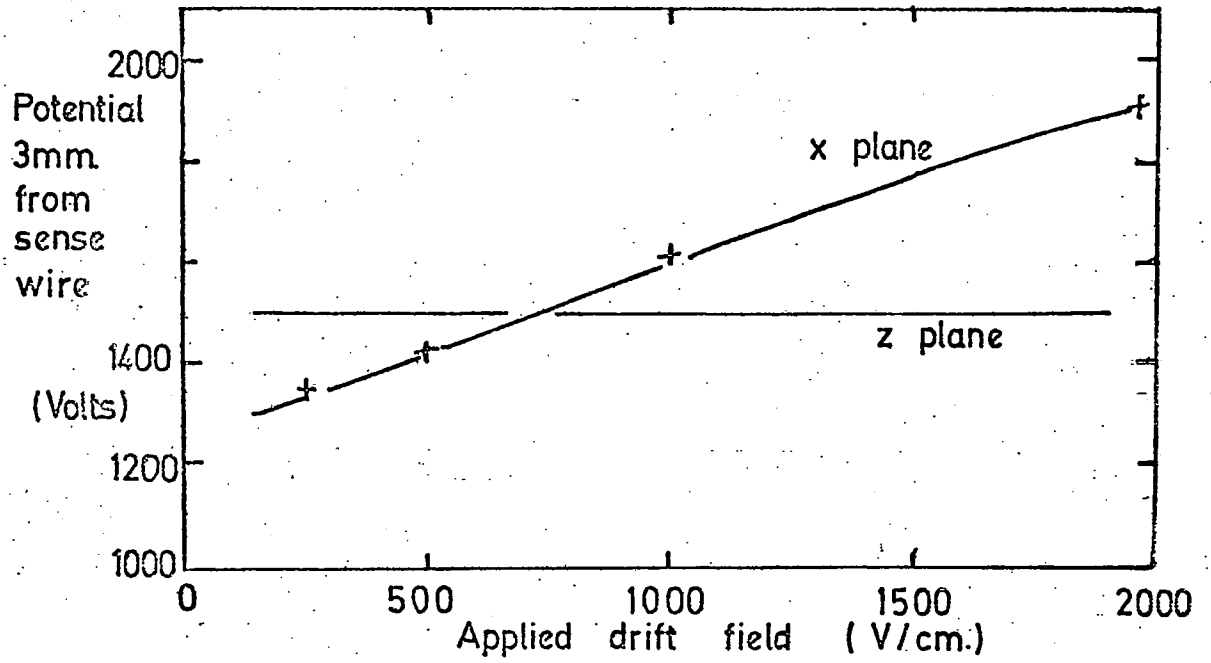

FIG 3.11 Potential versus drift field for an operating voltage of 1·5 kV

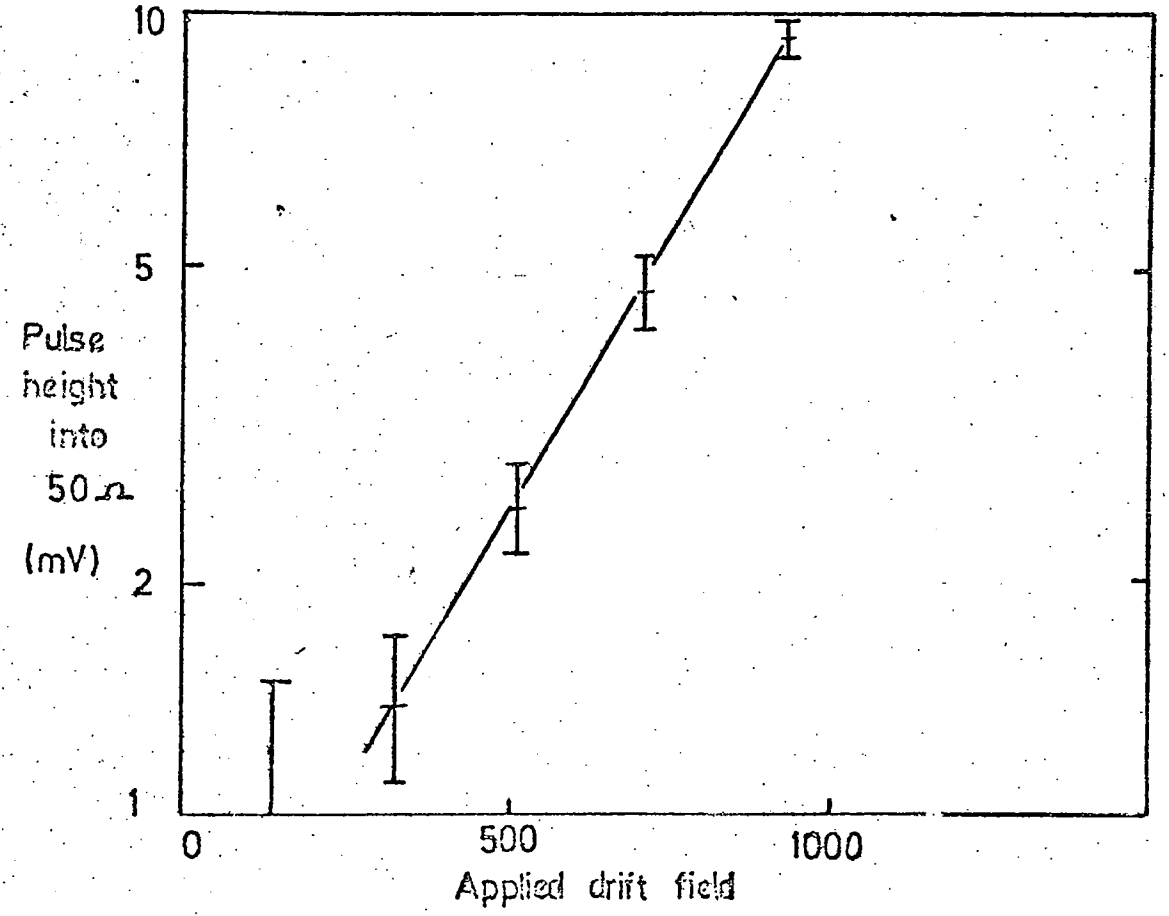

FIG 3·12 Pulse height versus drift field for a constant operating voltage of 1·42 kV

compared with figure 3.7. To clarify the rising edges of the pulses, the amplified pulses for the same conditions were displayed on the oscilloscope via a linear gate which was opened with a pulse from the scintillator (figure 3.6). The pulses were then displayed coincidently as shown in figure 3.14. (Note that the gate attenuates the pulses and also saturates at less than 1 volt).

The variation in pulse height with drift distance is shown in figure 3.15 for a drift field of 950 V/cm and V_{min} = 1.41 kV. Figure 3.16 shows the same results using 5.9 KeV X rays from a collimated iron 55 source. There is good agreement with similar results which have since been published from C.E.R.N. (14) for chambers containing argon-isobutane- methylal (67.2% - 30.3% - 2.5%) as shown in figures 3.17 and 3.18 for electrons and X rays respectively.

The reduction in pulse height close to the sense wire can be explained as being due to some of the primary ionisation occurring within the multiplication field so that the resulting electrons do not experience the maximum multiplication process. The effect would be significant at distances for which there was a reasonable probability of secondary ionisation taking place, (i.e. even for very low values of α), possibly up to 1 mm from the wire, and its extent would increase with V_{min}. Imperfect collimation of the sources would also increase the apparent extent of the effect.

The rise in pulse height across the full width of the cell (particularly noticeable for X rays) is however more difficult to explain. Probably the most satisfactory explanation involves the assumption that under conditions of high gain, avalanches originating from several adjacent electrons, will interact and result in reduced multiplication. Charpak et al (14), have assumed that interaction between avalanches occurs when their separation is less than 220 μm, which is greater than the separation of charges produced by the conversion of a 5.9 KeV photon (15).

Figure 3.13. - Amplified pulses from drift chamber for

V_{min} = 1.51 kV

Vertical scale 500 mV/div

Horizontal scale 20 nsec/div

Figure 3.14. - The same pulses displayed coincidently (with some attenuation and saturation)

Vertical scale 200 mV/div

Horizontal scale 20 nsec/div

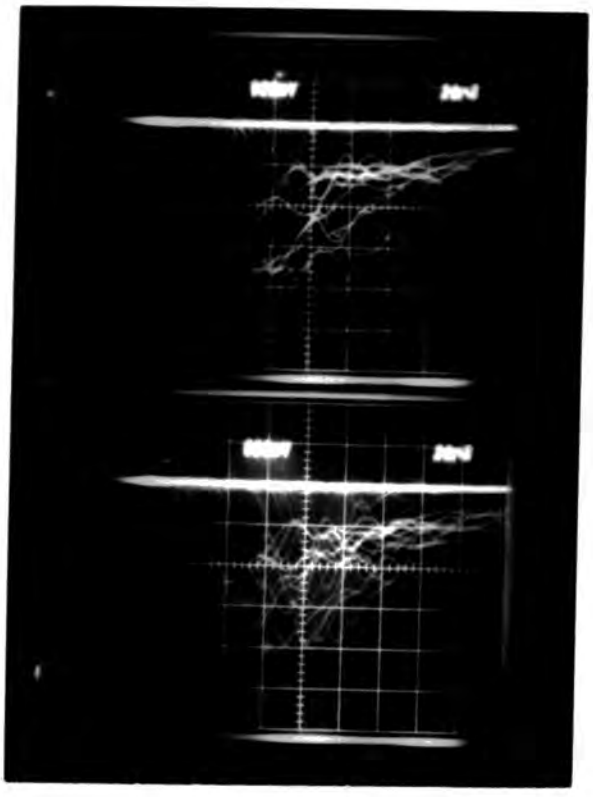


200mV 20nS
200mV 20nS

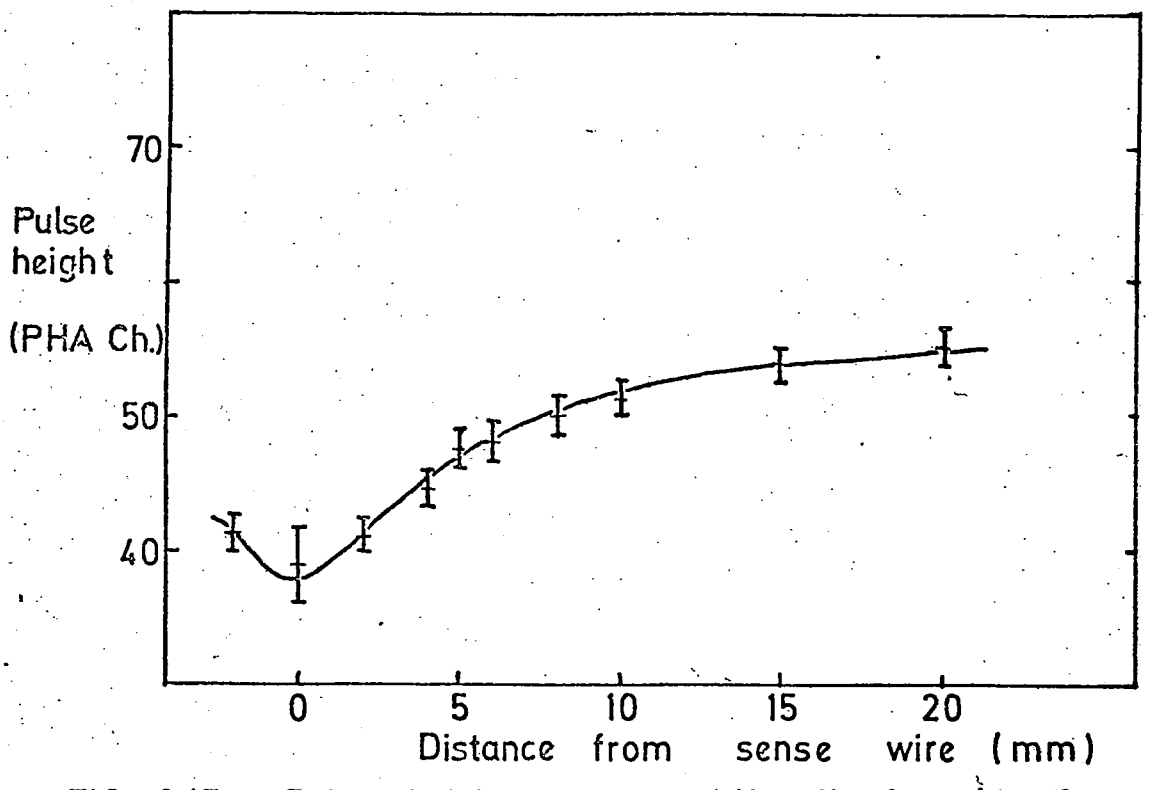

FIG 3.15 Pulse height versus drift distance (for ß particles)

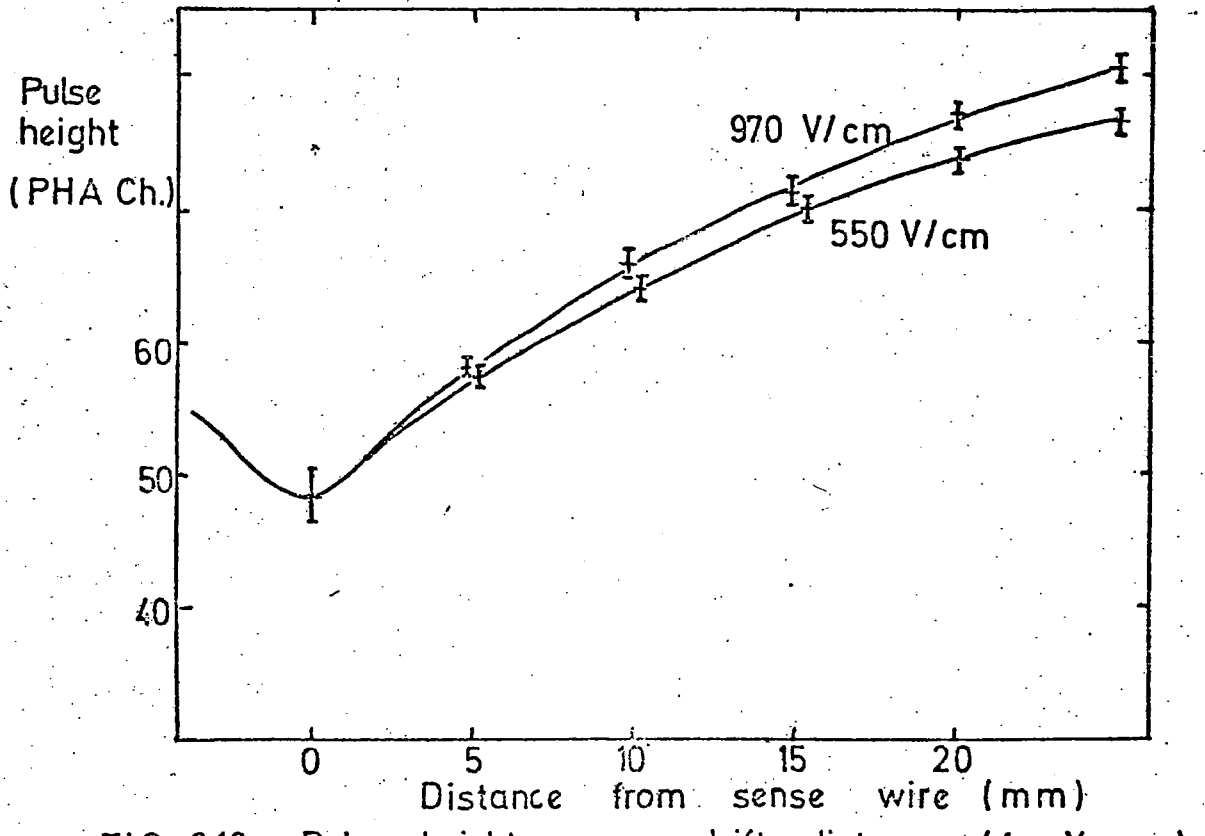

FIG 3.16 Pulse height versus drift distance (for X rays)

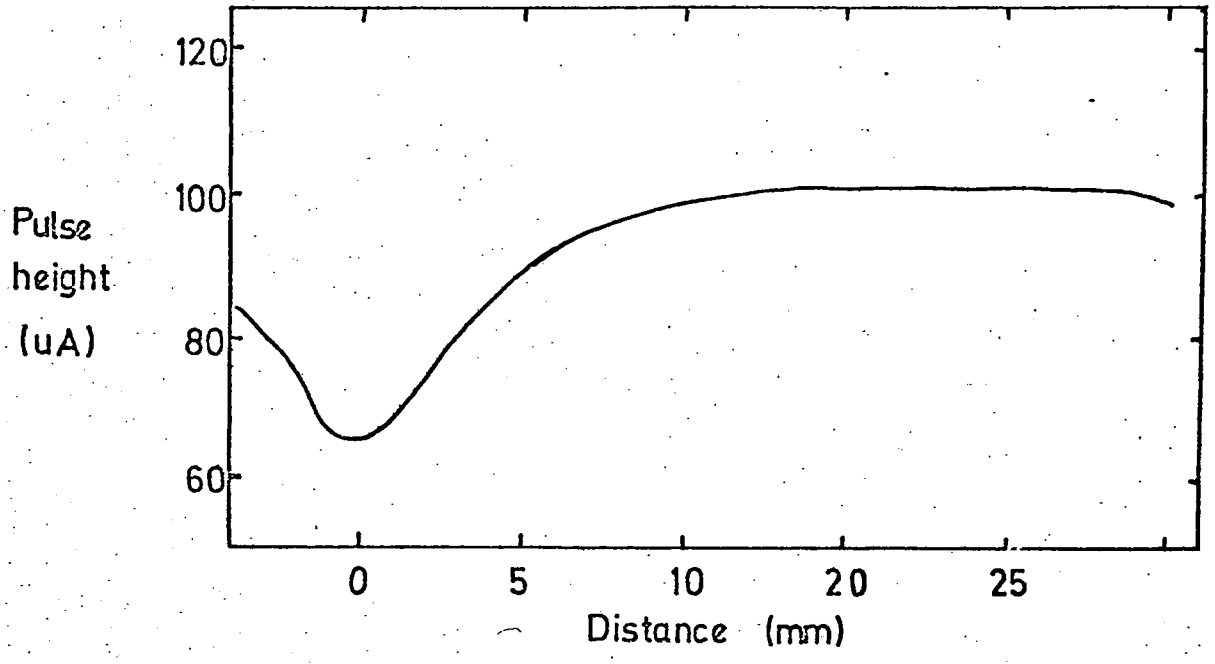

FIG 3.17 Pulse height versus drift distance for a minimum ionising beam (Charpak et al)

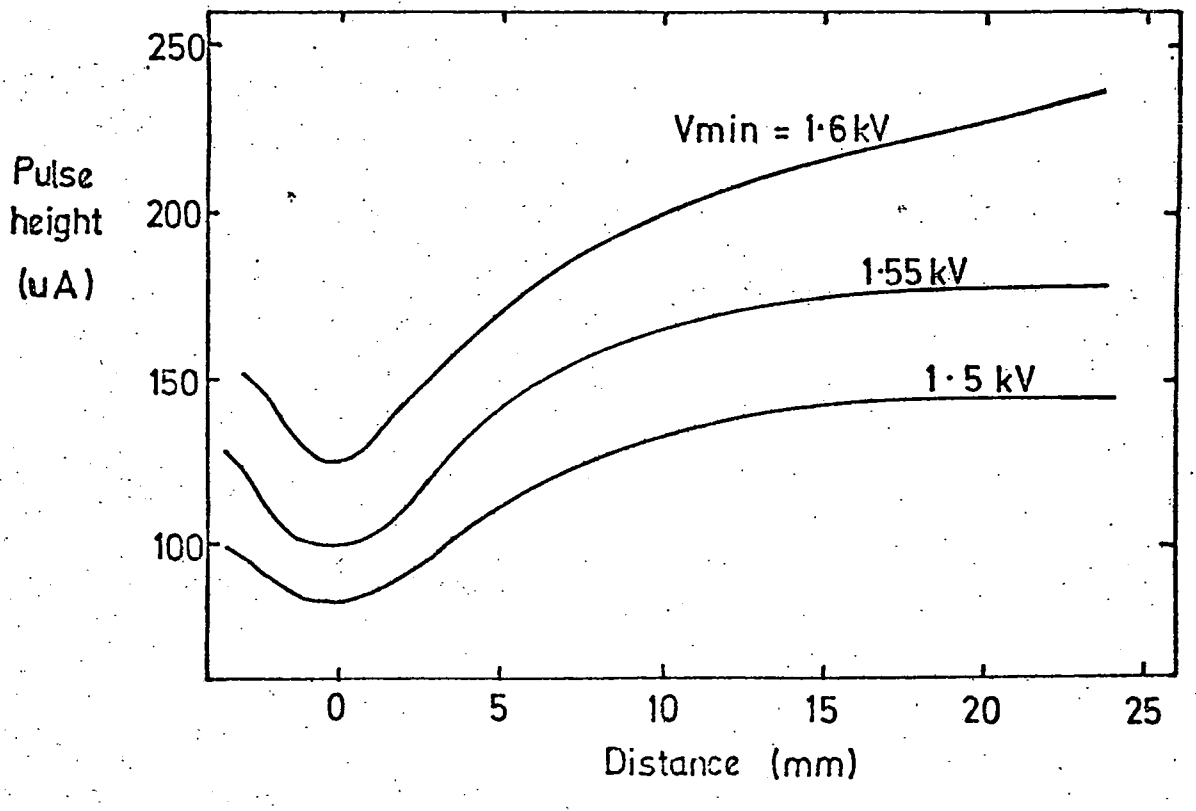

FIG 3.18 Pulse height versus drift distance for X rays (Charpak et al)

Thus electrons produced by an X ray incident near to the sense wire will cause avalanches which interact considerably, and give correspondingly low pulse heights. The electrons from the same event at a greater distance from the sense wire however, will have time to diffuse as they drift, and so the resulting avalanches will not interact to the same extent.

Such an explanation would also account for the rise in pulse height with distance being more pronounced for larger values of operating voltage (by increasing the extent of avalanche interaction) as shown in figure 3.18.

For β rays or high energy particles where the dispersion of the primary electrons is larger than for an X ray pulse, the effect would not be expected to be as significant. In such an event however, the time spread of avalanches from a single track may cause pulse height variation, especially when differentiating type circuits are used to observe the pulses. That is there will be a greater time difference between the arrival at the sense wire of electrons from the centre, and extremities, of a track near the sense wire than for a track further away, for purely geometrical reasons. Thus although the total charge movement may be the same, the initial rise of the pulse will be slower, resulting in lower pulse heights after differentiation.

3.3.3 Variation with particle energy

Although in principle the pulse height from a drift chamber should be proportional to the energy deposited in the chamber by an incident particle, the results of the preceding section indicate that this is not strictly true. In particular, proportionality breaks down between X ray photons and other more energetic particles because of the increased avalanche interaction for X ray events. Thus the difference in energy

deposited by the β rays (~2 KeV for our chambers) and 5.9 KeV X rays is not reflected in the respective pulse heights obtained during these tests.

Proportionality is maintained however for similar events. Figure 3.19 is the pulse height spectrum (obtained with a P.H.A.) for the chamber irradiated with an iron 55 source, showing the main peak at 5.9 KeV and the smaller 'escape' peak due to only one of the two photoelectrons created by the photon conversion ionising within the chamber. The energy resolution as shown is of course affected by the variation in pulse height with distance and the divergence of the radiation from the source. The energy proportionality was further investigated by irradiating the chamber with several different energy X rays and recording the resulting peaks of the pulse height spectrums. The results of these tests are presented in figure 3.20, which shows good linear agreement between energy and pulse height.

3.4 Efficiency Measurements

There are two reasons why a particle passing through a drift chamber may not be detected. Either it does not produce ionisation in the chamber or the output pulse produced does not trigger the detecting electronics. The probability of a high energy charged particle not causing ionisation in our chambers has been shown (section 3.2.1) to be insignificant, although this does not apply to X ray or γ ray detection, where the probability of an interaction in the chamber depends on photon energy, chamber gas, and chamber dimensions. As an example, figure 3.21 shows the probability of a photon interacting in a 6 mm chamber filled with a mainly argon mixture, for varying photon energy (16). This has neglected the transparency of the chamber windows, which will reduce the detection efficiency for lower photon energies.

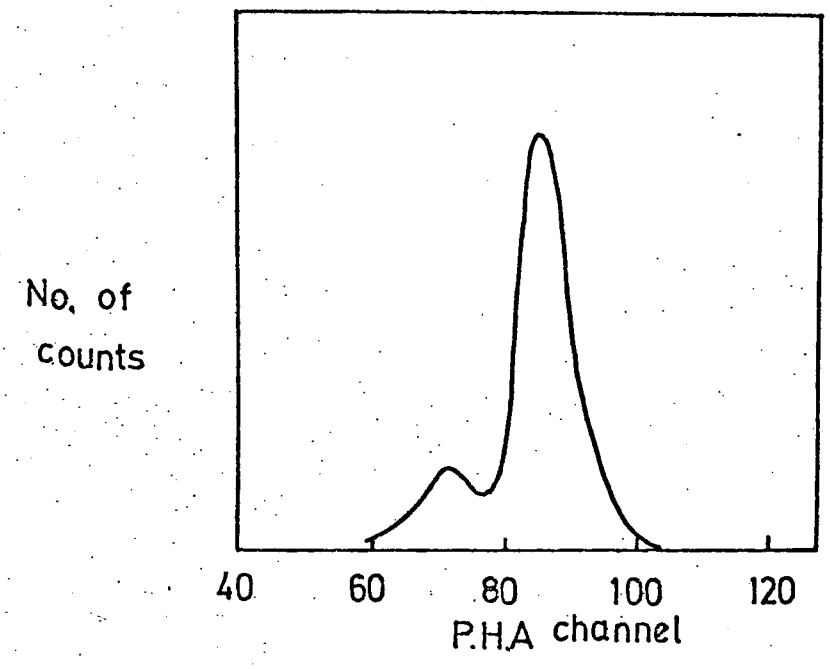

FIG 3.19 Pulse height spectrum for Iron 55 X ray source

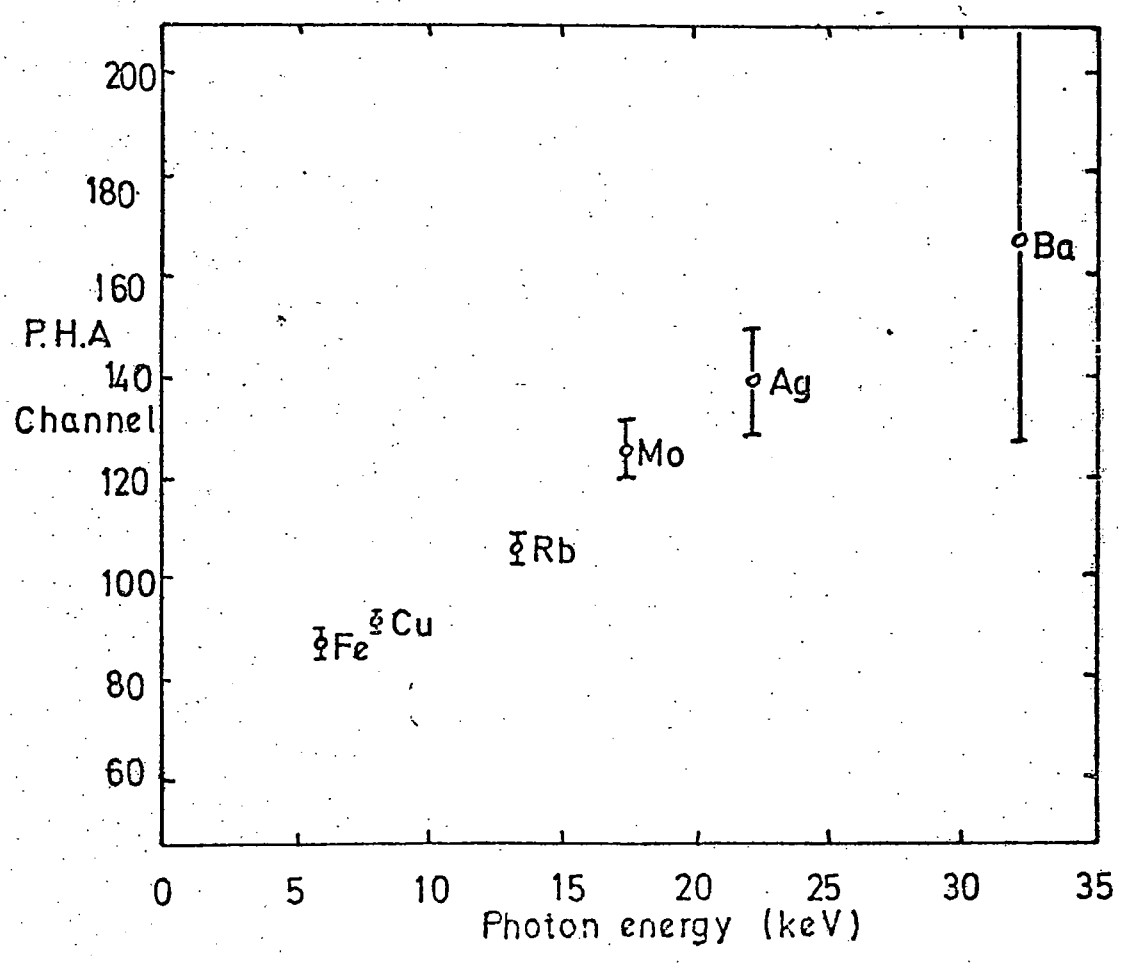

FIG 3.20 Pulse height versus energy for X ray photons

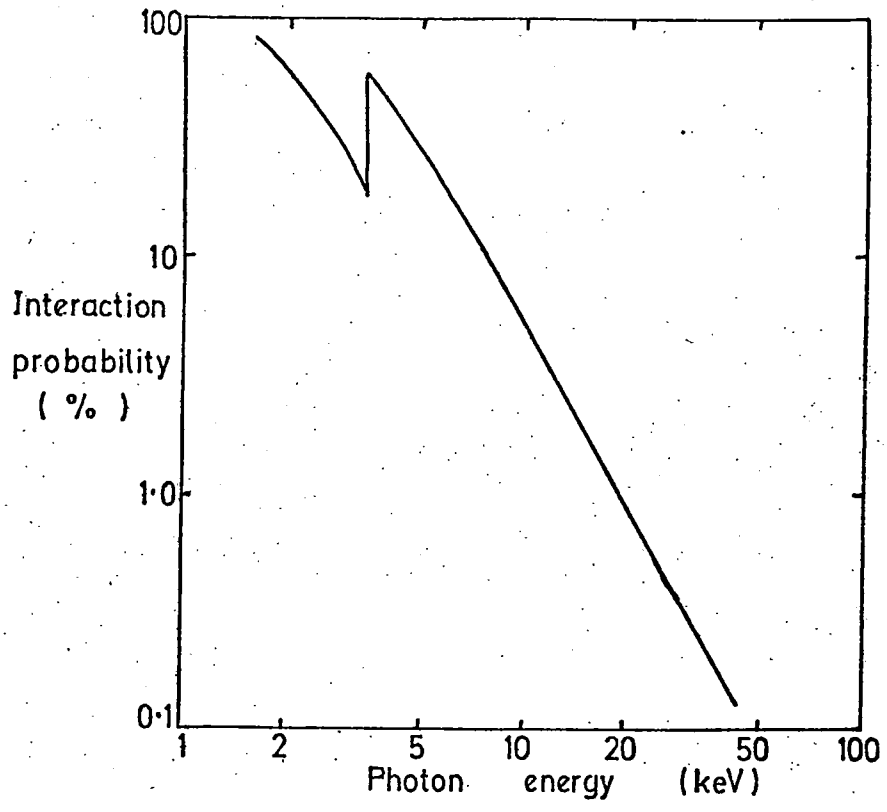

FIG 3.21 Probability of X ray photon interacting in 6mm argon

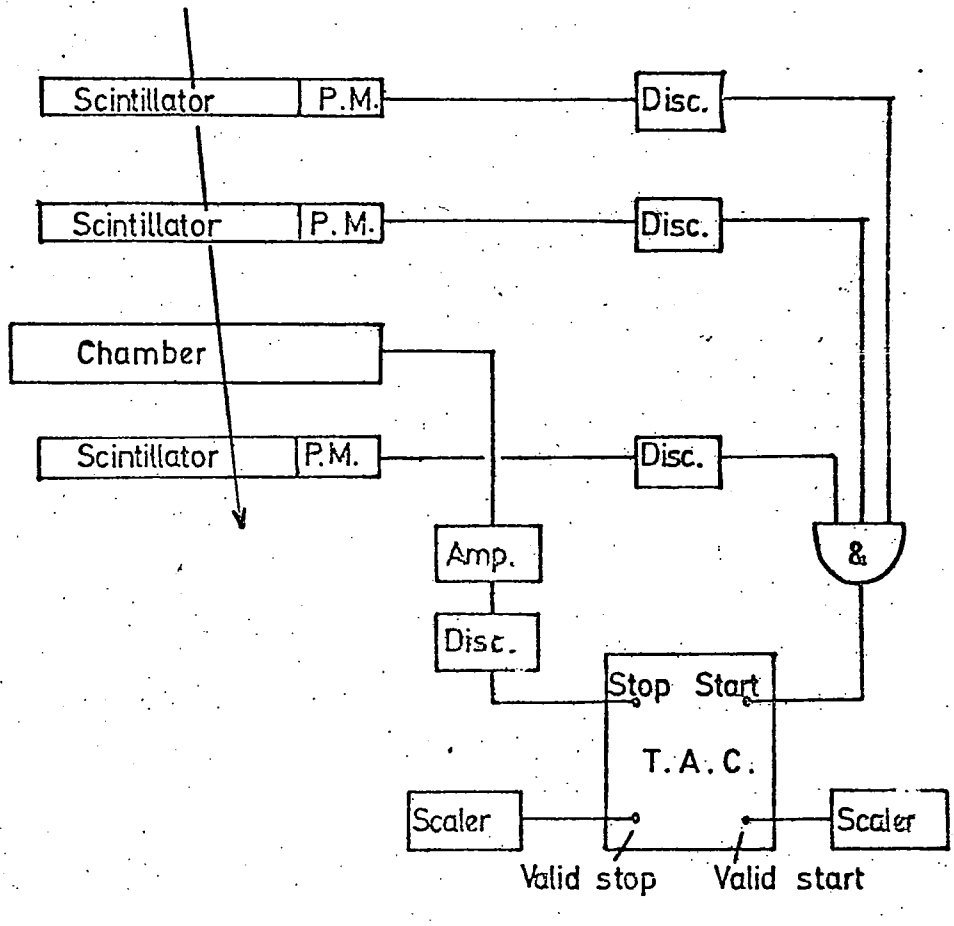

FIG 3.22 System for investigating chamber efficiency using cosmic rays

The efficiency with respect to high energy particles was investigated using cosmic rays and the system shown in figure 3.22. The T.A.C. module was found to be useful, for measuring efficiencies, as a start signal generates a 'valid start' output and then disables the start input for a time set by an external control. This time was set to be greater than the maximum expected drift time, and if a stop pulse arrives during this time a 'valid stop' output is generated. If no stop pulse arrives there is no 'valid stop' signal and the start input is enabled again. Thus the ratio of valid stops to valid starts gives the efficiency of the chamber.

The results from this system are presented in figure 3.23 showing the variation in efficiency with operating voltage for the different discrimination levels and a constant drift field of 330 V/cm. The dependence of efficiency on pulse height is demonstrated by the increased efficiency (below saturation) as the discrimination level is lowered. Unfortunately this level cannot be lowered indefinitely because of electrical interference problems and the practical minimum was found to vary between 100 mV and 400 mV depending on the experimental environment. Even at high discrimination levels, maximum efficiency is still attainable merely by operating at slightly higher voltages.

The fact that the efficiency does not saturate at 100% is attributed to three possible factors.

i) The efficiency is measured over the whole chamber, that is including the region around the sense wire, where it is known that pulse heights are reduced. To demonstrate the effect of this on efficiency, figure 3.24 shows the variation of efficiency with position around the sense wire. This data was obtained from tests on a multi-cell chamber (described in section 5.2) using 600 MeV positrons in the test beam facility at the Daresbury Laboratory during the

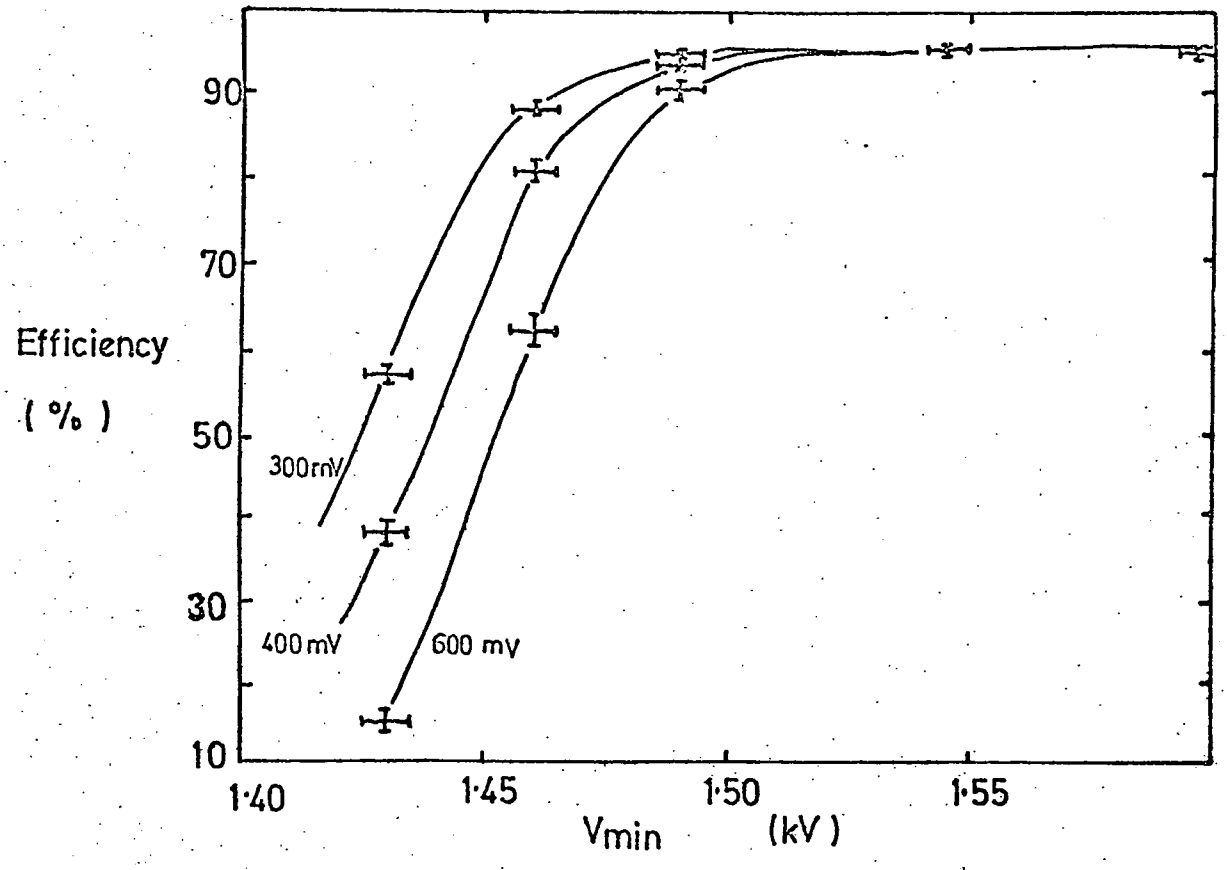

FIG 3.23 Efficiency versus operating voltage for various discrimination levels

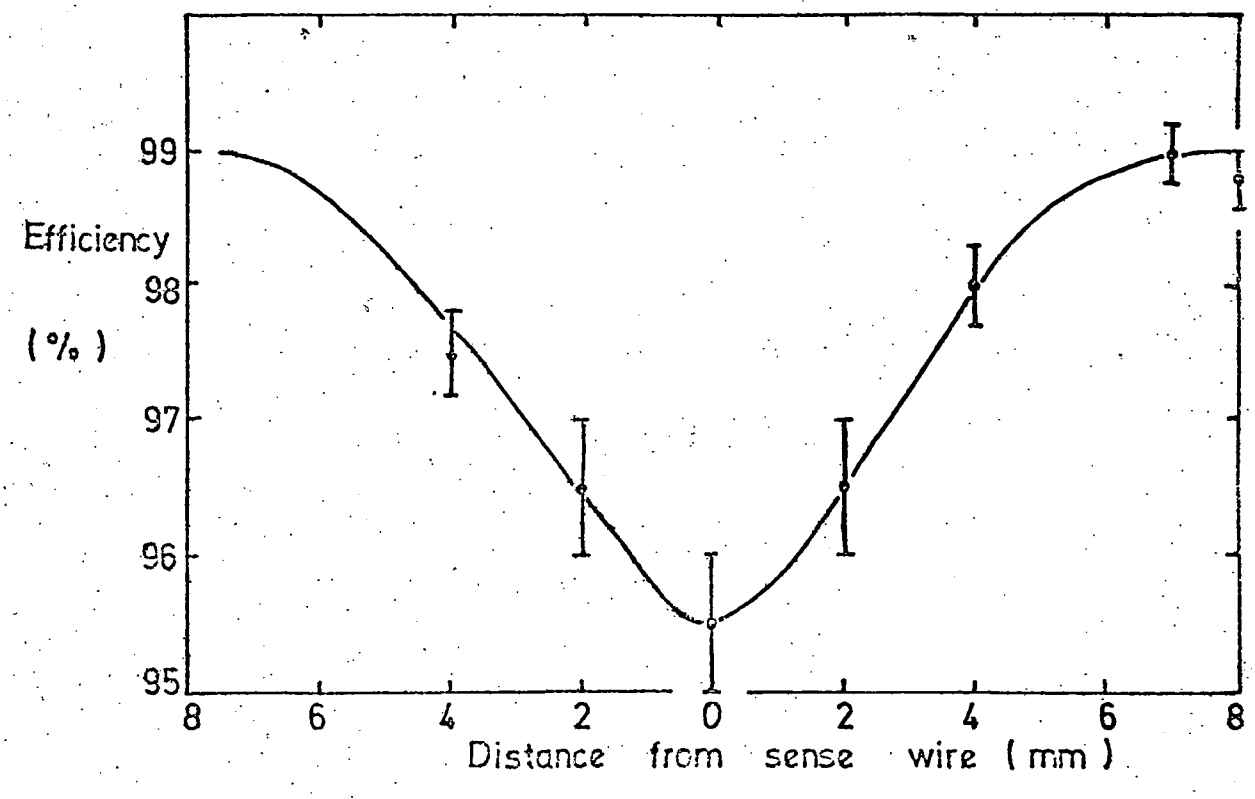

FIG 3·24 Variation of efficiency near sense wire

testing of prototype experimental chambers.

ii) The experimental system itself may not be stringent enough to allow 100% efficiencies to be measured (due possibly to non-vertical cosmic ray showers). For example in the system shown in figure 3.22, removal of one of the coincidence scintillators reduces the maximum measurable efficiency to 83%. Referring to the Daresbury tests mentioned above, detection efficiencies of above 99% were measured using a coincidence system comprising five scintillation counters (17).

iii) There may be an intrinsic loss of efficiency due to the statistical nature of the initial energy loss mechanism, i.e. abnormally low number of collisions producing a reduced number of ionisation electrons and hence a lower pulse height which may not exceed the discrimination level.

The dependence of efficiency on pulse height is further illustrated in figures 3.25 and 3.26. The former shows the variation in efficiency for three drift fields and constant discrimination level (400 mV). The operating voltage necessary to maintain a 50% efficiency can then be plotted against drift field (figure 3.26, full line). The crosses on this figure show the operating voltage required to maintain a constant pulse height for various drift fields and good correlation can be seen.

3.5 Conclusion

These tests have shown that the gas chosen for our drift chambers has the requisite properties for producing observable pulses after the passage of an ionising particle. It is also apparent that using the output pulse height to provide information about the incident particle should be attempted with caution as this pulse height depends on many factors. It is not only related to the particle energy (this dependence

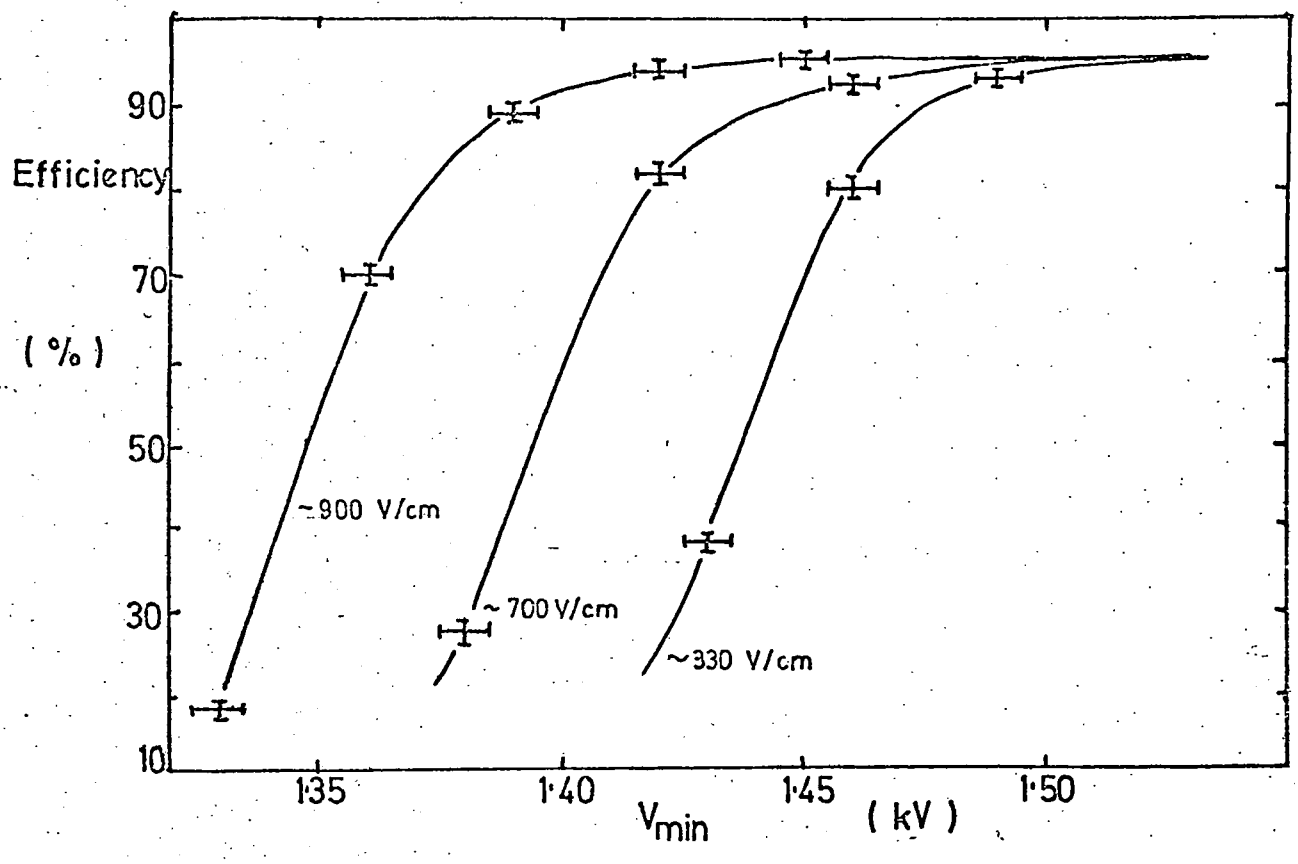

FIG 3.25 Efficiency versus operating voltage for various drift fields.

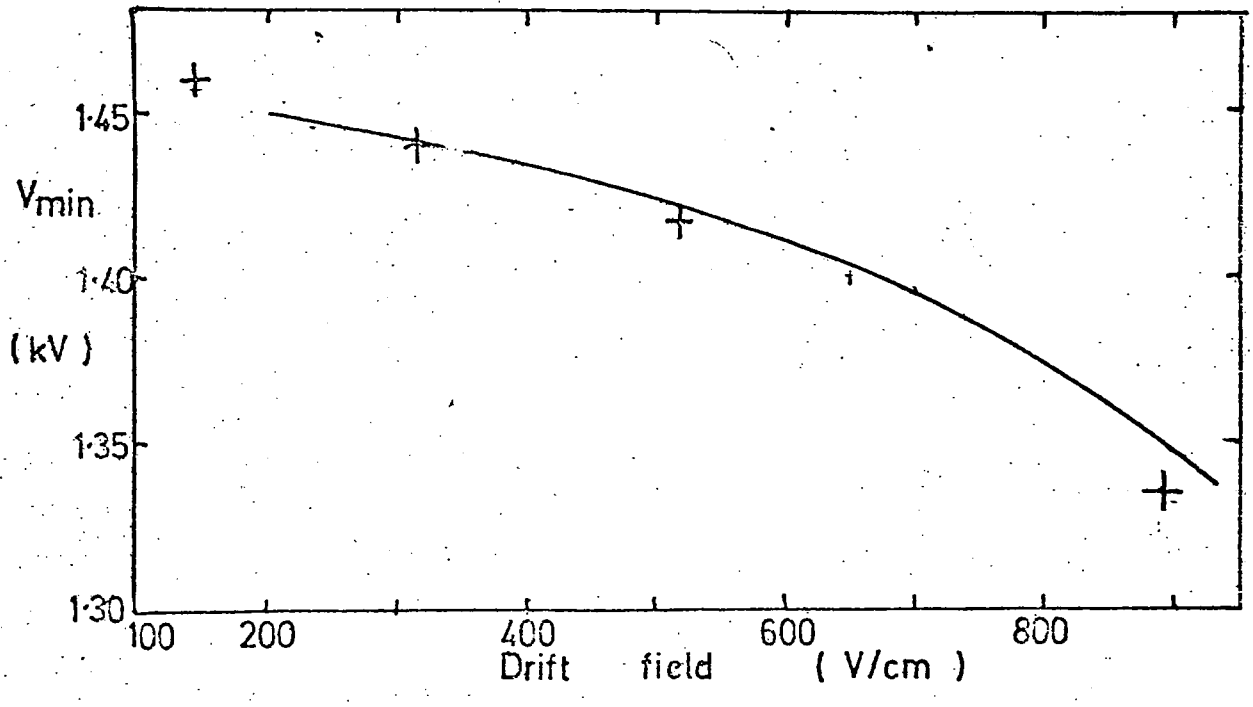

FIG 3.26 Conditions to maintain constant efficiency (line) and pulse height (crosses)

being statistical) but also to operating voltage, applied drift field, distance of particle track from the sense wire, and angle of track to the sense wire plane (see section 4.5).

These variations of pulse height with various parameters are however, adequately explained and appear to be in good agreement with results from workers using other mixtures. From our tests using another popular gas mixture, argon + 30% isobutane, during drift velocity investigations, it was found that this mixture operated successfully at operating voltages about 20% higher than for argon + 10% methane, and was able to withstand higher voltage gradients without breaking down.

CHAPTER 3 - References

1. For example D.H. Wilkinson, 'Ionisation Chambers and Counters,' Cambridge (1950)
or
S.A. Korff, 'Electron and Nuclear Counters ..... Theory and Use', Van Nostrand, (1955)

2. B. Rossi, 'High Energy Particles' Prentiss-Hall New Jersey (1965)

3. H.A. Bethe and J. Askin 'Experimental Nuclear Physics' Ed. E. Segre J. Wiley, New York, (1953)

4. R.M. Sternheimer. Phys. Rev. 145 (1966) 247.

5. Z. Dimcowski, C.E.R.N. N.P. Divison Internal Report 70-30. (1970)

6. G. Charpak, D. Rahm, and H. Steiner, Nuc. Intr. Meth. 80(1970) 13

7. V. Palladino and B. Sadoulet, Lawrence Berkeley Laboratory Internal Report LBL 3013 (April 1974)

8. W.P. Jesse and J. Sadauskis, Phys. Rev. 97 (1955) 1668

9. L. Landau, J. Phys. USSR. 4, 8 (1944) 201

10. O. Blunck and S. Leisegang, Z. Physik 128 (1950) 500

11. P.V. Ramana Murthy and G.D. Deemster, Nuc. Instr. Meth. 56 (1967) 93

12. M.W. Charles, J. Phys. E. Sci. Instr. 5 (1972) 95

13. B. Makowski and B. Sadoulet, Nuc.Inst.Meth. 3 (1973) 189.

14. A. Breskin, G. Charpak, F. Sauli, M. Atkinson and G. Schultz, Nuc.Inst.Meth. 124 (1974) 189.

15. J. Hough, Nuc.Inst.Meth. 105 (1972) 323.

16. R. Browell, Durham University Internal Report, NI-72-15 (1972).

17. J. M. Breare, R. Browell and K. A. Short, Durham University Internal Report NI-74-5 (1974).

CHAPTER FOUR

MEASUREMENT OF ELECTRON DRIFT VELOCITY

4.1 Introduction

Since in a drift chamber it is the drift times of electrons which are directly measured to give the location of the initial ionisation, it is obviously of prime importance to know accurately the velocity at which the electrons drift in the gas used in the chamber. Furthermore this drift velocity w, must be known for any of the conditions which may exist inside a practical chamber, with particular regard to variations in electric field. To obtain 100 μm accuracy over drift distances greater than 1 cm requires that the drift velocity be known to better than 1% over the whole drift length.

Also, to ensure successful operation of drift chambers, a gas must be chosen such that the drift velocity fulfils certain conditions. Two particular properties with respect to drift velocity were considered as basic requirements for our chambers.

i) The magnitude of the velocity must be such that the necessary spatial resolution could be obtained with relatively simple timing systems (analogue or digital) over the drift distances involved.

ii) The drift velocity must be relatively independent of electric field, at least over a certain range of operating conditions, so that the drift time-distance relationship will be linear across the whole chamber, thus avoiding the need for non linear timing systems or complex software. As it has already been shown that the electric field rises sharply in the region of the sense wire, it is of particular importance that the velocity saturates at high fields. It is also an advantage if local variations in the drift field due to constructional defects do not affect the time-distance linearity.

It was with regard to these points that the electron drift velocity in argon + 10% methane was investigated and compared with results for other mixtures.

4.2 Experimental System

Unless specified all the results in this chapter were obtained at Durham using the experimental system shown in figure 4.1. The basic mechanical part of the system consisted of a rigid aluminium frame having three separate horizontal platforms, each adjustable vertically. The top platform supported the drift chamber under test, and the lower platform included a system of secondary collimators positioned above the zero-time scintillation counter.

The source was 2 mCi of strontium 90, emitting β rays up to 2.27 MeV positioned behind two thick steel blocks with a 0.25 mm x 50 mm slit between them, which both collimated the β rays and absorbed many of the gamma rays radiating from the source. Even with this degree of collimation, scattering of the beam was still a problem, so that the chamber was positioned as close as possible to the collimating slit. As a further aid, a secondary collimating slit ($\sim$ 4 mm wide) was located above the scintillation counter in order to reject the more severely scattered particles, although this also had the effect of substantially reducing the good event rate. During the experiments the upper and lower slits were accurately positioned to be in the same vertical plane and their platforms clamped in position.

The centre platform was adjustable along two horizontal runners, movement being controlled by a lockable screw thread attached to the platform and passing through the main frame. The relative position of the platform was measured by means of a scale attached to one of the runners and a vernier attached to the platform, with a resultant accuracy of 0.1 mm.

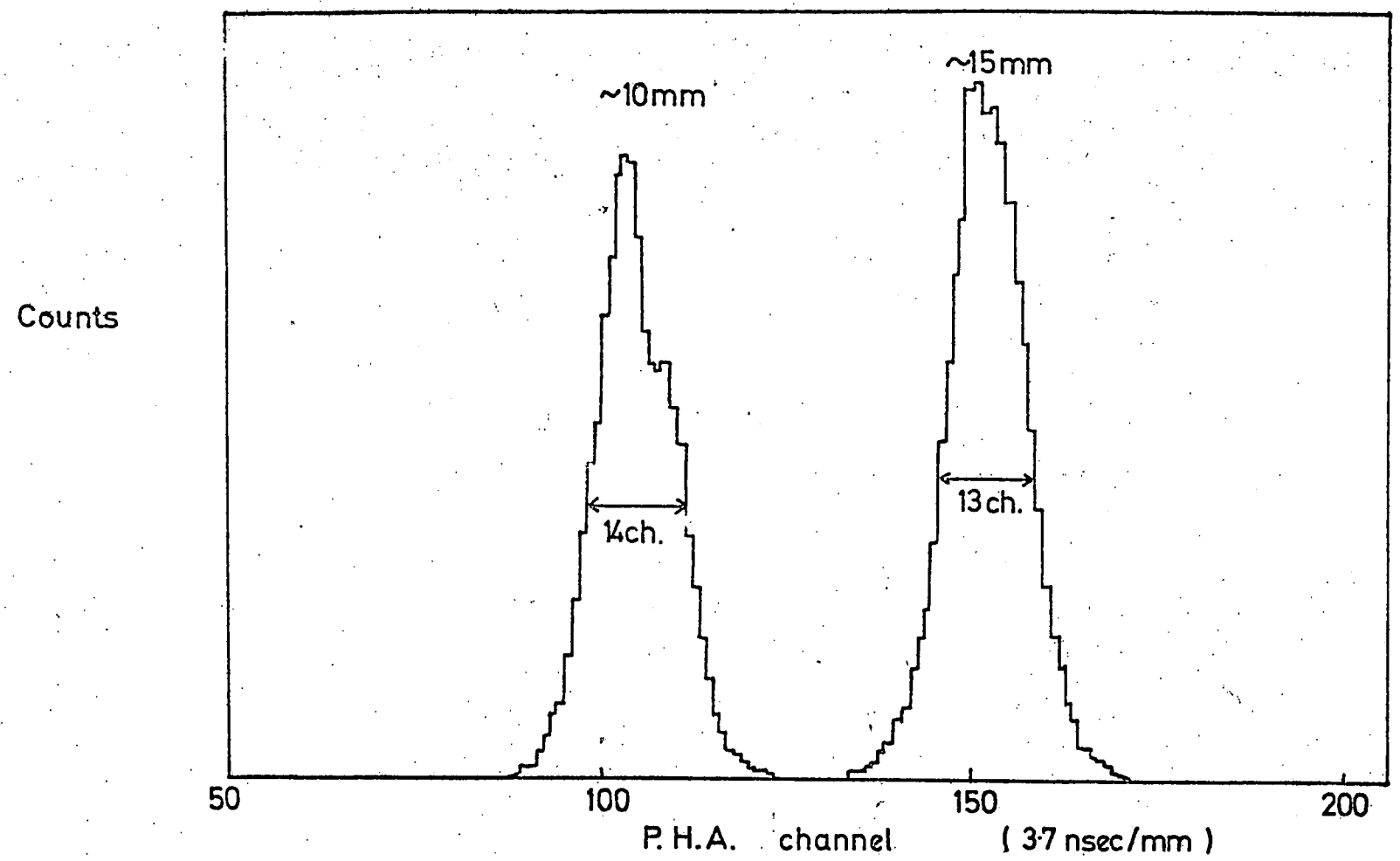

FIG 4.2 Typical drift time distributions

4.3 Result for argon + 10% methane

4.3.1 Drift time-distance relationship

Using the system described above, the variation in electron drift time with position was measured for several different applied drift fields, using our standard gas mixture in the chamber. The results of these tests for four of the drift fields used are shown in figure 4.3 and two main features are apparent. Firstly the time-distance relationship is linear over most of the cell, with the velocity being lower for higher applied fields. Secondly there exists a region near to the sense wire where the drift velocity tends to a uniform value independent of E_a. The relationship in the vicinity of the sense wire is shown in more detail in figure 4.4. Note that most of the experimental points have been omitted from this region for clarity.

Using figures 4.3 and 4.4, the position of the sense wire can be accurately established, and data from both sides of the cell can be combined to draw figure 4.5, an accurate picture of drift time against drift distance.

From a study of the numerically evaluated equipotential plots described in chapter 3 for various applied fields, it is possible to calculate the variation of electric field along the central plane of a chamber. This is shown in figure 4.6 for four values of E_a, and again in figure 4.7 in terms of percentage distortion of the applied field. Referring to these figures we see that the linear sections of figure 4.5 correspond to those regions in the chamber where E is independent of position and equal to E_a. Hence the inverse slopes of these sections of figure 4.5 were plotted against E_a in figure 4.8, to show the variation of drift velocity in a uniform field against the value of that field.

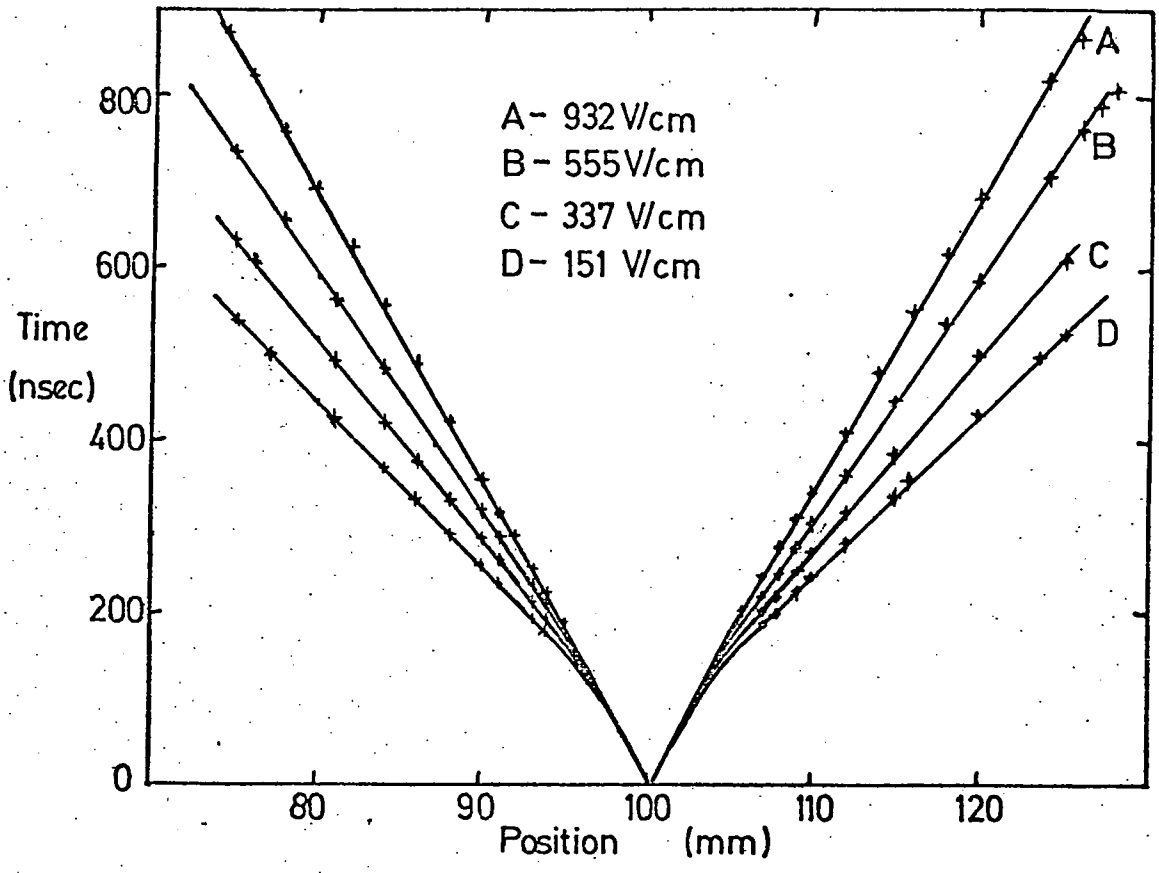

FIG 4.3

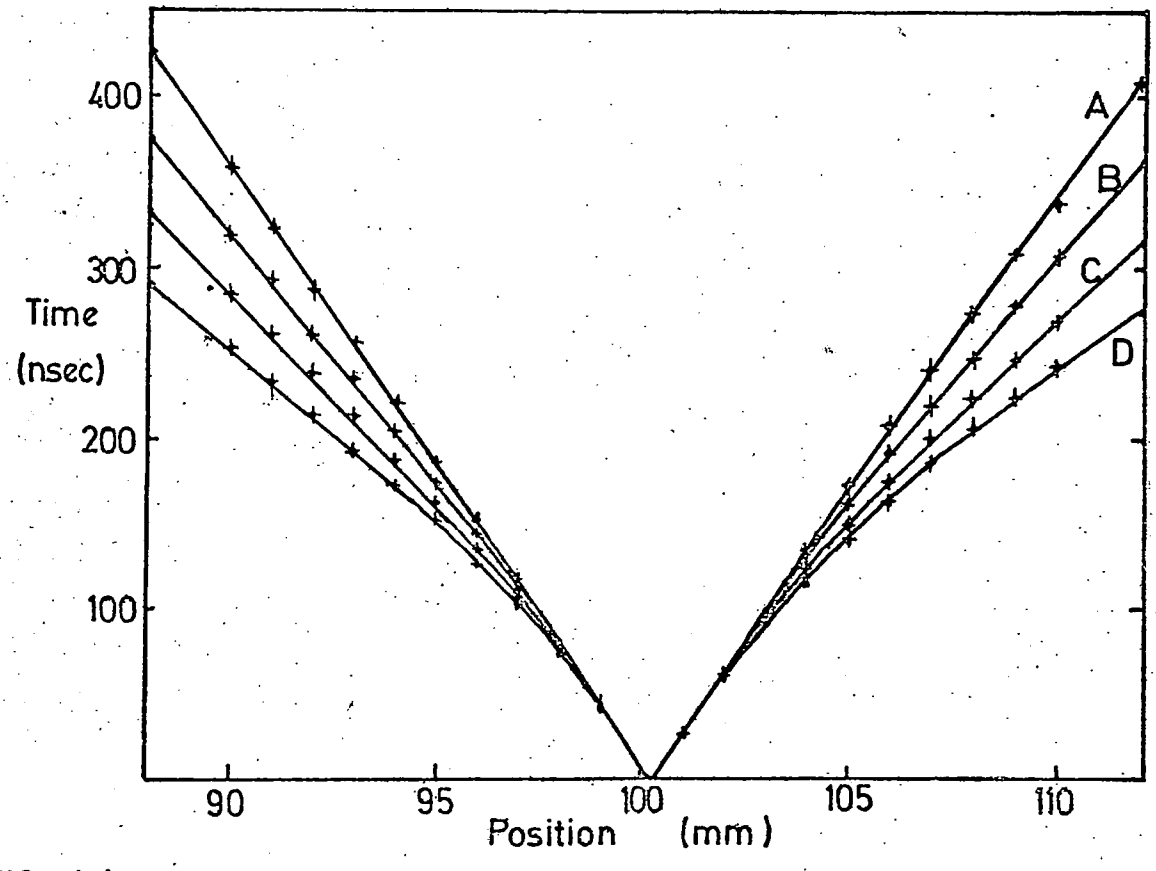

FIG 4.4

FIGS 4.3& 4.4 Drift time versus position of radiation source with respect to the sense wire

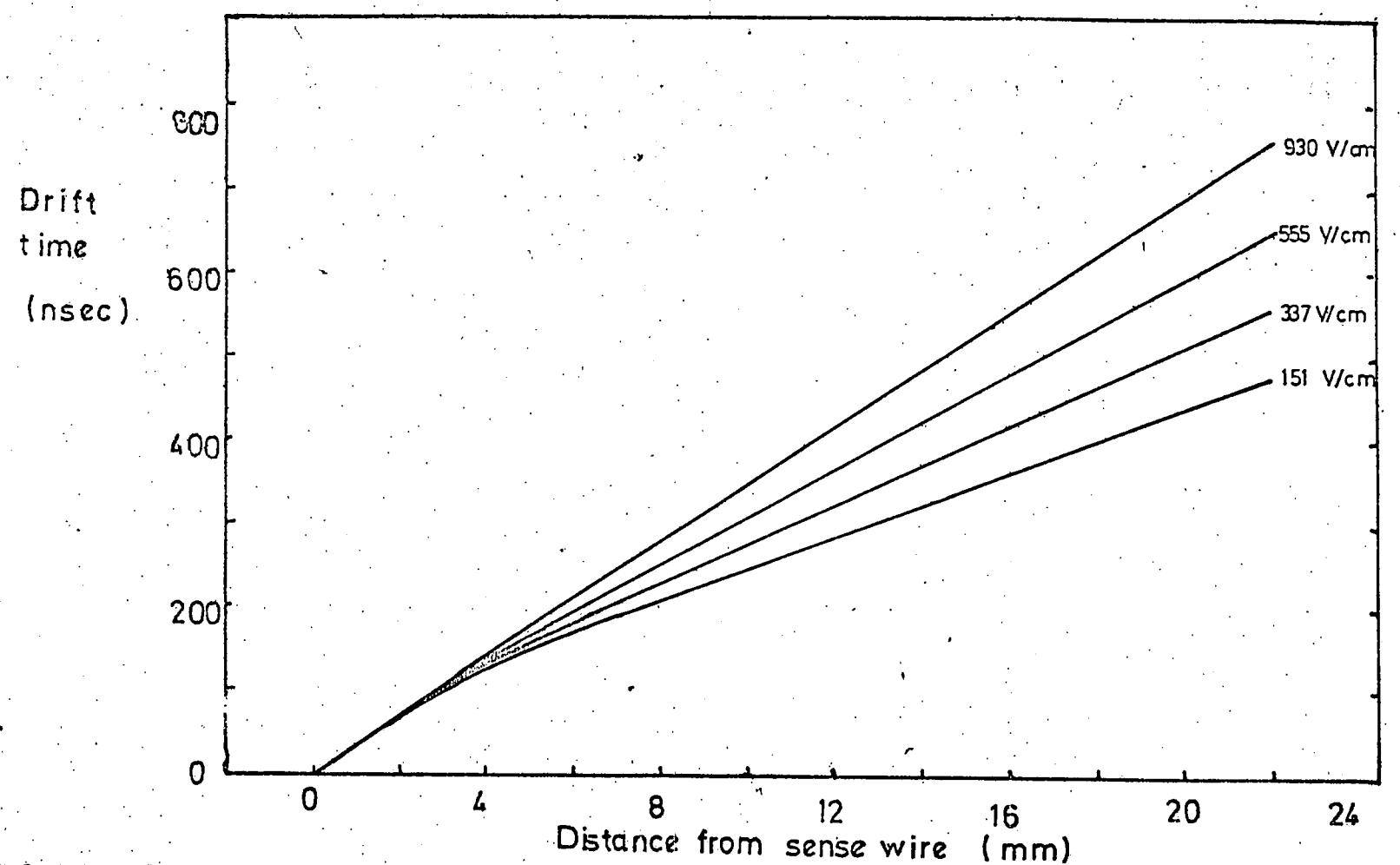

FIG 4.5 Drift time versus drift distance for various applied fields

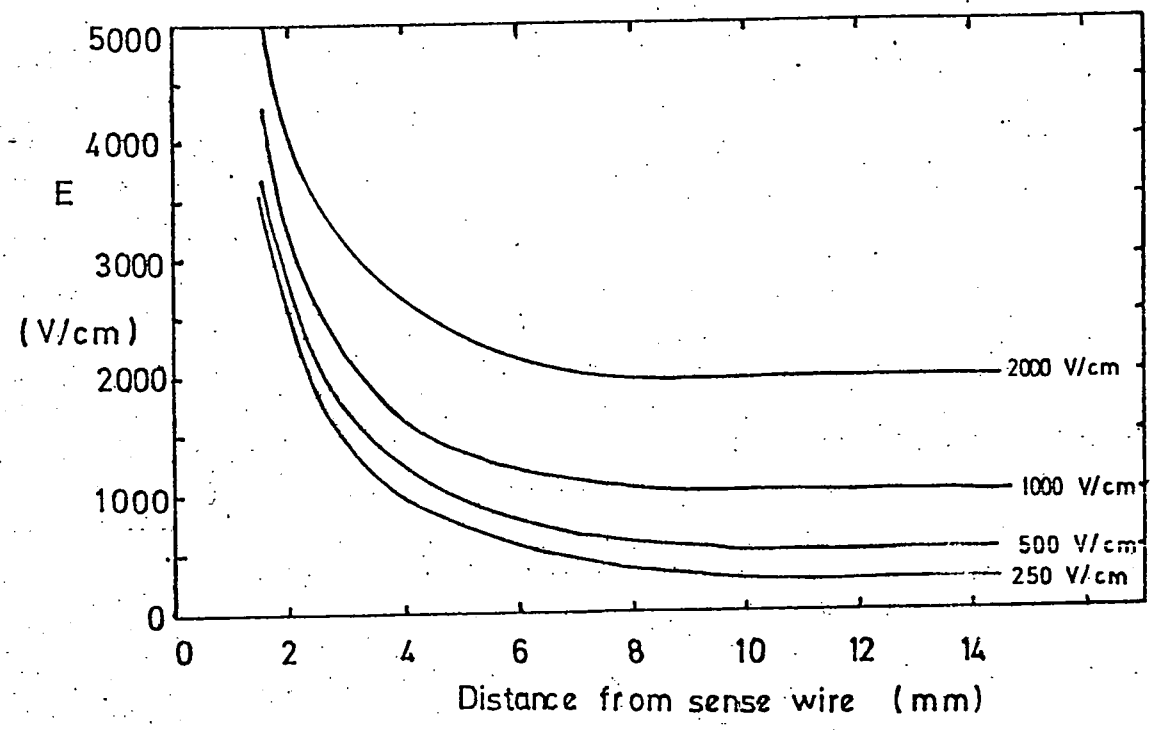

FIG 4.6 Electric field along central plane for various applied fields

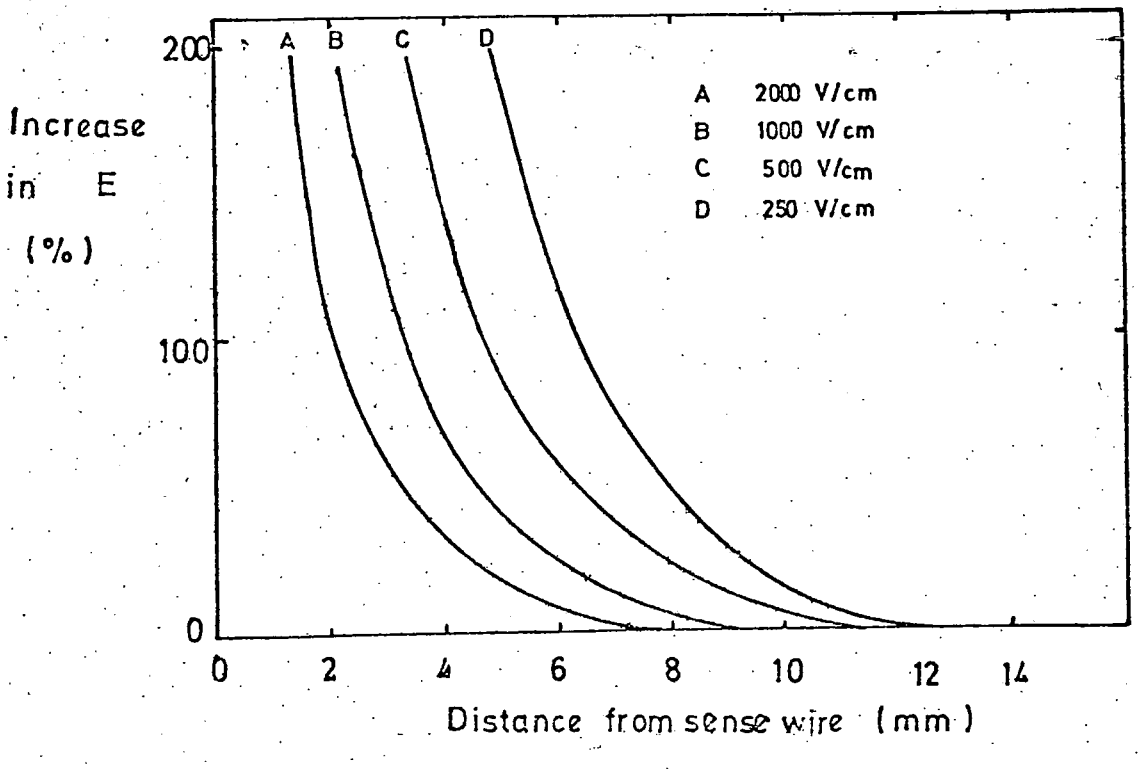

FIG 4.7 Distortion of electric field for various applied fields

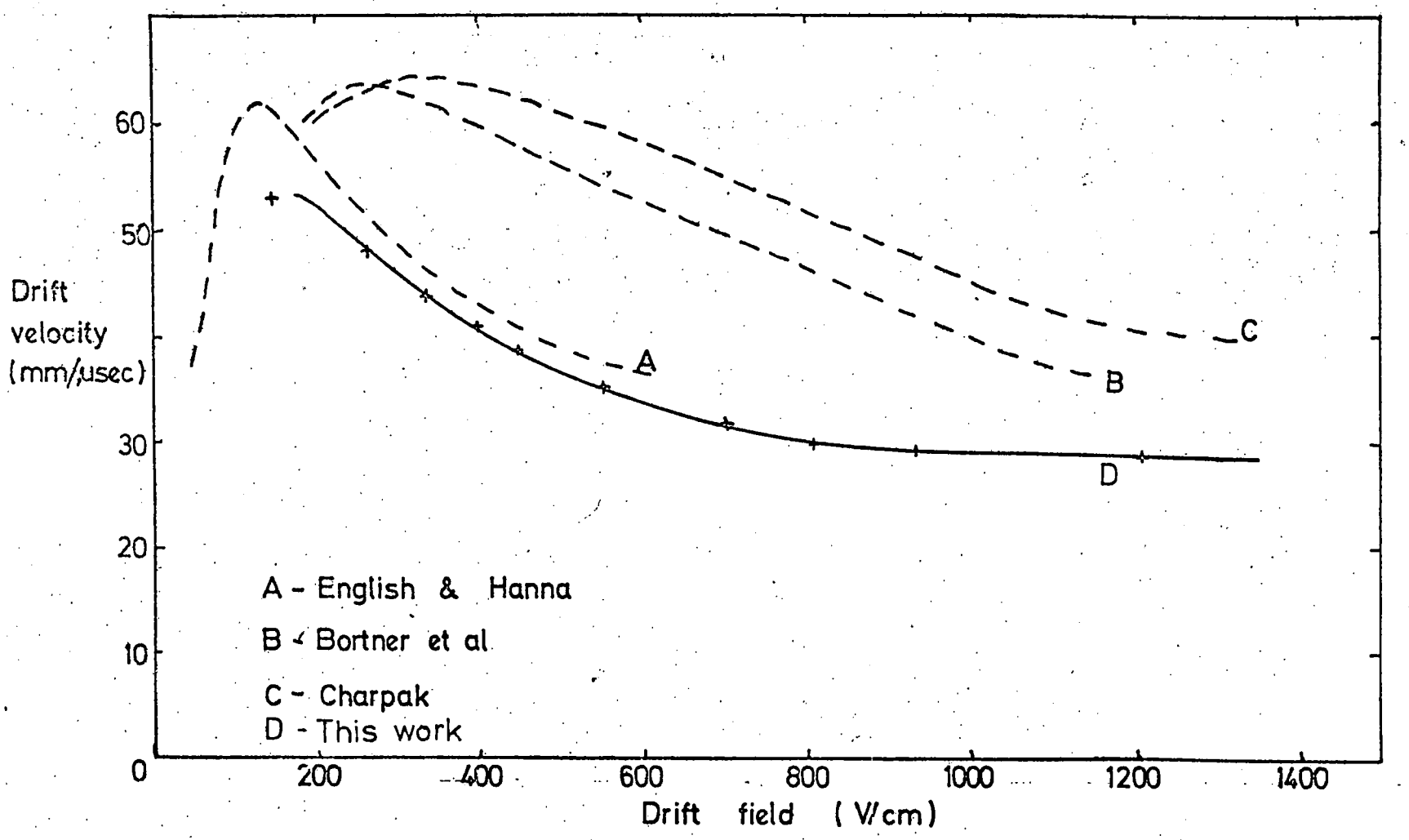

FIG 4.8 Drift velocity of electrons in argon +10% methane at 1 atmosphere versus electric field.

The behaviour of the drift velocity over the whole chamber is now exactly explained by combining the information from figures 4.8 and 4.6. Thus the rise in E near the sense wire, and the saturation of drift velocity at high E, predicts the region of uniform, low, velocity independent of E_a, around the sense wire. Furthermore, for lower applied fields, this distortion of velocity will extend further from the sense wire as E is distorted at greater distances from the wire (see figure 4.7). The magnitude of the velocity distortion is also increased at lower applied fields, as the variation of drift velocity with E is more marked in this region.

For higher fields the distortion of the drift field is reduced, and as the velocity is tending to saturate anyway, the velocity remains constant over the whole chamber. The fact that under these circumstances the time distance curve remains linear right up to the wire implies that the drift velocity curve of figure 4.8 is saturated up to much higher fields than those shown.

4.3.2 Drift velocity and chamber operation

It can be seen from figure 4.8 that the two basic requirements for the behaviour of drift velocity mentioned in section 4.1 are satisfied for our gas mixture.

The value of drift velocity at saturation, $\sim$ 30 mm/μsec, is well suited to small chamber operation. For instance digital timing at 250 MHz would yield a potential resolution of 4 nsec or 120 μm. For the analogue system used in these tests, the 1 μsec range on the T.A.C. enables distances up to 30 mm to be measured, to an accuracy of better than 5 nsec or 150 μm (maximum non-linearity of 0.5%).

The saturation of drift velocity at high fields appears satisfactory, the velocity change with field, above about 800 V/cm being less than 1% per 100 V/cm. Thus it is clear that operating the chambers at high fields (say $>$ 1kV/cm) offers many advantages, such as linear time distance

calibration and stability against local field variations.

To illustrate these advantages further let us consider the calibration of chambers. It is obviously desirable to assign one drift velocity to the whole chamber, and figure 4.9 shows how the error introduced by this assumption varies with applied field. This error was found by extrapolating the linear sections of figure 4.5 back to the distance axis and measuring the negative intercept. It can be seen from figure 4.9 that constant drift velocity may be assumed (for the general testing of chambers) only for high fields, and that for use in the accurate location of particles or at lower applied fields, the corrections indicated by the figure may have to be considered.

4.3.3 Comparison with other results

There is quite a large variation amongst the published data for electron drift velocities in argon + 10% methane, and included in figure 4.8, showing the results of this work, are three curves by other workers.

The best agreement is with the results of English and Hanna (1) which were obtained using a grid ionisation chamber and an α particle source. The drift velocity was calculated by measuring the rise time of the pulse due to the collection of electrons from an α particle track of known length. The tests were carried out at atmospheric pressure and an accuracy of about 10% was quoted.

Curve B comes from Bortner et al (2) who measured the time of arrival of ionisation electrons at two proportional counters situated a known distance apart in a constant electric field. It is not clear at what pressures these tests were carried out.

Curve C is from Charpak (3) with no information on the method of measurement although it is referenced as having been collected from a Thesis by Walenta (4).

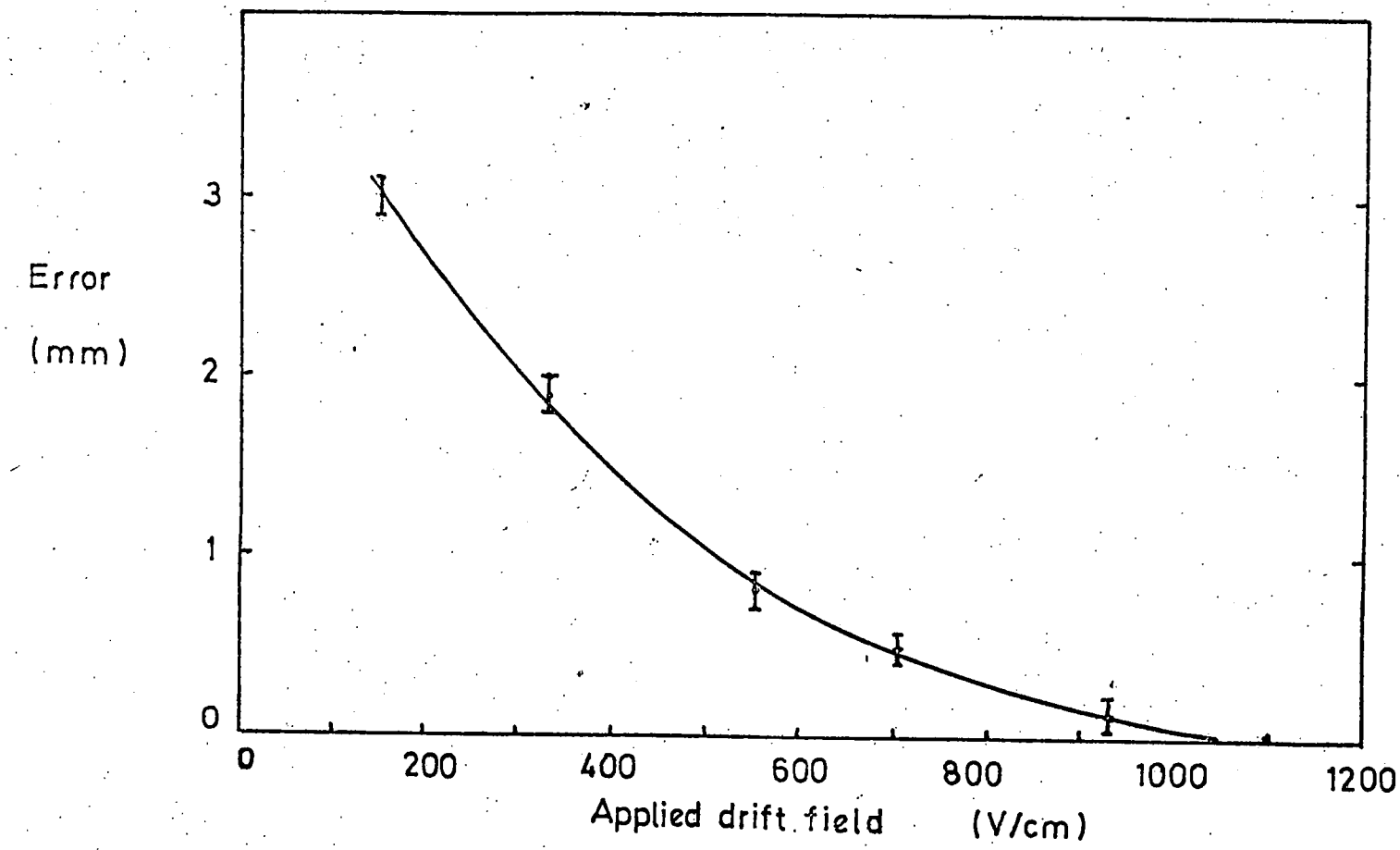

FIG 4.9 Error involved in assuming constant drift velocity across cell, versus applied field

It is difficult to explain the quite large discrepancies involved, other than by variations in gas composition, pressure, electric field measurement etc, between different experiments. The results of this work have however been found to describe consistently and accurately the operation of our chambers, and have been verified by the results of several consequent observations obtained with our chambers under various operating conditions.

4.4 Results for other gas mixtures

It was decided not only to study the electron drift velocity in our standard mixture, but to investigate its behaviour in a range of possible drift chamber gases.

Thus the drift velocity measurements were repeated for various gas mixtures, obtained by mixing gas from cylinders via calibrated 'Rotameter' flow meters. The drift velocity was allowed to stabilise between each different gas mixture, which sometimes took several hours particularly when the actual gas was changed, as distinct from merely varying the percentage composition.

The most obvious first choice was to investigate argon methane mixed in proportions other than 90:10, as this would also give an indication of the stability of velocity in the standard mix to fluctuations in gas composition. As it was difficult to obtain small concentrations of methane using a simple two flowmeter system with argon and methane, the same effect was achieved by mixing argon with argon + 10% methane from the premixed cylinder.

The results of this series of tests are presented in figure 4.10. During the tests, 4% was found to be the lowest practical proportion of methane which allowed satisfactory operation of the chamber, less methane resulting in severe electrical breakdown presumably due to lack of discharge quenching and to secondary emission.

Also shown on figure 4.10 are curves for 'pure' argon obtained from references 1, 5 and 6. These results indicate the strong effect on drift velocity caused by the presence of impurities in a gas, as the difference between curves marked I and II is that the argon of curve I was only 'commercially' pure (99.6%) compared with the specially purified argon of curve II. English and Hanna (1) were aware of this during their tests, but reported that the effects of any original impurities become negligible after the addition of even small amounts of a molecular gas ($\sim$1%).

The rise in drift velocity with percentage of methane in this range is seen from figure 4.10 to be constant in the region of velocity saturation, and equal to 1.5mm/μsec per 1% of methane. Thus at 10% methane, the velocity varies by about 5% per 10% variation in methane content.

Further tests indicated that this dependance on methane content is reduced for higher methane concentrations (to less than 1 mm/μsec per 1% of methane) and figure 4.11 shows the results of the tests carried out on argon + 50% methane and 100% methane. Reasonable agreement is seen with results for 100% methane from English and Hanna (1) and Hurst et al (6), both shown in figure 4.11. Considerable discrepancies do exist however, and results from other sources give a maximum value of w in methane of 100 mm/μsec (see for instance references 3 and 7) compared with our value of 135 mm/μsec. Discrepancies apart it appears agreed that pure methane is a 'fast' gas and as such is well suited to drift chambers with long drift distances, such as the ones used at Saclay by Saudinos et al (8). Methane may also be useful in 'non-drift' gaseous detectors, in order to reduce time jitter.

The behaviour of drift velocity in other gas mixtures, specifically those containing isobutane, was investigated using a simpler technique. Using a chamber with a smaller unit cell width (28 mm) so that higher drift fields could be achieved for lower V_{max}, the position of the ionising beam was set at 1 cm from the sense wire and the corresponding

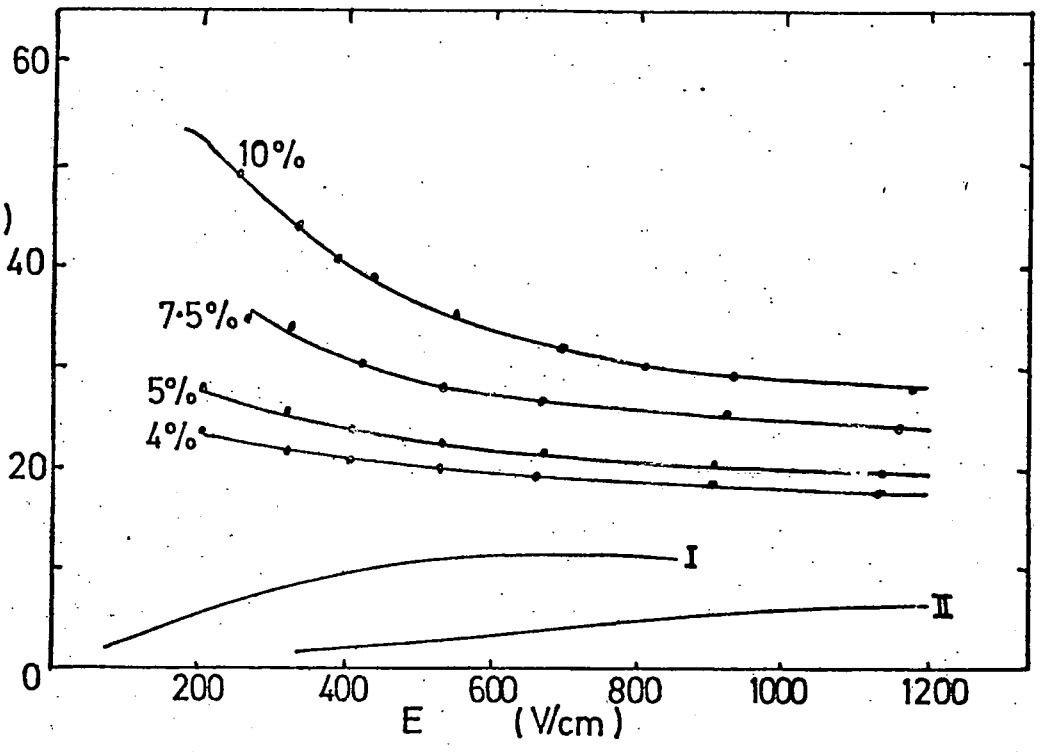

FIG 4.10

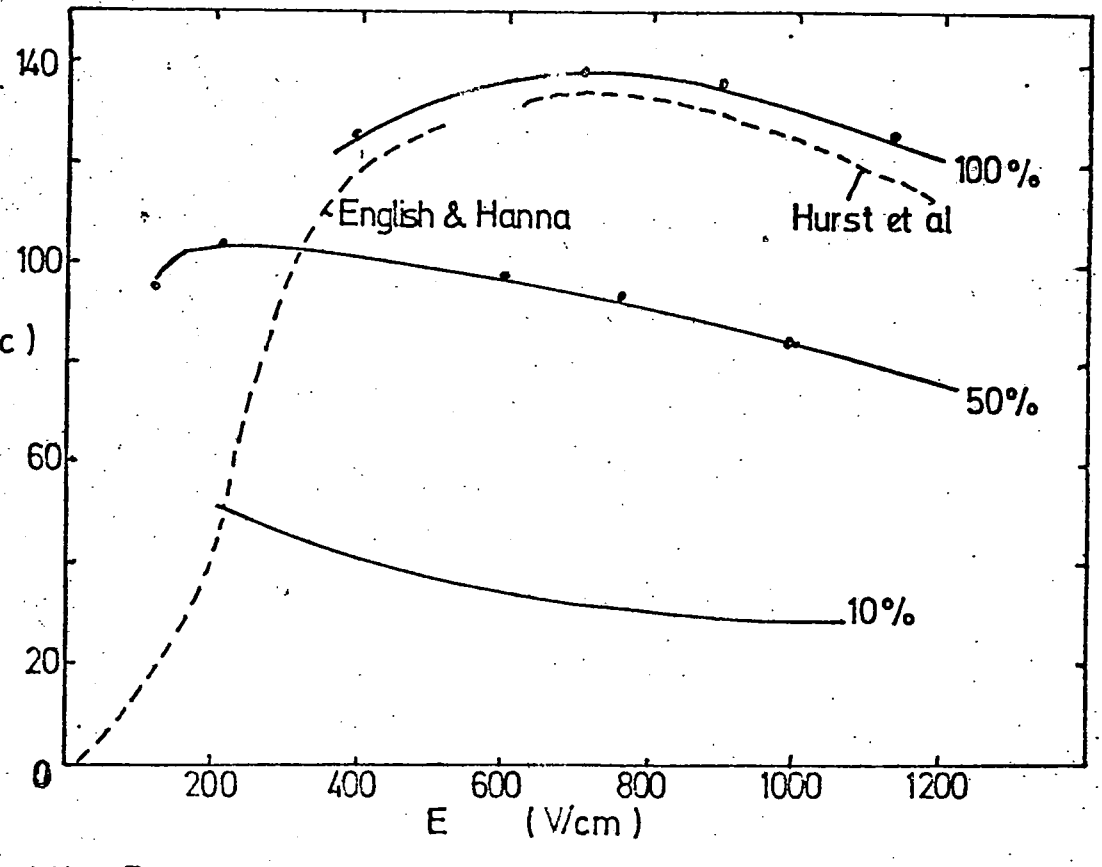

FIG 4.11

FIGS 4.10 & 4.11 Drift velocity curves for various methane proportions in argon. Curves I (1), and II (5,6) for 'pure' argon.

drift time measured for various fields. The drift velocity was then calculated by assuming constant velocity over the whole length, although as shown previously this will introduce some error, particularly at low fields or where the velocity does not saturate.

Figure 4.12 then shows the drift velocity obtained in this manner for three different proportions of isobutane in argon. It can be seen that for high isobutane content ($\sim 25\%$) a region of velocity saturation exists at fields above about 1000 V/cm. The form of these curves is in good agreement with similar curves from Charpak et al (9) although the absolute values seem about 15% higher, (one curve from reference 9 is shown on figure 4.12 for comparison). The discrepancy appears systematic and may be due to our less stringent method of measurement, an error in the positioning of the source for instance would result in such a constant percentage error in all results.

The effects of multiple component gas mixtures were investigated by repeating the previous tests with various mixtures of argon + methane + isobutane, some of the results being presented in figure 4.13. Comparing these results with those for argon-isobutane, both from these tests (figure 4.12) and from Charpak et al (9) (figure 4.14) considering the probable 15% discrepancy, it would appear that in the three part mixture both methane and isobutane have similar modifying effects on electron drift velocity. Thus the curves of figure 4.13 approximate to these for argon-isobutane if total hydrocarbon content in figure 4.13 is equated to isobutane content in the other figures. The effect is further demonstrated by observing the close similarity of the curves for argon + 7.5% methane (figure 4.10), 7% isobutane (curve D of figure 4.14), and 6% methane + isobutane (curve D of figure 4.13).

The actual mechanism of electron drift in gases and the effect of gas additives will be discussed in detail in Chapter 6.

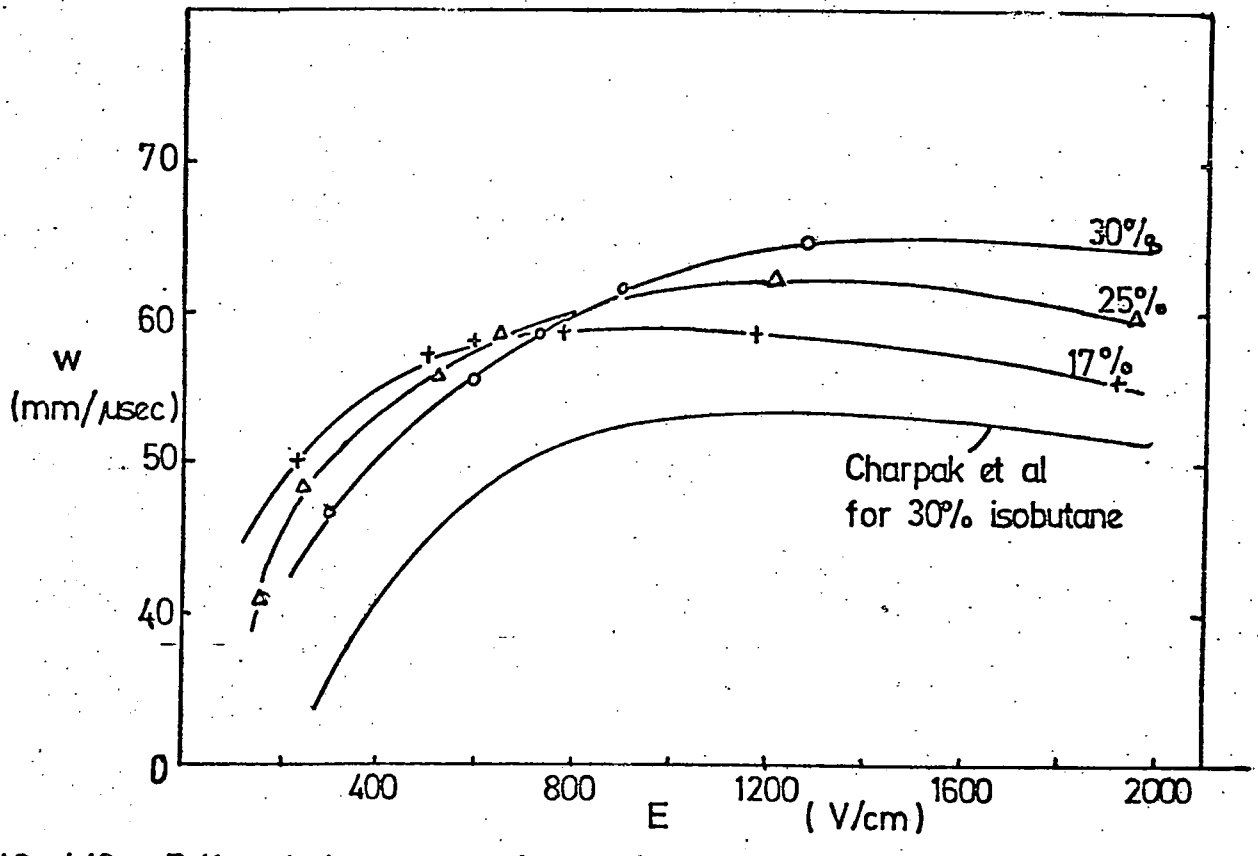

FIG 4.12 Drift velocity curves for various proportions of isobutane in argon

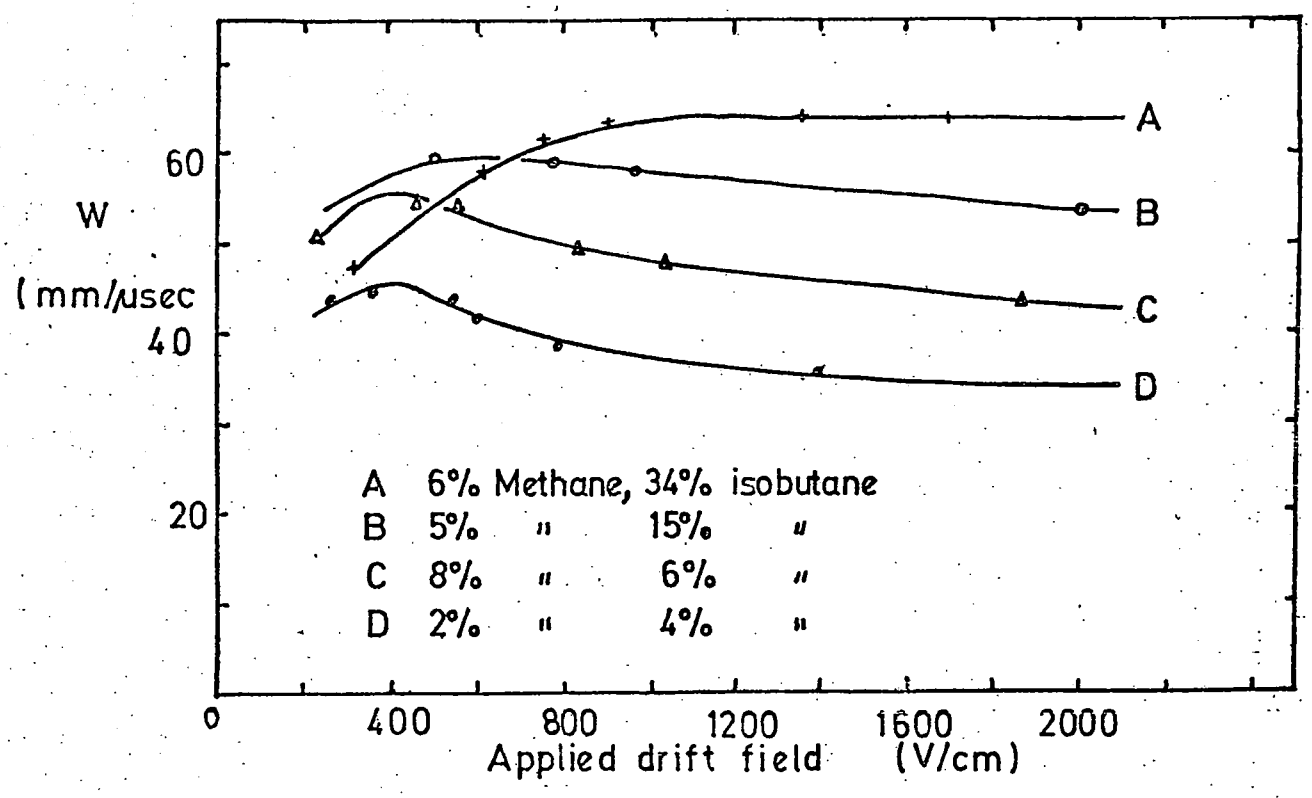

FIG 4.13 Drift velocity curves for various hydrocarbon proportions in argon. (This work)

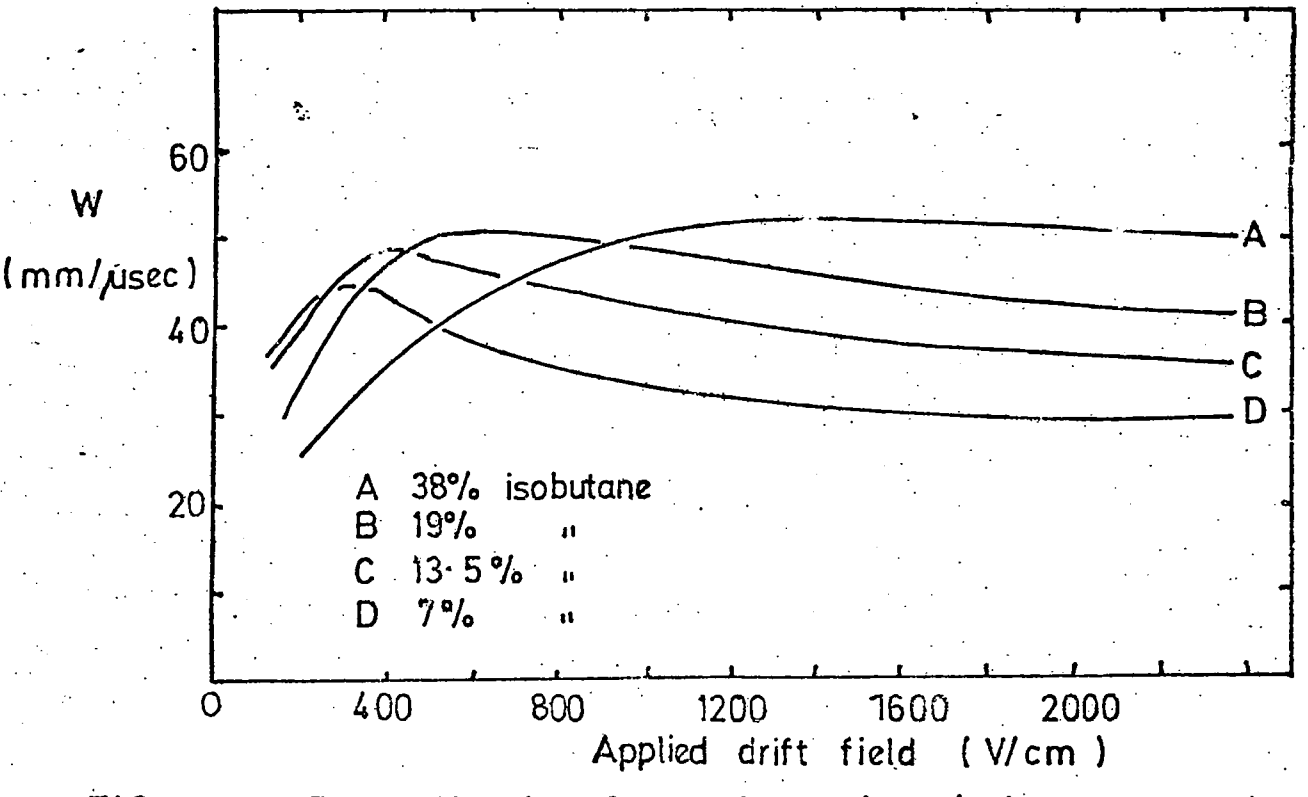

FIG 4.14 Drift Velocity Curves for various isobutane proportions in argon (Charpak et al)

4.5 Effect of angled particle trajectories

The tests on drift velocity described in the preceding sections were all carried out for particles traversing the chamber approximately orthogonally to the sense wire plane. The first electrons to reach the avalanche region will be those created nearest to this plane, as this represents the shortest possible drift path. This will not be true however for particles crossing the same wire plane at the same point but at an angle θ to the normal to the plane. Thus a different drift time will be recorded for the angled track due to the change in the shortest drift path although w remains unchanged. Calculation of the shortest drift path by geometrical means should then explain variations in measured drift times for angled tracks.

In order to determine these paths it is necessary to know the distribution of electric field lines within a chamber, and figure 4.15 shows such a distribution from Charpak et al (9). To simplify calculations they have assumed that the shortest drift path is in a direction perpendicular to the track where possible, or else coincident with the cathode plane. Referring to figure 4.16, showing three tracks at angle θ crossing the sense wire plane at S_1, S_2 and S_3, the corresponding shortest paths would be taken as PA, QA, and RQA. Expressions for the shortest path, d, for a chamber of half thickness g are then

$$d = S \cos\theta \quad \text{for } S \leqslant \frac{g}{\sin\theta \cos\theta} \qquad (1)$$

and

$$d = S - \frac{g}{\sin\theta}\left(\frac{g}{\cos\theta}\right) \quad \text{for } S \geqslant \frac{g}{\sin\theta \cos\theta} \qquad (2)$$

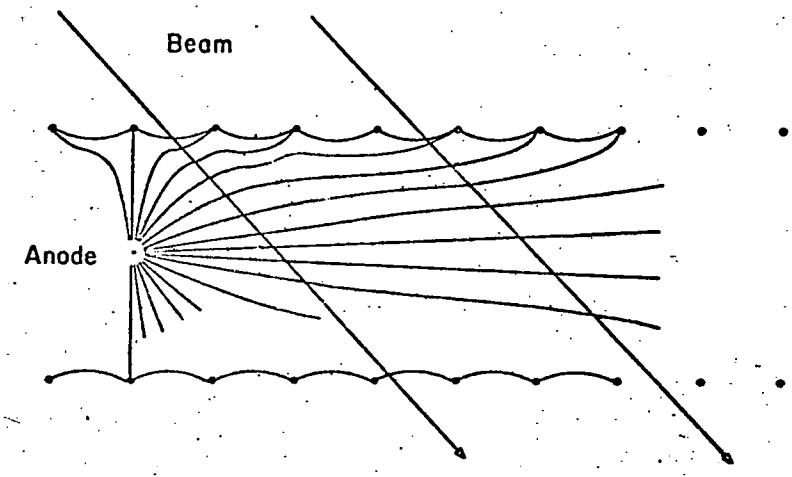

FIG 4.15 Field lines in an A.F.D.C. (from ref. 9)

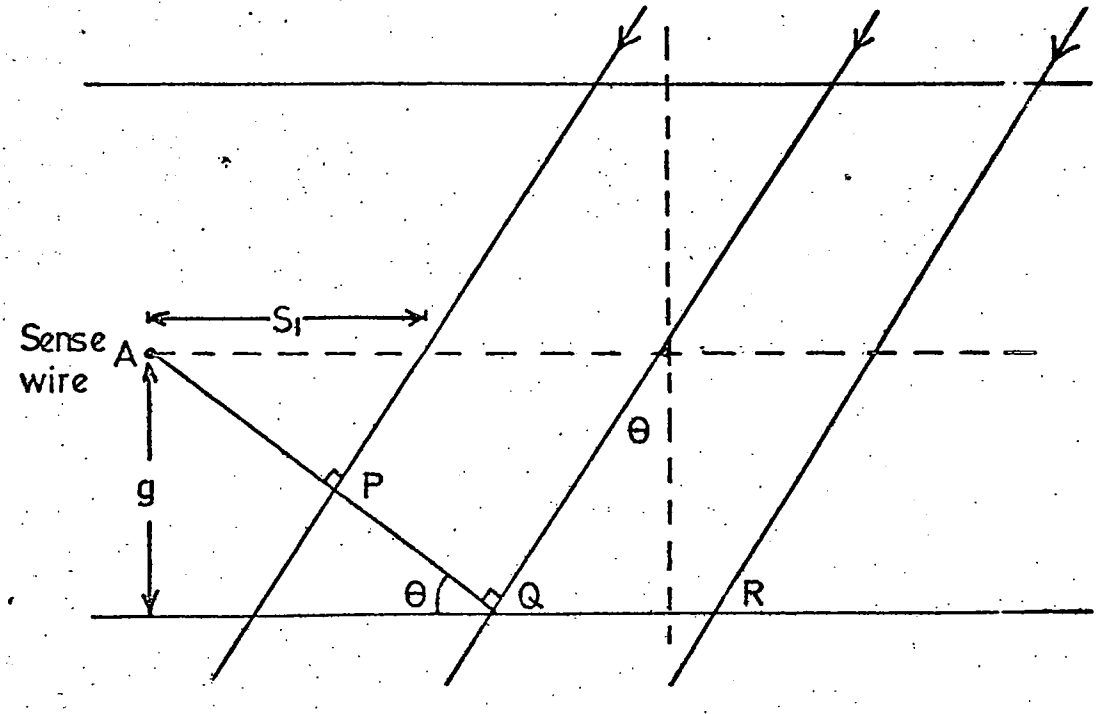

FIG 4.16 Angled tracks in a drift chamber

These expressions fit the results of Charpak et al for drift time against S, for tracks at 42^{o}, as shown in figure 4.17, where the line through the experimental 42^{o} points represent the expressions above.

However results obtained at Durham for constant s and variable θ disagree with this theory, and in fact if variable angle tracks are considered we see that the theory leads to the anomaly of different drift paths from the same point in space. Figure 4.18 shows the results of the Durham tests in which drift times were recorded for particles passing through a chamber at various angles but at the same position in the sense wire plane. This was achieved by pivoting a chamber, between a fixed source and scintillator, about an axis parallel to the sense wires and in the same plane. Also shown in figure 4.18 as curve A is the theoretical variation given by equations 1 and 2 above, and here the fit is poor, particularly in the region where 1 is replaced by 2 (around 24^{o}). Better agreement is obtained with a different theory, assuming a simplified field distribution as shown by figure 4.19. Electrons drifting from an angled track will have their path lengths reduced by x tan θ, but increased by $\sqrt{A^2 \pm x^2} - A$, where x is the variable shown on the figure.

The net reduction, R, in path length is then given by:

$$R = x \tan \theta - \sqrt{A^2 + x^2} + A \qquad (3)$$

The value of x for maximum R, and hence shortest path is given by differentiating. For constant θ and $\tan \theta = B$ we have:

$$\frac{dR}{dx} = B - \frac{x}{\sqrt{A^2 + x^2}}$$

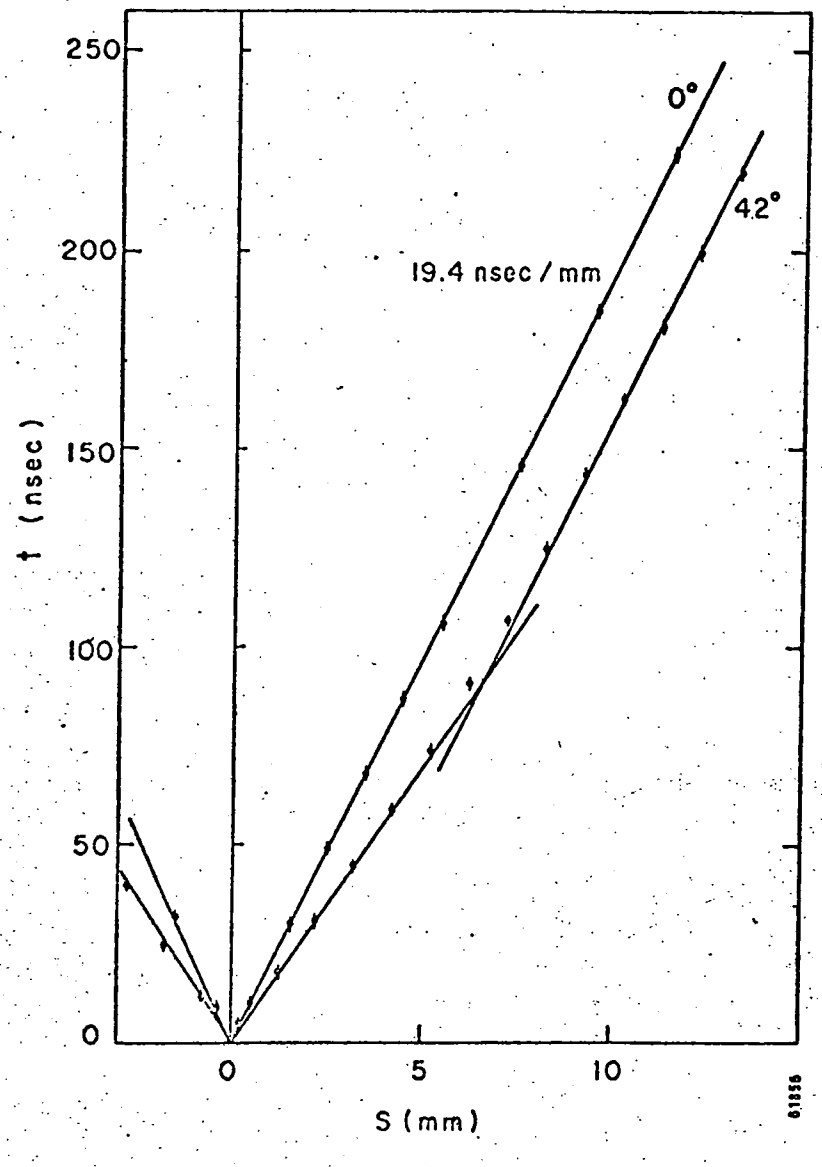

FIG 4.17 Drift time - distance relationship (experiment and theory) for angled tracks, from Charpak et al (9).

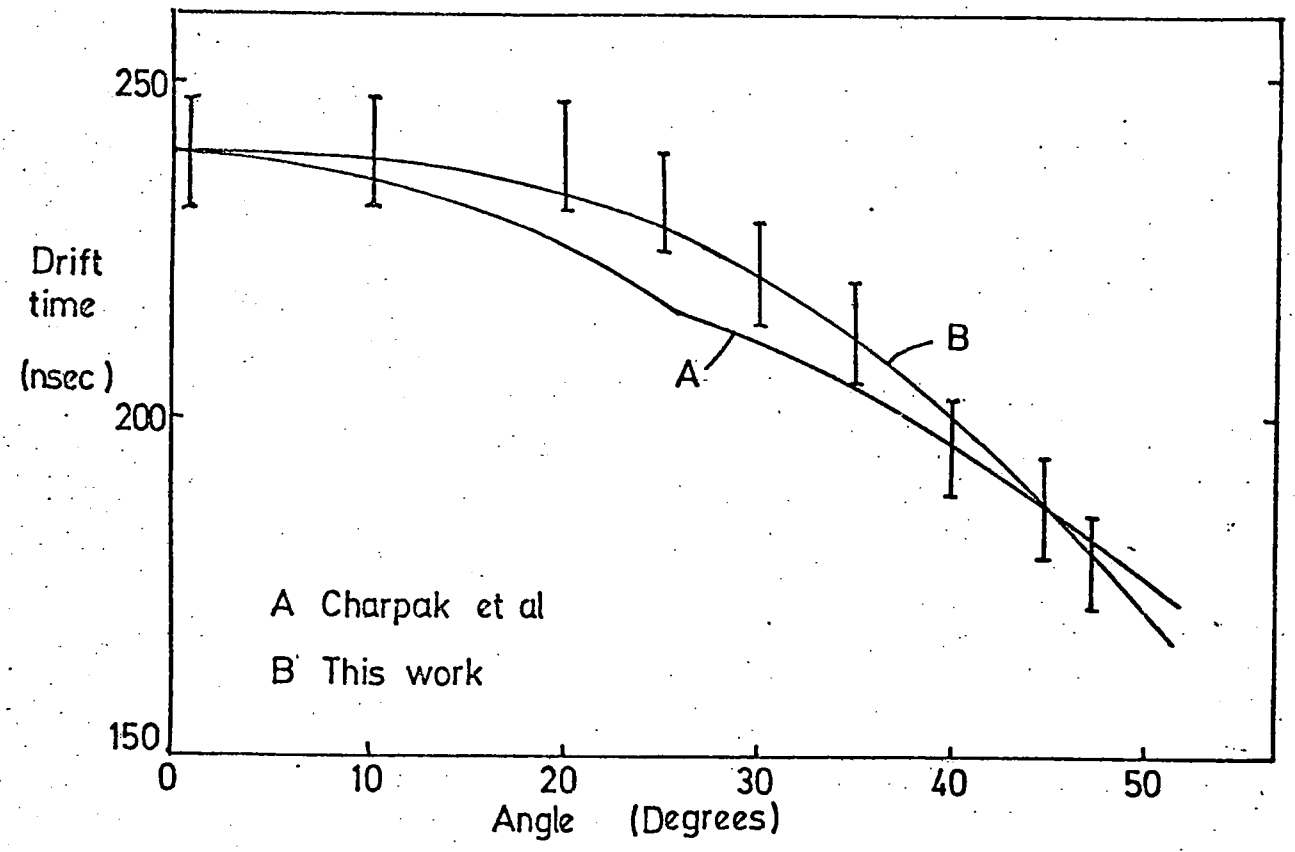

FIG 4.18 Variation of drift time with track angle, experimental and theoretical

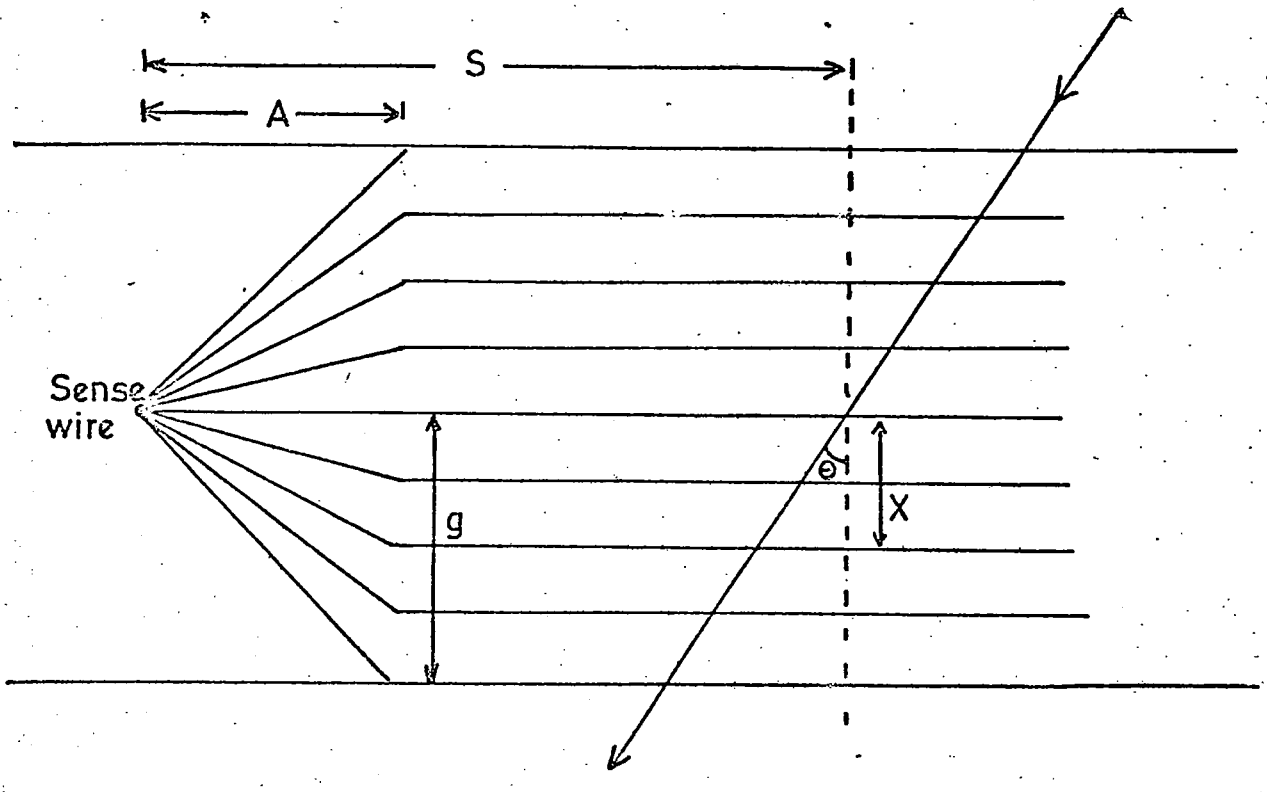

FIG 4.19 Model for predicting effect of angled tracks.

For maximum R

$$B = \frac{x}{\sqrt{A^2 + x^2}}$$

or

$$x^2 = \frac{A^2}{(1/B^2 - 1)} \qquad (4)$$

Thus x for the shortest path is found and substituted in 3 to find the reduction in path length against angle θ remembering that B, and hence x, are both functions of θ.

The relationship will break down for a track which enters the 'radial' field region, to be replaced by:

$$d = S \cos \theta$$

as before. The full relationship for angled tracks is then given by:

$$d = S \cos \theta \quad \text{for } S - A \leq g \tan \theta \qquad (5)$$

and

$$d = S - (x \tan \theta - \sqrt{A^2 + x^2} + A) \text{ for } S-A > g \tan \theta \qquad (6)$$

where x is given by 4 above, with a maximum of $x = g$.

Assuming a value of 3 mm for A, values of expected drift time against θ were calculated (for S = 8 mm) and shown on figure 4.18 as curve B showing good agreement with experiment. Expressions 5 and 6 also fit the data for angled tracks at various distances such as that shown in figure 4.17.

There are two points to note with respect to the use of the above expressions however, the first being that the value of A should change with the applied drift field, reducing as the field is increased (see for example figure 3.10). Secondly it may not be obvious in an experimental system at what angle any particular track is incident, and two or more chambers along the particle path may be necessary to define approximate track angle before making the drift time corrections above.

One useful property to emerge from the above work is that except very close to the sense wire track angles of up to 20° can be accepted without correction if errors up to 200 μm can be tolerated.

4.6 Conclusion

The work described in this chapter has indicated that the behaviour of the electron drift velocity in argon + 10% methane is suitable for successful utilisation in drift chambers, particularly when high drift fields are applied to the chambers. The behaviour of drift velocity, w, for an applied field of 1 kV/cm can be summarised as follows.

(i) A value of 29 mm/μsec can be assumed over the whole chamber, this involving a maximum overestimation of distance of less than 100 μm.

(ii) The stability of w with drift field is 1% per 100 V/cm

(iii) The stability of w with gas content is 1% per 2% variation in methane proportion (i.e. $\pm$ 0.2% methane)

(iv) The stability of w with temperature was not measured but is not expected to differ significantly from other results (9) for argon + 30% isobutane, quoted at 0.4% variation per 14°C.

(v) Tracks traversing the chamber at an angle do not affect w, but do introduce errors in the estimated particle position which may be corrected for by the appropriate expressions. Tracks at angles up to 15° however will introduce errors of up to 100 μm only.

Comparison with argon + 30% isobutane, the standard gas mixture used at C.E.R.N., indicate that argon + 10% methane has the advantages of simplicity (no mixing systems required) and lower drift velocity ($\sim$ 30 mm/μsec against $\sim$ 50 mm/μsec) resulting in the use of less stringent timing systems. The isobutane mixture however has a slightly better stability of w with applied field, and much better stability with isobutane content (9).

Chapter 4 - References

1. W.N. English and G.C. Hanna., Can. J. Phys. 31 (1953) 768

2. T.E. Bortner, G.S. Hurst and W.G. Stone, Rev. Sci. Instr. 28 (1957) 103

3. G. Charpak 'Drift chambers' Presented at the Workshop on Research Goods for Cosmic Ray Astrophysics in the 1980's, ESRIN (Frascati) October, 1974.

4. A.H. Walenta, Ph.D. Thesis - Heidelburg University (1972)

5. N.E. Bradbury and R.A. Nielson, Phys. Rev. 49 (1936) 388

6. G.S. Hurst, J.A. Stockdale and L.B. O'Kelly, J. Chem. Phys. 38 (1963) 2572

7. T.L. Cottrel and I.C. Walker, Trans. Faraday Soc. 63 (1967) 569

8. J. Saudinos, J-C Duchazeaubeneix, C. Laspalles and R. Chaminade, Nuc. Instr. Meth. 111 (1973) 77.

9. A. Breskin, G. Charpak, B. Gabioud, F. Sauli, N. Trautner, W. Duinker and G. Schultz, Nuc. Instr. Meth. 119 (1974) 9.

CHAPTER FIVE

MEASUREMENT OF SPATIAL RESOLUTION

5.1 Introduction

The primary reason for the development of drift chambers as particle detectors is that they offer the best potential spatial accuracy at present available in a relatively simple, large area device. Hence in the study of a practical chamber, or in deciding the suitability of a new gas mixture, the investigation of the resulting spatial resolution is particularly relevant.

In an early paper on drift chambers, Walenta (1) discussed the various contributions to the overall accuracy of a chamber, defining σ as the standard deviation of the location inaccuracies measured for many events. The contributions to σ relevant to our chambers are listed below.

(i) The distribution of the primary ionisation (σ_i). The drift length measured is not the shortest distance to the particle track, but the distance to the nearest ion pair created by the particle, and the possible error thus introduced depends on the density of ion pairs (or as quoted by Walenta, the density of ionisation clusters containing several pairs). The number of such 'clusters' is not expected to be less than the number of primary ion pairs created, which was shown in chapter 3 to be about 16 (or about 27 per cm) and the resulting contribution to inaccuracy is then $\sigma_i \sim 40$ μm.

(ii) The diffusion of drifting electrons (σ_d). The theory of this process is discussed in chapter 6, and it is this contribution which gives rise to the variation in resolution for different gas mixtures. Walenta's calculation of the value of this contribution for his gas or argon + 9% methane + 7% isobutane was $\sigma_d = 80$ μm, for drift distances less than 1 cm.

(iii) Measurement of drift time (σ_t). The errors involved in the various electronic timing systems were discussed in chapter 2, and the contribution to σ would not be expected to be greater than 50 μm for the tests described in sections 5.3 and 5.5.

(iv) Estimation of drift velocity (σ_v). During the resolution tests a linear drift time - distance relationship was assumed over the whole chamber and this will have some effect on the total σ. The fact that the actual velocity is only estimated to within 1% will also be significant and the combined contribution of these effects is estimated at 50 μm.

(v) Mechanical tolerances (σ_m). The total displacement of a sense wire from its expected position will not affect the width of the distribution of location inaccuracies, although of course it will cause the absolute position of the incident particle to be wrongly estimated. Non parallelity of sense wires in an array of chambers due either to constructional defects or misalignment of chambers, will however contribute to σ. The actual magnitude of such a contribution is difficult to estimate as it will be unique to any particular array of chambers. For the system described in section 5.3 a maximum estimate of σ_m = 50 μm seems reasonable.

Taking into account all the rather simply estimated contributions above, the quadratic sum for the overall σ is in the order of 130 μm, and hence this is the sort of result expected in the following tests on resolution.

It should be noted that of the contributions listed above only (i) and (ii) are actually inherent to drift chambers, i.e. in theory the other effects could be reduced to an insignificant level. Thus it is important to differentiate between the inherent resolution and the contribution from the system as a whole, although in any resolution tests it will be the combined effect of both which is measured. It must also be stressed that

σ_m and σ_v represent maximum estimates only. For any particular test system, merely by chance the drift velocity may be estimated exactly and the wires aligned perfectly. Such a series of tests would discover a lower overall σ ($\sim$ 110 μm).

5.2 Preliminary results

During the investigation of drift velocity described in the last chapter, the raw data was in the form of drift time distributions obtained from drift chambers (see for example figure 4.2) and the width of these distributions obviously gives a measure of the resolution of the system. Unfortunately in this system there is a contribution to the spread of drift times not mentioned in 5.1, this being that the positions of the ionising tracks are only poorly defined. This is due in part to the geometrical divergence of particles emerging from the collimating slit (proportional to d, the distance between the slit and the sense wire plane) but mainly to the multiple scattering of the relatively low energy electrons. This latter contribution introduces a possible spread of the particle beam approximately proportional to d^2 for the intervening air, plus a fixed contribution from the Melinex window.

When the full width at half the maximum (f.w.h.m) of the drift time distributions for identical conditions was measured for various values of d, the points of figure 5.1 were obtained. The full line on the figure gives the theoretical variation of beam width calculated by considering the combined effects of the geometrical divergence and scattering. A useful approximation to the angular spread of an electron beam after travelling distance d through air, due to multiple scattering, is given as (2),

$$\theta_s = \frac{7000d}{k^2}$$

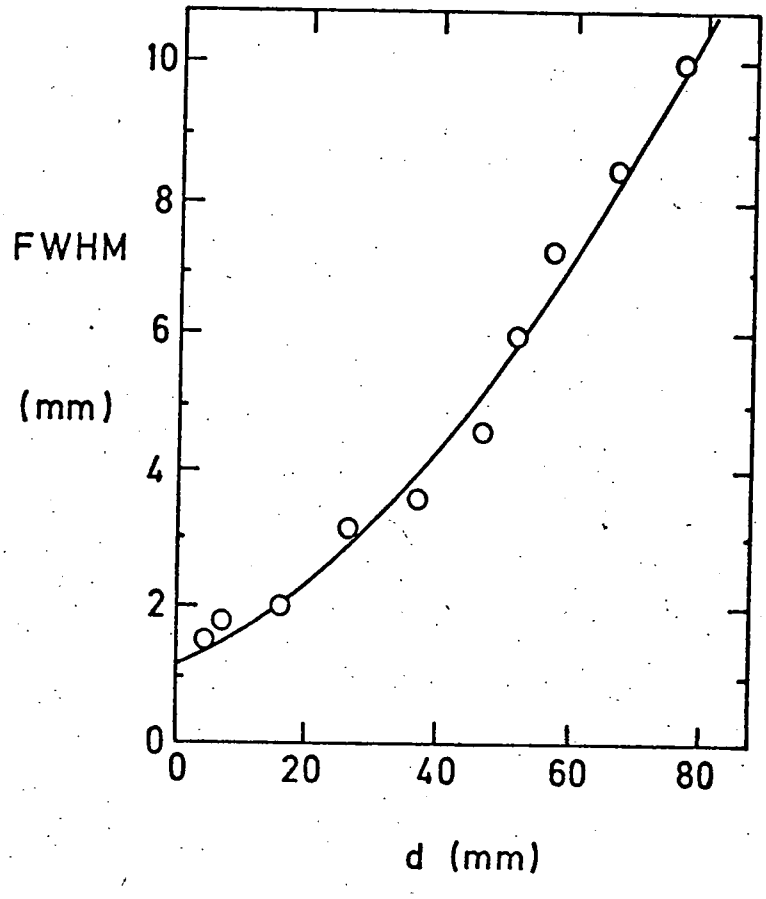

FIG 5.1 Width of drift distance distribution versus separation of sense wire and collimator (circles), compared to theoretical spread of 1·0 MeV electron beam.

where k is the electron energy in keV. The resulting widening of the beam was added to the geometrical spread, the actual line on figure 5.1 being calculated for 1.0 MeV electrons emerging from a slit 50 mm long and 0.25 mm wide, assuming the Melinex window to be equivalent to 20 mm of air. From this sort of agreement it was obvious that the resolution of the system was completely masked by the dispersion of the beam, and that to investigate the locational properties of drift chambers would require the use of much higher energy ionising particles.

Further investigation of resolution was continued using the test beam facility at Daresbury Laboratory, which provided a mono-energetic ($\pm$ 1.0%), collimated ($\sim \pm$ 2 cm) beam of positrons with selectable energy in the range from 200 MeV to the maximum operating synchrotron energy (usually 2 - 4 GeV). Details of the test beam are described elsewhere (3), and figure 5.2 shows the main features of the beam line with respect to the electron synchrotron.

These resolution studies were carried out as part of the tests on 28 mm multicell chambers designed for use in the g-2 experiment (see chapter 8), and are more fully described in the report of these tests (4). The main points and results will however be mentioned below.

The tests were made using one multicell chamber, several scintillation counters to define the beam, and a T.A.C. - P.H.A. system of time measuring. A plan of the whole system is shown in figure 5.3 where the acceptable beam through the chamber is defined by the overlap of scintillators S_3 and S_4, which were both mounted on movable platforms controlled by micrometer screws. Figure 5.4 shows some P.H.A. outputs for various overlaps of S_3 and S_4. All these results were taken with an applied field of 756 V/cm, argon + 10% methane, and a sensitivity of 8.75 nsec/channel (or 0.27 mm/channel). An overlap of 0.25 mm was found to be a practical minimum, mainly because of the background 'plateau' of drift times seen in figure 5.4. The plateau was thought to be due to

FIG 5.2 Daresbury e^+ line

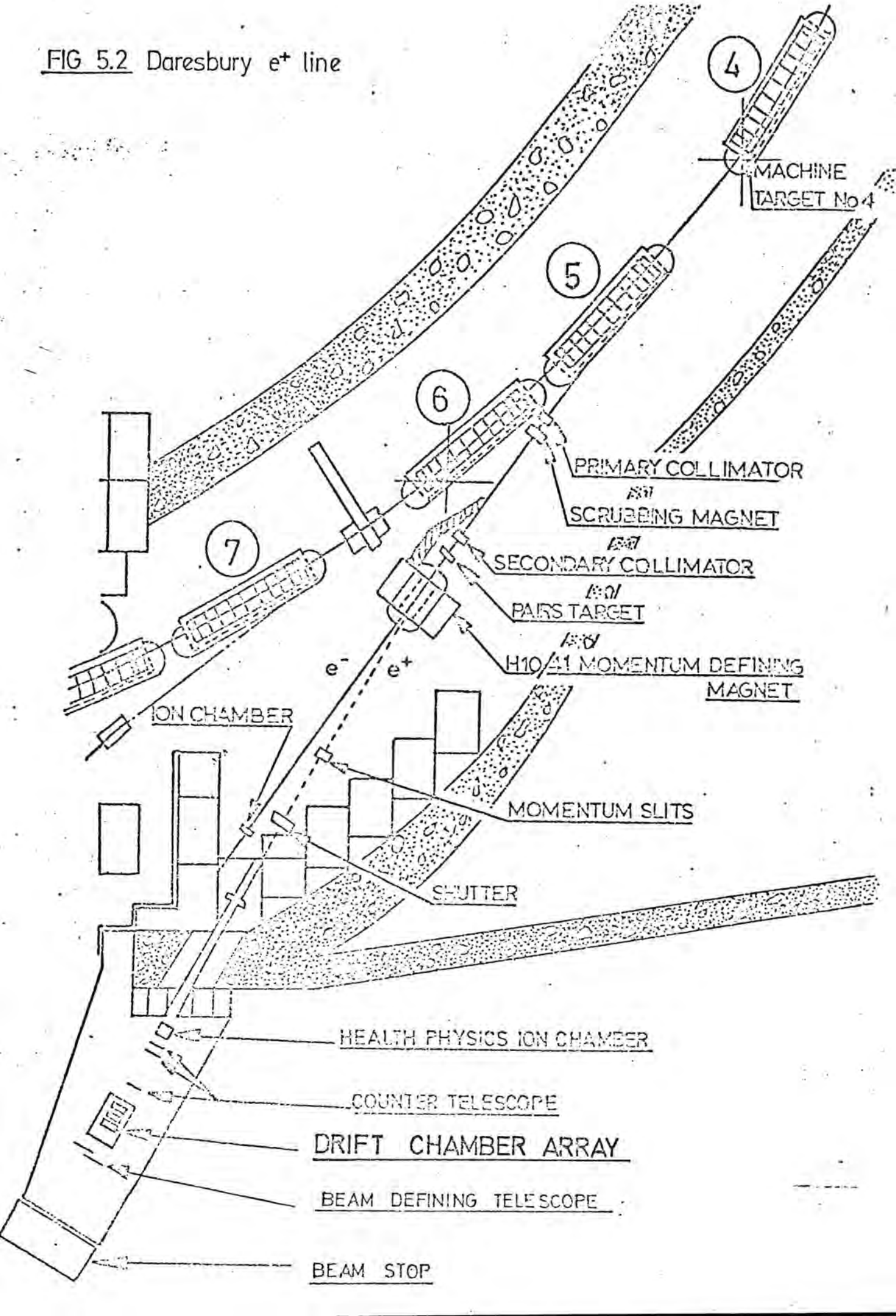

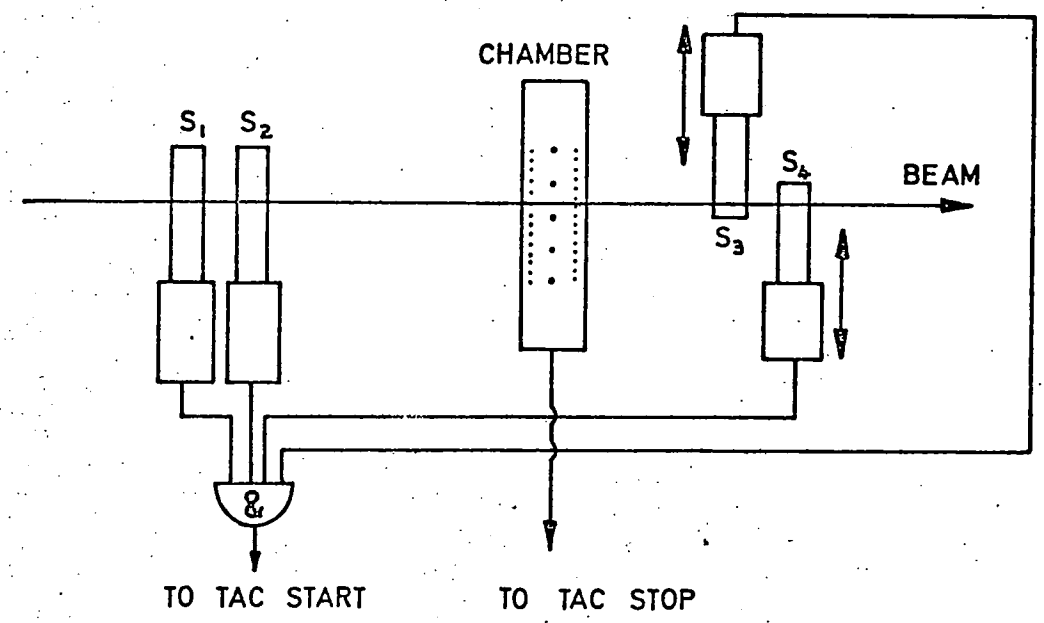

FIG. 5.3 Schematic of first resolution tests on e^+ beam

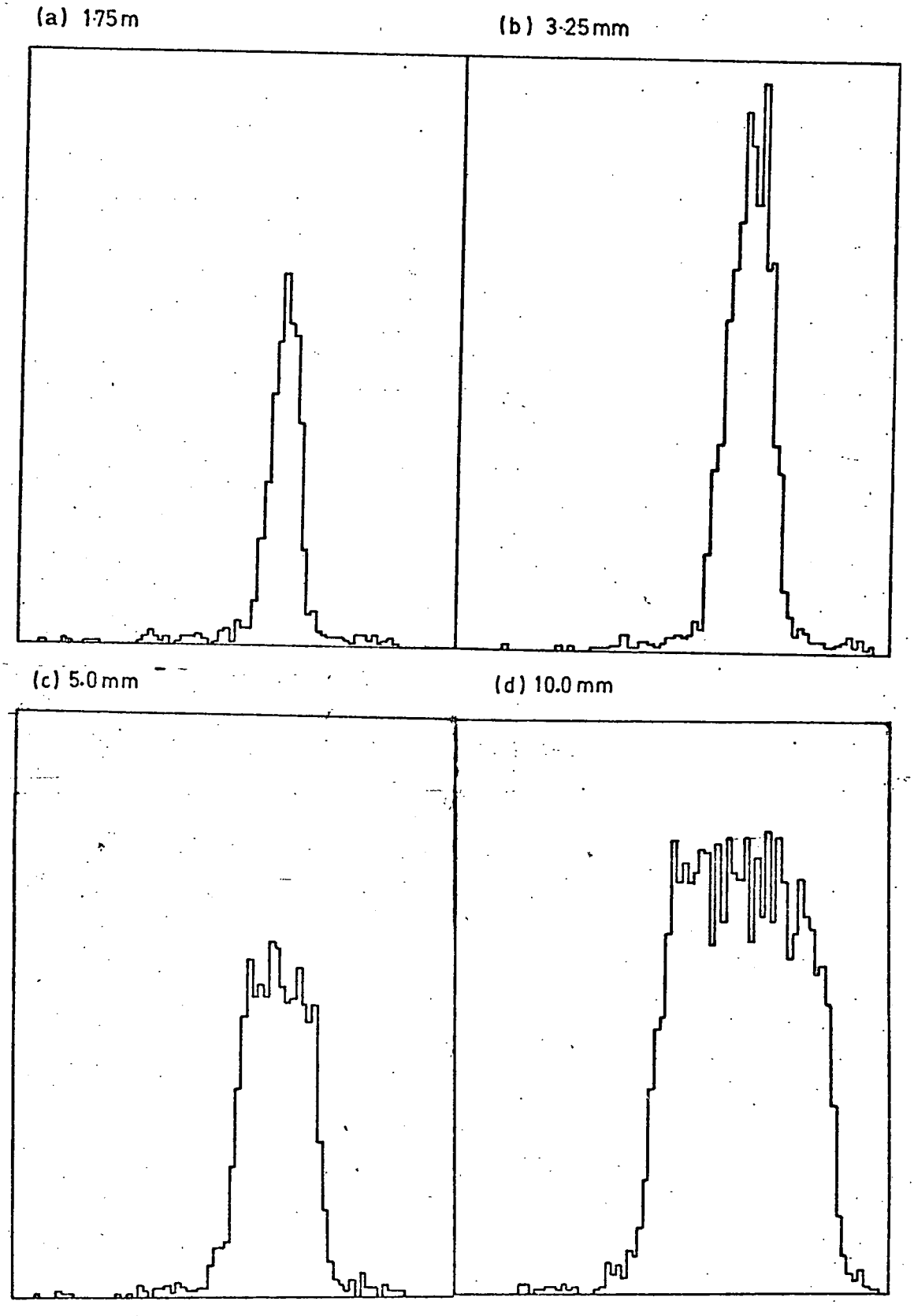

FIG 5.4 Drift time distributions for various defined beam widths

the triggering of the system by a shower rather than a particle passing through the overlap, and the stop pulse coming from one of the shower components being detected in the chamber. In fact even with S_3 and S_4 separated slightly, the 'plateau' was still observed, and assuming it was caused by stop pulses from the whole of a cell (maximum drift length 14 mm), the width of the plateau corresponded to a drift velocity of 31 $\pm$ 2 mm/μsec (i.e. excellent agreement with the results of chapter 4 which give a corresponding value of W = 30.5 mm/μsec).

The resolution of the chamber as measured by this method was still masked by the uncertainty on the position of any particular particle within the beam, and the best resolution measurable was a f.w.h.m. of ~1 mm for a beam width of 0.25 mm (see figure 5.5). This figure also shows the variation of resolution with drift distance, showing the time distributions obtained by positioning a 0.25 mm overlap at various positions in the chamber. The sensitivity is again 8.75 nsec/channel and the distances of the beam centre from the sense wire are given. Within the errors imposed by the system, it is seen that the resolution does not vary significantly with distance.

At this stage it was realised that the only valid method of studying resolution would be to use an array of chambers to define particle tracks (preferably straight) and thus deduce the mean locational errors.

5.3 Tests with an array of multicell chambers.

5.3.1 Experimental System.

The basic system used is shown in figure 5.6, where the three chambers were mounted on a flat rigid baseplate and alignment of the sense wires was achieved by means of externally scribed reference lines on the chamber frames. During chamber construction the sense wires were

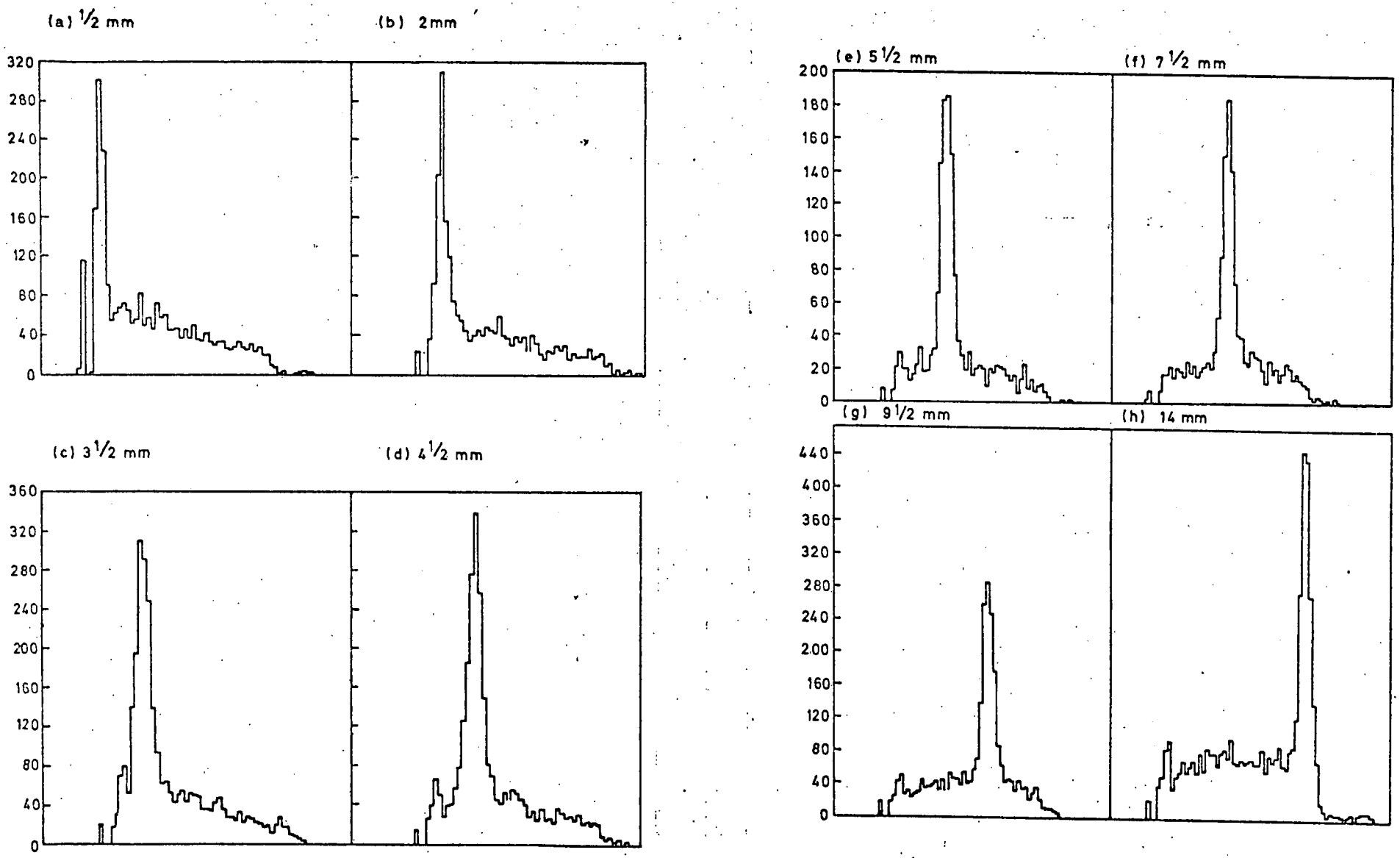

FIG 5.5 Drift time distributions for various positions of beam

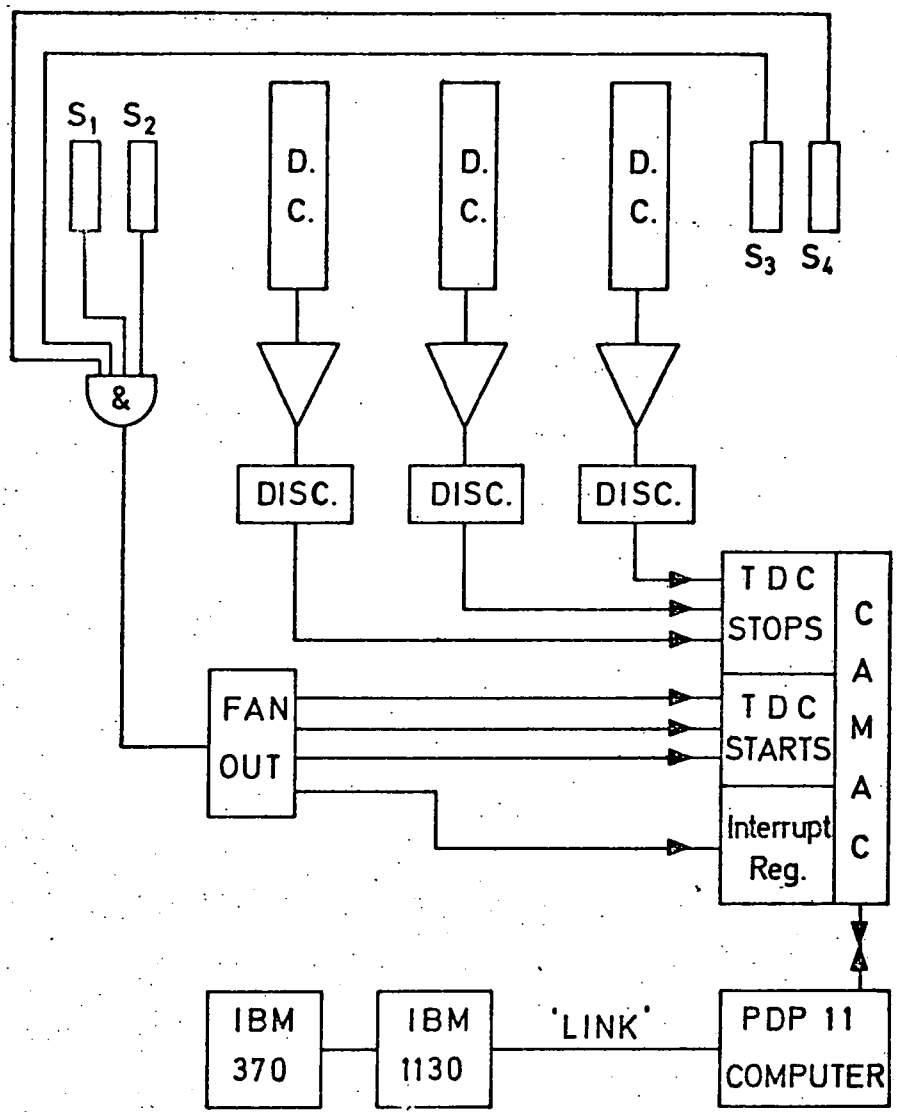

FIG 5.6 Resolution test system using an array of 3 drift chambers.

attached so as to be parallel to this line and at set distances from it. The chambers were mounted on the baseplate so that the lines were coincident with another fiducial line running the full length of the baseplate, and the final system was surveyed with a theodolite to ensure parallelity of the sense wires.

The gas (argon + 10% methane) was supplied, from one cylinder, to the chambers connected in parallel with a flowmeter monitoring the input and output to each chamber to ensure that no leaks developed (small amounts of air entering the chamber would be extremely detrimental to the drift process).

The drift field in all chambers was maintained at 600 $\pm$ 10 V/cm giving a drift velocity of 33.8 $\pm$ 0.2 mm/μsec. Preamplifiers were connected to one sense wire in corresponding positions in each chamber, via a short ($\sim$30 cms) length of miniature co-axial cable, all the remaining electronics being mounted in a nearby rack.

The timing was carried out in one Quad T.D.C. module manufactured by LeCroy Electronics Ltd. This module was in the form of a CAMAC component, so that its operation could be controlled by means of a programme in an associated small computer (Digital Electronics P.D.P 11). The output from the T.D.C's was stored in the computer and could be either displayed on a Visual Display Unit, or sent down a permanent link into the main laboratory computer (I.B.M. 370) via an I.B.M. 1130 as interface. This data handling system is also shown in figure 5.6.

5.3.2 Computer Control

Two programmes were used to control the data taken during the course of the various resolution tests although they both performed basically the same function. As an example the flow diagram for the first programme used, written in CAT 11, a form of 'Basic' specially written for CAMAC control purposes (5) is shown in figure. 5.7.

FIG.5.7 COMPUTER FLOW DIAGRAM

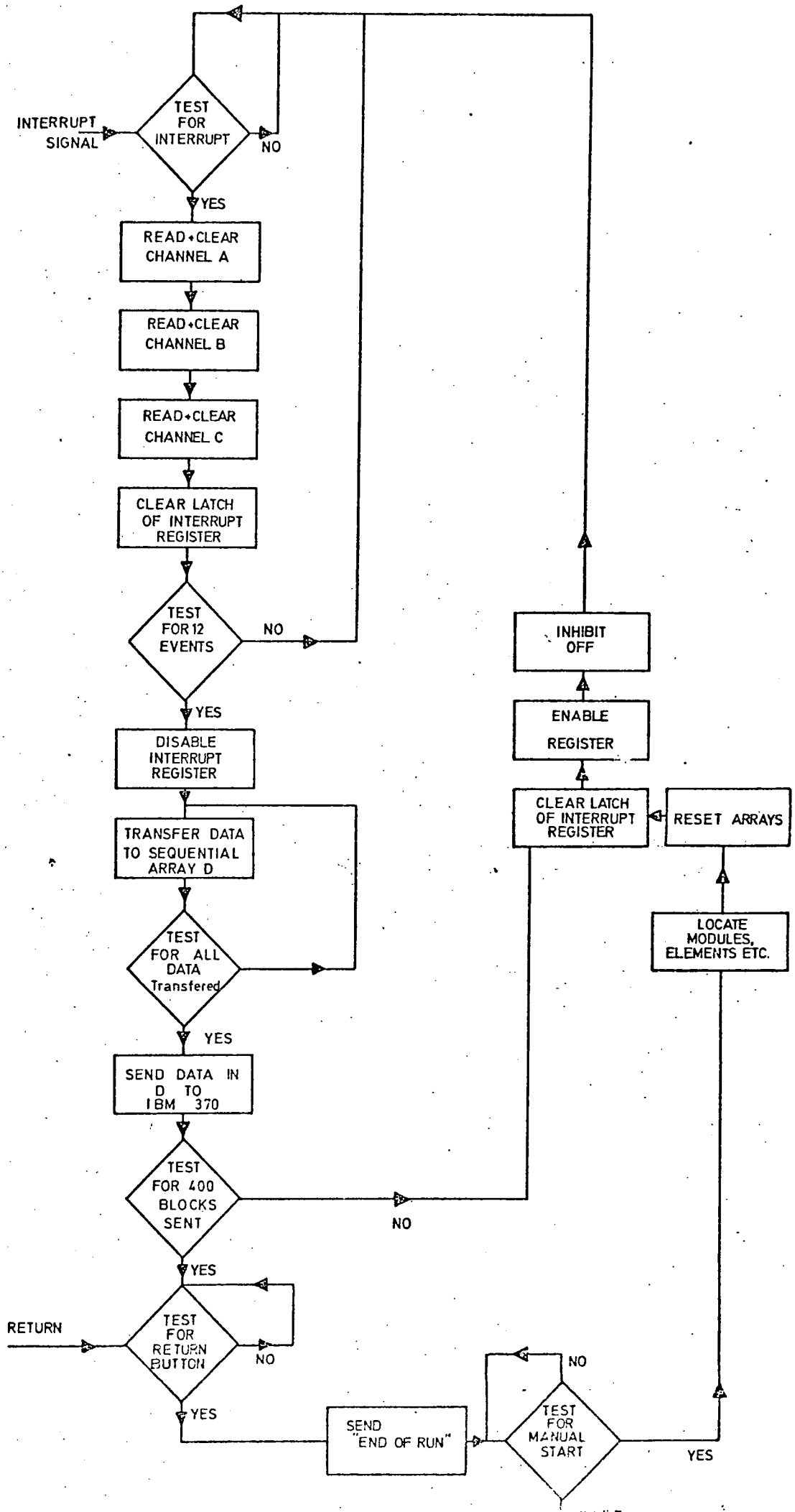

The programme was started by means of a manual command entered via a keyboard terminal (bottom right of figure 5.7). After setting up conditions for data taking the programme entered a loop to await an interrupt signal. This signal was generated, via an interupt register from the scintillator coincidence and thus signified that a valid event had occurred. This caused the three T.D.C. channels to be read, the data to be stored in the computer as one event, the system to be reset and the wait loop re-entered. The process was repeated until the available core was almost full whereupon the data was transferred into one array for convenience and then transmitted down the link (as one block of n events) to the IBM 370 where it was stored on disc.

The data obtained from these tests was quickly transferred to magnetic tape storage for later processing, thus freeing the discs for further data-taking.

During setting up procedures, and at times during an experiment, it was convenient to display the recorded times on a V.D.U. in the experimental area. With the first programme this was achieved by deleting the 'send' command and inserting one to display the values stored in the arrays. In the second of the programmes (written by P. Ridley, Daresbury) separate start commands were used to specify display or send modes of operation.

5.3.3 Data processing

The method of determining the locational errors in the chambers from the three recorded drift times can be explained with reference to figure 5.8, showing the predicted occurrence of ionisation in 3 chambers at X, Y and Z, for corresponding drift times T_1, T_2 and T_3. The estimated trajectory of the particle was constructed through the mean values of T_1 and T_2, and T_2 and T_3 (points A and B) and a deviation D defined as the difference between the measured location and the estimated track. This

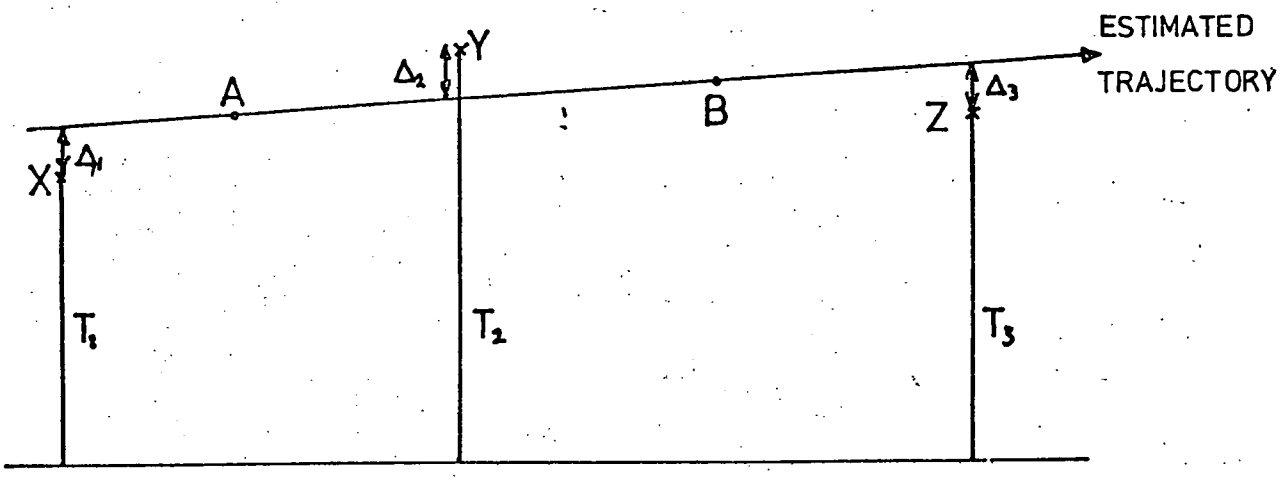

FIG 5.8 Trajectory fitting diagram

method results in equal deviations in each chamber ($D_1 = D_2 = D_3$).

Using a least squares method of determining the best estimated track would result in deviations given by $D_1 = D_3 = \sim 0.5\ D_2$ and the r.m.s. average of these three is only 4% lower than the equal deviations of the first method. Thus the equal deviation construction was retained for the determination of chamber resolution in order to simplify calculations.

It should be noted that the true deviations on figure 5.8 are $D_1 \cos\theta$ etc. where θ is the angle of the track to a line through the sense wires, but the collimation of the test beam and acceptance angle of the system were such that θ was always less than 1° (6), so that $\cos\theta \sim 1$

Deviations were only calculated for those events which were recorded as three significant drift times, any events containing a zero time or a T.D.C. range maximum (indicating no particle detected within that time) were rejected from the analysis.

5.4 Results from multicell chamber array

The deviations for each experimental run under a certain set of conditions were arranged in the form of a histogram, where the widths of such distributions give a measure of the resolution of the chambers. Two typical histograms obtained with a 2.5 GeV beam are shown in figure 5.9. The most immediate feature of the distributions is that they are not centred about zero. This was attributed to a slight displacement of the chambers in the horizontal plane and is not expected to affect the estimation of σ, which comes from the shape of the distribution only. It was realised that this shape could be analysed more simply if the histograms could be approximated by Gaussian distributions and so a comparison was made.

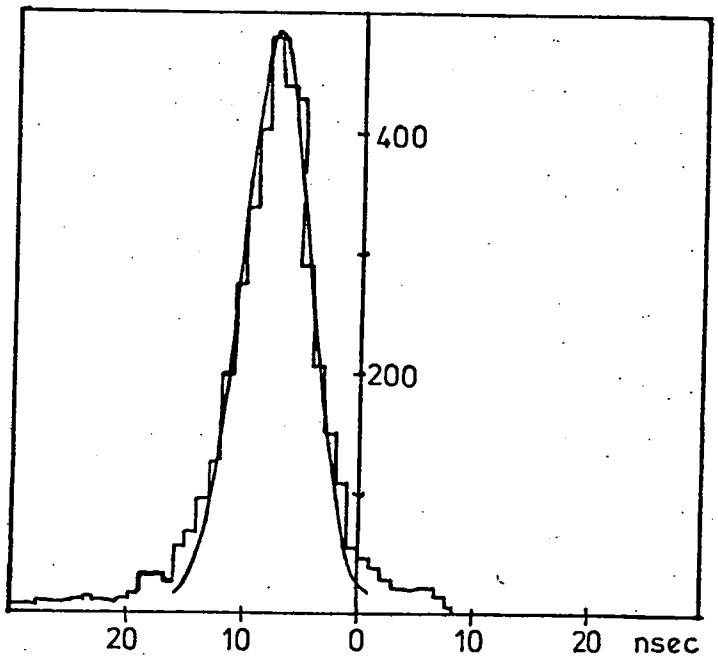

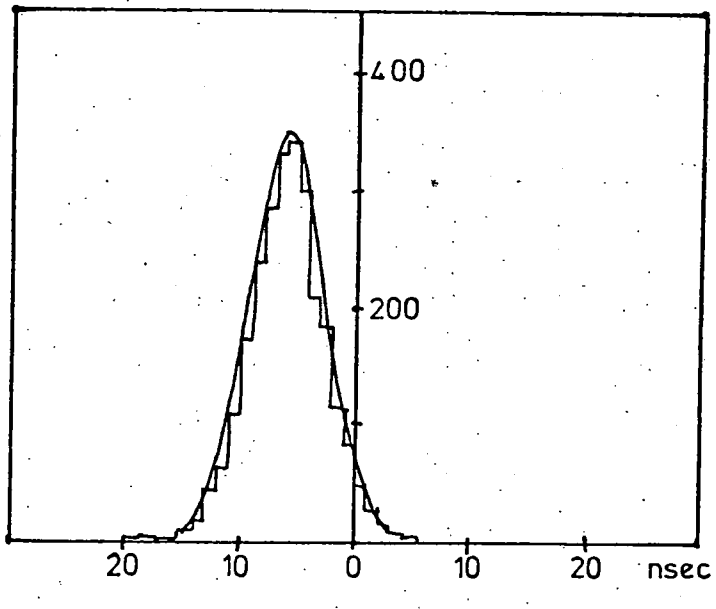

FIG 5.9 Deviation distributions showing fitted Gaussian curves. (2·5 GeV positrons)

It can be shown that the equation of a Gaussian distribution may be expressed in terms of its mean (X), its height (h) and its width (T) as follows:

$$g(x) = h \exp\left[-\alpha \left(\frac{x-X}{T}\right)^2\right] \qquad (5.1)$$

where α is a constant, and if T is given by the f.w.h.m. of the distribution (W) then $\alpha = 4 \ln 2$. Also shown on figure 5.9 are Gaussian curves calculated from 5.1, using X, h and W from the data histograms. The correlation between the data and the fitted Gaussian curves (for these and other runs) was considered adequate to allow the use of appropriate Gaussian expressions to estimate σ values for our data. A useful relationship can be found by equating expression 1 with the more usual equation for the probability function of a variable defined by Gaussian statistics and having a standard deviation σ:

$$P(x) = \frac{1}{(2\pi)^{\frac{1}{2}}\sigma} \exp\left[-\frac{(x-X)^2}{2\sigma^2}\right] \qquad (5.2)$$

Comparing the exponential terms of 1 and 2 gives

$$\sigma = \frac{T}{2\alpha} = \frac{W}{2.35}$$

i.e. standard deviation $\sigma = 0.425$ x f.w.h.m.

Applying this method to several runs (at high beam energy to minimise particle scattering) a value of $\sigma = 100 \pm 15$ μm was obtained for the spatial accuracy of the chamber.

The effect of scattering on the measurement of resolution at low beam energies is demonstrated in figure 5.10 showing drift time distributions obtained with various beam energies.

FIG 5.10 DEVIATION HISTOGRAMS FOR DIFFERENT BEAM ENERGIES

(Nanosecond Binwidths)

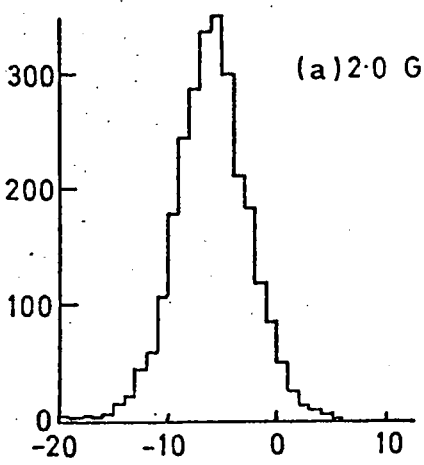

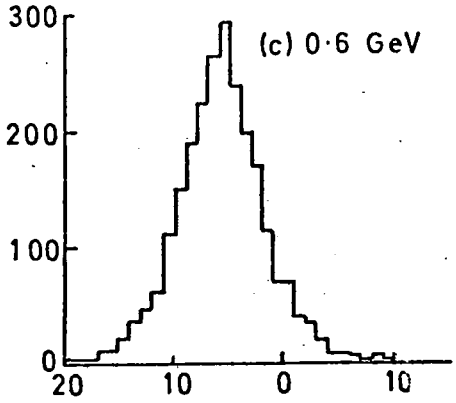

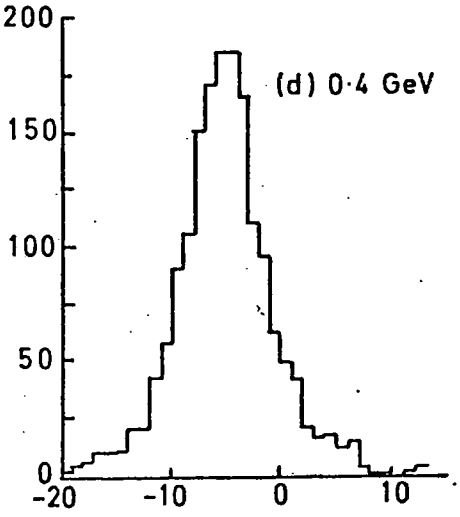

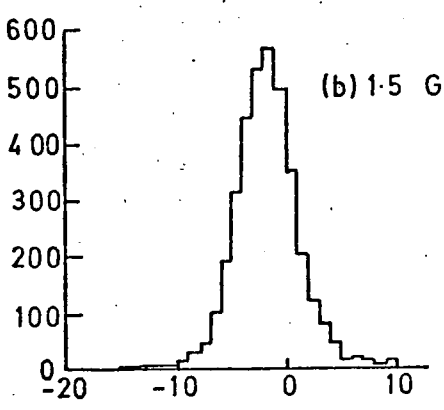

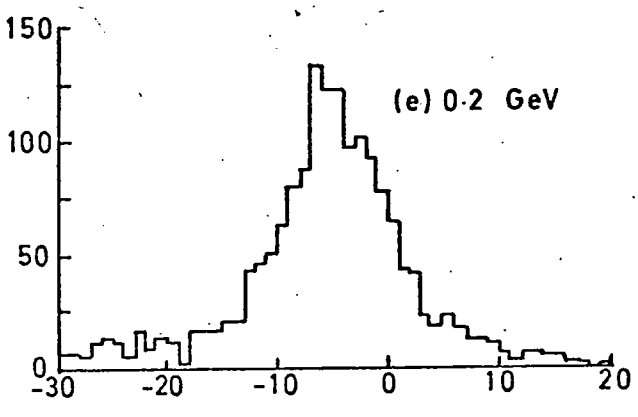

The use of f.w.h.m. to estimate σ is not so valid at low beam energies as the Gaussian shape is lost (the distribution being now partially due to non-straight tracks rather than just locational errors). A more general analysis of the data is presented in figure 5.11 which shows the percentage of measured deviations which are included between given limits on either side of the mean, for various energy runs. Thus at 2.4 GeV, approximately 70% of the deviations lie within $\pm$ 3.5 nsec of the mean value; at 0.6 GeV the figure is down to 60%; and at 0.2 GeV less than 40% of data lies within these limits. It would appear from these curves that above 1 GeV the scattering of particles has a very small effect on the distribution width.

Three further points should be noted with respect to the curves of figure 5.11.

(i) As the displacement of the distributions from zero is assumed to be due to system misalignment, the deviation distribution for one chamber would be expected to have a mean value of zero. Thus for the example above, 70% of 2.4 GeV particles would be located to within 3.5 nsec (118 μm) of their actual position in any one chamber. If rapid display of deviation histograms were possible it may be feasible to align arrays of chambers by careful adjustment until the distribution for the whole system is centred about zero.

(ii) For a Gaussian distribution, 68.3% of data is expected to lie within $\pm$ σ of the mean value, and this gives another method of estimating σ for our data, particularly at high beam energies. For the 2.4 GeV run, 68.3% of the data (marked on the axis) lies within $\pm$ 3.3. nsec, indicating a value of σ = 110 μm. The agreement with the estimation from the f.w.h.m. is supporting evidence for the Gaussian approximation.

FIG.5.11 Amount of data within given resolution — various energies of beam.

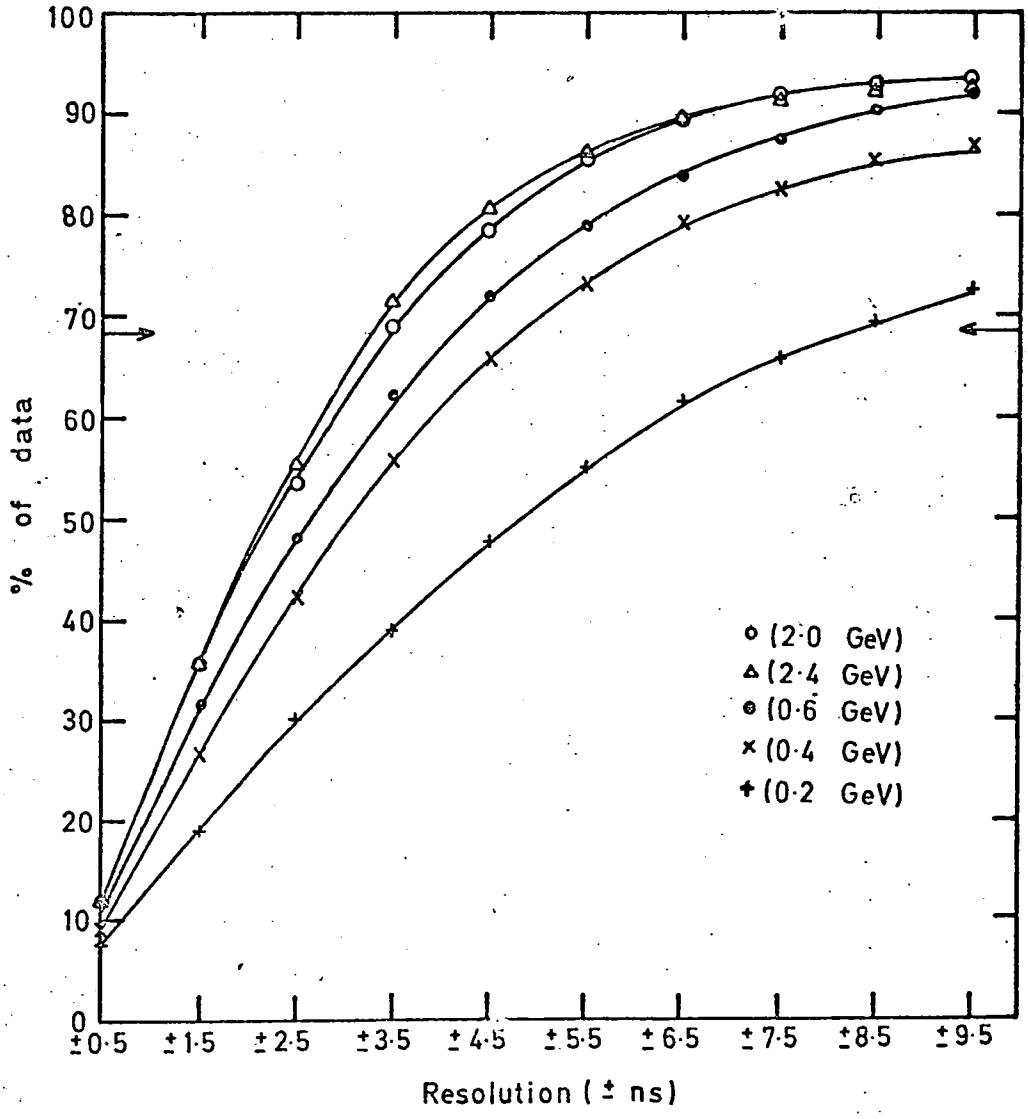

(iii) The percentage of data plotted is a percentage of all data (calculated from the raw data rather than the histograms), including deviations so large that they would almost certainly be due to non-valid events, e.g. showers or random background stop pulses (c.f. the 'plateau' of section 5.2). Consequently the estimates of σ from these curves will include this small extra contribution.

5.5 Measurements with an array of single cell chambers

Some further information on resolution was obtained from tests on an array of single cell chambers on the Daresbury test beam. The system was designed to test the operation of chambers in strong magnetic fields and will be fully described in chapter 7, but some preliminary data taken without the magnetic fields is relevant here.

The experimental system, data handling and data processing were all basically the same as in section 5.3 (see figures 5.6, 5.7 and 5.8), although the method of mounting the chambers was different (see section 7.4) and in consequence the sense wire alignment may not have been as accurate.

Runs were carried out with high energy particles ($\sim$ 2 GeV) for two applied drift fields, 500 V/cm and 900 V/cm, the drift velocities being 37 mm/μsec and 29.4 mm/μsec respectively. Figure 5.12 shows a deviation histogram for each field. The double peak was attributed to a lateral displacement of one of the sense wires combined with a beam which passed through both sides of the chamber. Thus for a track passing on one side of the displaced sense wire the drift times will be reduced resulting in a constant negative deviation superimposed on the distribution, whilst the opposite will occur for tracks on the other side. Limiting the analysis to particles in one side of the chamber only, the distributions of figure 5.13 were obtained, which include values for σ

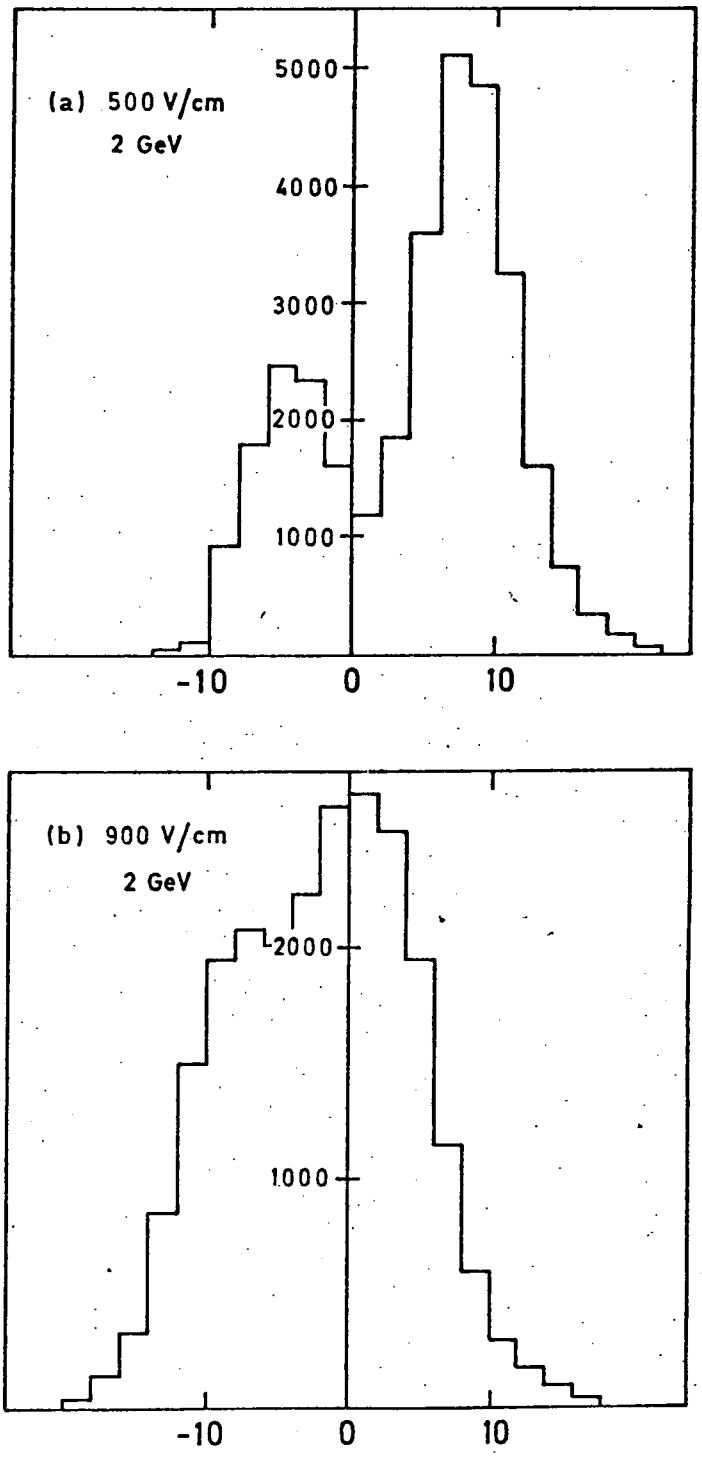

FIG 5.12 Deviation distributions from single cell chamber array.

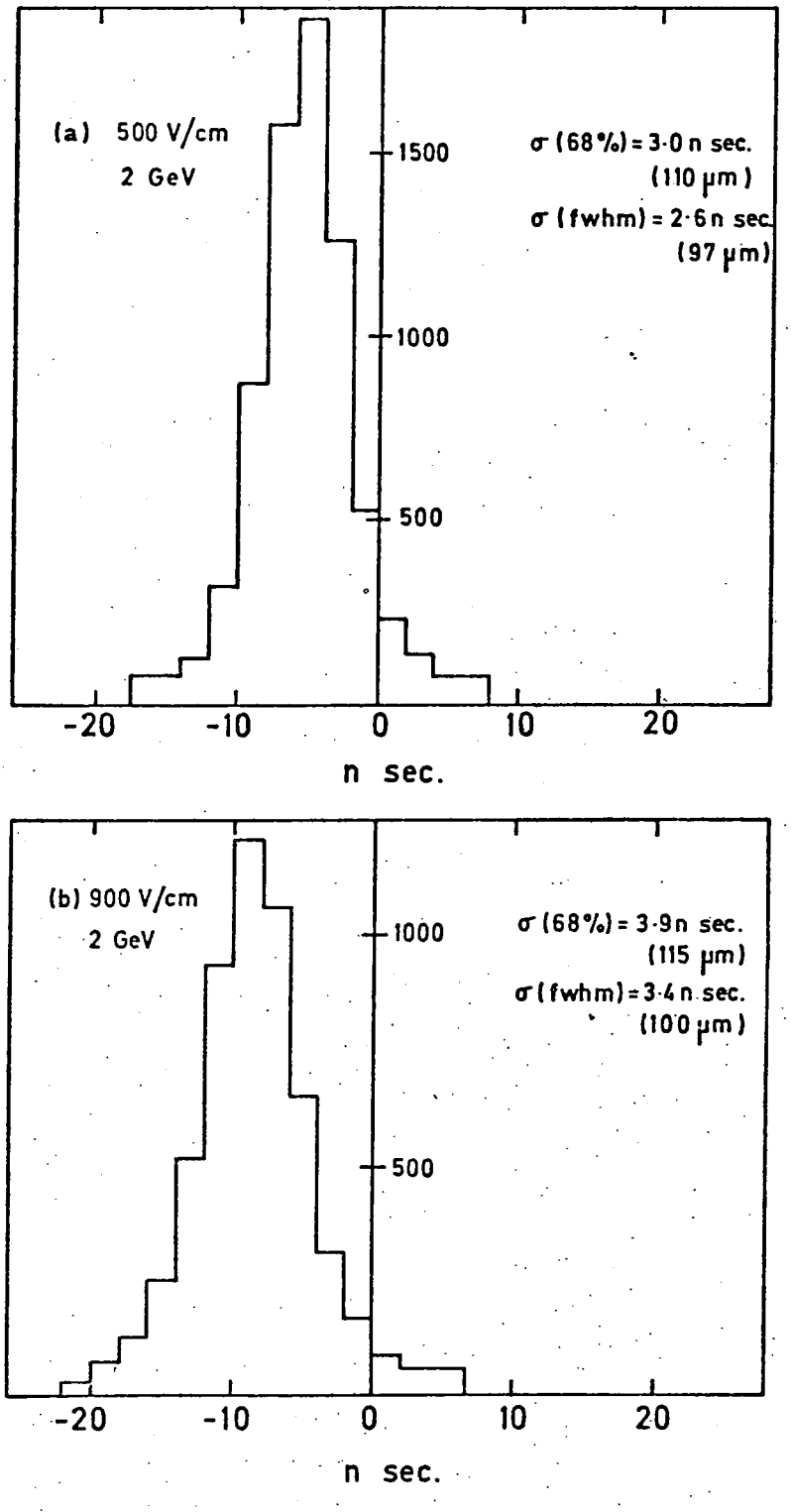

FIG 5.13 Deviation distributions from one side of single cell chambers.

calculated by the two techniques (68% of data and f.w.h.m.) described previously. The results show good agreement with those calculated from the multicell chamber tests.

The values of σ calculated up to this point have been derived from the combined results of tracks at all possible distances from the sense wire and it was decided to investigate the variation, if any, of σ with drift distance.

The data from one side of the chamber then was divided up according to the drift time recorded in the middle chamber, and the corresponding distributions from one run (at 500 V/cm) are shown in figure 5.14. Unfortunately the procedure for selecting only tracks on one side of the sense wire does not appear to have been stringent enough and a small secondary peak is evident. (This is a good example of the trouble caused by the so-called L-R ambiguity in drift chambers which will be discussed in more detail in chapter 8). Subtracting the effect of this secondary peak by eye, values of σ for the four distributions were calculated using the '68% of data' technique. The results and similar ones for a drift field of 900 V/cm are presented in Table 5.1.

Drift time nsec	σ (500 V/cm) μm	σ (900 V/cm) μm
50-150	122 ± 4	109 ± 3
150-250	125	106
250-350	120	109
350-450	127	106

Table 5.1 - σ versus drift time for two drift fields

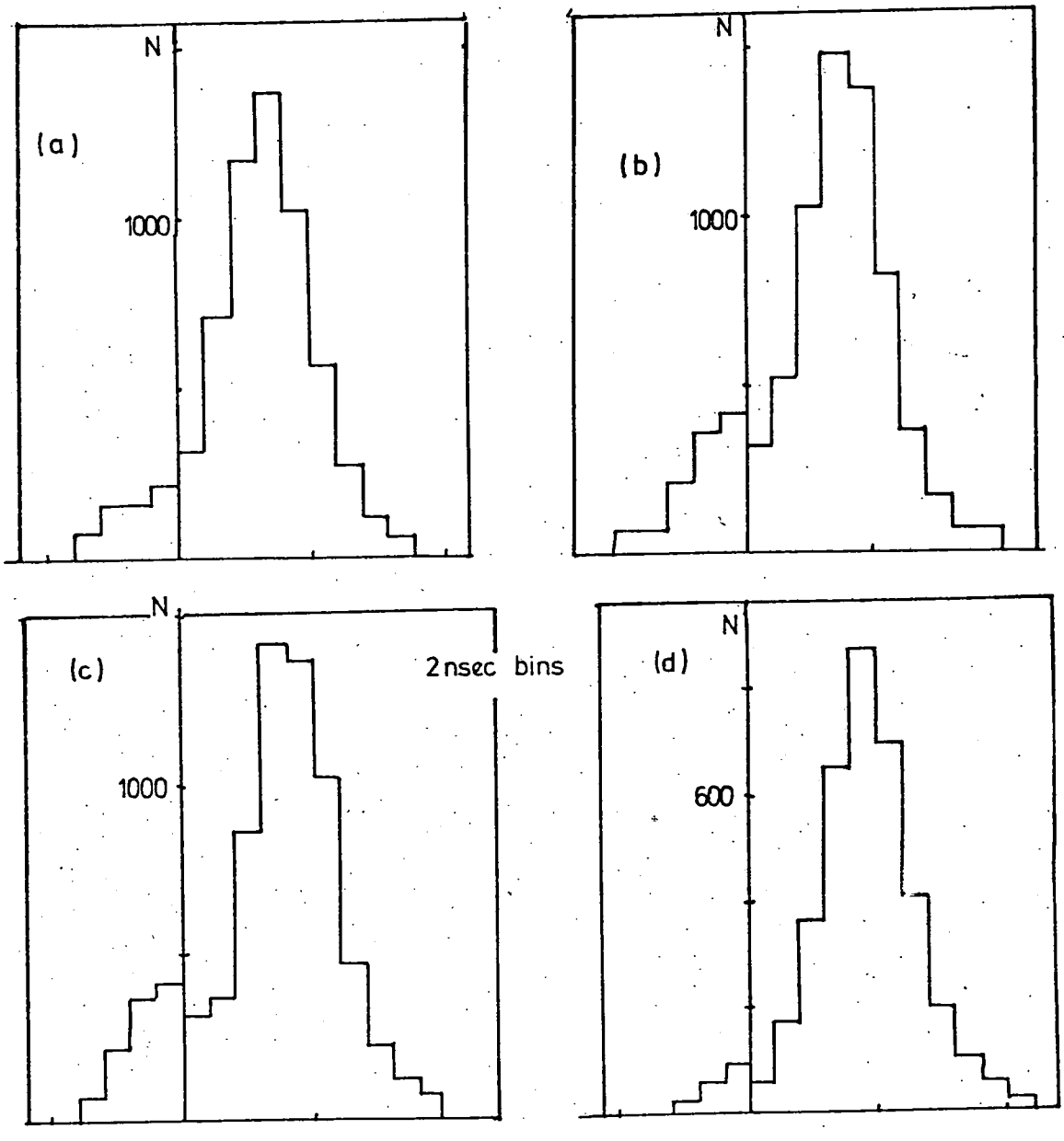

FIG 5.14 Deviation distributions for different ranges of drift times (a) 50-150, (b) 150-250, (c) 250-350 (d) 350-450 nsec.

The values of σ at 500 V/cm are higher than those calculated previously for the whole range of drift times, although a slight change in the proportion of random background events between runs (possibly due to changes in beam parameters) would be sufficient to cause such a small effect. Of more significance is the uniformity of σ across the range of drift times. Within the limits of the method of calculation there was found to be no change in the resolution of the chambers for drift distances in the range 1-16 mm.

5.6 Conclusion

The final value for the spatial resolution (σ of the error distribution) of the Durham drift chambers using argon + 10% methane and the timing system as described was estimated to be in the region of 110-120μm, which shows agreement with the rough predictions of section 5.1. The experimental values do correspond to the lower limit of the predictions however, suggesting that either the system contributions (particularly σ_v and σ_m) were lower than expected, or the intrinsic accuracy (particularly σ_d) for our gas mixture is lower than that calculated by Walenta. This latter point is investigated in the next chapter.

These values for resolution compare favourably with results by other workers for various gas mixtures, indicating further the suitability of argon + 10% methane as a drift chamber gas. For instance figure 5.15 shows the resolution results by Charpak et al (7) for their mixture of argon + 30% isobutane + 2.5 methylal, including data for tracks inclined at 42°. The rise in σ near to the sense wire is attributed to the increased effect of σ_i (section 5.1) in this region. For example for a track incident on the sense wire, the uncertainty in position will be equal to half the mean separation of the primary ionisation, P. (i.e. $P/2 \sim 150$ μm)

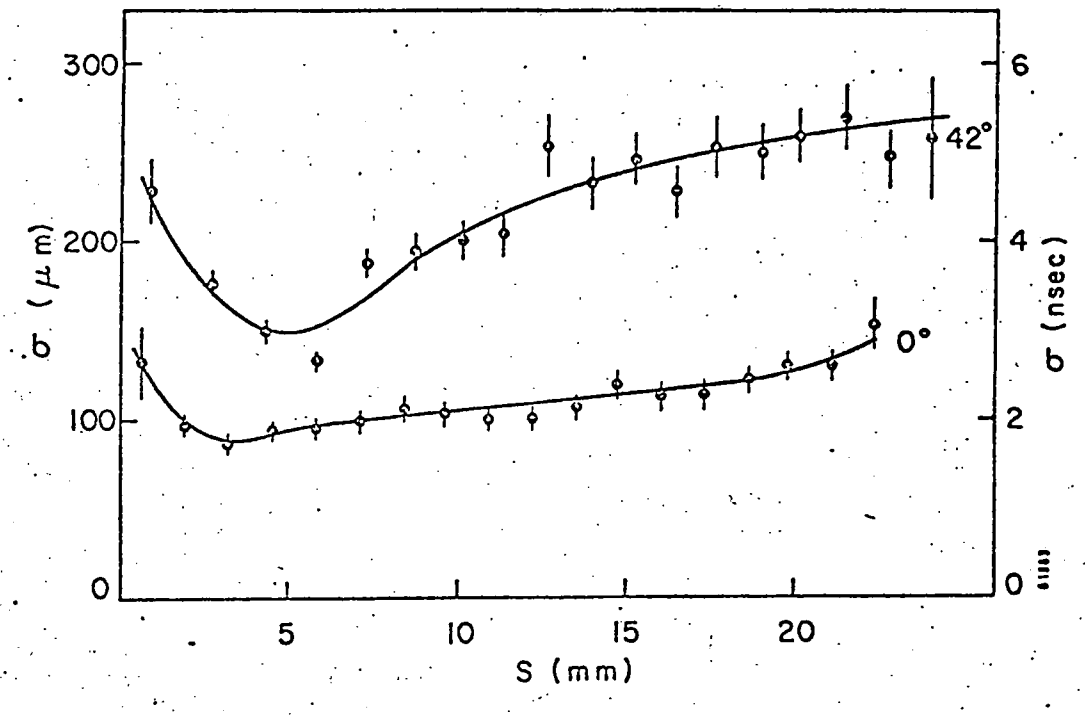

FIG 5.15 Resolution versus drift distance, (s), for argon/isobutane from Charpak et al (7)

The decreased accuracy for tracks at 42^{o} to the normal as indicated on figure 5.15 can be explained by reference to the contribution of σ_i. Using the model for inclined tracks shown in figure 4.19, we see that for a track in the 'parallel field' region, inclined at an angle θ to the normal, there will be a possible spread of measured drift lengths given by $p_p \sin\theta$. This is in addition to the other contributions to σ which should remain constant. For $\theta = 42^{o}$, $p_p \sin\theta$ will be approximately 200 μm.

Results from the tests on angled tracks at Durham using a radioactive source, and described in section 4, indicate that the resolution for angled tracks varies with the direction of tilt as well as angle. Figure 5.16 shows the full width half maximum of drift time distributions (converted to distance) for two independant runs. As the field in the drift chambers is symmetrical about the sense wires, the effect is presumably due to the divergence of the beam of particles. Taking the mean of the data from both runs and both tilt directions gives the variation of resolution shown in figure 5.17. A slight worsening of resolution with angle is seen, although once again any effects are swamped by the uncertainty on the particle position.

Other measurements of resolution in argon + 30% isobutane have been made, for instance by Sadoulet and Litke (8), and Bateman and Connolly (9). Sadoulet and Litke obtained the values shown in figure 5.18, with a chamber having single voltage cathode planes 8.5 mm apart, and potential wires. The field appears to have been about 700 V/cm. They claim their results represent the intrinsic accuracy of the chambers, other errors being accounted for in the analysis. Bateman and Connolly have reported $\sigma = 190$ μm for drift distances of 1 cm, although this is thought to have been limited by the scattering of the 1 GeV/c π^{+} particles of their beam. Saudinos et al (10) working with pure methane

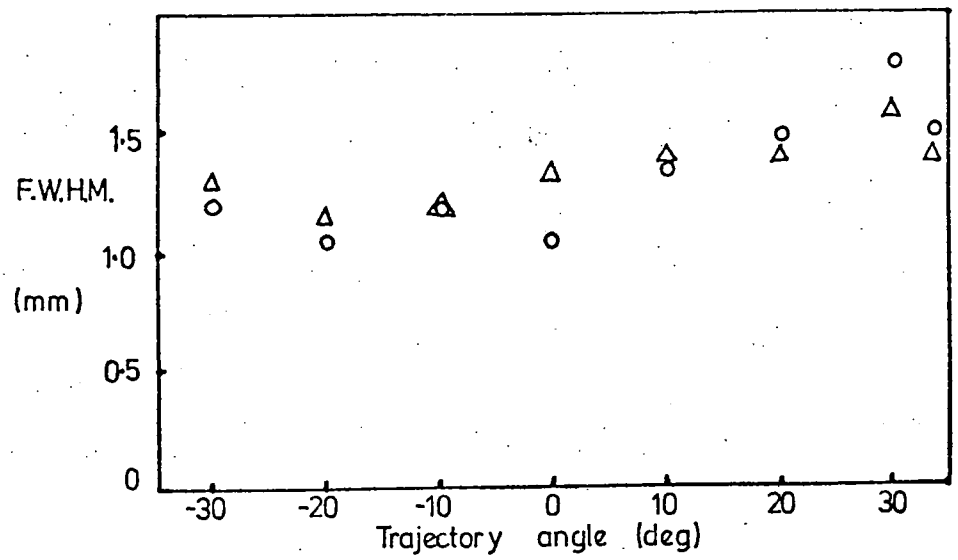

FIG. 5.16 Resolution versus angle of track to normal.

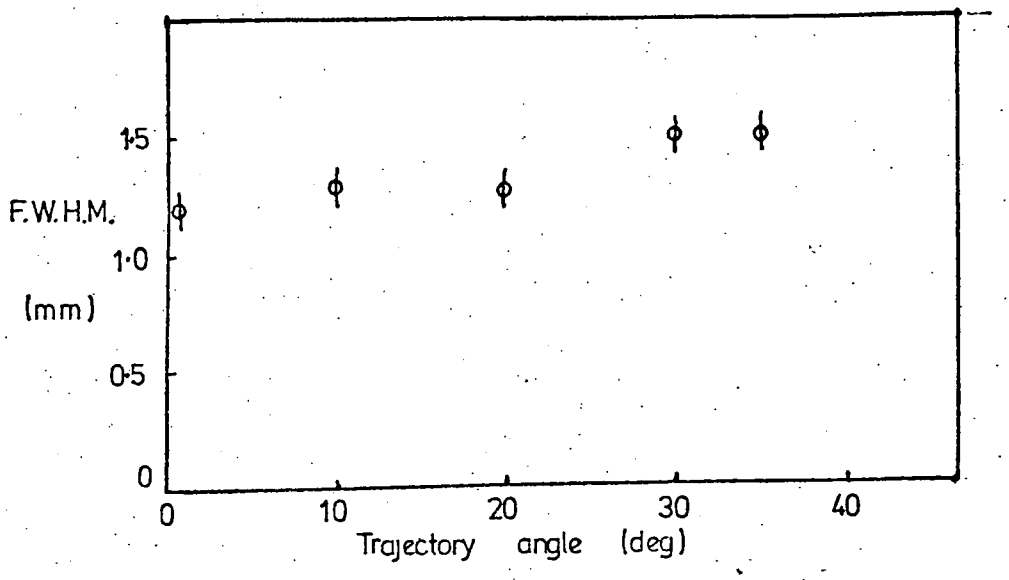

FIG. 5.17 Resolution versus track angle, averaged over 2 runs and 2 directions of tilt.

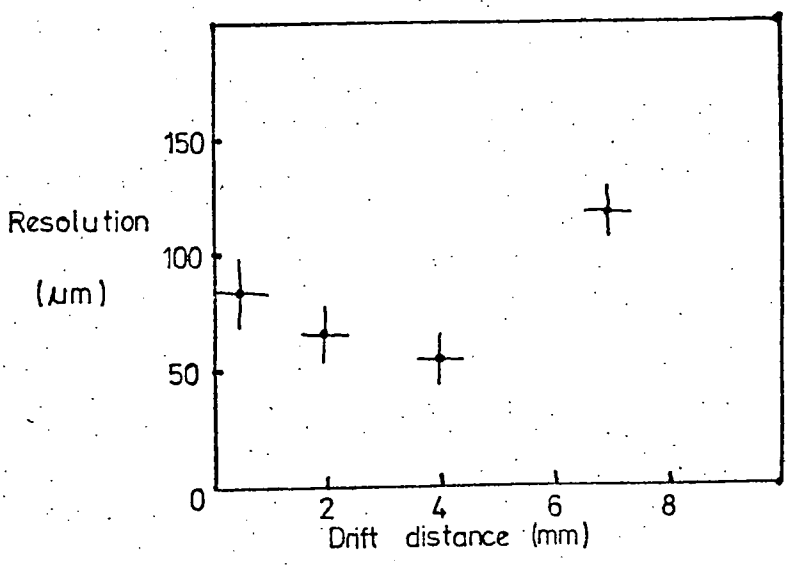

FIG 5.18 Resolution versus drift distance, from Sadoulet and Litke.

in differently designed chambers have quoted $\sigma = 170$ μm for 7 cm drift lengths, going to $\sigma = 550$ μm for 50 cms. 350 μm was the overall resolution of large (4 m^2) chambers described by Cheng et al (11) using argon + 80% ethylene, but again this is thought to be due to scattering of their beam (160 MeV protons).

CHAPTER 5 - References

1. A.H. Walenta, Nuc. Inst. Meth. 111 (1973) 467

2. C.S. Wu, 'Interaction of Beta particles with matter' in Nuclear Spectroscopy (Ed. F. Ajzenberg-Selove), Academic Press, New York, (1960).

3. D.J. Thompson, Daresbury Laboratory Internal Report, TM/70 (1972)

4. J.M. Breare, R. Browell and K.A. Short, Durham University Internal Report NI-74-5 (1974)

5. F. Golding, Daresbury Laboratory Internal Report (April 1973)

6. J.M. Breare, R. Browell and K.A. Short, Durham University Internal Report NI-75-1 (1975)

7. A. Breskin, G. Charpak, B. Gabioud, F. Sauli, N. Trautner, W. Duinker and G. Schultz, Nuc. Inst. Meth. 119 (1974) 9

8. B. Sadoulet and A. Litke, Nuc. Inst. Meth. 124 (1975) 349

9. J.E. Bateman and J.F. Connolly, Rutherford Laboratory (High Energy Physics Division) Internal Report RL/75/044 (1975)

10. J. Saudinos, J.C. Duchazeaubeneix, C. Laspalles and R. Chaminade, Nuc. Inst. Meth. 111 (1973) 77

11. D.C. Cheng, W.A. Kozanecki, R.L. Piccioni, C. Rubbia, L.R. Sulak, H.J. Weedon and J. Whittaker, Nuc. Inst. Meth. 117 (1974) 157.

CHAPTER SIX

THE ELECTRON DRIFT PROCESS

6.1 Introduction

The mechanism by which electrons move through a gas under the influence of an applied electric field is the process which directly determines the operating characteristics of a drift chamber. The two parameters of particular importance which can be derived from a study of this mechanism are the electron drift velocity w, and the diffusion coefficient D, which limits the intrinsic spatial accuracy of such devices.

This chapter attempts to describe and explain the factors affecting these parameters and thus predict actual values for various gases, particularly argon + 10% methane. This will be achieved by the application of simple classical models combined with experimentally determined relationships.

A much more rigorous and mathematical treatment of the whole theory of electron drift and diffusion is presented by Huxley and Crompton (1) who have also collected experimental data on various transport coefficients for many gases. Their work and that of Palladino and Sadoulet (2) on the same subject, have provided the basis of much of the theoretical work included in this and the next chapter.

6.2 General theory of electron motion in electric fields

A free electron in a gas with no external electric fields, moves with a velocity v_o in thermal equilibrium with the gas molecules, undergoing elastic collisions with them, as shown in figure 6.1(a). Kinetic theory indicates that under these conditions there will be

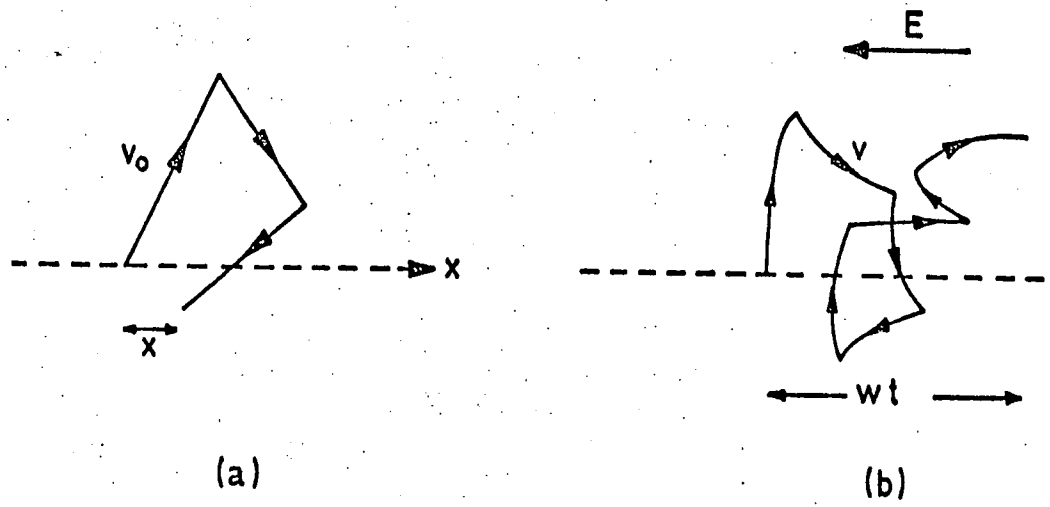

FIG. 6.1 Electron motion in a gas, with and without electric field.

a definite distribution of electron velocities (Maxwellian Distribution), and correspondingly of electron energies. The mean velocity, $\bar{v}$, at temperature $T^{o}K$ is given by

$$\tfrac{1}{2} m \bar{v}_o^2 = \frac{4}{\pi} k T \qquad (6.1)$$

where m is the electron mass and k is Boltzmann's constant. At $15^{o}C$ this gives $\bar{v}_o \sim 10^7$ cm/sec and the corresponding electron energy as approximately 3×10^{-2} eV.

Note that from figure 6.1, there will be some spatial displacement of the electron from its original position after a time t seconds. This constitutes the principle of electron diffusion which will be dealt with in section 6.4.

In the presence of an electric field E, figure 6.1(b) applies. That is the electron still exhibits its random motion but with a new velocity v, and due to the accelerating force exerted by E there is a net drift velocity w superimposed on the motion. This velocity describes the overall effect of the field, and at no time is the electron actually moving at this velocity. Typical values of w lie between 10^5 and 10^7 cm/sec, and are usually functions of E. The diffusion effects are still applicable to this motion and so w represents a mean value of drift velocity for a single electron or alternatively the velocity of the centroid of a group of electrons.

A useful concept in considering the motion of charged particles in electric fields is that of mobility, μ, given by,

$$w = \mu E \qquad (6.2)$$

For the motion of ions, μ is virtually independent of E, at least for values of E/p up to about 20 V/cm torr, where p is the gas

pressure in mm of mercury (torr). The first simple theory of ionic mobility was put forward by Langevin (3) in 1903 and gave a value of

$$\mu = \frac{e\lambda}{M\bar{v}} \qquad (6.3)$$

where λ is the ionic mean free path, M is the common ionic and molecular mass and e is electronic charge. The theory made many simplifying assumptions and several more rigorous theories have since been developed although all indicate $w \propto E$ at low E/p. A comprehensive review of these theories, including Langevin's original is presented by McDaniel (4).

Unfortunately the picture for electron motion is more complex and the concept of mobility must be used with caution, as in general μ for electrons is a function of E. The main reasons for the greater complexity of electron motion are summarised below.

(a) The mean fractional energy loss Q, by a particle of mass m, in collision with a particle of mass M, is given by,

$$Q = \frac{2mM}{(m+M)^2} \qquad (6.4)$$

For ions, $m \sim M$ and $Q \sim \frac{1}{2}$, so that ions do not gain much energy from an electric field. For electrons however $M \gg m$ and Q reduces to $2m/M$ which is very small. Thus electrons even at very low values of E/p rapidly acquire energies far in excess of thermal energies. The Townsend energy factor η is defined as the ratio of the mean electron energy to the thermal molecular energy, and figure 6.2 from Healey and Reed (5) shows this energy factor for electrons in neon

and argon. Thus electrons in argon at E = 1000 V/cm and atmospheric pressure may be expected to be at 250-300 times thermal energy, (i.e. 7-9 eV), and therefore random velocities will be ~ 17 times v_o. The effect of inelastic collisions (with larger Q values) prevents η from increasing indefinitely and also lowers it for molecular gases.

(b) Whereas ions in the electric fields which we are considering rarely attain sufficient energy to cause excitation of the gas molecules, so that all their collisions are elastic, this is not the case with electrons. For instance in argon, the threshold for electronic excitation is 11.5 eV (6) and this energy will be attained by increasing numbers of electrons as E is increased above a few hundred volts/cm. For such inelastic collisions, Q is increased, effectively limiting the mean energy of the electrons and thus distorting the shape of the electron velocity distribution. The effect is more pronounced in molecular gases such as methane, where inelastic collisions due to vibrational and rotational excitation are a significant process at energies below 1 eV.

(c) The process of electronic elastic scattering is not so straightforward as is predicted by simple classical theory. This states that the mutual potential energy of an electron and molecule is proportional to r^{-4} where r is their separation, and that the cross section for elastic scattering is therefore inversely proportional to electron velocity v. Simultaneous work by Ramsauer (7) and Townsend and Bailey (8) discovered that for certain gases, notably the heavy noble gases, there exists an anomolous region of low cross section for low electron energies (~ 1 eV). Figure 6.3 shows the variation of scattering cross section for noble gases,

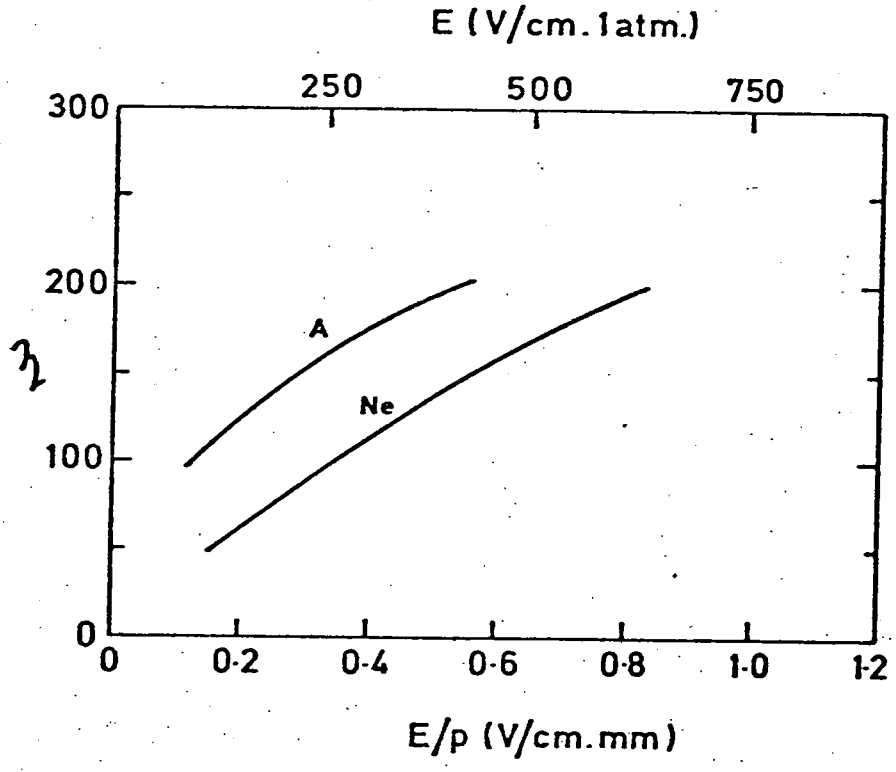

FIG 6.2 TOWNSEND ENERGY FACTOR η FOR ARGON AND NEON.

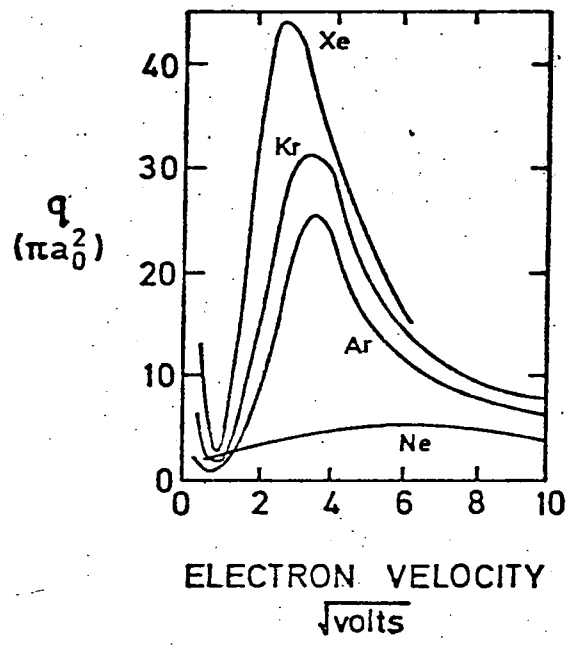

FIG 6.3 COLLISION CROSS SECTIONS FOR NOBLE GASES, FROM BRODE (9)

collected and averaged from many sources by Brode (9). The explanation of the effect requires the use of quantum theory, and in particular the method of partial waves. It can be thought as an interference effect involving the major component of the incoming wave (electron) and the deep, narrow potential well representing the gas atom.

(d) Because of the effect of inelastic collisions and the complex dependence of cross section on electron energy, the distribution of electron velocities $f(v)$ is no longer necessarily Maxwellian, which is derived by assuming only elastic collisions and a cross section, q, proportional to v^{-1}. A different distribution was derived by Druyvesteyn (10) again assuming elastic collisions, but this time with q independent of v. The form of the velocity distribution is obviously relevant in calculations where averaging is performed over all electron velocities, although the difference introduced in the final results of such calculations merely takes the form of a dimensionless 'averaging' factor. The value of this factor is discussed in Appendix I. In general because of inelastic collisions, the form of the distribution is not necessarily dependent on $q(v)$. It is found however that most practical situations can be described by assuming one of the distributions mentioned above, and by selecting a suitable value of r, such that $q \propto v^{-r}$, from experimental data.

In view of the points listed above it is clear that the rigorous analysis of electron drift is a complex problem, particularly when the gas involved is a mixture of noble gas and molecular gas and several mechanisms will be competing. This is indicated from the measured drift velocity in our mixture of argon + 10% methane

(figure 4.8) when above 200 V/cm, w is decreasing with increasing E, contrary to the conventional concept of mobility.

In the following section the above points will be applied to estimating w for argon and methane and then by combining parameters in the appropriate proportions, the behaviour of w for argon methane mixtures may be explained.

6.3 Drift velocity for specific gases

6.3.1 General

The method of calculating the variation of w with electric field, used in this section is to first derive a simple expression for w, which includes terms involving mean electron velocity $\bar{v}$, mean free path λ between collisions ($\alpha\ q^{-1}$) and averaging constants. This can then be solved for any E using experimentally determined data for mean electron energy and collision cross section. An alternative technique has been used by Palladino and Sadoulet (2) based on a theory first developed by Morse et al (11). This involves solving, by numerical methods and using experimental cross section data, expressions based on the Boltzmann transport equations. This allows both w and electron energy to be determined theoretically, and further reference to this work will be made later.

The expression for w derived here comes from simple equations of motion. We consider an electron after a collision with a gas molecule in a field E, having a velocity v at angle θ to the field direction x. The distance covered by the electron in the x direction in time t is given by,

$$d = t\ v \cos\theta + \tfrac{1}{2}\ \frac{eE}{m}\ t^2 \qquad (6.5)$$

if we assume the elastic scattering cross section is isotropic then averaging over many collisions

$$d = \tfrac{1}{2} \frac{eE}{m} t^2 \qquad (6.6)$$

In order to find the mean displacement in the x direction ($\bar{d}$) between collisions we replace t by t_c the time between collisions and then average over the distribution of t_c. This distribution is given by

$$g(t_c) = \frac{1}{T} \exp(-t_c/T) \qquad (6.7)$$

where T is the mean free time between collisions, $= \lambda/v$ where λ is the mean free path. The mean of the t_c^2 distribution is thus given by,

$$\overline{t_c^2} = 2T^2 \qquad (6.8)$$

Thus

$$\bar{d} = \frac{eE}{m} T^2 \qquad (6.9)$$

For a hypothetical electron with constant velocity v there are 1/T collisions per second and hence the net velocity in the x direction (i.e. w) is given by

$$w = \bar{d} \cdot \frac{1}{T} = \frac{eE}{m} T \qquad (6.10)$$

or

$$w = \frac{eE}{m} \frac{\lambda}{v} \tag{6.11}$$

Taking an average over the distribution of electron velocities

$$w = \frac{eE}{m} \left(\frac{\bar{\lambda}}{v} \right) \tag{6.12}$$

it can be shown that equation 12 is only valid for the special case of constant T, and that in general

$$w = k_{\lambda} \frac{eE}{m} \left(\frac{\bar{\lambda}}{v} \right) \tag{6.13}$$

where k_{λ} depends on the variation of λ with v. Even more generally we have

$$w = k \frac{eE}{m} \frac{\lambda}{v} \tag{6.14}$$

where k now also depends on the particular 'mean' value of v used and on the assumed electron velocity distribution f(v). The evaluation of k is discussed in Appendix I but as an example table 6.1 shows the value of k for Maxwell and Druyvesteyn distributions, for $\lambda \propto v^r$, and a value of v obtained from mean electron energy measurements (i.e. $\sqrt{\bar{v}^2}$)

	r		
	1	0	-1
Maxwell	1.38	0.92	0.46
Druyvesteyn	1.24	0.82	0.41

Table 6.1 - Value of k in equation 14 using $\sqrt{\bar{v}^2}$.

To solve equation 14 we need to know the value of the mean electron velocity, usually determined from the mean electron energy ϵ and its variation with E. A useful parameter in this context is the characteristic energy ϵ_k, which is closely related to the actual mean energy ϵ. It is defined as the ratio between the diffusion coefficient D and mobility μ, and is readily determined experimentally (12). The diffusion coefficient D is discussed further in section 6.4 but it is relevant here to mention that it was first given by Townsend (13) as

$$D = \frac{\lambda \bar{v}}{3} \tag{6.15}$$

From equation 14,

$$\mu = \frac{ke}{m} \lambda v^{-1} \tag{6.16}$$

and so we see that the ratio D/μ is proportional to $m v^2/e$, thus,

$$\frac{D}{\mu} = \frac{F}{e} \frac{1}{2} m \bar{v}^2 \tag{6.17}$$

$$= \epsilon_k \text{ in electron volts.}$$

or

$$\sqrt{\bar{v}^2} = \sqrt{\frac{2 \epsilon_k}{Fm}} \tag{6.18}$$

As with k, the value of F is dependent on $\lambda(v)$ and $f(v)$, and is discussed in Appendix I. Table 6.2 shows F values for $\lambda \alpha v^r$ as before,

	r		
	1	0	-1
Maxwell	0.44	0.66	1.33
Druyvesteyn	0.51	0.76	1.52

Table 6.2 - Values of F in equation 17.

In the following calculations the value of v used to solve equation 14 comes from $\mathcal{E}_k$ measurements. Thus our value of k in equation 14 is the product of the k of table 6.1 (because we are using $\sqrt{\bar{v}^2}$) and $\sqrt{F}$ from equation 6.2 (because we are using $\mathcal{E}_k$ rather than $\mathcal{E}$). The resulting constant is tabulated in table 6.3

	r		
	1	0	-1
Maxwell	.92	.75	.54
Druyvesteyn	.89	.71	.5

Table 6.3 - Values of k in equation 14 using v obtained from $\mathcal{E}_k$ measurements.

6.3.2 Argon

Figure 6.4 shows the variation of $\mathcal{E}_k$ with applied electric field. The curve is drawn from Palladino and Sadoulet (2) and represents both the experimental data of many authors (12) and their own theoretical predictions. The variation of $\mathcal{E}_k$ are as expected, that is high $\mathcal{E}_k$ even at low fields because of the low energy loss per collision, and $\mathcal{E}_k$ rising with E until part of the electron distribution reaches 11.5 eV, the threshold for excitation, when the large energy loss per collision keeps $\mathcal{E}_k$ relatively constant.

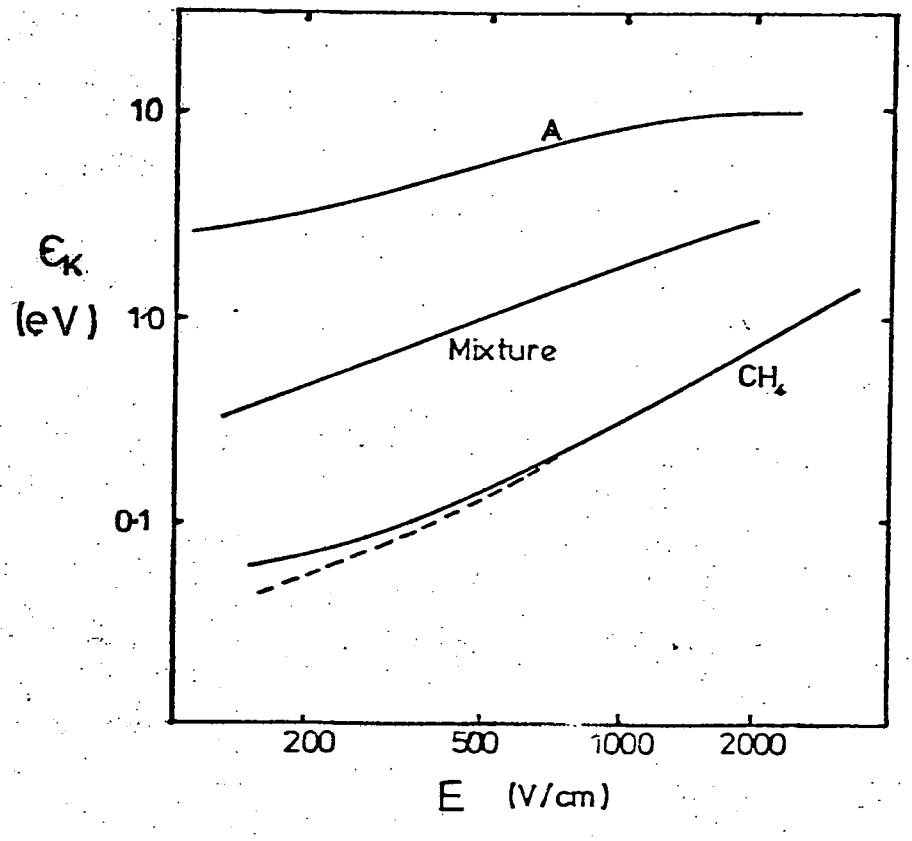

FIG 6.4 Electron energy versus electric field.

Figure 6.5 shows the accurate variation of momentum transfer cross section q_D with electron energy from Frost and Phelps (14). The parameter q_D differs from the total collision cross section q_s in that it includes a factor to account for any non-isotropy of scattering. For isotropic scattering $q_D = q_s$ and the results of Massey and Burhop (15) show that for electrons the two values agree closely at low electron energies ($<$10 eV) and that $q_D > q_s$ at higher energies. It is however the value of q_D which is more relevant in calculations of drift velocities. The corresponding value of mean free path λ is found from

$$\lambda = \frac{1}{Nq_D}$$

where N is the number density of gas molecules ($2.7 \times 10^{19} cm^{-3}$ at N.T.P.). Using values from figures 6.4 and 6.5 equation 14 can now be solved for any value of E, but the following discussion will indicate the general form of the variation of W with E.

From equation 14 we have

$$w \alpha E.\lambda.v^{-1} \qquad (6.19)$$

For E between 100 and 2000 V/cm we see that ϵ_k is between 2 and 8 eV. Assuming $\epsilon_k \sim \epsilon$, then for this range $q_D \alpha \epsilon$ and therefore $\lambda \alpha \epsilon^{-1}$ As v is obviously proportional to $\epsilon^{\frac{1}{2}}$ we have

$$w \alpha E \epsilon^{-1.5} \qquad (6.20)$$

Figure 6.4 shows that for E$<$1000 V/cm, $\epsilon \alpha E^{.45}$, and therefore $w \alpha E^{.33}$. For E$>$1000 V/cm ϵ is approximately independent of E and therefore $w \alpha E$.

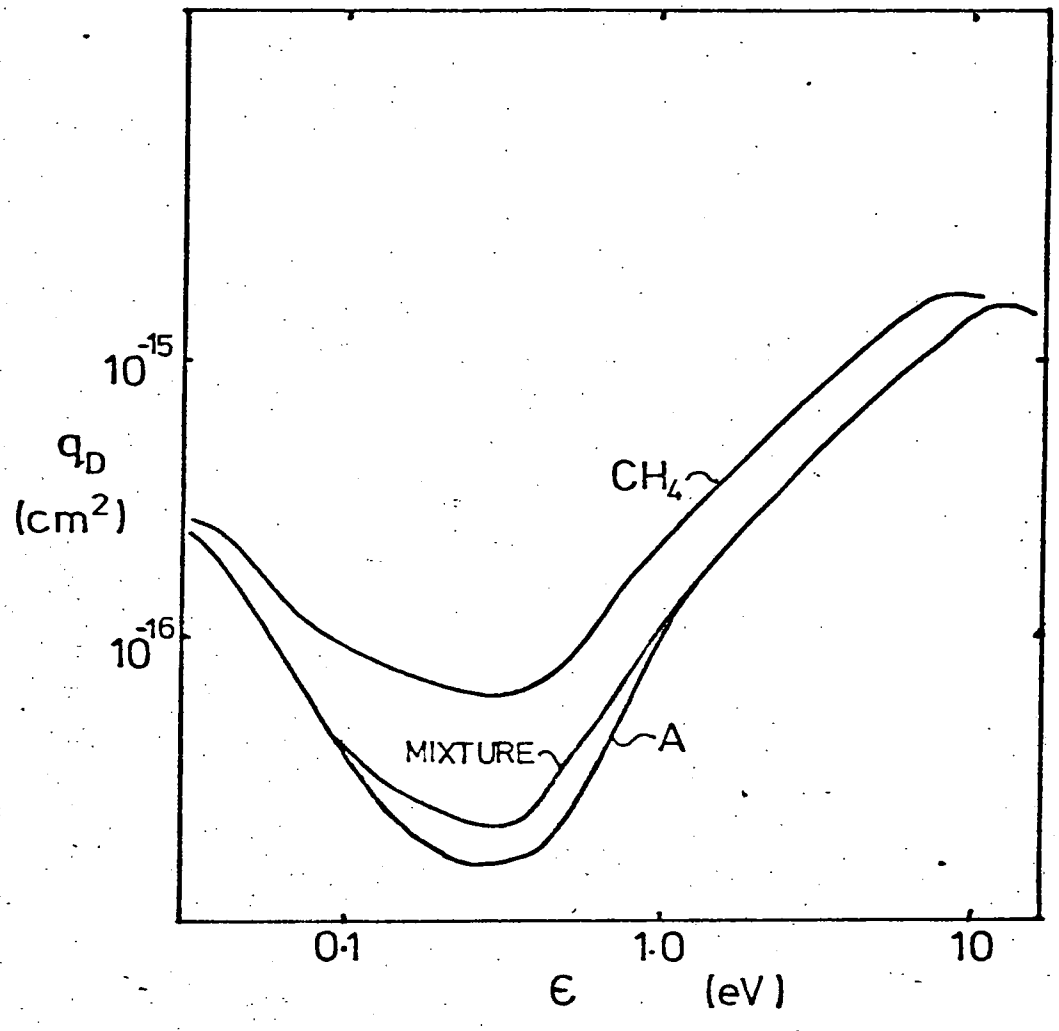

FIG 6.5 Momentum transfer cross section versus electron energy.

Substituting experimental values of λ and v into equation 14 gives the actual values for w, and the results of these calculations are shown in figure 6.6, compared with the experimental variation of w determined by Nielsen (16). The shape of the experimental curve is accurately predicted and the best numerical agreement is obtained by assuming a value of $k \sim 0.7$ as shown in the figure.

Figure 6.7 showing experimental data for w in argon, collected from many sources (2), shows that the simple model is accurate over several orders of magnitude of E.

6.3.3 Methane

We can make the same predictions for methane, using the energy versus E variation from figure 6.4. The solid line represents the experimental variation found by Cochran and Forester (17) and the broken line is the theoretical prediction of Palladino and Sadoulet (2) The overall electron energy is much lower than for argon because of the possibility of large energy loss collisions causing molecular vibrations which occurs in methane below about 0.4 eV. The energy does rise steadily with E however as the actual cross section for these collisions is small. ($5 \times 10^{-17} cm^2$(2)).

Unfortunately the overall momentum transfer cross section is difficult to accurately establish below about 1 eV, and in figure 6.5 the q_D curve in this region is drawn by assuming a similar shaped curve to argon and adding the constant 5×10^{-17} cm^2 due to inelastic collisions. The variation of w with E was calculated as for argon, and the results are shown in figure 6.8, compared with our experimental data taken from figure 4.11. The fit as shown was obtained by assuming a value of $k = 0.8$. The agreement here is worse than for argon, presumably due to the imprecise values of collision cross section below 1 eV.

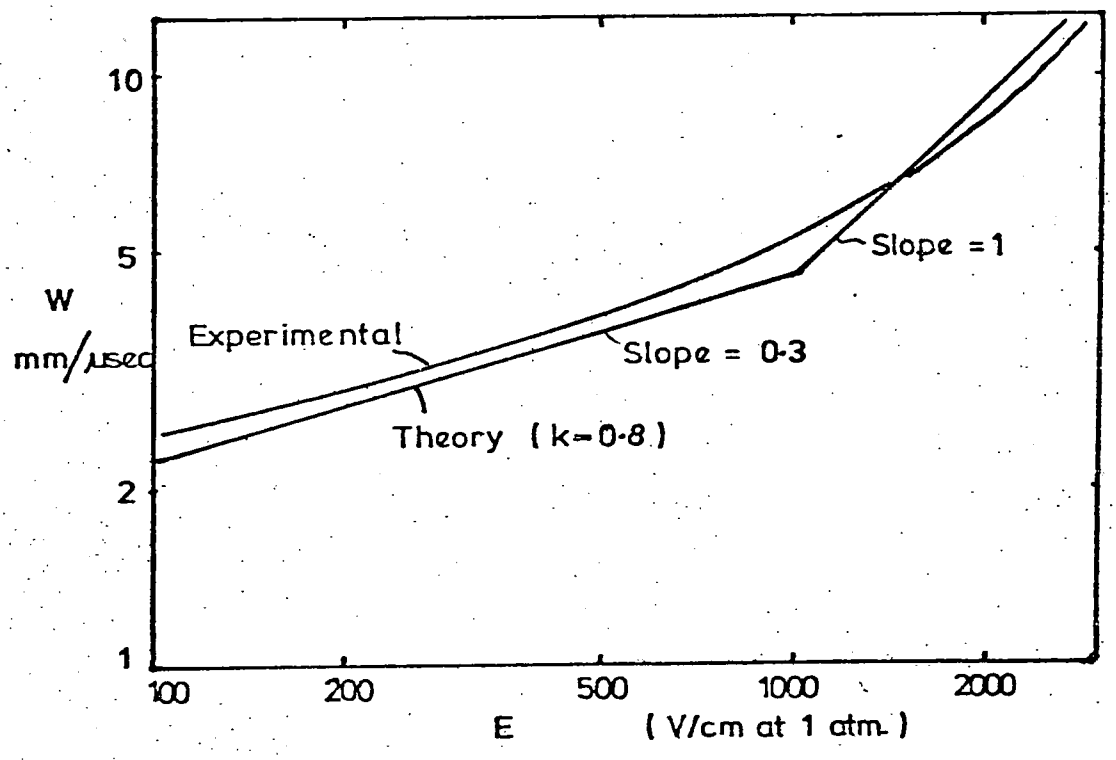

FIG 6.6 Comparison of theory and experimental data (16) for drift velocity in argon

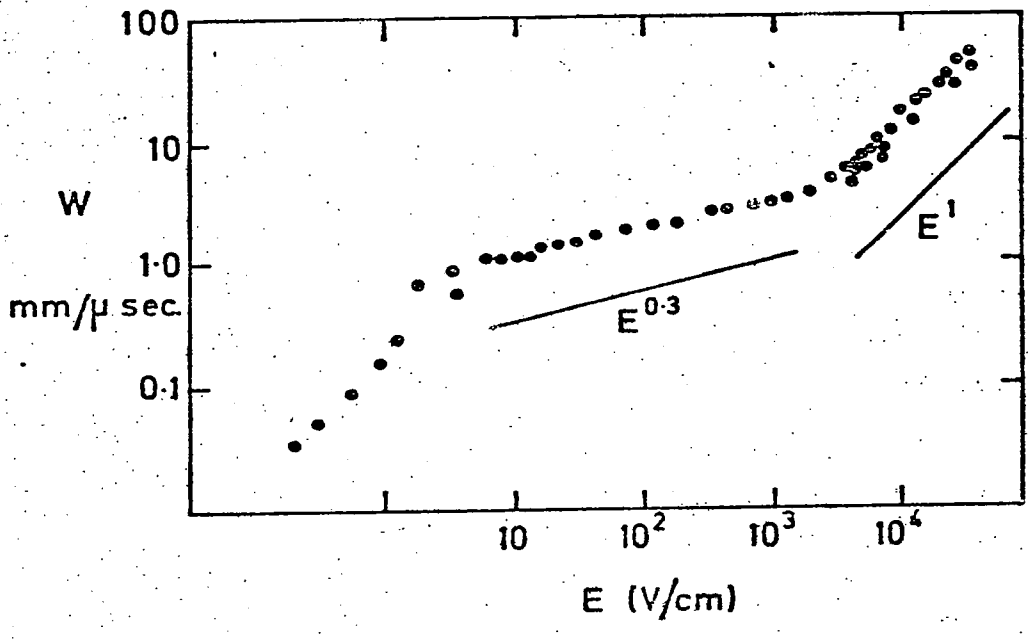

FIG 6.7 Drift velocity in argon over large range of E, (2).

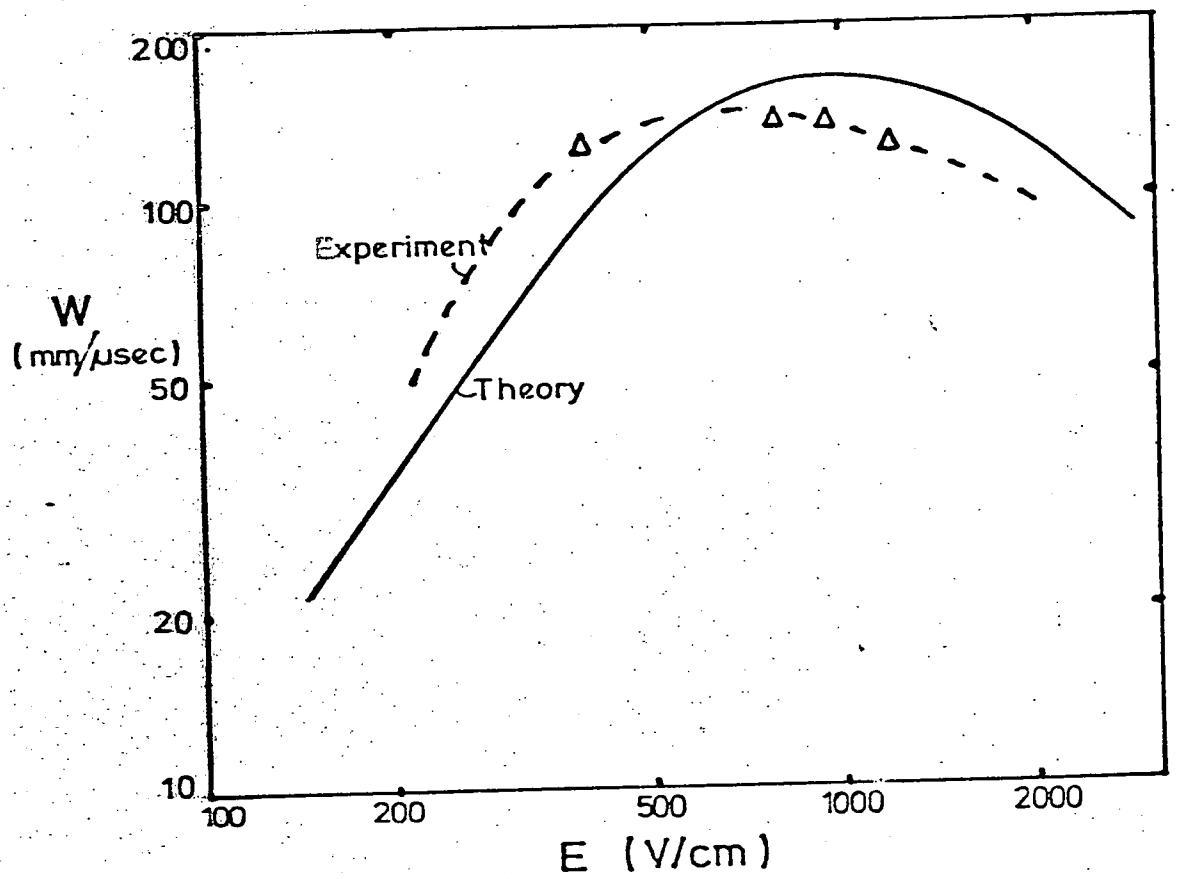

FIG 6.8 Drift velocity in methane, prediction and experiment.

6.3.4 Argon-Methane mixtures

The main problem here is in estimating the variation of electron energy with electric field. Calculations of electron energy for argon isobutane mixtures by Palladino and Sadoulet (2) indicate that for 10% hydrocarbon content, ϵ_k is given very approximately by ϵ_k (mixture) = $\sqrt{\epsilon_k(\text{Argon})\epsilon_k(\text{iso.})}$. Applying this to argon + 10% methane, and making adjustments to give the best final fit to the experimental values of w, gives the estimated variation of ϵ_k shown in figure 6.4, where ϵ_k is approximately proportional to $E^{.8}$.

The net cross section was obtained simply by adding the values for argon and methane in the appropriate proportions. The result is shown in figure 6.5.

The effect of the methane additive in argon is seen to be a slight 'filling in' of the Ramsauer minimum and a significant lowering of the electron energy, such that at about E = 200 V/cm it corresponds to the minimum value of cross section. For E less than 200 V/cm, λ/v is either constant or proportional to E^{-n} where n is less than 0.5, and so w rises with E. Above 200 V/cm λ/v becomes proportional to E^{-n} where n is greater than 1, and so w falls with E. Above 800 V/cm the value of n is only slightly over 1 and so w reduces very slowly with E.

Substituting actual values into equation 14 allows the variation of w to be calculated, and the resulting curve is shown in figure 6.9, compared with our experimental values from chapter 4. A value of k = 0.6 was assumed in the calculation, although good fits could be obtained for k between 0.5 and 1.0, depending on the precise position of the estimated ϵ_k versus E curve. Because of this strong dependence on the estimated ϵ_k values the preceding calculations for argon + 10% methane should be thought of as providing an explanation

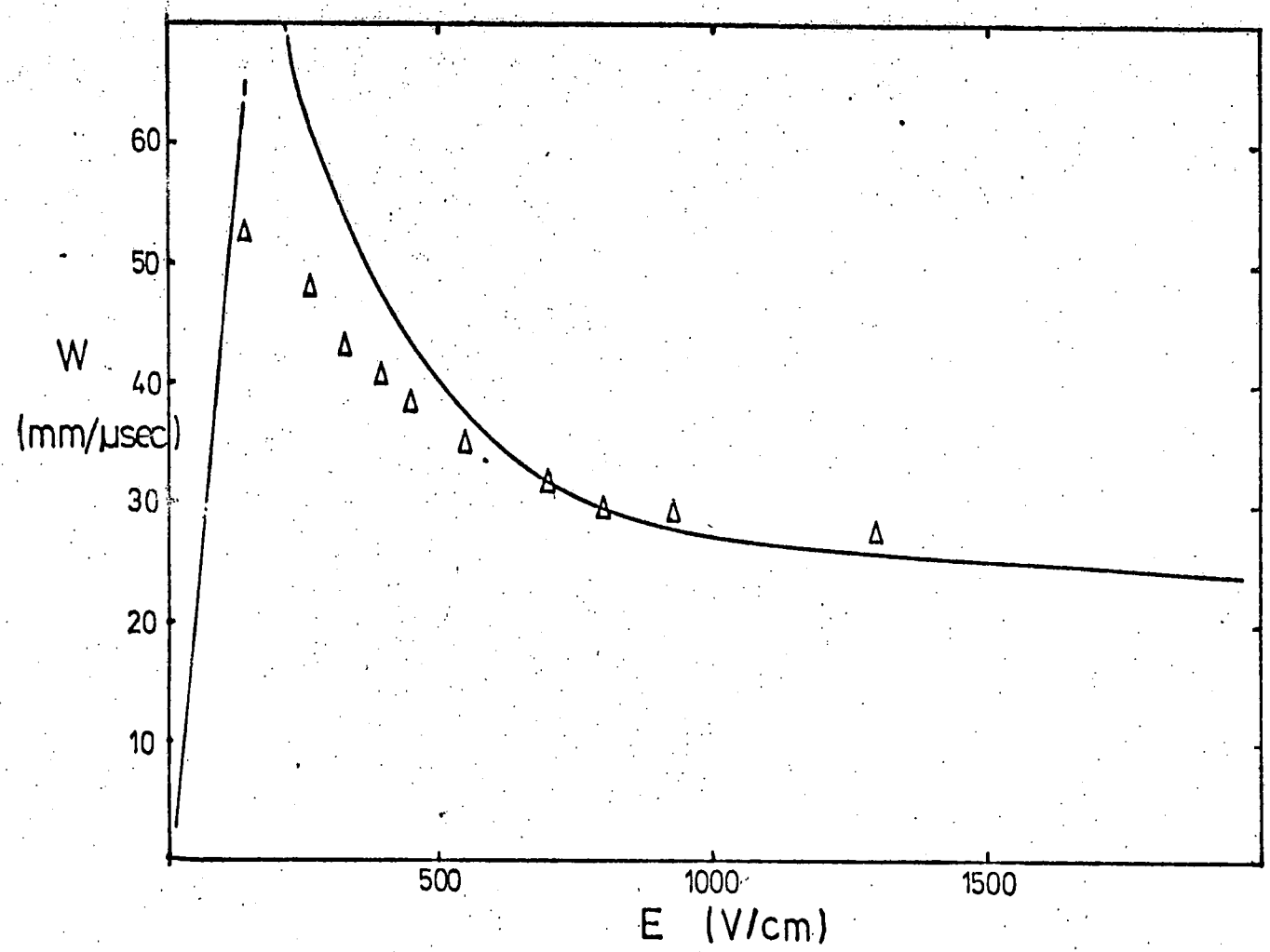

FIG 6.9 Theoretical prediction of drift velocity in argon + 10% methane compared with experimental data.

of the experimental variation of w with E, rather than an exact prediction.

The form of the w versus E relationship is however quite accurately described by the theory, as shown by figure 6.9, except that the predicted value for the peak of the curve is approximately twice as high as in practice. As this peak corresponds to the minimum of the cross section curve, it may be that because of the finite width of the electron energy distribution, the actual minimum value of q never represents the cross section for any particular distribution. That is, when in equation 12 we average over the velocity distribution it would be more accurate to also average over the corresponding range of λ values. The approximation of using only the λ value corresponding to the mean energy is valid unless the slope of the q versus C curve is significantly non-uniform (e.g. at the Ramsauer minimum).

The behaviour of w in other composition argon methane mixtures can also be examined qualitatively, using the same theory, and by noting that increasing the proportion of hydrocarbon in the mixture has two main effects, (a) the mean electron energy is lowered, and (b) the minimum in the cross section curve is 'filled in' to a greater extent. These have the corresponding results

(a) the peak of the w versus E curve is moved to higher values of E

(b) the peak is broadened, i.e. the change of slope of w versus E from positive to negative takes place more gradually and over a larger range of E.

These arguments apply equally to argon-isobutane mixtures, as isobutane has similar electron scattering properties to methane. Thus the general points mentioned above are illustrated by the results of Charpak et al for argon isobutane shown in figure 4.14, our own data for argon-methane-isobutane in figure 4.13, and the rigorous theoretical calculations of Palladino and Sadoulet (2)

For 38% isobutane content, the w peak is so broad that above $E \sim 1000$ V/cm, w is virtually independent of E. It is this saturation of w which is attractive to drift chamber designers. Note that the same effect, for lower values of w is achieved in argon + 10% methane for a different reason, namely the E^{-m} dependence of w at high fields, where $m \sim 0.1$.

6.4 Diffusion

As mentioned in section 6.2 the distance travelled by an electron parallel to the electric field in time t will be given by $d \pm x$, where $d = wt$ and x is a statistical variation due to the random motion of the drift process. For a group of electrons, w can be considered as the velocity of the centroid of the group, and x as due to the diffusion of electrons across a concentration gradient. This concept leads to the definition of a diffusion coefficient D as the ratio between the net number of particles flowing through unit area per second (J), and the density gradient of the diffusing particles (∇N)

Thus $J = - D \nabla N$ (Ficks Law of Diffusion)

In 1905 Einstein developed a relevant formula pertaining to particles in random motion. Assuming N_o particles at the origin of a three dimensional co-ordinate system at time $t = 0$ then the number density N at radius r and time t is given by

$$N = \frac{N_o}{(4\pi Dr)^{3/2}} \exp(-r^2/4Dt) \qquad (6.21)$$

where D is the diffusion coefficient as before. The root mean square radial displacement is given by

$$\sqrt{\bar{r}^2} = \sqrt{6\,Dt} \qquad (6.22)$$

and in one dimension

$$\sqrt{\bar{x}^2} = \sqrt{2Dt} \qquad (6.23)$$

It can be shown (see ref. 1, p 117) that equation 23 is applicable to a group of electrons in an electric field parallel to the x direction, where $\sqrt{\bar{x}^2}$ represents the r.m.s. displacement from the centroid. Under these circumstances however, D must be replaced by D_L, the coefficient of diffusion parallel to E, which in general is not equal to D. Diffusion at right angles to E is still described by the coefficient D. The difference between D_L and D was first noticed experimentally by Wagner et al (17) and has since been investigated theoretically by several authors (18-21). Assuming only elastic collisions and q independent of v, most authors calculate a ratio of $D_L/D \sim 0.5$, this value increasing for $q \propto v^{-n}$ and decreasing for $q \propto v^{+n}$. The effect is demonstrated by the experimental results of Wagner et al for D and D_L in argon and methane, as shown in figure 6.10. The broken line on figure 6.10 shows the estimated values of D_L/μ for argon + 10% methane. Defining $\epsilon_L = D_L/\mu$, we have for our mixture, and an electric field of 1000 V/cm, $\epsilon_L \sim 0.6$ eV (compared with $\epsilon_k \sim 1.5$ eV). We shall assume for the range of E that concerns drift chamber operation, that $\epsilon_L \propto \epsilon_k \propto \epsilon$, the mean electron energy.

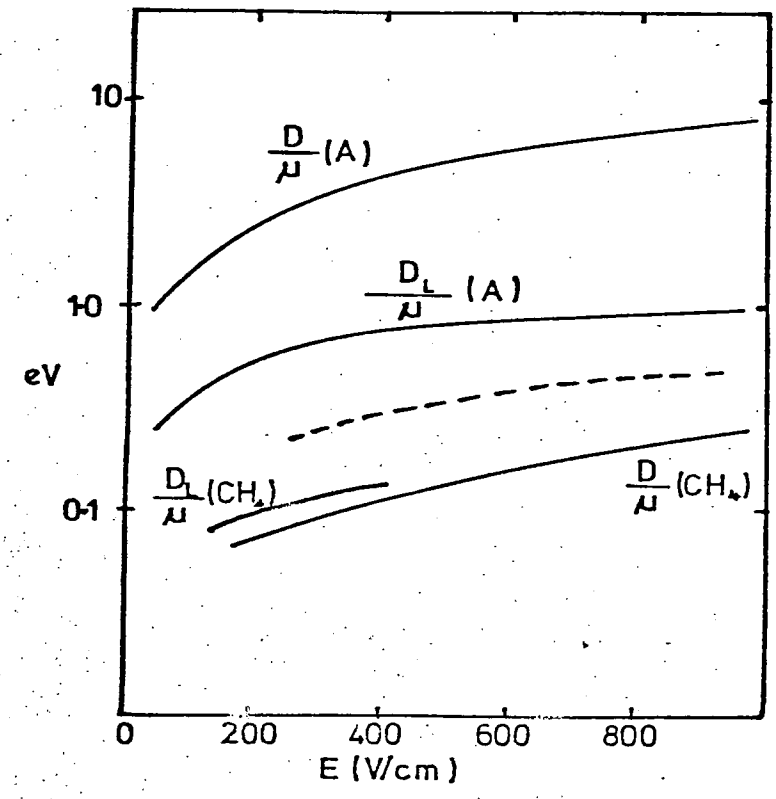

FIG 6.10 Ratio of diffusion coefficients to mobility, parallel (D_L) and orthogonal (D) to drift field. Broken line is D_L/μ estimate for argon+10% methane.

$$\sigma_x = \sqrt{\frac{2 D_L d}{w}} \tag{6.24}$$

$$= \sqrt{\frac{2 D_L d}{\mu E}} \tag{6.25}$$

$$= \sqrt{\frac{2 \epsilon_L d}{E}} \tag{6.26}$$

Thus to minimise the effects of diffusion we need to minimise ϵ_L/E (or ϵ_k/E) and we see that not only does the addition of hydrocarbon to argon improve its drift velocity characteristics but also improves its diffusion properties by lowering ϵ_k. It is also clear that for $\epsilon_k \propto E^n$ where n is less than 1 (as in our mixture for example) that there will be an improvement in spatial resolution by operating at high fields.

6.5 Application to Drift Chambers

The σ_x of equation 26 is not the final estimate of the contribution of diffusion to the spatial accuracy of a chamber however. The parameter which is more relevant in this context is σ_d, the uncertainty on the arrival time of the mth electron out of a group of n where it is the mth electron avalanching which triggers the timing system. The value of σ_d depends on σ_x, m and n. If the system was triggered by the centre of gravity of the group the the uncertainty would be given by

$$\sigma_d = \frac{\sigma_x}{\sqrt{n}} \tag{6.27}$$

This represents the best value of resolution (i.e. minimum of σ_d) but is very difficult to realise electronically. A more realistic example

is one where the timing is triggered by the first electron to reach the sense wire. In this instance it can be shown that

$$\sigma_d = \frac{1.28\sigma_x}{\sqrt{2 \log n}} \qquad (6.28)$$

This represents the worst value of resolution and although the general case for the mth electron is not reported, it seems reasonable to assume that σ_d will decrease with increasing m. Thus there is an advantage in not setting the discrimination level on the chamber pulses at the lowest possible level.

To calculate resolution in our chambers it is necessary to know both σ_x and n. For a drift distance d = 1 cm and an electric field of 1000 V/cm, σ_x is given from equation 26 as

$$\sigma_x = \sqrt{\frac{2.x\ 0.6\ x\ 1}{1000}}\ \text{cm}$$

$$= 345\ \mu\text{m}$$

for argon + 10% methane.

The value of n can be estimated with reference to figure 6.11 The assumption is made that electrons are considered to effectively originate from the same point if there is less than 100 μm difference in their drift lengths. Thus in figure 6.11 all the ionisation electrons formed in the distance y are considered to arrive at the sense wire with a time distribution characterized by σ_x. For d = 1 cm, y~2 mm, and as there are approximately 100 electrons/cm formed by an ionising particle traversing our chamber (see chapter 3), then n is about 20. Thus for triggering by the

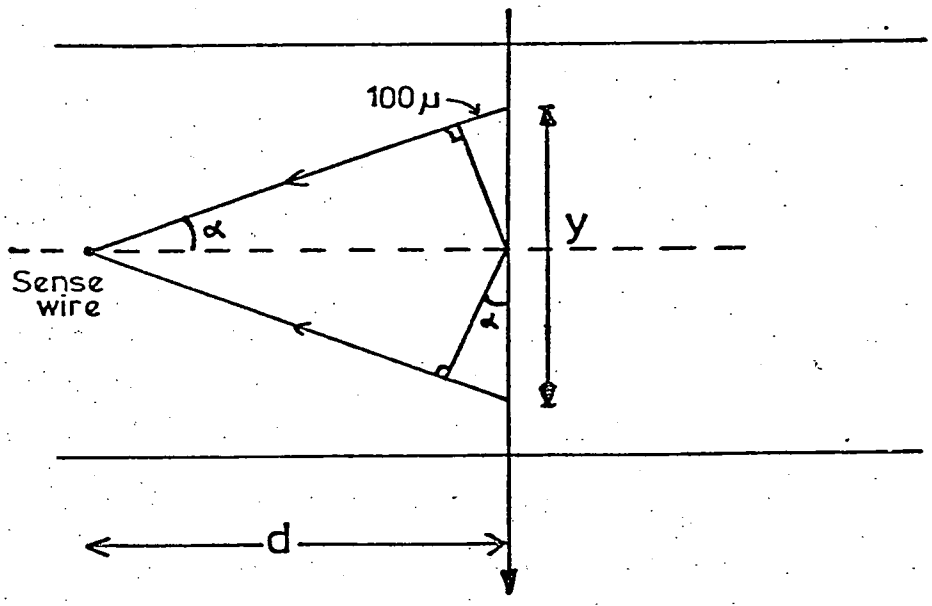

FIG 6.11 Variation in drift lengths from one track.

first electron σ_d is given by equation 28 as

$$\sigma_d = 0.52\ \sigma_x = 180\ \mu m$$

For the centre of gravity of the group, from equation 27

$$\sigma_d = 77\ \mu m$$

The experimental value of chamber resolution for these conditions, as described in chapter 5, was found to be 110 μm, where the pulse height discrimination level varied between 200 and 400 mV, or about 10 to 20% of the maximum pulse height.

Equations 27 or 28 show that any factor which decreases n will increase σ_d. Thus for tracks near to the sense wire, y of figure 6.11, and hence n, are reduced and so resolution is worsened. For large d (= drift distance) the model for field lines shown in figure 4.19 indicates that y becomes constant with d, but note that from equation 26 σ_d will increase with $\sqrt{d}$. Angled trajectories will also result in less electrons having similar drift lengths so that for the same d, σ_d will be increased.

Note that using σ_d instead of σ_x has to some extent incorporated the effect of σ_i of section 5.1 which was defined as the error due to the spread of the initial ionisation.

6.6 Conclusion

It has been shown in this chapter that it is possible to describe the behaviour of electron drift velocity w, and diffusion, by means of simple equations which involve values of mean free path λ and electron velocity v. Because of the complex variations of λ and v, no general numerical formula can be applied to cover the

variation of w and D with electric field E, and thus the original equations must be solved using specific values of λ and v appropriate to any particular value of E. Numerical constants appear in these equations as a result of averaging over the free path and velocity distributions, and these can have a significant range of values depending on conditions.

The main disadvantage of this technique is that the velocity (or energy) distributions, and their variations with electric field are not always well defined and in many cases no experimental data exists for them at all. An alternative procedure, using simulation techniques, which only requires knowledge of the mean free path versus energy relationship is outlined in chapter 9.

CHAPTER 6 - References

1. L.G.H. Huxley and R.W. Crompton. The diffusion and drift of electrons in gases, Wiley New York (1974)

2. V. Palladino and B. Sadoulet, Lawrence Berkely Laboratory Internal Report LBL-3013 (1974). A shortened version has been published in Nuc. Inst. Meth.

3. P. Langevin, Ann. Chim. Phys. 28 (1903) 289.

4. E.W. McDaniel. Collision Phenomena in Ionized Gases, Wiley, New York, (1964) Ch.9.

5. R.H. Healey and J.W. Reed. Behaviour of slow electrons in gases, Amalgamated Wireless Ltd., Sydney (1941)

6. American Institute of Physics Handbook, 3rd Edition, McGraw-Hill, New York, (1972)

7. C. Ramsauer. Ann. Phys. 64 (1921) 513, 66 (1921) 546

8. J.S. Townsend and V.A. Bailey. Phil. Mag. 43 (1922) 593, 44 (1922) 1033.

9. R.B. Brode. Rev. Mod. Phys. 5 (1933) 257

10. M.J. Dryvesteyn Physica 10 (1930) 61.

11. P.M. Morse, W.P. Allis and E.S. Lamar Phys. Rev 48 (1935) 412

12. Experimental determinations of D/μ are extensively summarised in references 1 and 4.

13. J.S. Townsend, Electricity in Gases, Clarendon Press, Oxford (1915)

14. L.S. Frost and A.V. Phelps, Phys. Rev. 136 (1964) A1538

15. H.S.W. Massey and E.H.S. Burhop, Electronic and Ionic impact phenomena, Oxford Univ. Press (1952)

16. R.A. Nielsen, Phys. Rev. 50 (1936) 950

17. E.B. Wagner, F.J. Davis and G.S. Hurst, J. Chem. Phys. 47 (1967) 3138

18. J.H. Parker and J.J. Lowke, Phys. Rev. 181 (1969) 290

19. H.R. Skullerud, J. Phys. B. 2 (1969) 696

20. L.G.H. Huxley, Aust. J. Phys. 25 (1972) 43.

21. R.E. Robson, Aust. J. Phys. 25 (1972) 685.

CHAPTER SEVEN

OPERATION OF DRIFT CHAMBERS IN STRONG MAGNETIC FIELDS

7.1 Introduction

The practical application of drift chambers often requires that they be operated in regions where strong magnetic fields are present. This may be intentional, as the accurate location of a particle trajectory in a known magnetic field provides a good method of determining particle momentum, hence the application of drift chambers to high resolution spectrometers. It may however, arise from the necessity of positioning the chambers very close to equipment involving strong magnets (e.g. accelerator or storage rings) in which case they will be subject to stray, maybe non-uniform, fields.

As the operation of drift chambers involves the movement of electrons through a gas it is to be expected that the existence of a magnetic field over the drift region would have a significant effect. Consequently the behaviour of chamber properties in magnetic fields is an important topic and one which will affect the suitability of any particular gas mixture for experimental applications. Furthermore, concurrent with this study, work was being carried out at Durham on the development of drift chambers for an experiment at CERN (see chapter 8) in which the chambers would have to operate in stray fields from storage ring magnets, up to a maximum of 15 kG. and so a quantitative study of the effects of magnetic fields with respect to argon + 10% methane was vital for successful calibration.

In almost all instances the orientation of chambers in magnetic fields is the same, and unfortunately this is the orientation in which the field has the maximum effect on drifting electrons. In order to detect the deviation of high energy particles in a magnetic field B, the chambers are placed so that this deviation is in the drift

direction, i.e. with B, parallel to the sense wires. Under these conditions the effect on the drifting electrons is to tend to remove them from the chamber. This is indicated in figure 7.1 showing a plan of a chamber. In all the following discussions and experiments this is the orientation of chamber and field which applies.

7.2 Basic ideas of magnetic field compensation

The initial thoughts (1), that the effect of a magnetic field on an electron having a drift velocity w, could be represented by a force Bew, acting on the electron were soon revised in view of the fact that w is only a net effect, the actual motion of the electrons at any time being as described in the previous chapter.

The actual effect of B, which was first investigated by Townsend (2), is to impose a drift velocity w_T orthogonal to the directions of B and E. The drift velocity parallel to the electric field, w_L, is also modified. Thus the electrons drift at an angle ϕ to the direction of the electric field at an absolute velocity w_A. The term w_o is now used to represent the value of drift velocity for no magnetic field. These velocities are indicated in figure 7.2.

A magnetic drift velocity is also defined by

$$W_M = \frac{w_T}{w_L} \frac{E}{B} \qquad (7.1)$$

and therefore

$$\tan \phi = w_M \frac{B}{E} \qquad (7.2)$$

The transverse displacement, Δy, of electrons after drifting a distance d in the E direction is given by

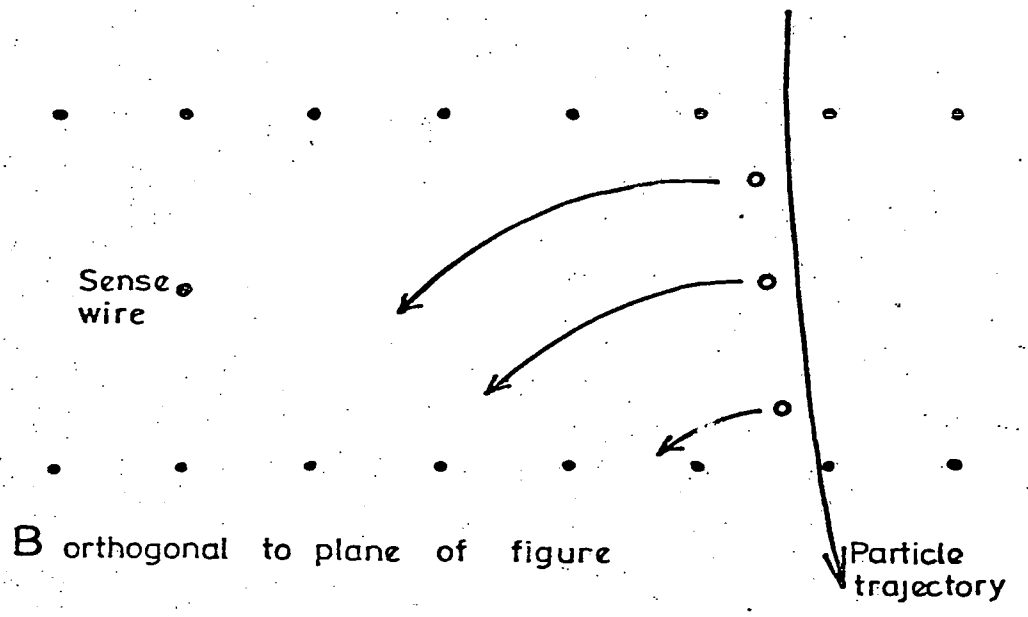

FIG 7.1 Usual configuration of magnetic field in drift chambers.

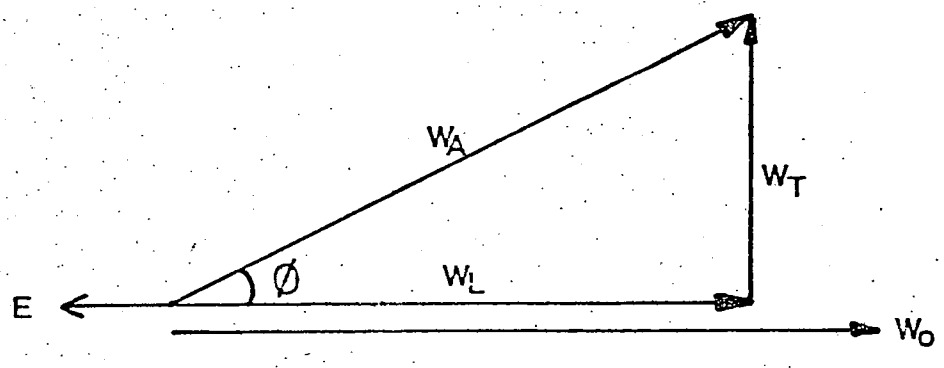

FIG 7.2 Drift velocity components in crossed electric and magnetic fields.

$$\Delta y = \frac{w_T}{w_L} d = w_M \frac{B}{E} d \qquad (7.3)$$

Assuming $w_M \sim w_o$ (it will be shown later that $w_M > w_o$), $E = 10^5$ V/cm, $B = 1.5$ Tesla, and $w_o = 3 \times 10^4$ m/sec, then $\Delta y \sim d$. For events where Δy is greater than the chamber thickness (6 mm in our chambers) electrons will tend to be removed from the chamber before reaching the sense wire region and hence the event will not be detected. For Δy less than this value, some of the electrons may still be removed and thus the detection probability (i.e. efficiency) will be reduced. Unless resolved this problem would have prevented the use of drift chambers with large drift spaces in strong magnetic fields.

An excellent method of counteracting the effect was suggested in a paper by Charpak et al (1) which involved slanting the applied electric drift field at an angle γ, such that the resultant drift velocity was restored to a direction in the sense wire plane. This is only exactly achieved of course if $\gamma = \phi$, where ϕ is a function of E and B.

The simple way in which this slant is realised is one of the major advantages of the adjustable field type of drift chamber as considered in this work. For such chambers the voltage distribution as applied to one of the H.T. wire planes is displaced by one or more wires with respect to that on the other plane. Figure 7.3 shows the equipotentials in a chamber with the drift field slanted by 3 wire spacings. The values were calculated using the numerical relaxation method mentioned previously. There are 3 main comments regarding the form of the equipotentials

i) Over much of the drift space the electric field is uniform and at an angle γ to the sense wire plane. The value of the field E in this direction is given by

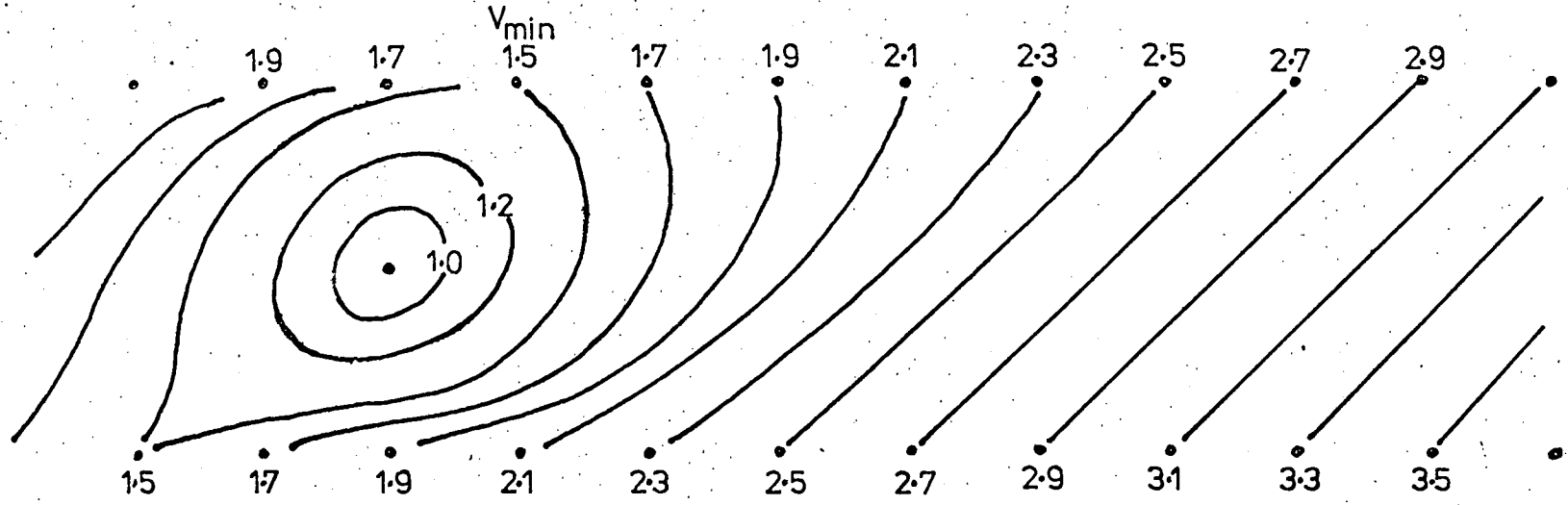

FIG 7.3 Equipotential lines (in kV) in a chamber with E slanted by 3 wire spacings ($\gamma = 45°$) and $E_a = 1000$ V/cm

$$E = \frac{E_{applied}}{\cos \gamma} \qquad (7.4)$$

ii) Nearer to the sense wire the field begins to become more radial and so the compensation effect will be upset. However in this region E is becoming much stronger and so the electrons tend to follow the electric field lines in spite of B.

iii) Very close to the wire E is identical to the non slanted case so that the avalanche process will be as before. The values of voltage on the wires opposite the sense wire are however now greater than V_{min}. In order to maintain similar operating conditions on slanting the electric field then, the value of the supply voltage must be lowered.

Note that no new voltages are required to achieve the slanted field, but also that only certain values of γ are allowed, i.e. for 6 mm thickness and 2 mm H.T. wire spacing only angles of 18.5^{o}, 33.7^{o}, 45^{o} etc. are obtainable, being referred to as 1, 2 or 3 unit slants respectively. Thus exact compensation ($\gamma = \phi$) can only be achieved for certain values of B and E. Figure 7.4 shows the various velocity components for the more general case of $\gamma \neq \phi$, where the drift velocity measured (i.e. parallel to the sense wire plane, $= w_s$) is given by

$$w_s = w_A \cos (\gamma - \phi) \qquad (7.5)$$

In experimental conditions B is usually fixed, with γ having its restricted number of possible values. The procedure for deciding on compensation conditions is to assume an approximate value of E, and knowing w_M, ϕ may be calculated. The closest available value of γ is then chosen as the slant angle. E can then be adjusted so as to make $\phi = \gamma$, bearing in mind that E is given by equation 4, regardless

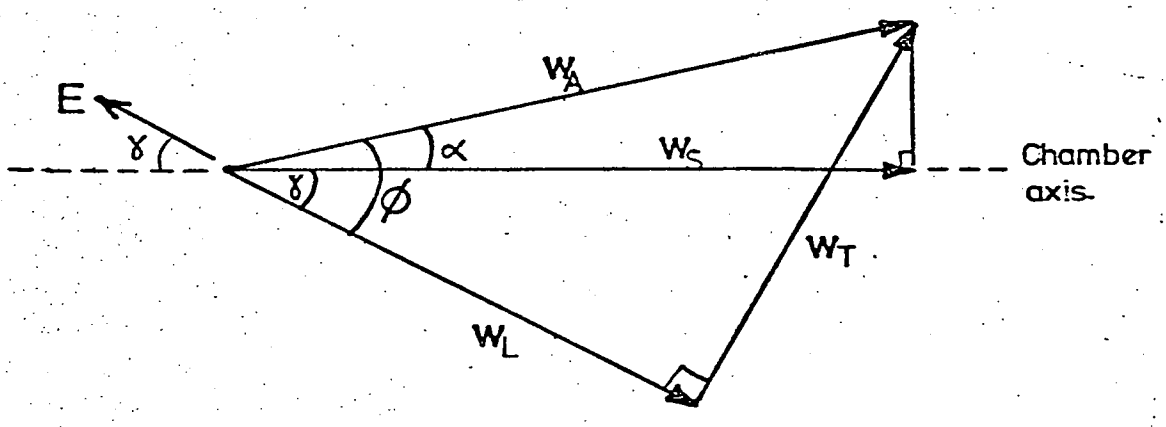

FIG 7.4 Drift velocity components in the prescence of magnetic and slanted electric fields.

of the actual direction of drift of the electrons.

7.3 Effect of Magnetic fields on the drift process

The differential equations describing the motion of an electron in fields of E in the x direction and B in the z direction can be written

$$\frac{d^2x}{dt^2} = \frac{eE}{m} + \frac{eB}{m}\frac{dy}{dt}$$

$$\frac{d^2y}{dt^2} = \frac{eB}{m}\frac{dx}{dt}$$

$$\frac{d^2z}{dt^2} = 0$$

Solving these equations it can be shown (e.g. Palladino and Sadoulet, reference 3) that to a first approximation $w_L = w_o$ and $w_T = w_o\,\omega\,T$, where T is the mean free time between collisions ($=\bar{\lambda}/v$) and $\omega = Be/m$. In general $w_T = w_o\,k_B\omega T$ where k_B is a constant depending on $f(\lambda)$ and $f(v)$ and is discussed in Appendix I For the present we shall assume $k_B \sim 1$.

Another factor affecting the drift process is that the paths of the electrons between collisions are now curved because of B, thus effectively decreasing the mean free path by a factor approximately equal to $(1+\omega^2 T^2)^{-1}$ (4). Taking this into account we have

$$w_L = \frac{w_o}{1+\omega^2T^2} \qquad (7.6)$$

$$w_T = \frac{w_o\omega T}{1+\omega^2T^2} \qquad (7.7)$$

so that

$$\tan \phi = \omega T \tag{7.8}$$

The diffusion coefficient D is similarly reduced, and these expressions are the same as those derived by Townsend (2).

From Chapter 6 and Appendix I we have,

$$w_o = k_\lambda \frac{e}{m} E T$$

so that

$$\omega T = \frac{w_o B}{k_\lambda E} \tag{7.9}$$

But by definition

$$w_M = \tan \phi \frac{E}{B} \tag{7.10}$$

and combining equations 8, 9 and 10 gives

$$w_M = \frac{w_o}{k_\lambda} \tag{7.11}$$

This relationship is only approximate however, as more precise expressions for w_L and w_T have been derived such that equation (8) is no longer valid. For example the value of w_L is more exactly given by Huxley (5)

As,

$$w_L = \frac{w_o}{1+\omega^2 T^2} \left(1+ \frac{\omega^2 T^2}{1+\omega^2 T^2}\right) \qquad (7.12)$$

In general then a magnetic deflection coefficient, ψ , is defined such that

$$w_M = \psi w_o \qquad (7.13)$$

where ψ is only approximately given by $1/k_\lambda$.

Theoretical expressions for ψ have been derived by Frost and Phelps (6) and Huxley (7) who found that,

$$\psi = \frac{3\left[\overline{v^{-2}\,(d/dv)(\lambda^2 v)}\right]}{\left[\overline{v^{-2}\,(d/dv)(\lambda v^2)}\right]^2} \qquad (7.14)$$

where obviously ψ depends on $f(\lambda)$ and $f(v)$. Using the same nomenclature as in the previous chapter ($\lambda \propto v^r$), table 7.1 gives several possible values of ψ calculated from equation (14)

	r		
	1	0	-1
Maxwell	1.0	1.18	3.0
Druyvesteyn	1.0	1.06	1.38

Table 7.1 - Values of Magnetic Deflection coefficient

Experimental evidence in support of these values of ψ has been obtained by Jory (8).

The work of chapter 6 has indicated that for argon + 10% methane, at the electric fields of interest, λ is decreasing sharply with v, and so relatively large values of ψ may be expected. (Results quoted later in this chapter indicate $\psi \sim 4$ for our mixture). Large ψ means large ϕ, and thus considerably greater compensation will be required than would have been expected by assuming the usual approximation $W_M \sim W_o$. In this respect a greater proportion of hydrocarbon is preferable, as this tends to 'fill' the Ramsauer minimum and lower the electron energy such that λ becomes largely independent of v. Then ψ is approximately 1 regardless of the velocity distribution and so ϕ is reduced, from

$$\tan \phi = \psi W_o \frac{B}{E} \qquad (7.15)$$

The benefits of higher hydrocarbon content are somewhat offset however as W_o tends to be larger, which will increase ϕ. These qualitative predictions are supported by the numerical calculations of Palladino and Sadoulet (3) on W_M values for various argon + isobutane mixtures. Figure 7.5 shows their calculated values of W_M compared with W_o, for pure isobutane, argon + 25% isobutane and argon + 7% isobutane. The increased values of ψ at low hydrocarbon content is clearly seen, and for 7% isobutane (which has a similar W_o variation as our mixture), $\psi \sim 3$ for E around 1000 V/cm and B = 20 kG. Experimental evidence of the behaviour of W_A and ϕ for argon + 30% isobutane + 2.5% methylal has been obtained by Charpak et al (9) who measured these parameters directly in a specially constructed chamber. Figure 7.6 from their work shows the calculated values of W_A and ϕ from the simple expressions 6, 7 and 8 compared with their experimentally determined points. In the calculations they assumed $k_\lambda^k = 0.75$ and the agreement with experiment is good, particularly at E = 500 V/cm. Agreement is not so good at

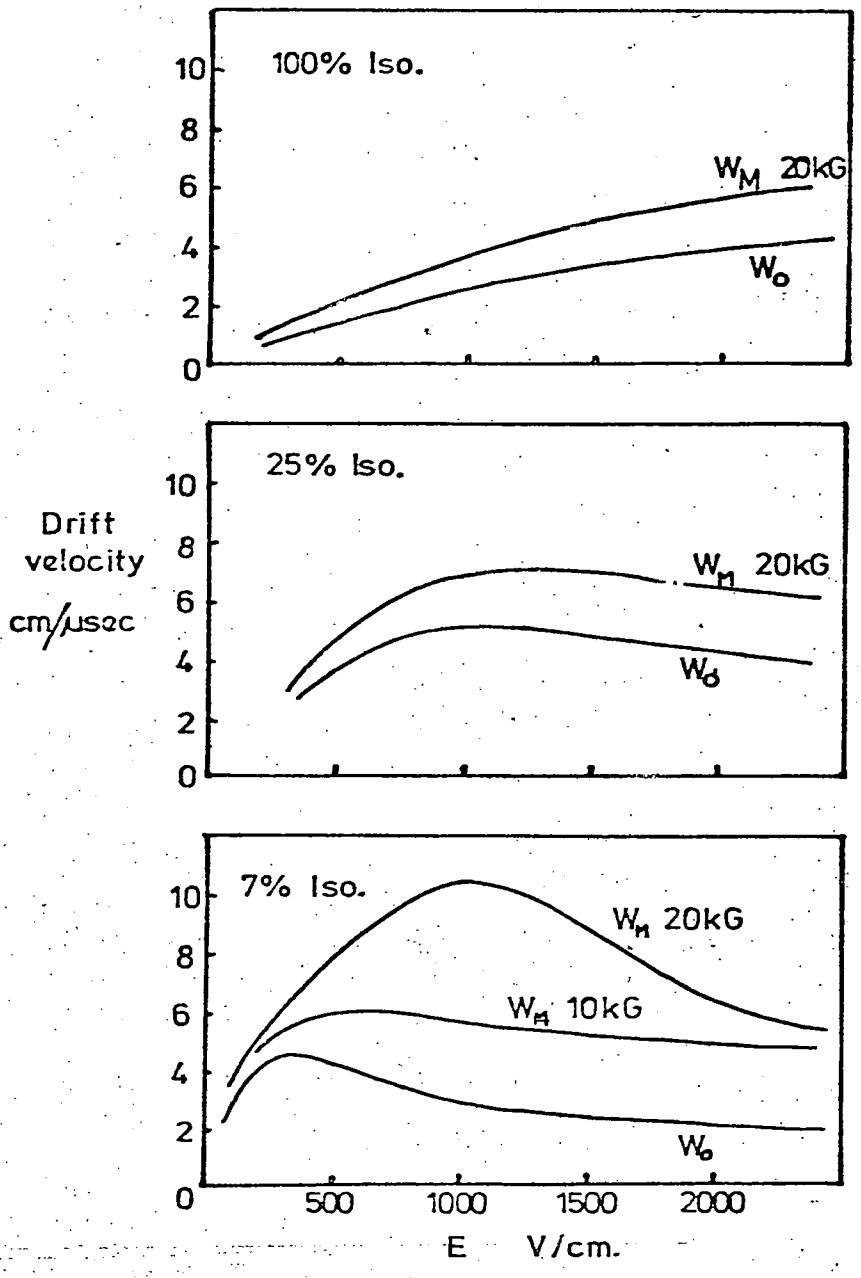

FIG 7.5 Predicted behaviour of W_M and W_o in argon–isobutane mixtures (Palladino and Sadoulet)

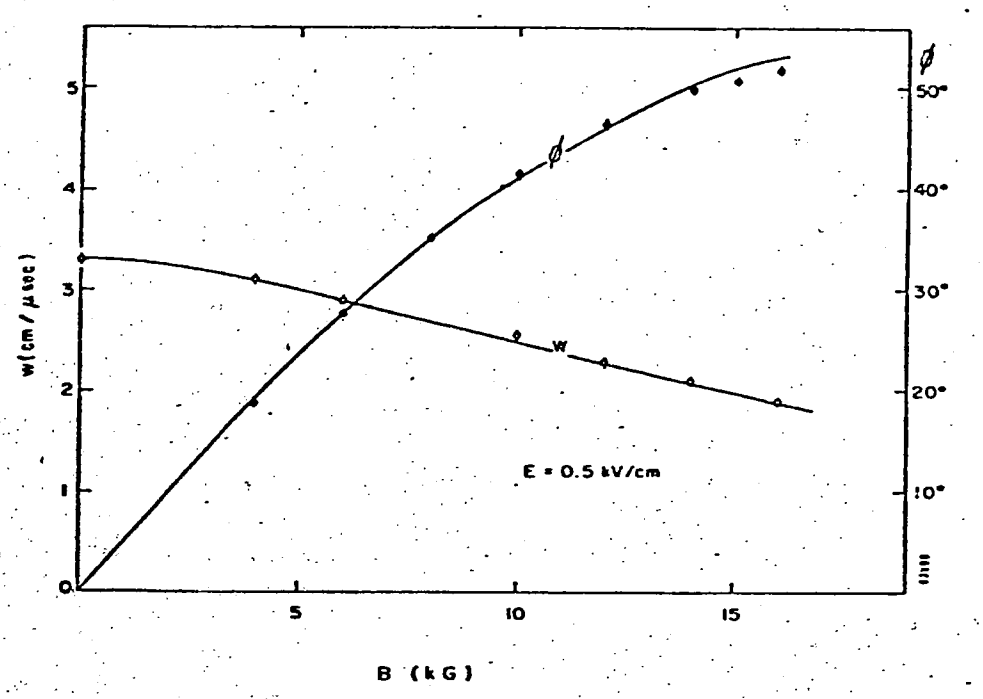

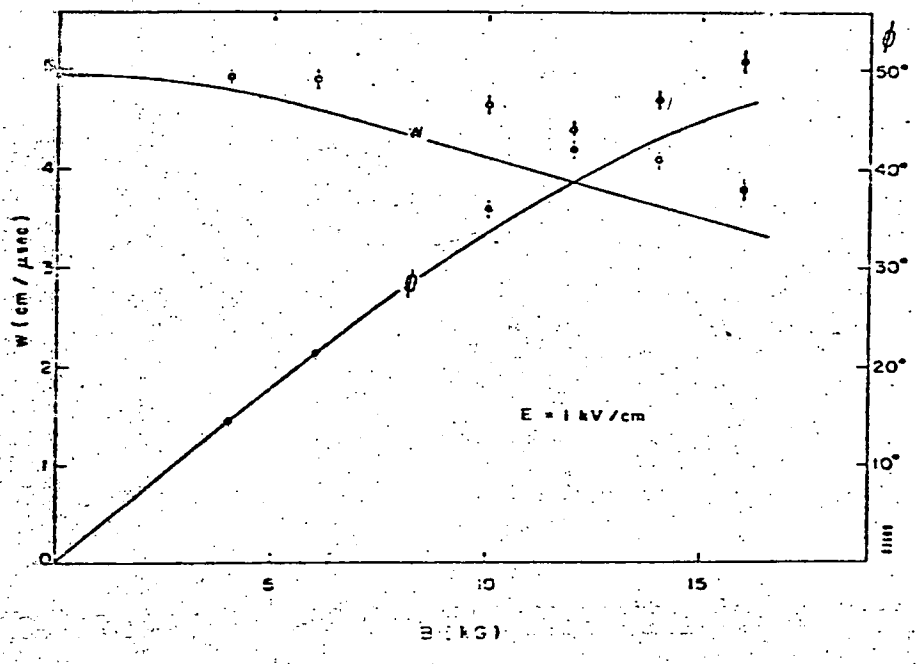

FIG 7.6 Variation of drift velocity and drift angle with B for argon + isobutane, theory and experiment, from Charpak et al.

E = 1000 V/cm however presumably because at higher E, $\lambda(v)$ and $f(v)$ are changed, such that ψ (and hence W_M) are increased.

7.4 Experimental system to investigate the effects of magnetic fields

In order to obtain experimental evidence of the effects described above, as applied to argon + 10% methane, a series of tests was planned using a high field magnet in the Daresbury Laboratory test beam facility (as described in section 5.2). The same array of 3 single cell chambers was used as for the resolution tests described in section 5.5, except that the third chamber was positioned between the pole faces of an electromagnet.

The magnet which was made available for the tests had a maximum magnetic flux rating of 13.5 kG and a pole piece aperture 5 cms high by 30 cms wide. The dimensions of the chambers to be used in these tests were therefore limited by this aperture size, which was particularly restricting in the height or sense wire direction (maximum 5 cm). This restriction precluded the use of either the large single cell test chambers or the prototype multicell chambers and hence a new series of chambers was designed.

7.4.1 Chamber Design

The main consideration in the design of these chambers was one common to most detectors for use between magnet poles, that is to achieve the maximum sensitive area in a usually restricted space. In this application the main problem involved supporting, and making electrical connection to, the sense and H.T. wires without using up too much of the available 5 cm height. This was achieved by soldering the wire planes to narrow strips of printed circuit board fixed to the frame of the chamber. These strips were connected to further

similar printed circuit board (by soldering each individual conducting strip) incorporated into the walls of the chamber and which ran in the 'open' direction of the magnet aperture. External connections were then made to the other end of this board, outside the sealed volume of the chamber. A section through the wire connection system is shown in figure 7.7, and this is basically the same system used in the design of the multicell chambers described in the next chapter (also for use between magnet poles).

Other features of the single cell test chambers are seen in figure 7.8 which also shows the external wiring used to provide the appropriate voltages to the H.T. wire planes (seen behind the chamber). The main frame of the chamber was machined from a single block of 'Perspex' (140 x 43 x 25 mm) for simplicity of construction and gas leak prevention. Gas connections were made via holes in the main frame at opposite ends of the chamber. The connection system for the nearest H.T. plane is well shown in figure 7.8. Solder joints between the wires and the strip, and between the strip and one of the external connection boards are clearly seen, as is the single connection to the sense wire on the adjacent plane. The inner H.T. plane connections protrude further than the outer so that any wires could be replaced from one side of the chamber.

Note that the particular chamber shown in figure 7.8 was unsuitable for operation because of two faults.

(i) A possible gas leak appears on the top seal of the front window due to crinkling of the Melinex. Such leaks could be effectively sealed with 'Sellotape' (temporarily) although replacing the window is more satisfactory.

(ii) Several H.T. wires in the inner plane are badly deformed, resulting in a distorted drift field. This

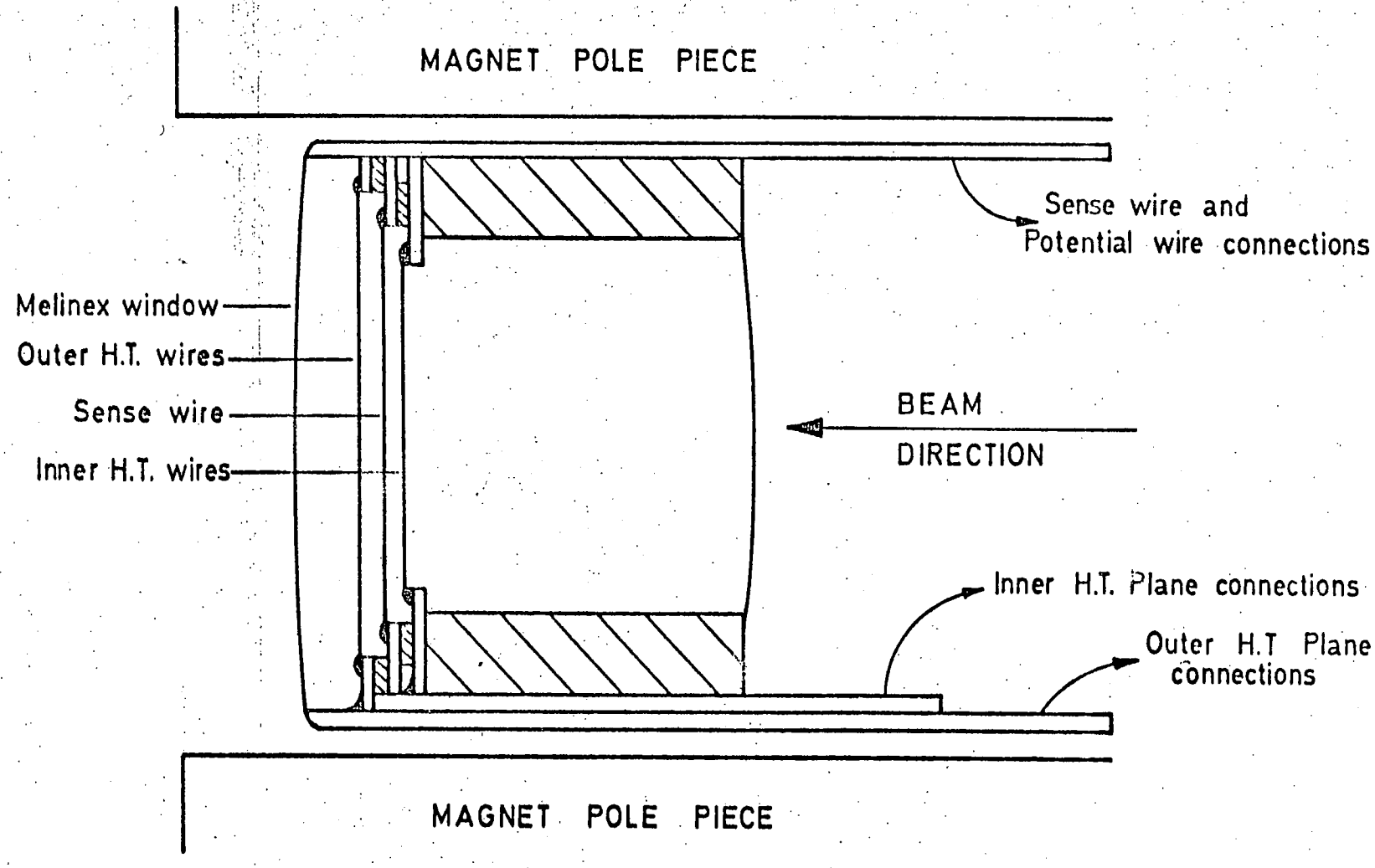

FIG 7.7 Section through chamber designed for high magnetic field tests.

Figure 7.8 - Single cell drift chamber for use with narrow gap magnets.

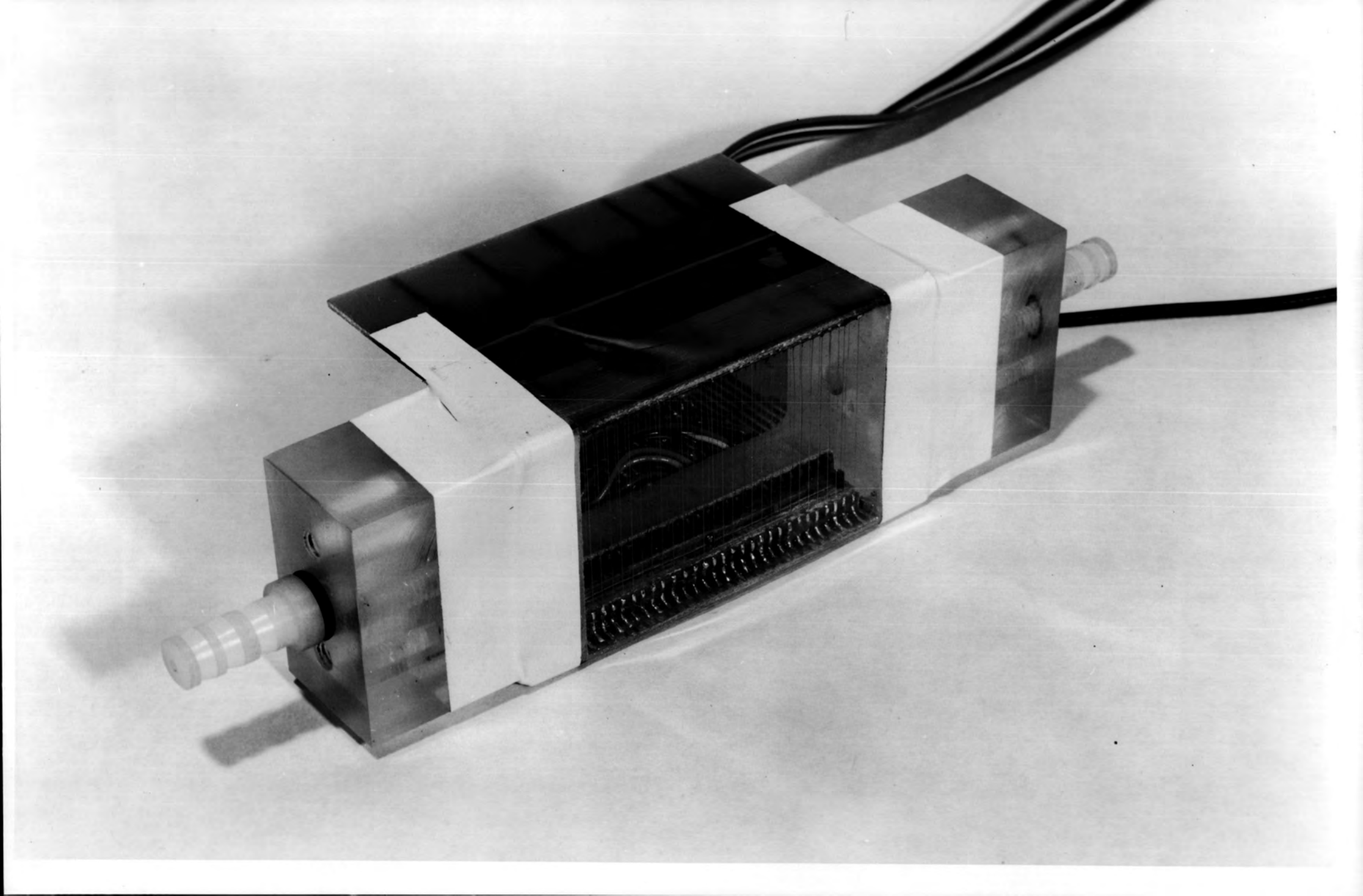

is presumably due to incorrect soldering of the wires to the strip, allowing the wires, which are attached under tension, to be pulled through the solder joint. Wire replacement is the only solution.

Several of these chambers were built, and proved to be simple, robust, easily maintained and satisfactory in operation.

7.4.2 Operational Details

Because of the lack of space beneath the chamber in the magnet, the assembly of 3 chambers used in these tests were supported by a rigid aluminium structure attached to the side of the chambers (attachment holes can be seen in figure 7.8 near to the gas ports). This support structure incorporated a circular 'Perspex' frame on which the third chamber was mounted, such that it could be rotated about an axis coincident with the sense wire.

One problem which arose from the use of the aluminium frame inside the magnet aperture, occurred during switching on or off of the magnet power. It was a property of the magnet power supply that the magnet could not be operated at less than half power. Switching the magnet on or off then produced a sudden large change in the magnetic field. This causes induced eddy currents in the aluminium and the result was that the aluminium frame tended to move slightly at these times, although the positions of the 3 chambers with respect to each other was not affected.

During the experiment values of E and γ were supplied to chamber 3 from an H.T. distribution box which contained the appropriate resistor network and four 64 way sockets. Each socket was wired to the resistor network in such a way as to provide 0, 1, 2 or 3 unit field slants respectively. The cathode wires of the chamber were connected to a corresponding 64 way plug and so various values of γ could be obtained depending on which socket was used. The value of R_E in the network

was selected by an external plug and several sockets, such that E could be easily varied. As stated in section 7.2 the supply voltage (and hence the applied field) had to be reduced on slanting the field, although from equation 4 the actual field E acting on the electrons is increased because of the slant of the equipotential lines.

B was varied by varying the current through the magnet coils, the appropriate field strength being read from a calibration curve, and θ was measured as the rotation angle of the third chamber in its circular mount.

Note that electric field conditions were only varied in chamber 3, chambers 1 and 2 were operated, at all times, at E = 520 V/cm, $\gamma = 0$, B = 0.

7.4.3 Tests with a single chamber

The first tests carried out in the magnetic field consisted of observing the drift times from the whole sensitive area of chamber 3. The start pulses were obtained from a single scintillator behind the chamber, having a larger area than that of the chamber to ensure that all relevant particles were recorded. The drift times were analysed using a T.A.C. - P.H.A. system (see chapter 2) and the resulting distributions were studied to give a general indication of chamber behaviour.

Figure 7.9 shows a schematic drift time distribution (with a displaced zero) from a whole chamber. The flat top to the distribution indicates an equal probability of detection across the whole chamber (i.e. uniform efficiency). The rounding off at A and B shows the extent of the expected efficiency dips around the sense wire and cell boundary respectively. The time interval between t_1 and t_2 corresponds to the maximum drift time allowable, i.e. the time of drift from the cell boundary, and knowing the cell width, the electron drift velocity

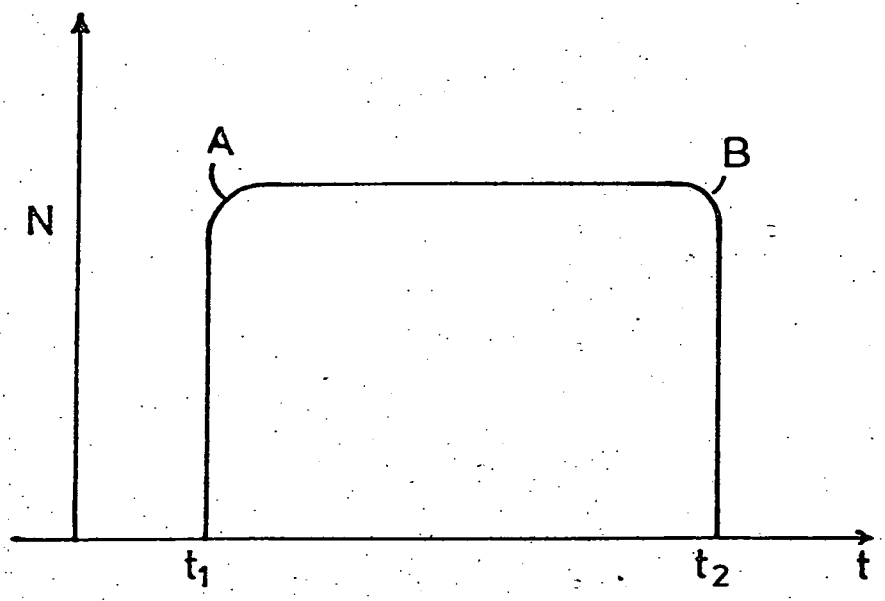

FIG 7.9 Idealised drift time distribution from whole cell.

can be estimated (assuming it to be uniform across the cell).

There are several points to note regarding this technique however,

(i) A uniform particle flux is required over the whole chamber to achieve the 'flat topped' distribution.

(ii) High particle fluxes (such that more than one particle may traverse the chamber within the maximum drift time) will result in short drift times being more probably recorded.

(iii) Estimates of W may be difficult if the end of the distribution is not well defined. This may be due to severe efficiency fall off, or geometrical effects (slanted fields or angled particle tracks).

The drift time distributions were expected however to give a reasonable picture of the effects of magnetic field compensation using slanted electric fields, and so distributions were recorded for various combinations of B, E and γ.

The ratio of stop to start pulses was also recorded during these runs to give a relative measure of chamber efficiency under various conditions.

7.4.4 Tests with an array of 3 chambers.

The main series of tests consisted of analysing the drift times resulting from the passage of a particle through an array of 3 chambers one of which could be subjected to magnetic fields of up to 13.5 kG. The experimental system used was the one described in sections 5.3 and 5.5, where figures 5.6 and 5.7 are relevant, the drift times being measured in T.D.C. modules, controlled and sorted by an adjacent PDP 11 computer and sent down a link to an IBM 370 for storage and later analysis.

The method of supporting the chambers in these tests did not allow for fine positional adjustment after assembly and so the alignment of the array was dependant on the accuracy with which the chambers spacers and frames were machined and constructed. To check that system misalignment would not be a significant source of locational inaccuracy several runs were carried out on the system with no magnetic fields present. The results of these runs were presented in section 5 as resolution tests, and showed that the resolution obtained with this system was not significantly worse than for the accurately surveyed multi-cell system. These results also provided a reference set of data against which the magnetic field tests could be compared.

The tests consisted of recording and analysing the data from many runs (usually comprising several thousand events), each run being carried out for a unique combination of E, γ, B and θ (in chamber 3).

7.5 Results of single chamber tests

Figure 7.10 shows the distribution of drift times obtained by the method described in section 7.4.3 for 3 different values of drift field E, with B = 0 and γ = 0. The main discrepancy between this and the idealised distribution of figure 7.9 is that the particle flux is not uniform across the chamber due to the collimation of the positron beam. So marked is the fall off in flux that all distributions shown in this section have logarithmic vertical scales (this being a feature of the P.H.A.). Despite this nonuniformity the full widths of the distributions are still obvious, and were found from the digital output of the P.H.A. to be 82, 71 and 63 channels for a, b and c respectively. With a system calibration of 11.2 nsec per channel and a cell half width of 28 mm, this gives values of W_o = 30, 35 and 40 mm/μsec. The corresponding values from the measurements of chapter 4 are 30, 36 and 41 mm/μsec respectively.

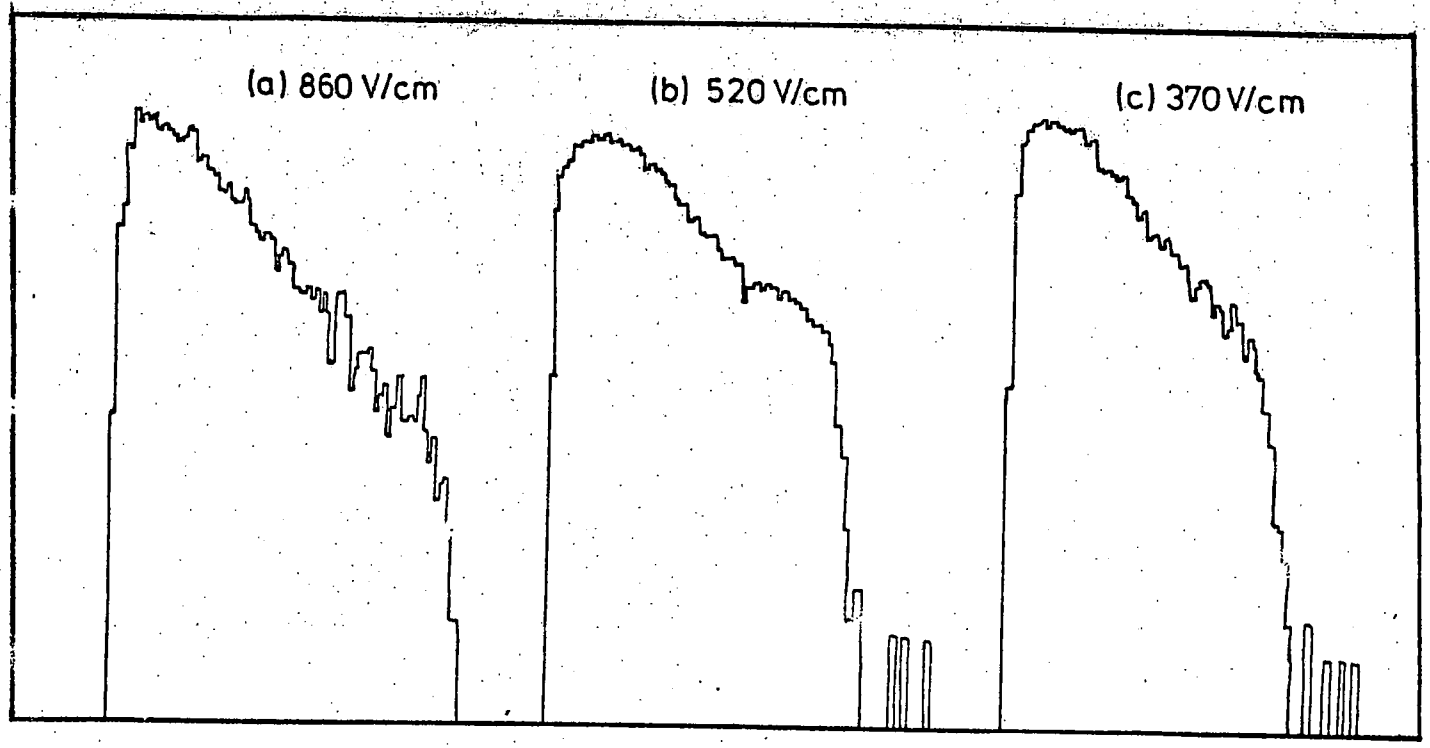

FIG 7.10 WHOLE CHAMBER DRIFT TIME DISTRIBUTIONS (B=0, γ= 0)

Figures 7.11 and 7.12 also show drift time distributions for various operating conditions and the effect of the magnetic field compensation system is demonstrated. Thus figure 7.10 represents the normal operating conditions with approximately 100% detecting efficiency across the cell. Applying a magnetic field of 13.5 kG (figure 7.11, a b and c) results in a drastic drop in efficiency for events with larger drift times, i.e. electrons drifting from the further parts of the cell are being lost. The effect is more drastic for lower E, and less pronounced at lower B (results not shown), being dependent on ϕ the angle of electron drift (more correctly $\phi - \gamma$) where from section 7.2, ϕ is proportional to B/E. Note that the reduction in distribution width is not due to variations in drift velocity, as the general effect of magnetic fields is to reduce drift velocity. Distributions d, e and f show the effect of applying compensation by slanting the electric field by 45°, with B still 13.5 kG. The compensation is good at 1100 V/cm, less so for lower E. The same compensation is better at these lower electric fields if the magnetic field is reduced. This is shown by the distributions of figure 7.12 for B = 8 kG. These results support the general expectations expressed in section 7.2 and from the fact that the compensation is good ($\gamma \sim \phi$) for conditions $\gamma = 45^{\circ}$, E 1000 V/cm, B$\sim$10 kG we estimate a value of ψ (from equation 15) of approximately 3, in accordance with section 7.3

Estimates of drift velocity (W_s) were only possible for those conditions where compensation was good enough so that the maximum possible drift time could be found, i.e. for $\gamma = 45^{\circ}$ and E = 1100 V/cm. Values of distribution width for these conditions indicated that W_s was reduced for increasing B, to a value of 25 ± 2 mm/μsec at 13.5 kG. This is in agreement with results of section 7.6.2.

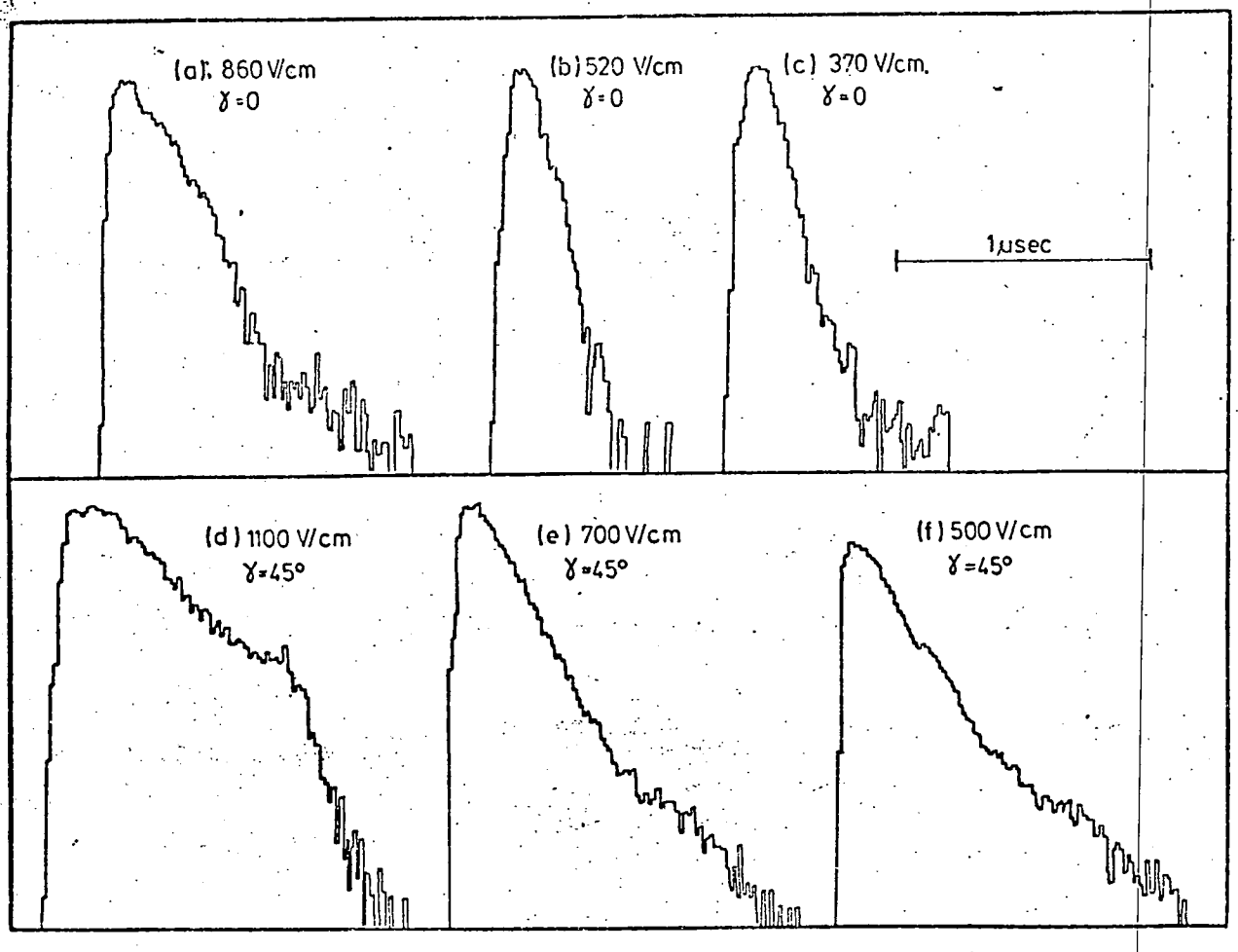

FIG 7.11 DRIFT TIME DISTRIBUTIONS FOR B = 13·5 kG

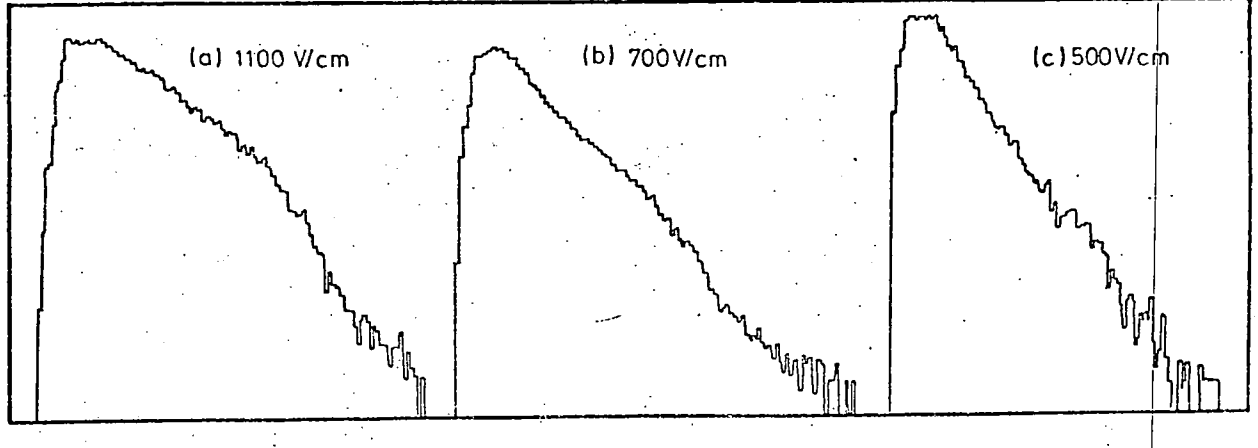

FIG 7.12 DRIFT TIME DISTRIBUTIONS FOR B = 8 kG, γ = 45°

Efficiency measurements were taken during these runs to determine the optimum compensation conditions ($\gamma = \phi$) which should be indicated by a corresponding maximum in relative efficiency. Figure 7.13 shows relative efficiency versus magnetic field for various conditions. The vertical scales on this figure are only relative efficiencies, scaled such that the efficiencies for $\gamma = 0$, $B = 0$ were unity. The same scaling factor was however applied to all the sets of data.

Assuming $\gamma = \phi$ at the value of B for which the efficiency begins to be reduced, figure 7.13 yields the following conditions,

(a) $\gamma = 45^{\circ}$, E = 1100 V/cm, B = 8 kG

(b) $\gamma = 45^{\circ}$, E = 700 V/cm, B = 5 kG

(c) $\gamma = 34^{\circ}$, E = 1000 V/cm, B = 5.5 kG

(d) $\gamma = 34^{\circ}$, E = 620 V/cm, B = 2.5 kG

Using this data and equation 15, corresponding values of magnetic deflection coefficient ψ were calculated to be, (a) 4.7, (b) 4.4, (c) 4.2, (d) 4.7.

7.6 Results of 3-chamber tests

The drift time data from these runs was first analysed in the manner described in section 5.3.3, but it was realised that as this method averaged effects over all three chambers, any deviations due to the magnetic field in chamber 3 would be reduced. Thus a new deviation was defined as the difference between the predicted drift time in chamber 3 obtained by extrapolating through the drift times in chambers 1 and 2, and the measured drift time. The frequency distributions of these deviations were plotted as before, although the method of defining the deviation meant that the widths of the

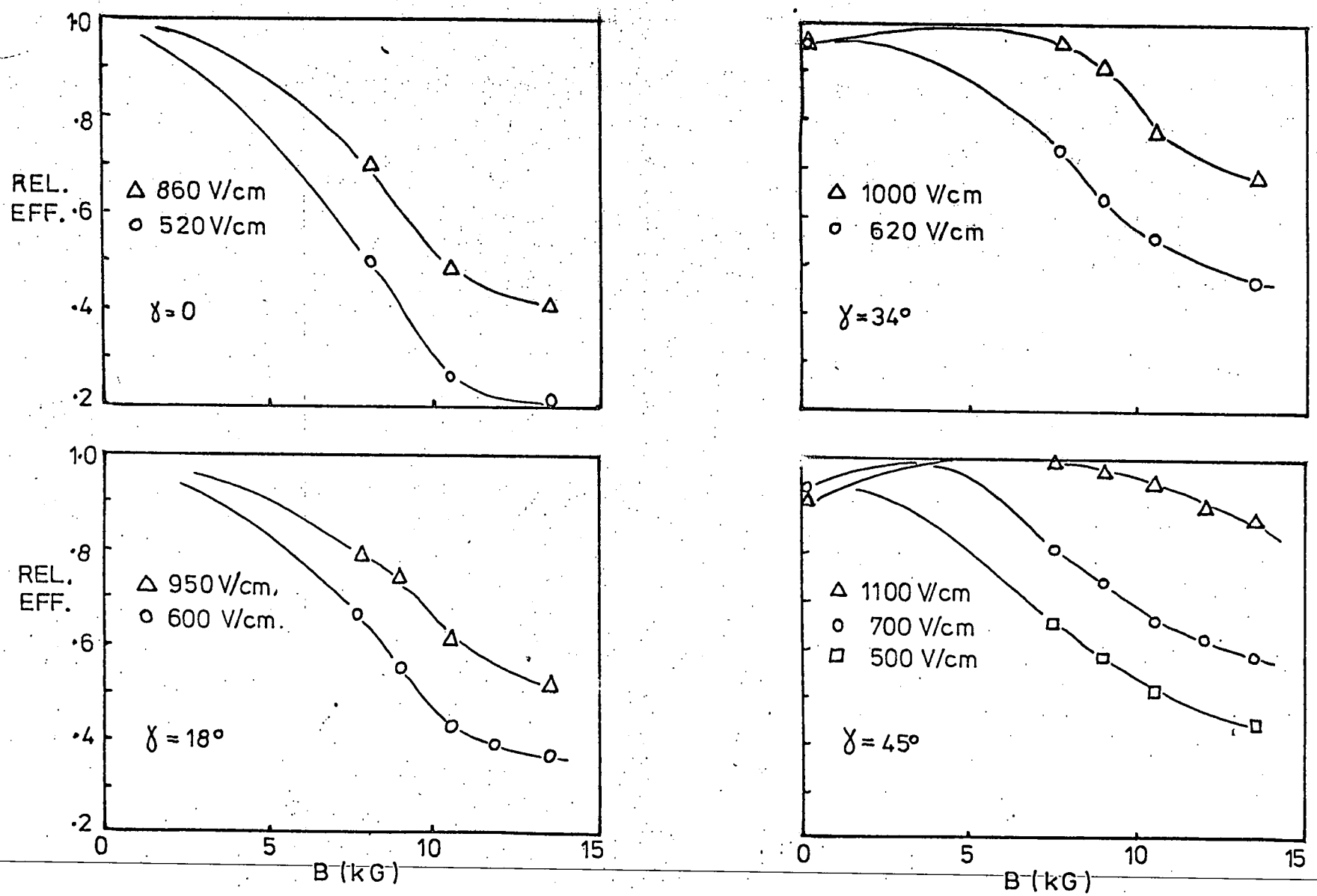

FIG 7.13 RELATIVE CHAMBER EFFECIENCY FOR VARIOUS VALUES OF B, E & γ.

distributions were much wider than before. With all chambers operated under identical conditions σ for the distribution was about 400 μm, i.e. about 3 times greater than for the individual chamber values of chapter 5.

Figure 7.14 shows a selection of deviation distributions for runs at various conditions, where the data has been divided up into four sections depending on the predicted drift time in chamber 3, these being (a) 50-150 nsec, (b) 150-250 nsec (c) 250-350 nsec, (d) 350-450 nsec. The bin width is 4 nsec.

Run 2 is for identical conditions in all chambers and is thus the reference data against which other runs are compared. Run 3, for E = 860 V/cm (in chamber 3 only), B = 0, γ = 0 shows up three notable features.

The mean values of the distributions are not constant. Since the drift fields are now different in chamber 3 compared with 1 and 2, the drift velocity is also different. Thus there will be a systematic discrepancy between the expected and measured drift times in chamber 3 which will be proportional to drift time and the ratio of the velocitiies. Knowing the change in W_o between 520 V/cm and 860 V/cm the displacements can be calibrated and thus used to estimate drift velocity for other runs.

Since each distribution is plotted for a range of drift times the above displacement is not constant across each distribution and hence they will be widened. Thus the distributions are wider for run 3 than for run 2 although the resolution is known to be slightly better. Changes in W therefore had to be considered when estimating resolution from the distribution widths.

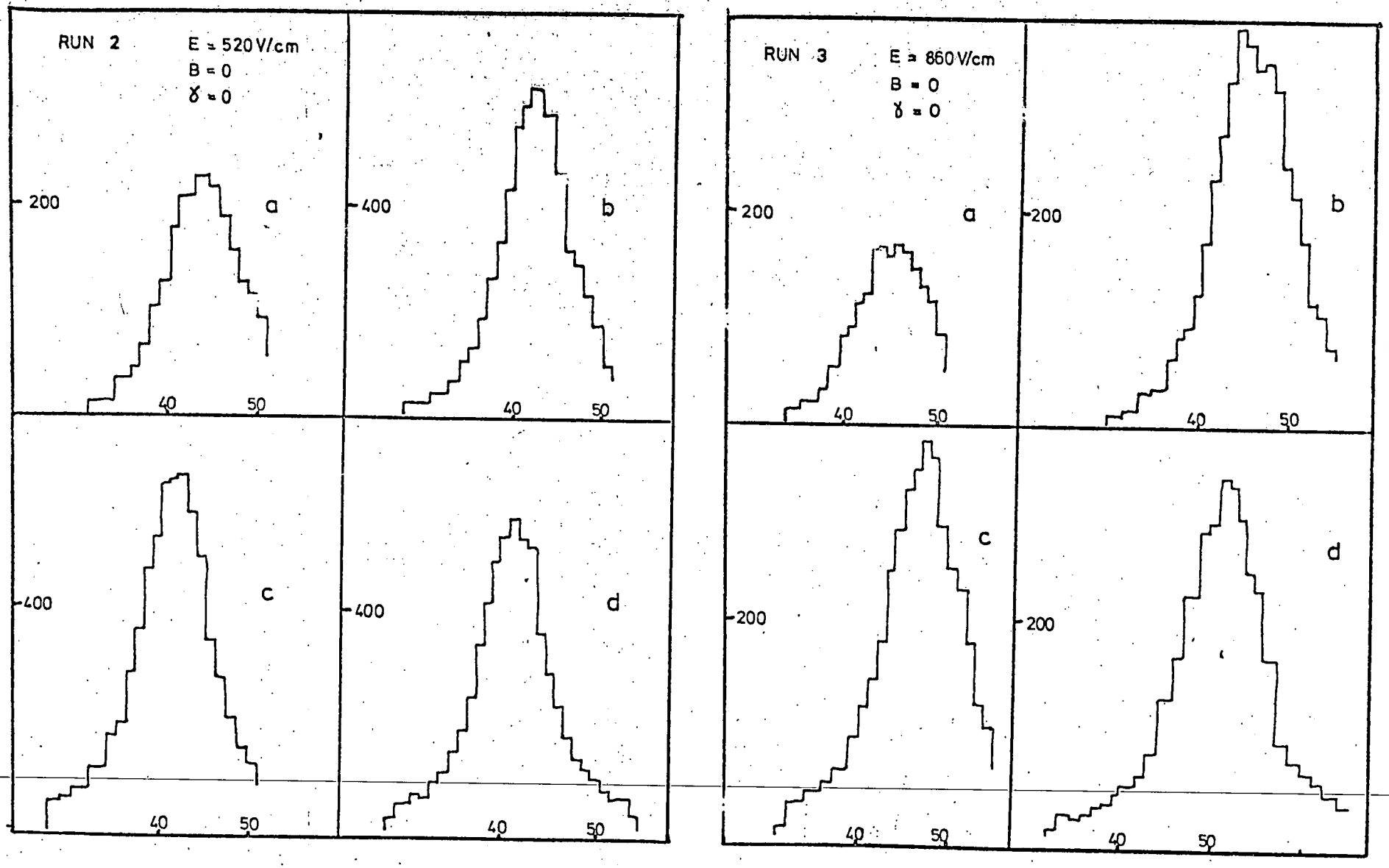

FIG 7.14 Some deviation distributions for various operating conditions.

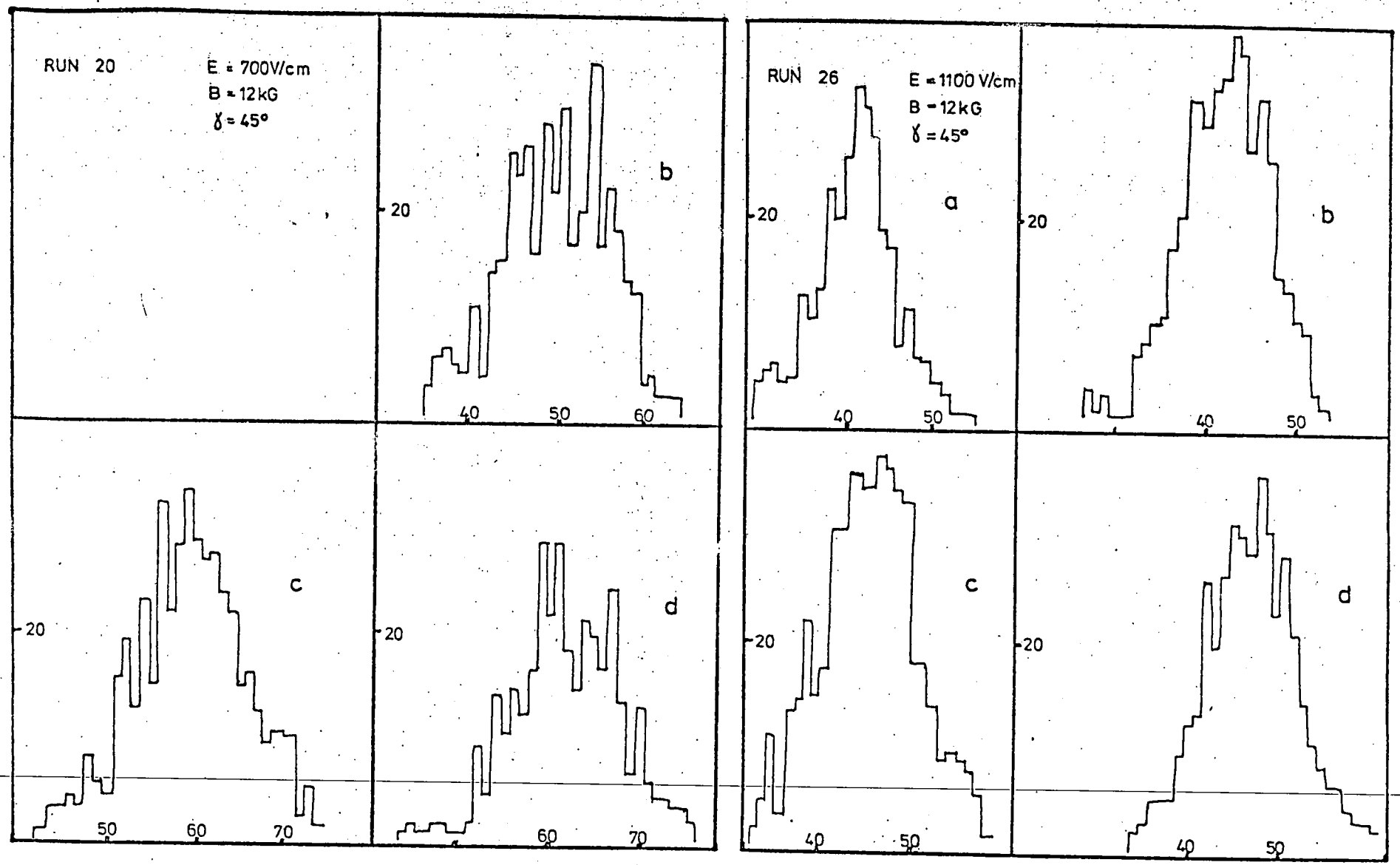

FIG. 7.14 continued

The number of events in each of the four distributions from one run will give a measure of the variation of efficiency across the chamber, assuming a reasonably even particle flux over the region.

Analysis of all the runs recorded during the tests yielded the following results grouped under headings of efficiency, resolution, and drift velocity.

7.6.1 Efficiency

Figure 7.15 shows the number of events making up each histogram in a given run, normalised with respect to the total amount of data taken in that run, and plotted against distance across the chamber for various runs. Unfortunately, this presentation also incorporates a measure of the beam profile across the chamber cell, as shown in the curve of figure 7.15 for B = 0, γ = 0, all E, where 100% efficiency is known to exist. As the beam profile will vary with B, the results of figure 7.15 are grouped into series of runs at the same B, so that differences between curves in the same series are directly attributable to variations in chamber efficiency.

These variations in efficiency support the ideas of magnetic field compensation presented earlier. That is for these values of B, good efficiency is achieved with $\gamma = 45^{\circ}$ and E = 1100 V/cm. At E = 700 V/cm the efficiency is similarly good for the lower B values, but at B = 13.5 kG it decreases with drift distance. A value of $\gamma = 34^{\circ}$ is seen to be insufficient compensation at these B values, efficiency decreasing rapidly with distance.

Note that for short drift distances the efficiency is similar for all conditions. This is an example of a general effect that for short drift distances, chamber operating characteristics are largely unaffected by magnetic fields, regardless of any compensation. This

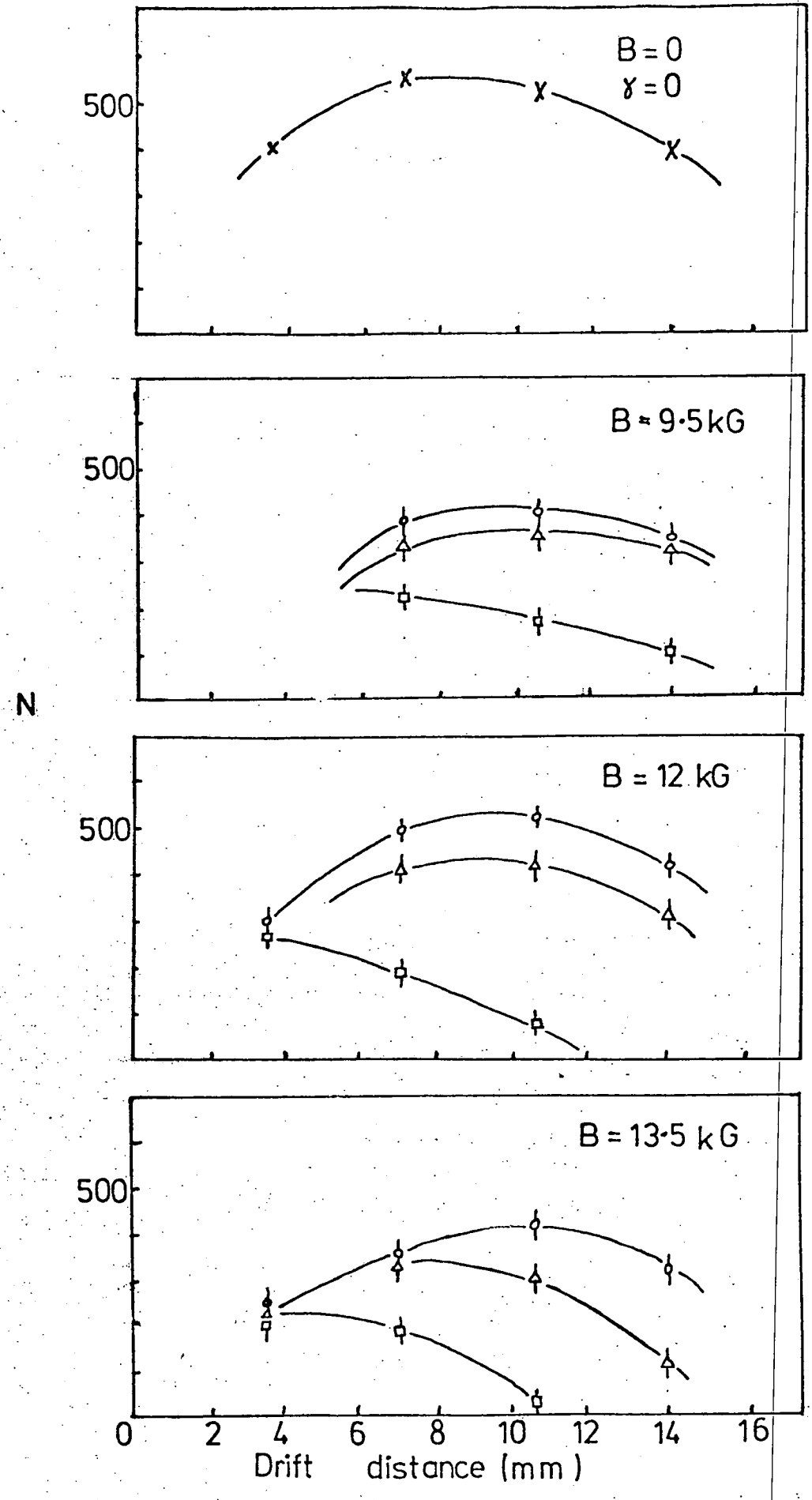

FIG 7.15 Number of events per distribution for different drift distances, and various conditions.

- 1100 V/cm, $\gamma = 45°$
- 700 V/cm, $\gamma = 45°$
- 1000 V/cm, $\gamma = 34°$

is also shown by the results of Sadoulet and Litke (10) for a chamber with wide gap and short cell length which was successfully operated in magnetic fields up to 15 kG with no electric field slanting.

Although no absolute values of efficiency in magnetic fields were obtained, results from other workers using argon isobutane mixtures (11) indicate that when compensation is correct, efficiencies of 100% are maintained across chambers similar to ours for drift distances up to 24 mm.

7.6.2 Drift Velocity

The data points on figure 7.16 show the experimental values of the measured drift velocity W_s against B for two values of E. These were obtained from the displacement of the deviation histograms as mentioned above. The variation of W_s with B depends on two factors. The first is the geometrical effect given by equation 5.

$$W_s = W_A \cos (\gamma - \phi)$$

where ϕ is a function of B, and the second is that W_A itself is a function of B.

In order to compare this data with theoretical predictions, values of W_s were calculated using equations given in this chapter, in the following manner. For E = 1100 V/cm, $\gamma = 45^\circ$, W_M was assumed to be approximately given by the results of section 7.5. In this case this was $\phi = 45^\circ$ for B = 8 kG. The value of ϕ could then be found for all B, assuming $\tan \phi \propto B$ (from equation 2). The corresponding value of ωT was found using the approximation $\tan \phi \sim \omega T$, and substituting this in equation 12, W_L could be calculated. W_A was then given by $W_L/\cos \phi$, and finally W_s was derived from equation 5 above.

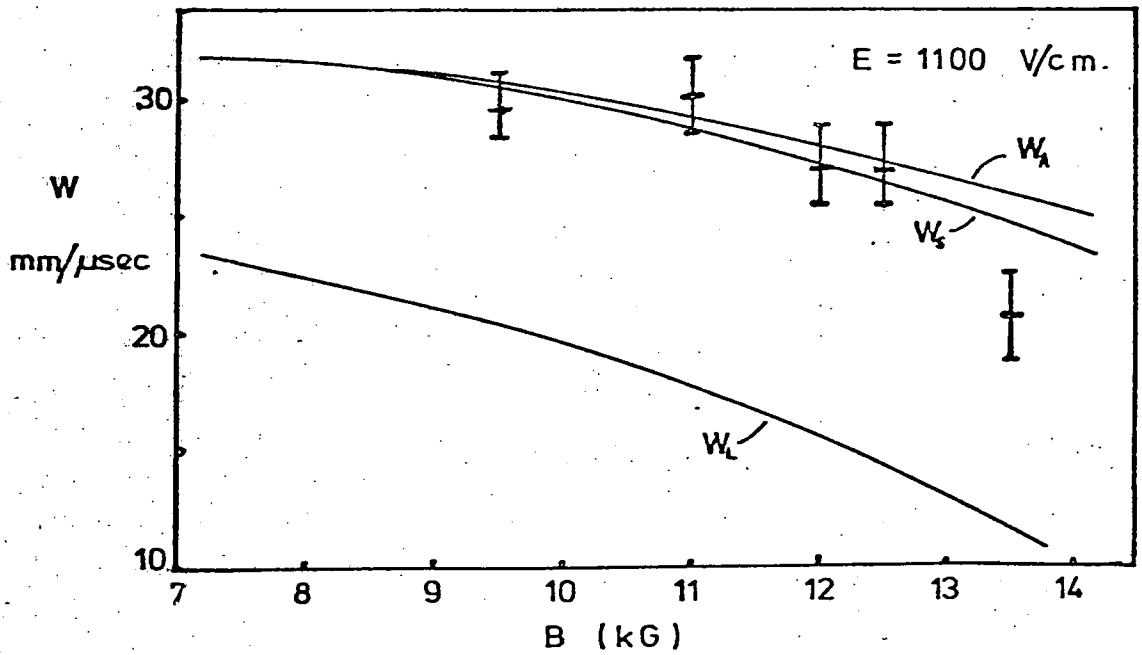

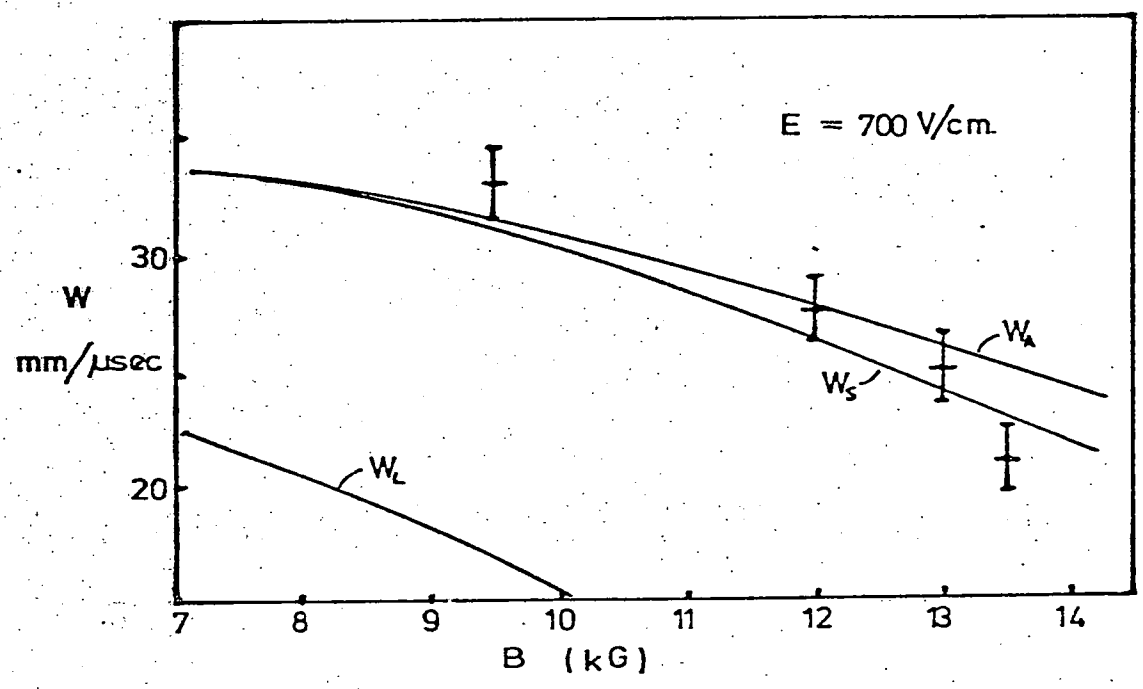

FIG 7.16 Variation of drift velocity with magnetic field (experiment and theory)

The calculated variations of W_L, W_A and W_s thus derived, are shown in figure 7.16(a). Similar calculations were made for E = 700 V/cm assuming $\phi = 45^\circ$ for B = 5.5 kG and the results are shown in figure 7.16(b). As the predictions seem reasonably accurate they are also shown in figure 7.17 calculated for a wider range of B values.

The only useful result obtained for the 2 slant field, ($\gamma = 34^\circ$) gave a value of $W_s = 23 \pm 2$ mm/μsec at 10.5 kG and E = 1100 V/cm. Applying the above theory to these conditions and assuming exact compensation ($\phi = 34^\circ$) at B = 5 kG gives a value of $W_A = 28$ and $W_s = 25$ mm/μsec.

The same theory can be used to present the variation of drift velocity with B in a different form. That is knowing the value of tan ϕ and ωT for one combination of B and E we can calculate the variation for B fixed and E varying. The resulting variation of W_A with E for three values of B is shown in Figure 7.18 as compared with the experimental variation for B = 0. This variation of W_A calculated by the above theory shows a similarity to the rigorous calculations of Palladino and Sadoulet (3) for argon-isobutane mixtures. Figure 7.19 shows their prediction for W_A against E and B, in argon + 7% isobutane.

7.6.3 Resolution

Two factors are expected to affect the resolution of drift chambers which are operating in strong magnetic fields. The first is due to the fact that unless the magnetic field is exactly compensated, the ionisation electrons will not drift orthogonal to the particle trajectory. The effect on resolution will be exactly the same as for angled particle tracks with B = 0, with the corresponding angle of the

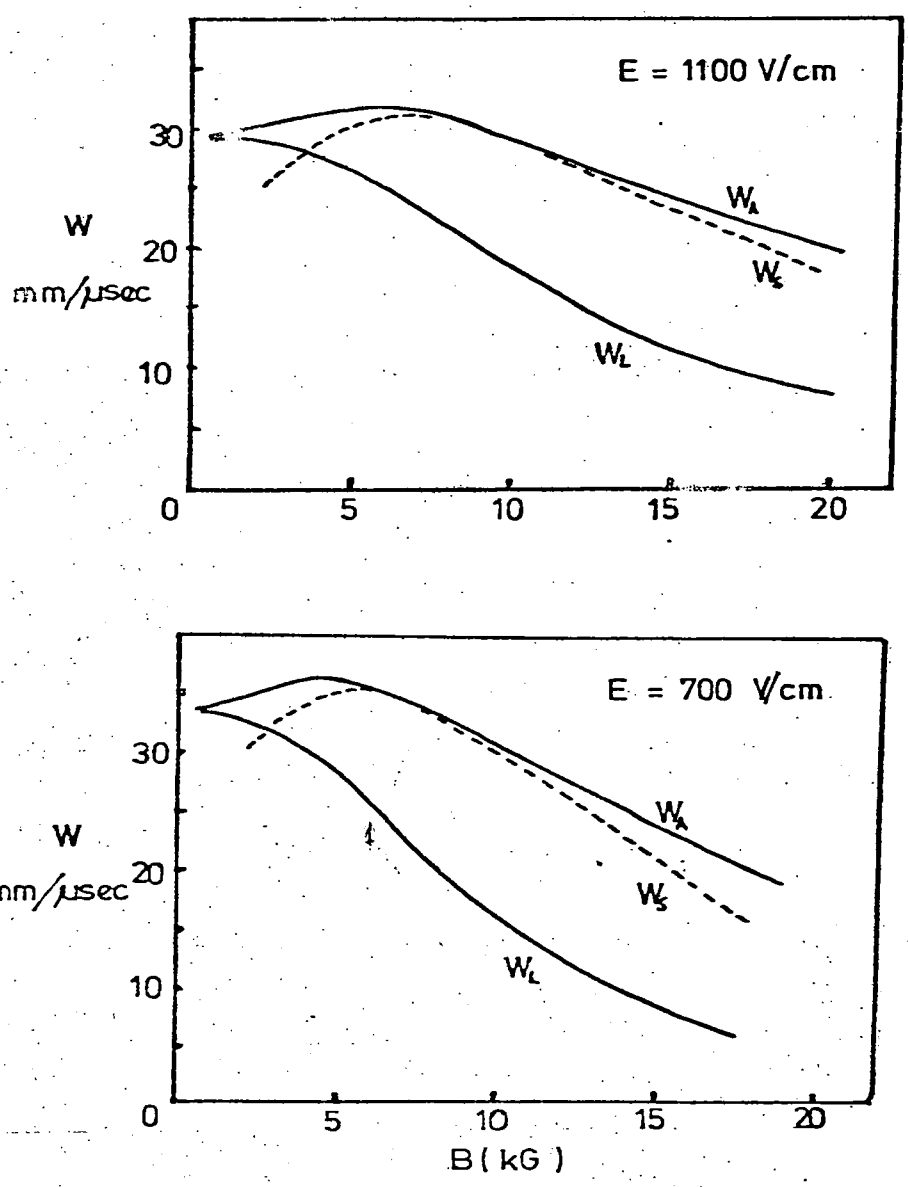

FIG 7.17 Theoretical variation of W for wide range of B. ($\gamma = 45°$)

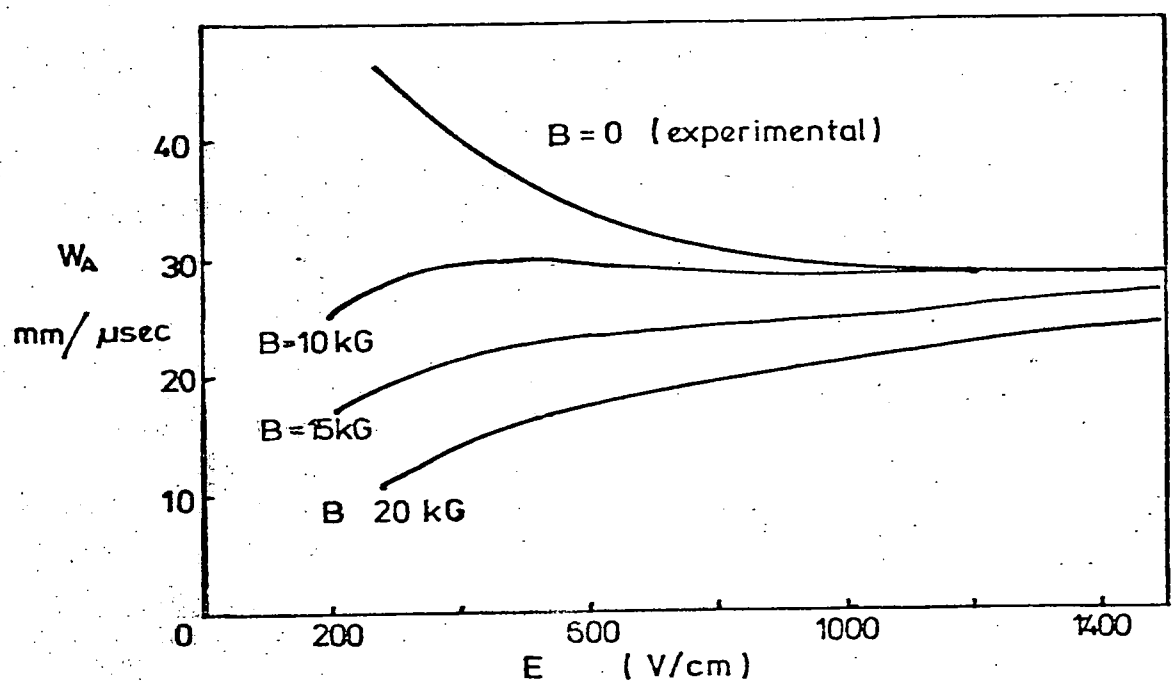

FIG 7.18 Theoretical variation of W_A with E for various values of magnetic field.

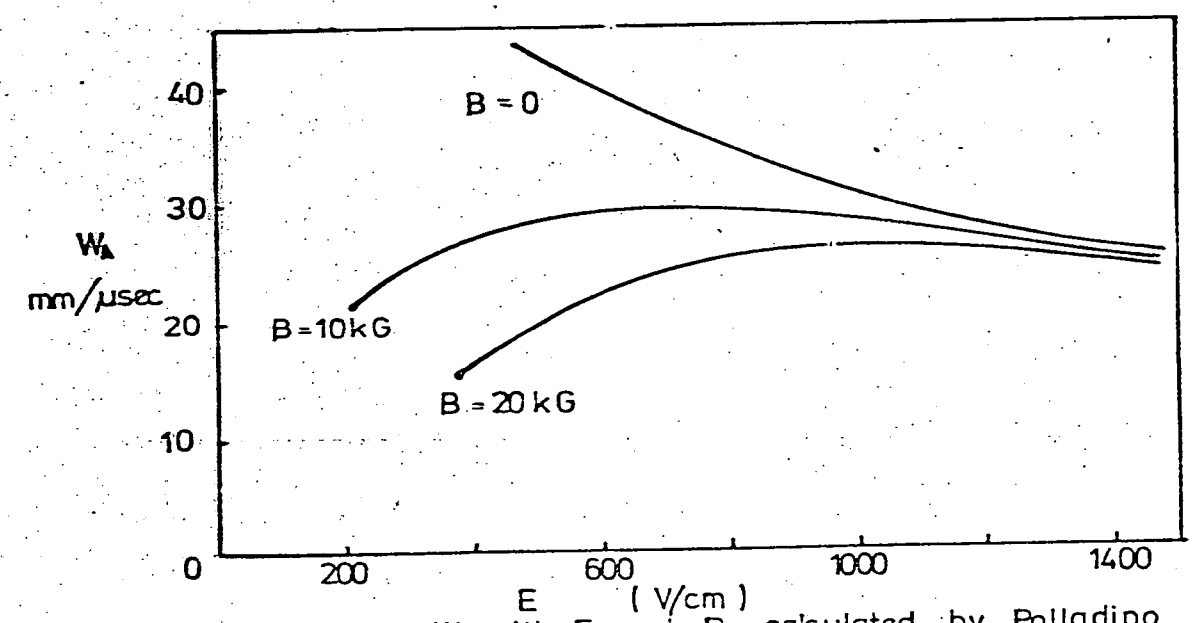

FIG 7.19 Variation of W_A with E and B, calculated by Palladino and Sadoulet for argon + 7% isobutane.

trajectory given by $\gamma - \phi$. As the purpose of compensation is to minimise $\gamma - \phi$, the general effect on resolution from this cause will be slight, except that there will be a tendency for resolution to worsen for those conditions when ϕ is greatly different from γ.

The second source of resolution variation is due to alterations in the value of the diffusion coefficient D. From the effective increase in gas density given in equations 6 and 7, D is expected to be decreased by the factor $(1 + \omega^2 T^2)^{-1}$. It was shown in chapter 6 however that chamber resolution for a drift distance d was dependent on the parameter σ_x where

$$\sigma_x = \sqrt{\frac{2Dd}{W_A}}$$

Thus any improvement in resolution due to the modified diffusion coefficient is partially nullified by the square root dependence, and simultaneous decreases in W_A

Figure 7.20 shows the variation of spatial resolution with drift distance for various values of B, E and γ. These were calculated from the deviation distribution widths, taking into account the variations of drift velocity between chamber 3 and the other two as mentioned previously. The conversion between distribution width and resolution was made by reference to the data for runs 2 and 3 where resolutions were already accurately determined for these conditions.

The experimental points on figure 7.20 are shown displaced about their mean drift distance for clarity, and in fact each point represents an overall resolution for a range of distances (3.5 mm) The data shows that at 1100 V/cm the resolution is slightly better with magnetic fields present than would be expected for the same

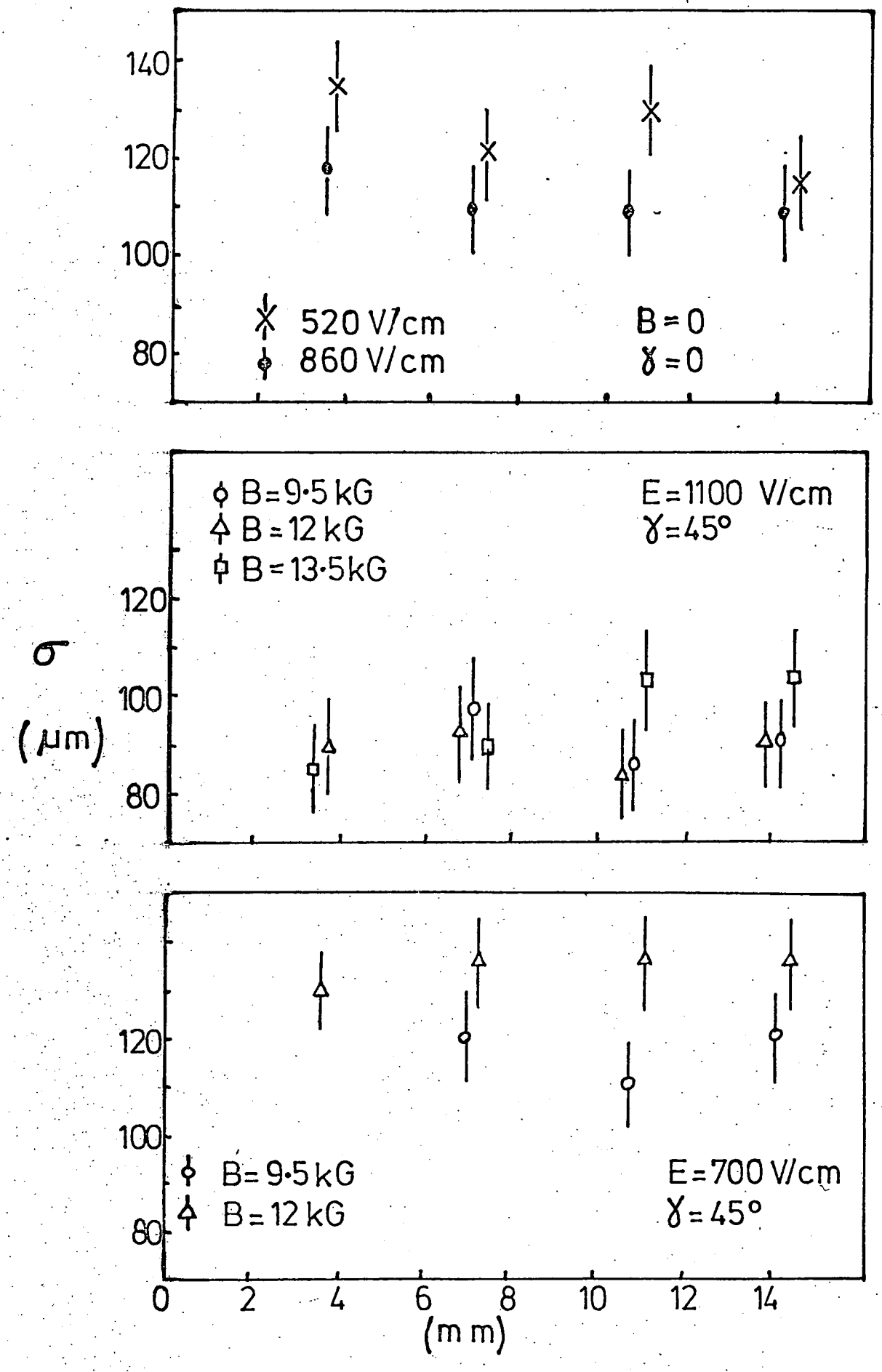

FIG 7.20 Spatial resolution versus drift distance for various conditions.

electric field and B = 0. This is presumably because the decrease in D is more significant than the geometrical effect, which is slight under these conditions, as compensation is good. For E = 700 V/cm the resolution seems little changed at B = 9.5 kG, although there may be some detioration at B = 12 kG, as the value of $\gamma - \phi$ is now becoming more significant.

7.7 Angled Trajectories

There are two basic points to be noted with respect to the combined effect of angled tracks and magnetic fields these being,

(a) The effects on chamber operating parameters are entirely due to geometrical considerations, involving the particle trajectory and the 'lines of drift' of the ionisation electrons. No fundamental changes would be expected therefore between different gas mixtures.

(b) When the slanted electric field compensation conditions are exact, the electrons drift parallel to the sense wire plane, and under these conditions the effect of angled tracks will be exactly as described for the case of B = 0.

This second point is illustrated by the work of Charpak et al (11) with argon + 30% isobutane (+ 2.5% methylal). Figure 7.21 from their work shows the time distance relationship and detection efficiency for normal and inclined tracks at B = 10 kG, E = 1400 V/cm and $\gamma = 32^{\circ}$ (correct compensation conditions for their gas mixture).

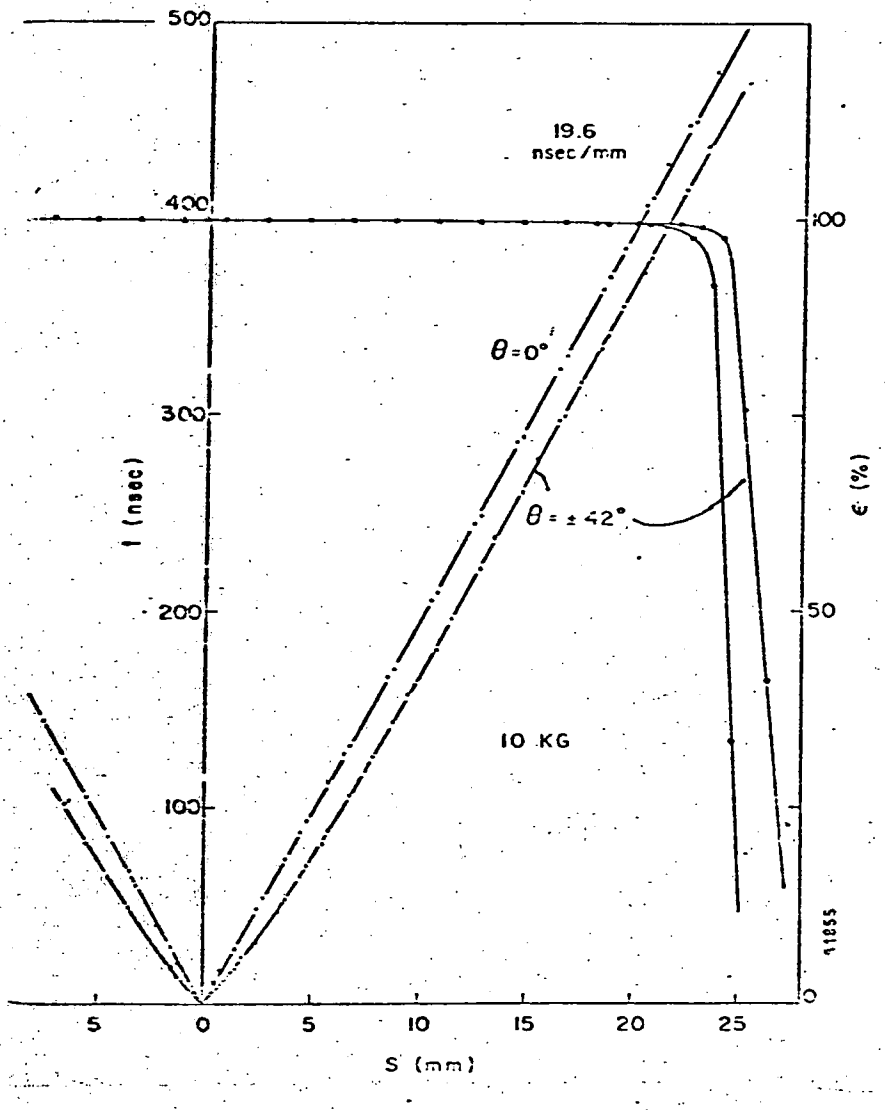

FIG 7.21 Time distance curves and effeciency for angled tracks in argon, isobutane (Charpak et al)

The efficiency is seen to be maintained at 100% for tracks at 42^{o} to the normal. The extension of efficiency beyond the cell width (24 mm) for the angled tracks is merely geometrical, the distance on the horizontal axis being measured in the sense wire plane. Furthermore, there is no reported difference between the track being tilted in the same direction to the field slant or opposite to it, as indicated by the $\pm$ sign on the figure. These results and the similarity with the B = 0 case, are supported by more extensive later work by the same group (9)

The similarity in spatial resolution for angled tracks, with and without compensated magnetic fields, is indicated by figure 7.22 which shows data collected from reference 11 for tracks at 42^{o}, for conditions B = 0 and B = 12 kG, $\gamma = 32^{o}$.

Angled track data taken as part of the tests described in this chapter was intended to investigate the effects of inexact compensation conditions. Thus the runs were carried out at B = 13.5kG, E = 1100 V/cm and $\gamma = 45^{o}$, which had a secondary advantage of approximating to the g-2 operating conditions. Previous results have shown that for the above conditions, the electron drift angle (to the drift field) should be 58^{o}, so that they will drift at 13^{o} to the sense wire plane.

For particle trajectories up to 15^{o} to the chamber normal, under these conditions, no discernable variation in either spatial resolution or efficiency was noted. The results for angles of 25^{o} are shown in figures 7.23 and 7.24, for resolution and efficiency respectively. Also shown on these figures for comparison are the corresponding results for normal trajectories. These figures indicate a possible slight worsening of resolution and efficiency for 25^{o} tracks at longer drift distances. This can be attributed, as for the

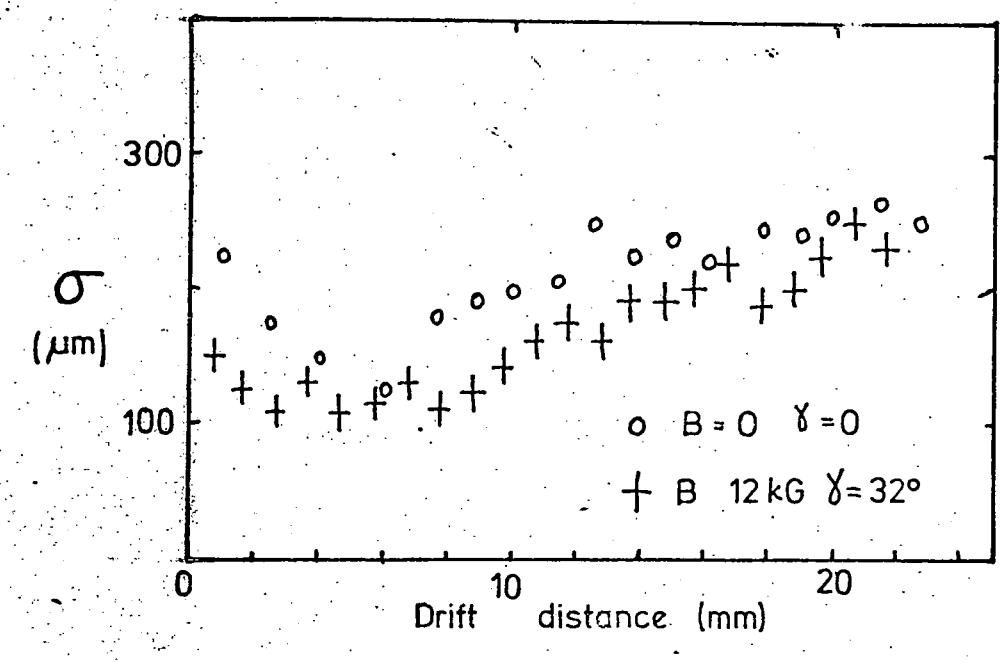

FIG 7.22 Results of Charpak et al for resolution due to tracks at 42° with and without magnetic fields.

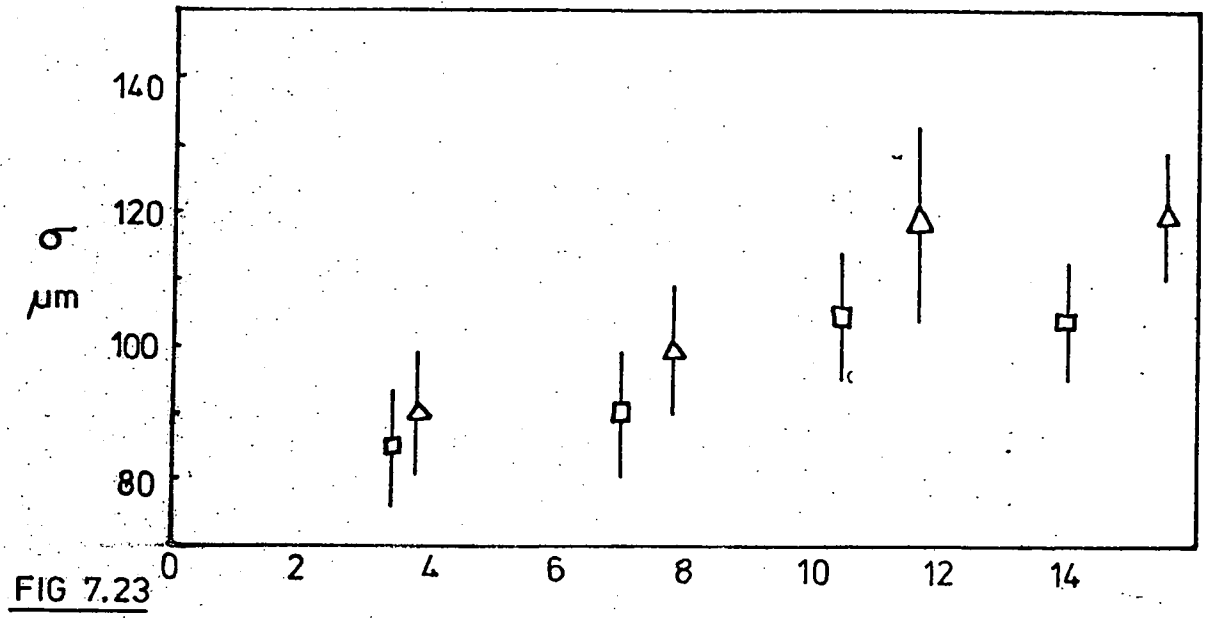

FIG 7.23

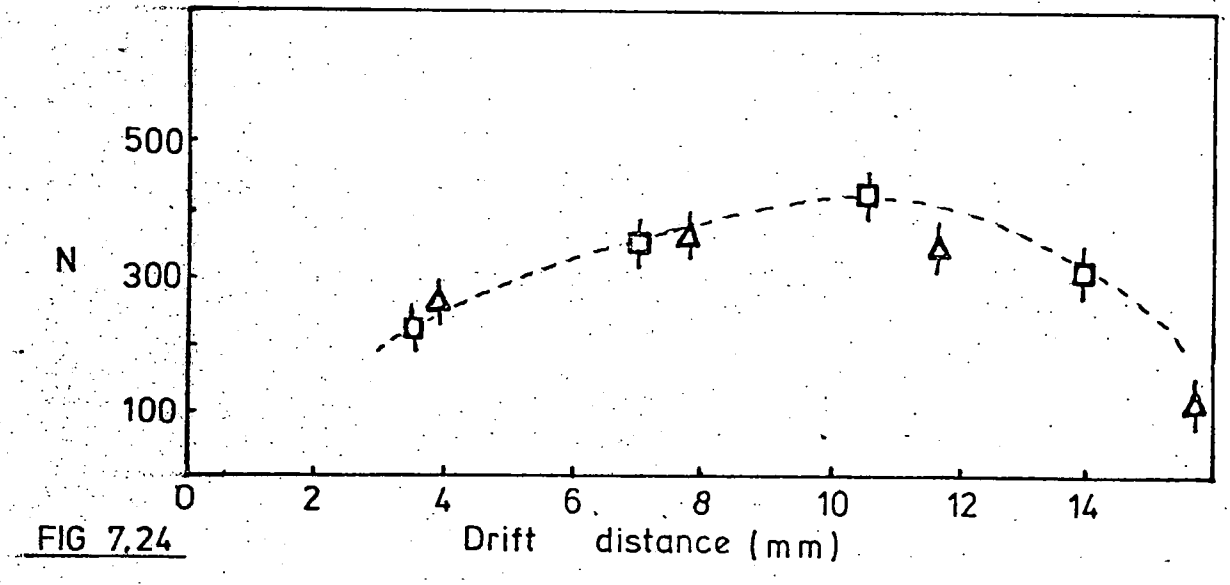

FIG 7.24

RESOLUTION AND NUMBER OF EVENTS PER HISTOGRAM FOR NORMAL AND ANGLED TRACKS AT 13·5kG, 1100 V/cm, δ=45°

NORMAL TRACKS

TRACKS AT 25°

zero magnetic field case, to the greater spread, in terms of drift path length, of the primary ionisation for angled tracks.

Figure 7.25 which shows the approximate lines of electron drift for the partially compensated magnetic field conditions above, indicates that for an angled track as shown, drift paths occur which are shorter than for the corresponding normal track. The results of the 25^{o} run support this, as they yield a drift velocity of 25 ± 2 mm/μsec, compared with the measured value of 21 ± 2 for normal tracks. With reference to figure 7.16(a) it is interesting to note that the measured velocity for the 25^{o} run is in better agreement with the theory than that for the normal track.

Although data was not taken for tracks angled in the opposite sense (as shown by the broken line in figure 7.25) it would appear from the figure that in this instance the shortest drift path would not be reduced to the same extent and thus different drift velocities would result. It is regretted that the time allocated on the Daresbury e^{+} beam was not sufficient to allow this and other effects to be studied in greater detail, although it is felt that other techniques (involving actual drift time-distance measurements) would be much more appropriate to the determination of drift velocity variations (see section 9.2).

7.8 Conclusion

The work of this chapter has shown that drift chambers containing argon + 10% methane can be operated successfully in magnetic fields up to 13.5 kG. (This also applies to trajectories angled at up to 25^{o} to the normal) by the application of slanted electric field compensation techniques. For high values of E (say greater than 1000 V/cm and a field slant of 45^{o} this can be achieved with no

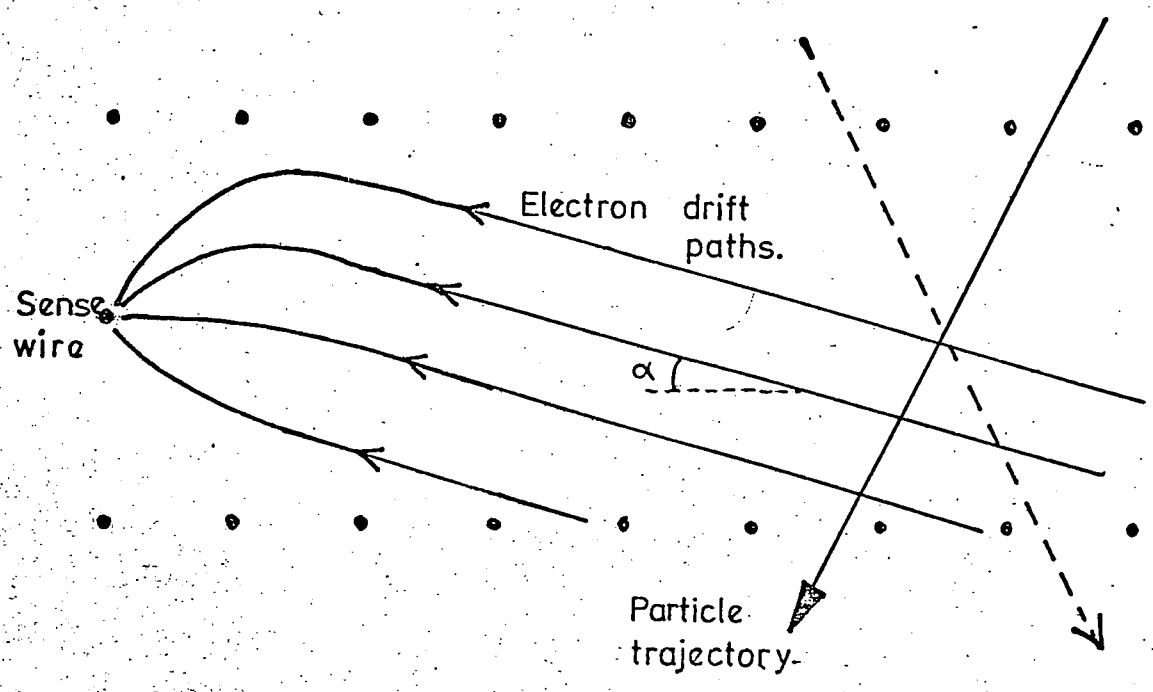

FIG 7.25 Model for angled tracks in the prescence of partially compensated magnetic fields.

significant worsening of resolution or efficiency, and the resulting drift velocity (required for calibration purposes) can be described by simple theory.

The results obtained are in reasonable agreement with those of other workers using argon-isobutane mixtures (9,11), the main difference being that for our mixture, the electron velocity distribution and collision cross section variation are such that a high value of magnetic deflection coefficient, ψ , is obtained. This is supported by the calculations of Palladino and Sadoulet (3) and leads to larger drift angles, ϕ, for our mixture and consequently a larger degree of compensation is required. This is offset to some extent however by our lower value of W_o, which tends to reduce ϕ (see equation 15)

It is lack of theoretical knowledge as to the precise value of ψ for argon + 10% methane which makes it difficult to predict drift velocity variations and exact compensation conditions without reference to some experimentally determined data. A value of between 4 and 5 appears to be the best fit to all our data, for B in the range 8 to 13.5 kG.

It is interesting to note the results of Sadoulet and Litke (10) who found that for conditions of radial electric field (i.e. near to the sense wire) drift chambers could be successfully operated in strong magnetic fields with no compensation techniques. This effect, combined with an efficiency fall off with distance from the sense wire, may explain some of our earlier test results (not described here) in which data from the whole cell was analysed collectively and appeared to give good resolution in magnetic fields regardless of compensation conditions (12).

CHAPTER 7 - References

1. G. Charpak, F. Sauli, W. Duinker, Nuc. Inst. Meth. 108 (1973) 613

2. J.S. Townsend, 'Electricity in Gases', Clarendon Press, Oxford (1915)

3. V. Palladino and B. Sadoulet, Lawrence Berkeley Laboratory Internal Report LBL-3013 (1974)

4. W.P. Allis, 'Handbuch der Physik', ed. S. Flugge, Springer-Verlag, Berlin (1950) Vol. 21, p. 383.

5. L.G.H. Huxley, Phil. Mag. 23 (1937) 210.

6. L.S. Frost and A.V. Phelps, Phys. Rev. 127 (1962) 1621

7. L.G.H. Huxley, Aust. J. Phys. 13 (1960) 718.

8. R.L. Jory, Aust. J. Phys. 18 (1965) 237

9. A. Breskin, G. Charpak, F. Sauli, M. Atkinson and G. Schultz. Nuc. Inst. Meth. 124 (1975) 189.

10. B. Sadoulet and A. Litke, Nuc. Inst. Meth. 124 (1975) 349.

11. A. Breskin, G. Charpak, B. Gabioud, F. Sauli, N. Trautner, W. Duinker and G. Schultz, Nuc. Inst. Meth. 119 (1974) 9.

12. J.M. Breare, R. Browell and K.A. Short, Durham University Internal Report NI-75-1 (1975)

CHAPTER EIGHT

DISCUSSION OF DRIFT CHAMBER APPLICATIONS

8.1 Drift chambers for the g-2 experiment

This section describes the development, undertaken by the Nuclear Instrumentation Group at Durham University, of drift chambers for use in an experiment at CERN, Geneva, and may be considered fairly typical of the application of such chambers to high energy physics. The author was actively involved in this development up to and including the installation and testing of prototype chambers in the muon storage ring at CERN.

8.1.1 The g-2 experiment.

The magnetic moment μ of a muon (spin $s = \frac{1}{2}$) in terms of the Bohr magneton μ_o is given by simple theory as

$$\mu = -g \mu_o s$$

where $g = 2$

The rigorous application of quantum electrodynamic theory (Q.E.D). however predicts a slight anomaly in the g factor for muons, described by a_μ, where

$$a_\mu = (g - 2)/2$$

Experiments in which a_μ is measured to a high degree of accuracy are known as $g - 2$ experiments. The importance of measuring a_μ to such high accuracy is that its value can be predicted by Q.E.D. very precisely (1,2) and so an accurate experimental determination provides

a good check of the theory. Current theory gives a_μ as $(1165889\pm17)\times10^{-9}$ (3) whilst the experimental value prior to this experiment was $(1166160\pm310)\times10^{-9}$ (2). Whilst these results may be only statistically different, they may in fact be the first sign of a discrepancy. Thus if a_μ can be measured to a precision of 10-20 ppm, then it should either resolve or confirm the deviation (4). This is the main purpose of the present g-2 experiment.

The theory behind the experimental method of determining a_μ is described in papers relating to earlier g-2 measurements (2,5) but basically it consists of measuring the count rate of decay electrons from a circulating beam of muons in a storage ring. The anomolous magnetic moment causes this count rate to be modulated by a factor dependent on a_μ. In the present experiment muons are stored in a 14 m diameter storage ring and the electrons are monitored, as they emerge from the beam vacuum tube, by 20 shower counters (4).

8.1.2 The need for drift chambers.

In order to achieve the necessary precision of measurement it is essential that all parameters affecting the experiment are accurately determined. One such parameter is the circulating beam profile. Although this can be measured internally to some extent, it was decided that an external system, determining the point of origin of each decay electron, would offer many advantages. The necessary information can be obtained by defining electron paths as they leave a section of the vacuum chamber, calculating their motion in the particular configuration of magnetic field present, and extrapolating the trajectories back to their point of origin within the muon beam. To ensure that this technique has any value it is necessary to define a minimum of 3 points on the electron trajectory to within 0.1 mm,

and also to introduce a minimum of scattering matter into the path. Thus the use of multiwire drift chambers was indicated.

The continuous sensitivity of drift chambers means that any variations in beam profile with time (after injection) should be measurable. As the chambers are still functioning as 'proportional' chambers, the momentum of incident electrons will be measurable from the output pulse data thus providing a check on the discrimination level of the shower counters (which provide the timing start pulses and thus define valid events).

Information on the relative number of events occurring as multiple particle events (due to electron showering) will also be available.

8.1.3 Positioning of the chambers

Figure 8.1 shows the general layout of the g-2 muon storage ring and the position of the drift chamber system in a section of the ring directly opposite the inflector. This region was chosen as at this point the ring had no electrostatic focussing electrodes which would have scattered the decay electrons. To further reduce the possible electron scattering, a thin section of vacuum wall (0.8 mm titanium) was installed in this region, so thin in fact that it bowed inwards under the pressure differential, producing a curved cross-section. This factor was of importance in designing the shape of the chambers (see next section).

Figure 8.2. shows the more detailed arrangement of 8 drift chambers and 3 M.W.P.C.s (the responsibility of the Daresbury Laboratory) which make up the planned final track recording system. The counter shown is one of the 20 monitoring the modulation of the electron count rate, and provides the zero time pulse for the drift chamber electronics. Hence only those electrons tracks which inter-

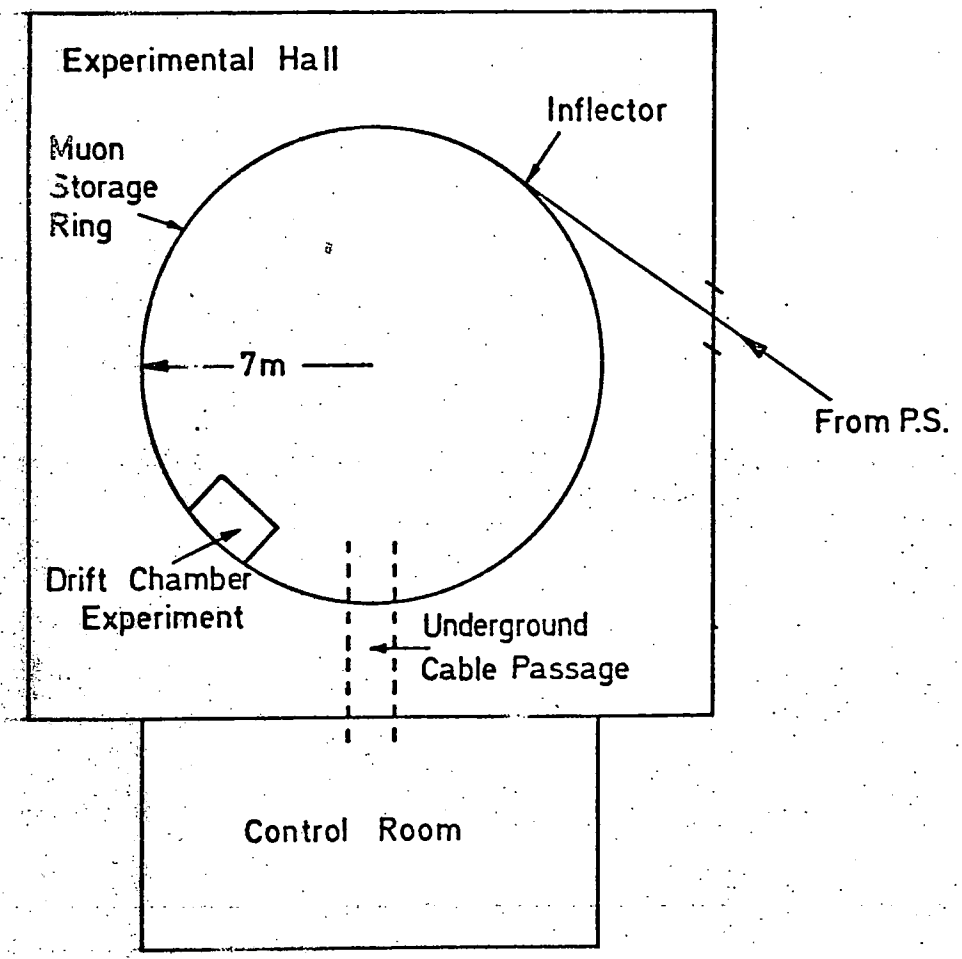

FIG 8.1 Plan of g-2 experiment

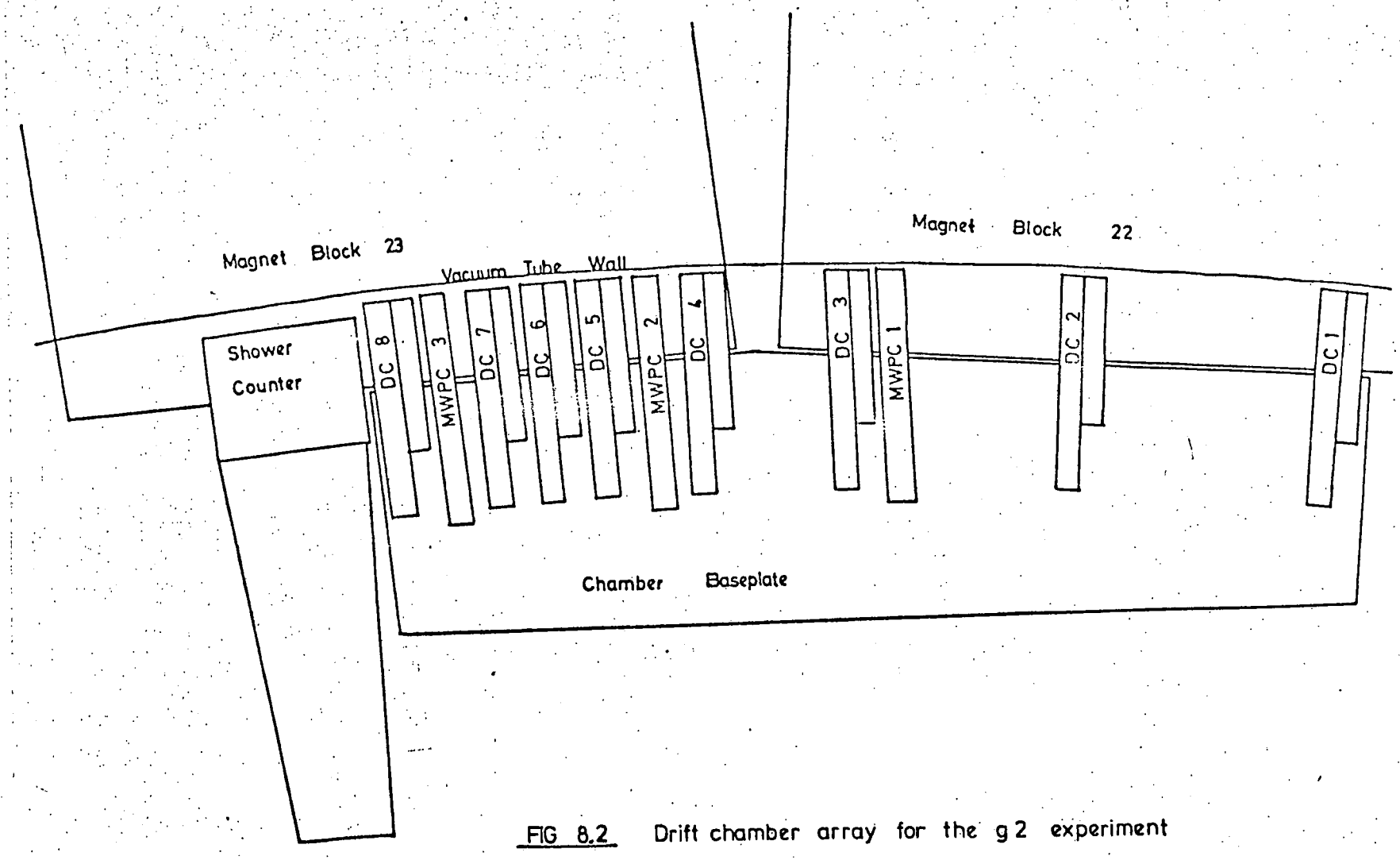

FIG 8.2 Drift chamber array for the g 2 experiment

sect this counter will be recorded by the drift chambers, and they may be due to high energy electrons passing through the system from chamber 1, or low energy electrons bending sharply out of the ring through the last few chambers. In order to ensure the maximum number of recorded points on such sharply bending tracks, the chambers are packed close together near to the counter.

In order to obtain information on the electron tracks very near to their source it is necessary to position the sensitive volume of the chamber as close as possible to the vacuum wall, and in figure 8.2. the chambers are seen to be inside the boundaries of the magnet blocks. Figure 8.3. shows this more clearly in the form of a section through a magnet block with a chamber in position. Some major dimensions are indicated on the figure (in mm). One problem associated with the position of the chamber as shown in figure 8.3. is that the sensitive volume is subject to a non-uniform magnetic field, varying between about 15 and 5 kG.

8.1.4 Chamber Design.

Figure 8.4 shows a sketch of the final design of chamber to be used in the experiment. The following mechanical details are relevant here.

The concave vacuum wall section required a similarly curved thin end section on the chamber. Attempts to machine this section were unsuccessful, and it was finally constructed from a piece of laminated glass fibre epoxy resin (G.10) 0.5 mm thick, bent into the required shape and held in place under tension by adhesion to the side members. This section of the sensitive volume raised several problems associated with maintaining uniform electron drift velocities. In general the resolution from this region is 2 or 3 times worse than in 'normal' regions (6).

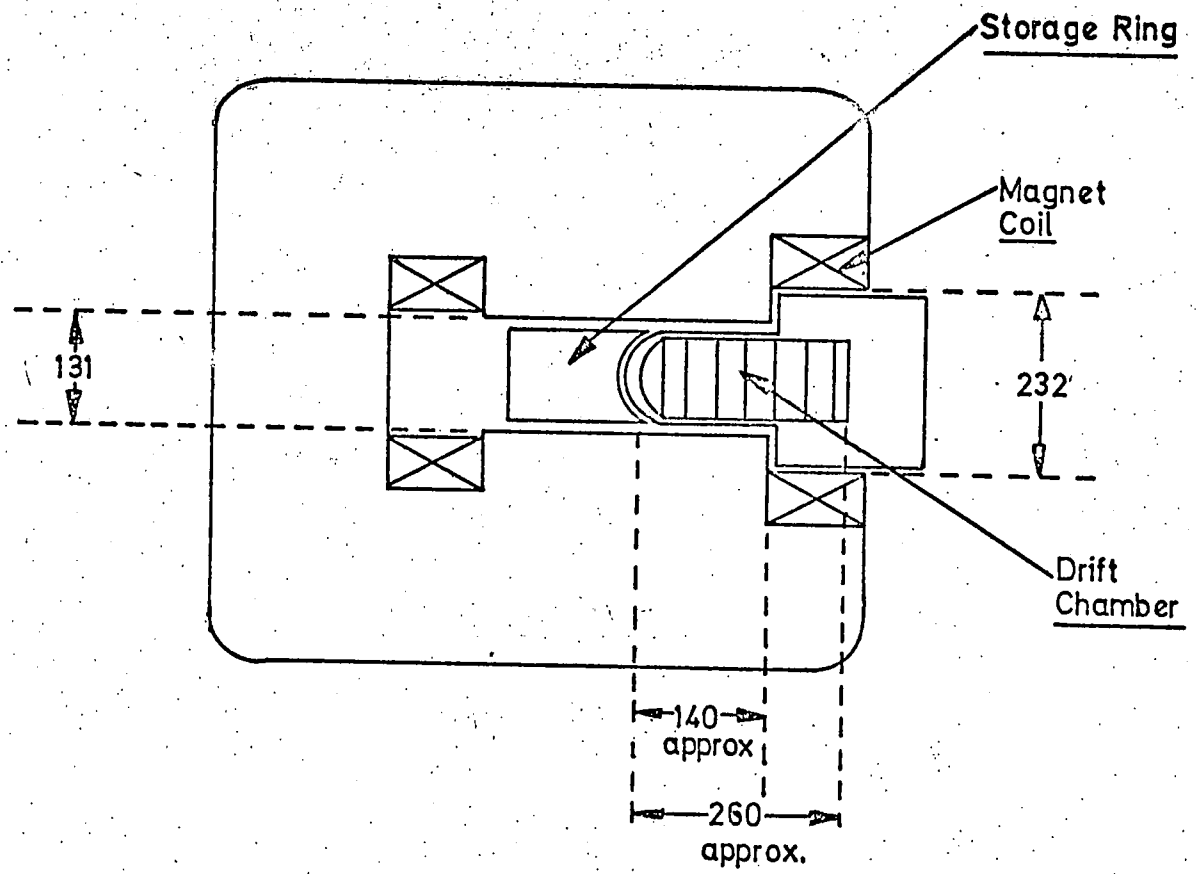

FIG 8.3 Section through storage ring, dimensions in mm.

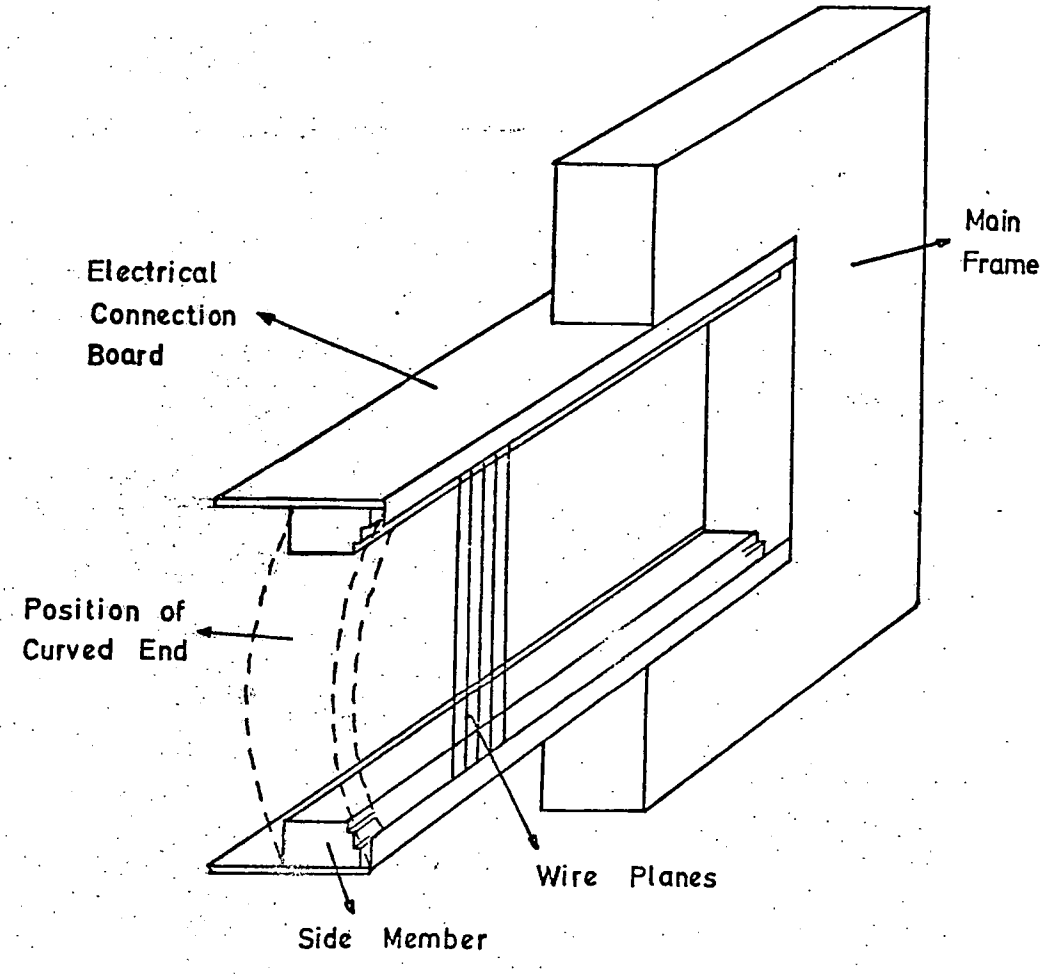

FIG 8.4 Sketch of g-2 chamber

The side members had to be thin enough to make maximum use of the restricted space between the magnets and yet strong enough to support the considerable tension of the wire planes without flexing. G10 bars, 11 mm thick were used at first, but these would support the wire tension only after a complex prestressing construction technique, which was considered unsatisfactory. It was finally suggested by International Research and Development Co. Ltd. (I.R.D.) who were to manufacture the actual chambers for the experiment (to Durham specifications), that glass might be a more suitable material, having a Young's Modulus value 30 times greater than G10. After some problems with machining and adhesives, the final chambers were constructed with glass side members and proved satisfactory.

The main frame(G10) is as massive as possible to provide overall rigidity for the chamber and to facilitate mounting on the baseplate. Fiducial lines are scribed on the main frame, parallel to the sense wires and at an accurately determined distance from them. These lines can then be optically surveyed during the system alignment procedure much more easily than the actual sense wires.

In order to simplify the alignment procedure each chamber in the array is mounted in a cradle having vernier adjustment of horizontal position and vertical orientation. Figure 8.5 shows three of the actual experimental chambers (manufactured by I.R.D.) mounted on these cradles. The H.T. distribution boxes are mounted on top of the main frames.

The configuration and construction of the wire planes was the same as for all chambers described previously, except that the g-2 chambers consisted of 8 adjacent cells 28 mm wide. The electrical connection system was identical to that described in section 7.4.1 (figure 7.7 applies).

Figure 8.5 – Three g-2 drift chambers mounted in adjustable cradles.

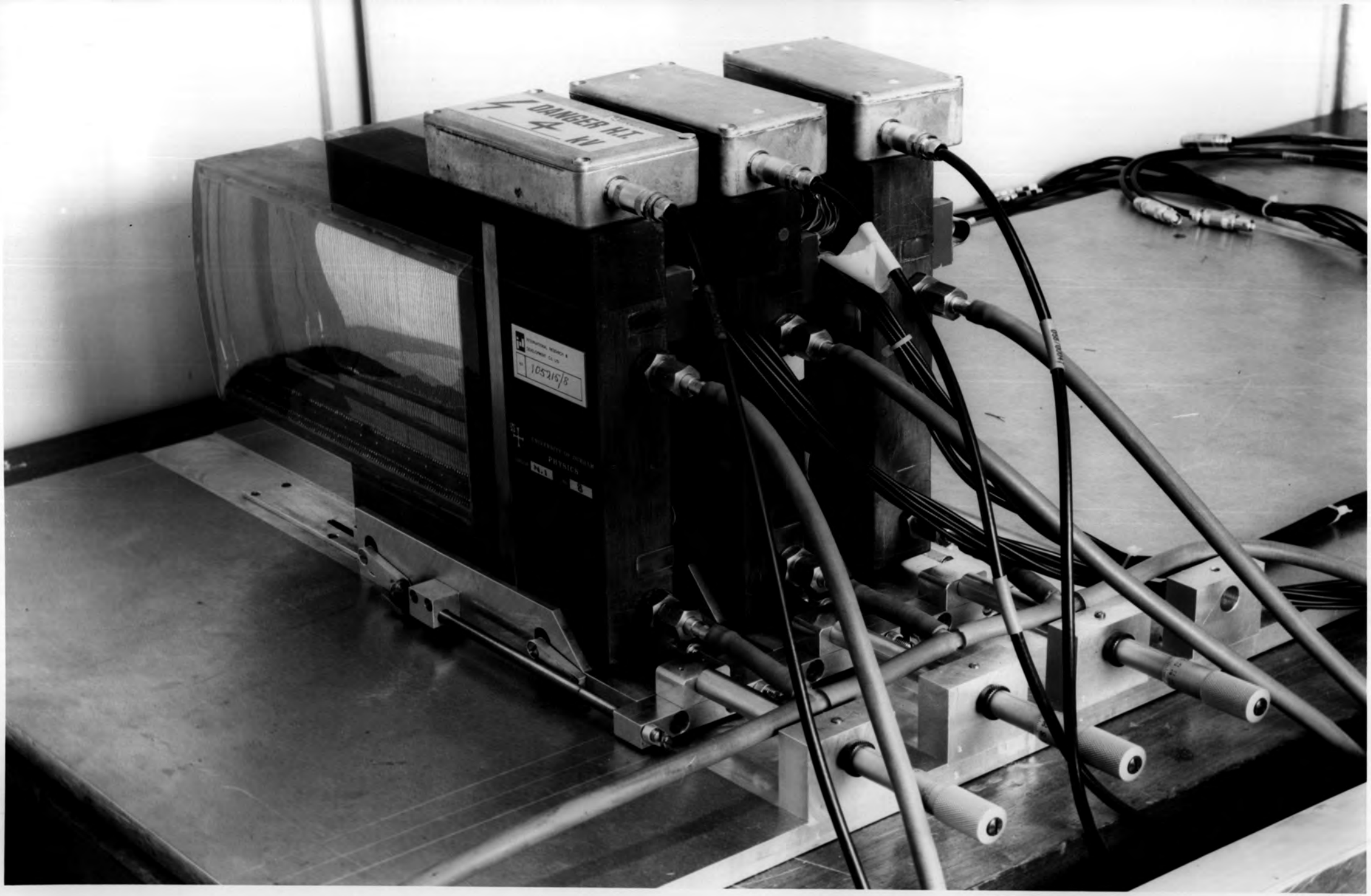
DANGER H.T.
4 KV
105215/5
PHYSICS

8.1.5 Operation of chambers

As the chambers function partially in the leakage field of the storage ring magnets, the value of B across the chamber is not constant. Figure 8.6 shows this variation versus distance from the vacuum tube wall, up to the end of the chamber sensitive volume. Obviously one set of conditions will not compensate exactly for B over the whole chamber, and three solutions to the problem were considered.

With one value of γ the applied drift field E_a could be varied from cell to cell to suit the magnetic field. The idea was rejected as it required a very complex H.T. distribution system and resulted in regions of excessively high or low values of E.

Alternatively, keeping E_a constant, the value of γ could be varied for different regions across the chamber. This method was tried during the initial tests in the storage ring (7), but again it was rejected because of practical complications and uncertainties around the interface of 2 different γ values.

The method adopted for the final system was the practically simpler one of applying the same E and γ across the whole chamber, with values such that good efficiency is maintained throughout. The resulting variation of drift velocity across the chamber (as B varies) must of course be accurately known for calibration purposes. Conditions chosen for the experimental chambers were a slant of 3 ($\gamma = 45^{\circ}$) and $E_a = 600$ V/cm (E$\sim$900 V/cm), although a higher electric field value may have been more satisfactory.

Using these values, and the results of chapter 7 we can estimate the values of α ($= \phi - \gamma$) and w_s across a g-2 chamber. These are shown in figures 8.7 and 8.8 respectively.

Figure 8.7 shows that for g-2 chambers α is less than 20°

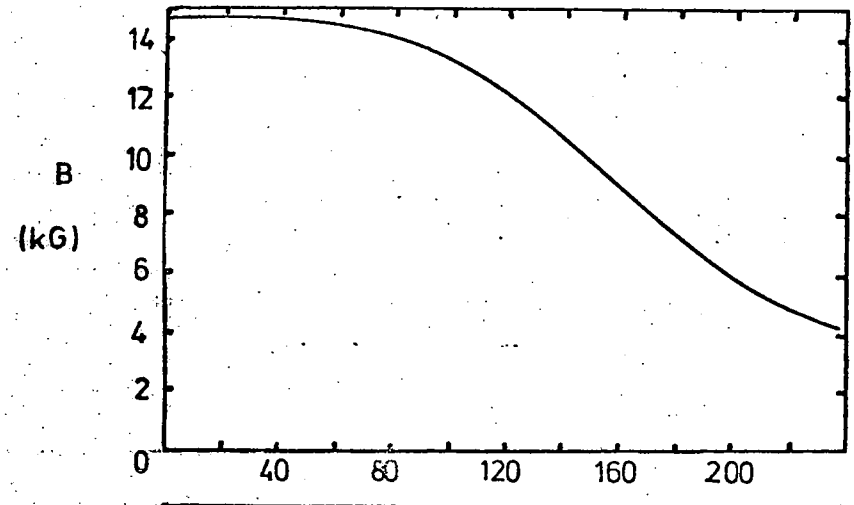

FIG 8.6

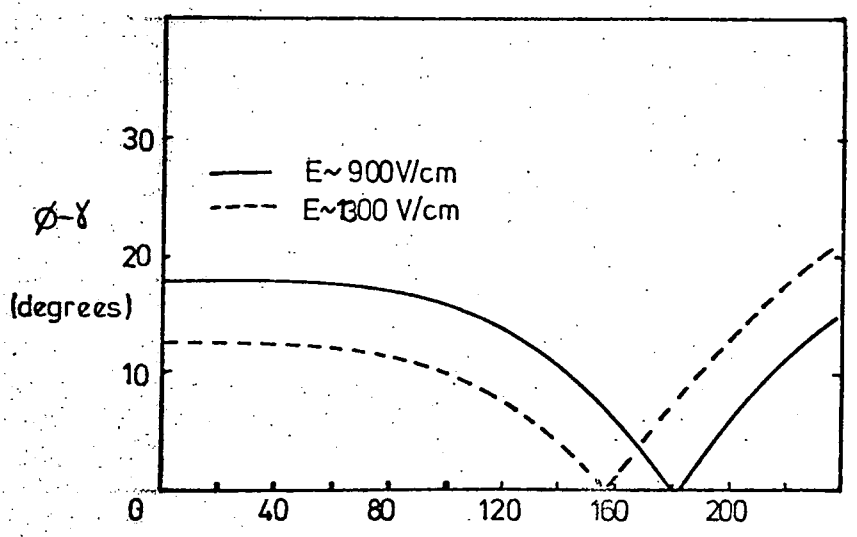

FIG 8.7

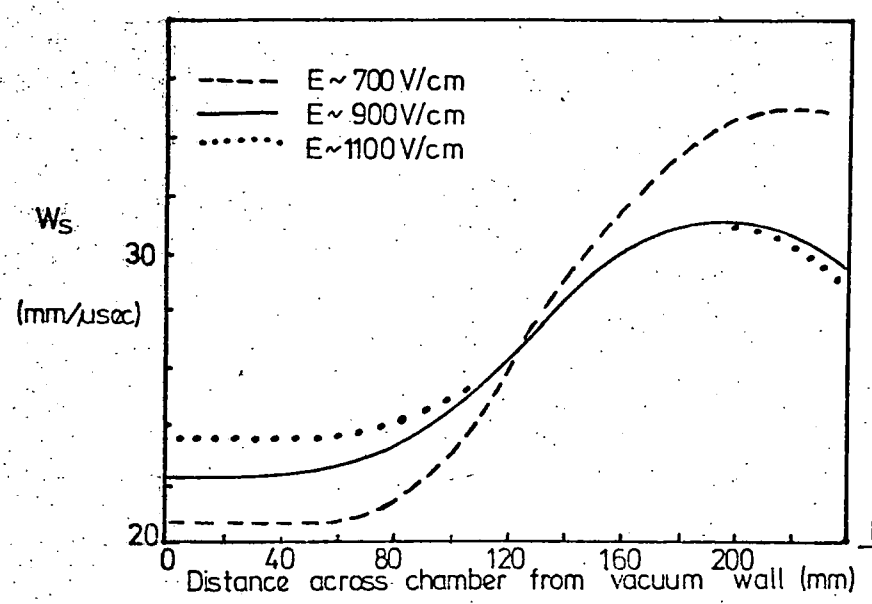

FIG 8.8

Variation of magnetic field, Ø-γ, and drift velocity, across a chamber installed in g-2 storage ring.

over the whole chamber, so that high efficiency should be attainable, except possibly for the longest drift times. This figure also shows the effect of increasing E_a to about 900 V/cm (E~1300 V/cm). This would improve the compensation in the region of main interest (i.e. near to the vacuum tube) at the expense of cells further out.

Figure 8.8 shows the expected variation of w_s across the chamber for 3 drift fields, including the one used in the g-2 runs. Figure 8.9 shows the corresponding values of average drift velocity across each individual cell (for E = 900 V/cm).

8.1.6 Results

Results of the preliminary tests on chambers in the storage ring are described in an internal report (7) but will be summarised here.

A significant problem was found to be one of electrical interference arising from many sources. For instance the chamber sense wires acted as extremely efficient aerials for the receiption of the local Suisse-Romande television transmissions. Shielding the chambers in aluminium foil reduced the background noise level to an acceptable level. Larger noise signals were generated by the actual experiment (e.g. from the inflector and pulsed electrostatic focussing field) but were generally of short duration and occurring at regular intervals, and so could be gated out in the electronics. More serious was the large flux of pions through the chamber at the time of injection. The actual pulse due to the pions was quite short (1 μsec) and could be easily gated out, but the flux was so large that the chamber was then saturated with positive ions which may take a considerable time to clear. Results of later runs (6) indicate that this is still a problem and chamber sensitivity is reduced up to 175 μsec after the initial pion burst. Some sort of clearing field applied

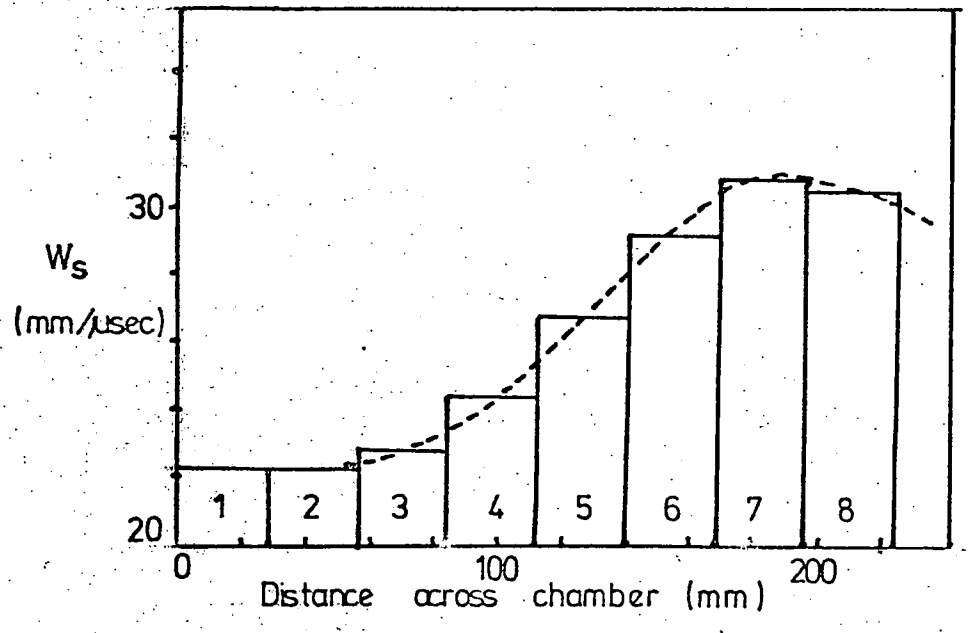

FIG 8.9 Average drift velocity in each cell of g-2 chamber for E=900 V/cm.

during the initial burst to remove the ionisation electrons rather than let them avalanche, may be the solution.

Figure 8.10 shows the sequence of events during a g-2 cycle and figure 8.11 shows the gating system and sequence of system pulses. This system formed the basis of the final experimental system. Using the simple system of figure 8.11 a drift time distribution from one cell of one chamber was obtained as shown in figure 8.12 (Note that this entailed successfully sending amplified chamber pulses down 32 metres of cable from the storage ring to the electronics in the control room). The distribution indicates the low signal to background ratio present during the runs, although coincidences between several chambers should eliminate random background. The width of the estimated 'real event' distribution indicates a drift velocity of $w_s = 29 \pm 1$ mm/μsec, in good agreement with the predicted value for the conditions existing in the cell ($B \sim 9$kG, $E \sim 900$ V/cm, $\gamma = 45^{\circ}$) i.e. $w_s = 30$ mm/μsec, from figure 8.8.

Other tests were carried out, including an investigation to determine the number of decay electrons accompanied by another associated particle, and generally the whole series of initial tests indicated that the drift chamber system designed at Durham would function adequately in its assigned task. Although the author's active involvement in the g-2 project ended at this point, the results of later runs are quoted in figure 8.13 (6). These indicate that the compensation conditions were adequate for the range of magnetic fields across the chamber shown by the uniform detection efficiency across each cell. The variation in 'plateau' level corresponds to the decay electron flux density. The fact that the distributions are continuing up to 500 nsec indicate that the drift velocity is less than 28 mm/μsec for most cells. Cell 7 seems to cut off about 450 nsecs however, indicating a value of $w_s = 31$ mm/μsec. This

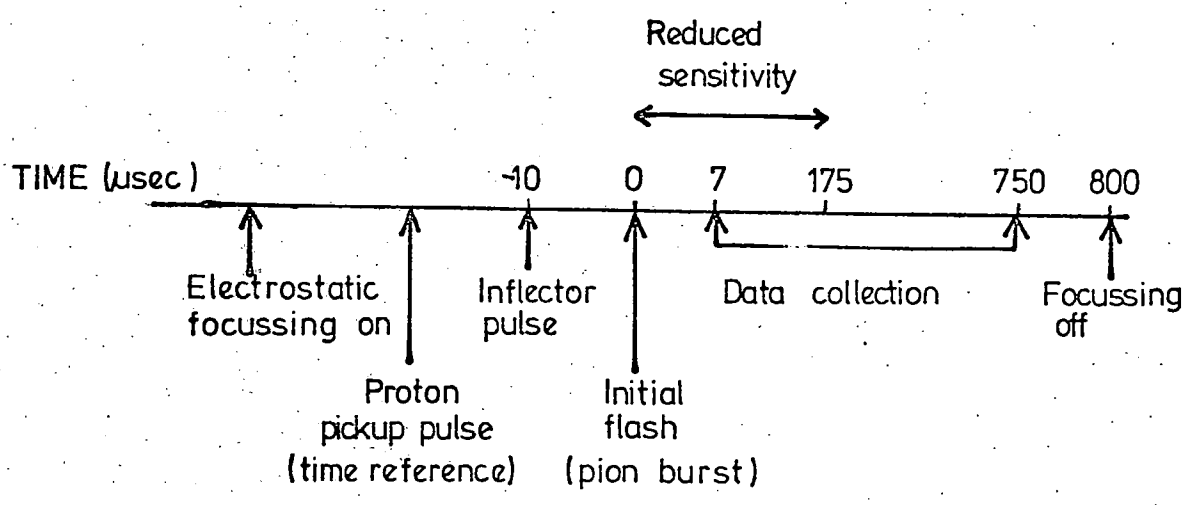

FIG 8.10 Sequence of events during a g-2 cycle

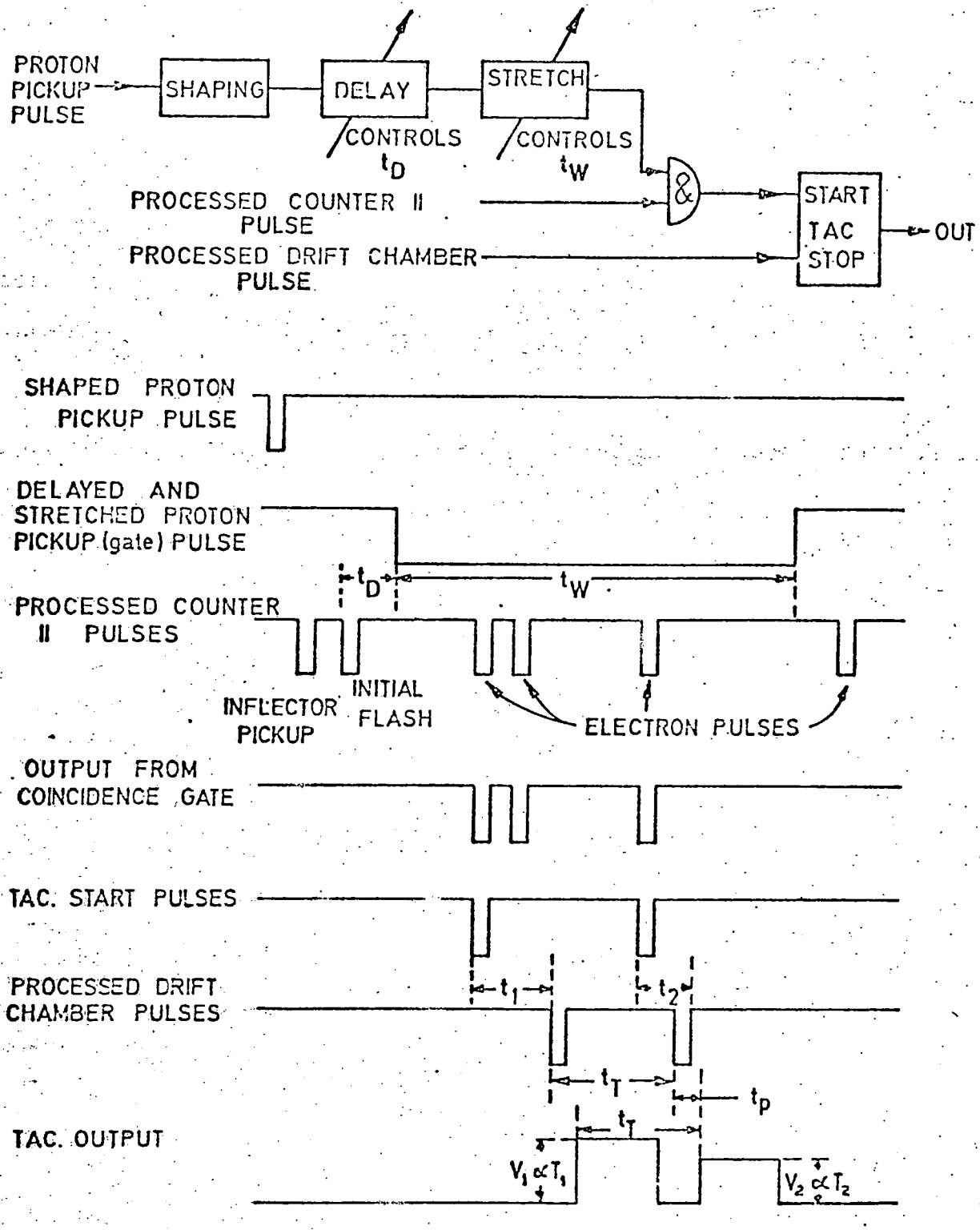

t_D = Delay between initial flash and start of gate.
t_W = Gate width.
t_1 , t_2 : Drift times
t_T : Separation time of events.
t_p : Processing time of TAC.

FIG 8.11 Basic g-2 gating system and sequence.

FIG 8.12 DRIFT TIME DISTRIBUTION FROM CELL 5 IN g-2 STORAGE RING. (HORIZONTAL SCALE : 4·2 ns/channel)

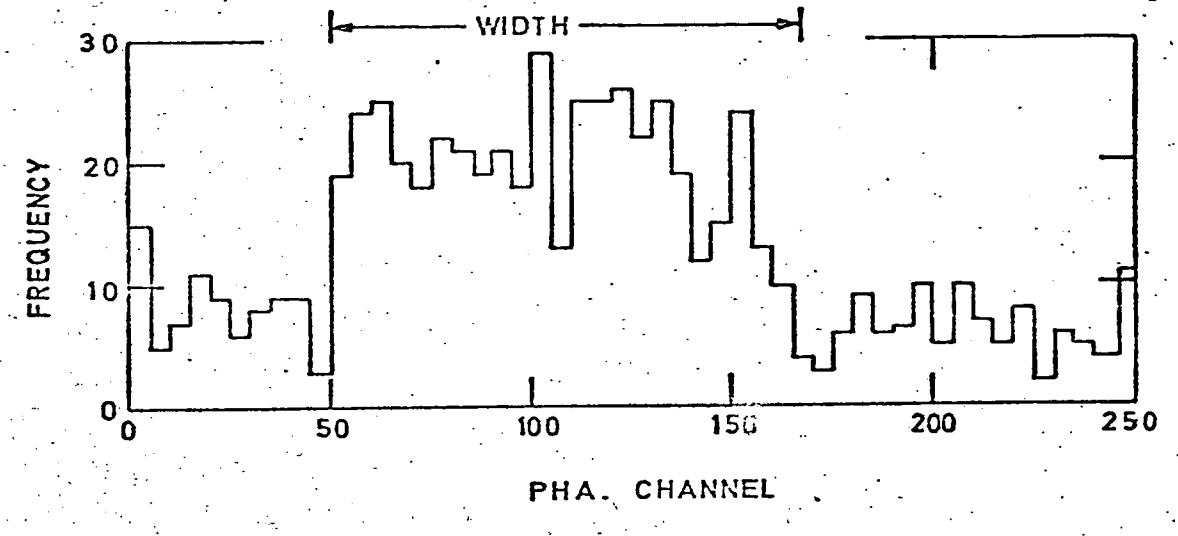

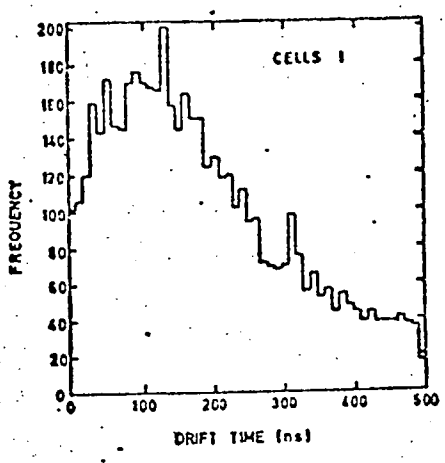

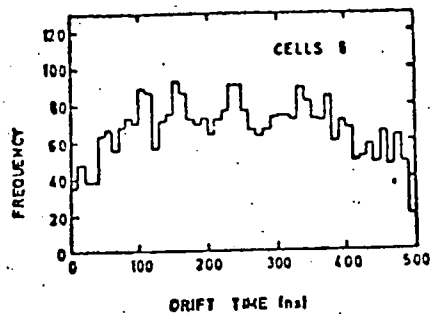

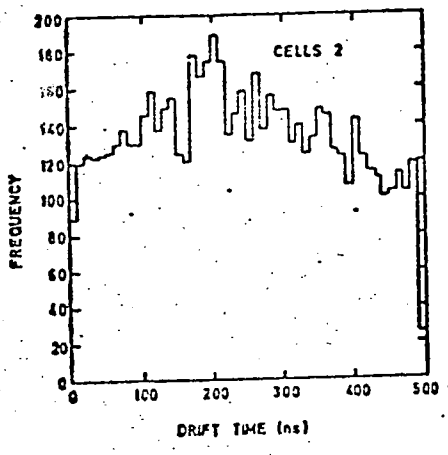

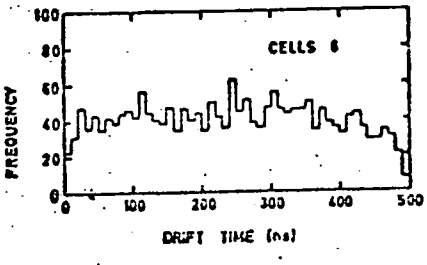

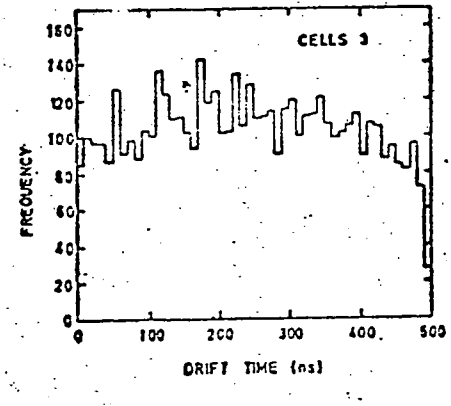

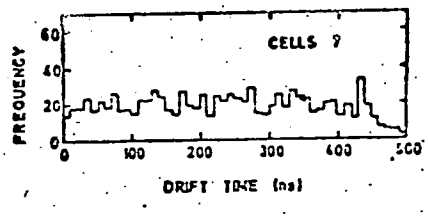

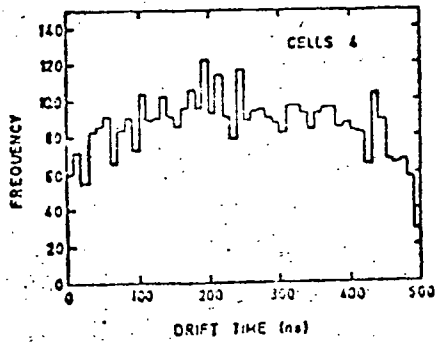

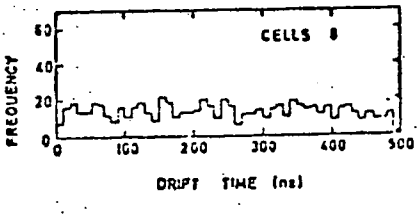

FIG 8.13 Drift time distributions from chambers in the g-2 storage ring.

is in agreement with the predictions of figure 8.9.

8.2 Other examples of Drift Chambers for experimental applications.

8.2.1 High Energy Physics.

One of the most successful applications of drift chambers to high energy physics was one of the earliest examples. This was the use of drift chambers by a CERN-Heidelburg group in an experiment to measure the branching ratio $K^+ \rightarrow e^+\nu / K^+ \rightarrow \mu^+\nu$ at the CERN PS from 1971-1972. The experiment used 7 large area (1 m^2) conventional multicell chambers, described by Walenta (8), with cells 21 mm wide, chamber thickness 10 mm and a gas mixture of argon + 9% methane + 7% isobutane.

Even larger chambers (13 m^2) have been built by a Harvard University group (9) as part of a high energy muon magnetic spectrometer for an experiment at N.A.L. The cell dimensions were 3.6 m long by 100 mm wide. A single voltage H.T. plane was used with field wires between each cell and a chamber thickness of 50 mm. The gas used was ethylene + 20% argon and resolutions during tests were as quoted in section 5.6.

Detectors based on the original drift chamber concept of separate drift space and detection regions have been developed at Saclay (10) and used in conjunction with the 1 GeV spectrometer there in 1972. The chambers comprise 2, long (500 mm), drift spaces with a uniform electric gradient maintained from one end to the other. Particles traverse the spaces (orthogonal to the long dimension) and the resulting electrons are drifted into single wire proportional counters (one for each space). Neon + 50% methane as the gas mixture gave resolutions from 0.61 to 1.63 mm for drift lengths from 120 to 500 mm. Pure methane gave corresponding values of 0.4 to 1.3 mm.

An interesting result of this work was that no reduction in efficiency was noted for drift lengths up to 500 mm, and the pulse height spectrum from a beam of 1.04 GeV protons was unchanged for drift lengths of 50 to 250 mm, suggesting that electrons can be drifted without attenuation over this sort of distance.

A somewhat different application has been put forward by a group at Oxford University (11). The principle is shown in figure 8.14. Particles pass through the device as shown and the resulting ionisation electrons are drifted towards a plane of 300 sense wires. Thus there will be 300 estimates of distance of the trajectory from the plane (from the drift times) and 300 samples of the energy deposited, allowing particle identification to be made.

None of the experimental applications up to now have involved operation in strong magnetic fields (except g-2), although two future experiments will. These are, (i) A neutron experiment on the OMEGA spectrometer at CERN for which Charpak's group have developed large (3 m^2) multiplane chambers designed to operate in fields of up to 18 kG (ii) A programme of muon physics again at CERN, for which many drift chambers have been proposed (12). Future applications relating to work at Durham University are covered in the next chapter.

8.2.2 Drift Chambers for X-ray detection

Major problems in using drift chambers to localise X or γ ray photons are the difficulty in providing a zero time pulse without absorbing or significantly affecting the photons, and the generally poor detection efficiency of gaseous detectors for photons, particularly those at high energies.

The first of these virtually precludes the use of conventional drift chambers with X radiation, unless it is emitted in the form of a pulse with good time resolution, or possibly accompanied by an

associated ionising particle to give a trigger.

A form of drift chamber which overcomes these problems can be achieved however, based on the original idea of a separate drift space added to a M.W.P.C. (13). Figure 8.15 shows this principle. (Note that this is not strictly a drift chamber as locational information is not provided directly by measurement of the drift time. In fact no timing systems are needed. However as such devices rely on the electron drift process and are commonly known as drift chambers they are included here). The principle has recently been extended by Charpak et al (14) to cope with X rays emitted from a point source (e.g. 'X ray crystal diffraction experiments). This is achieved by having a spherical section photon conversion region and a radial drift field such that the coordinates of the conversion point are transferred to the M.W.P.C., as shown in figure 8.16, from this work.

For high energy γ ray detection the efficiency problem is magnified. In this context work is now being carried out at CERN (20) in the U.S.A. (21), and now at Durham, into photon detectors like those of figure 8.15 but having metal converter material in the conversion space. This takes the form of blocks of thin perforated sheets, with the perforations aligned, insulated from one another so that a drift field can be applied across them. High energy photons are converted in the metal and there is a probability that one of the products will escape the metal into the nearest one of the perforation 'channels' causing ionisation. The resulting electrons are drifted down the channel into the M.W.P.C. as before. The resolution is obviously related to the separation of the perforations, and the efficiency depends on the geometry of the converter. The best published results at present are from CERN (20) for 0.66 MeV photons, having a spatial resolution of 1 mm and an efficiency of 5%.

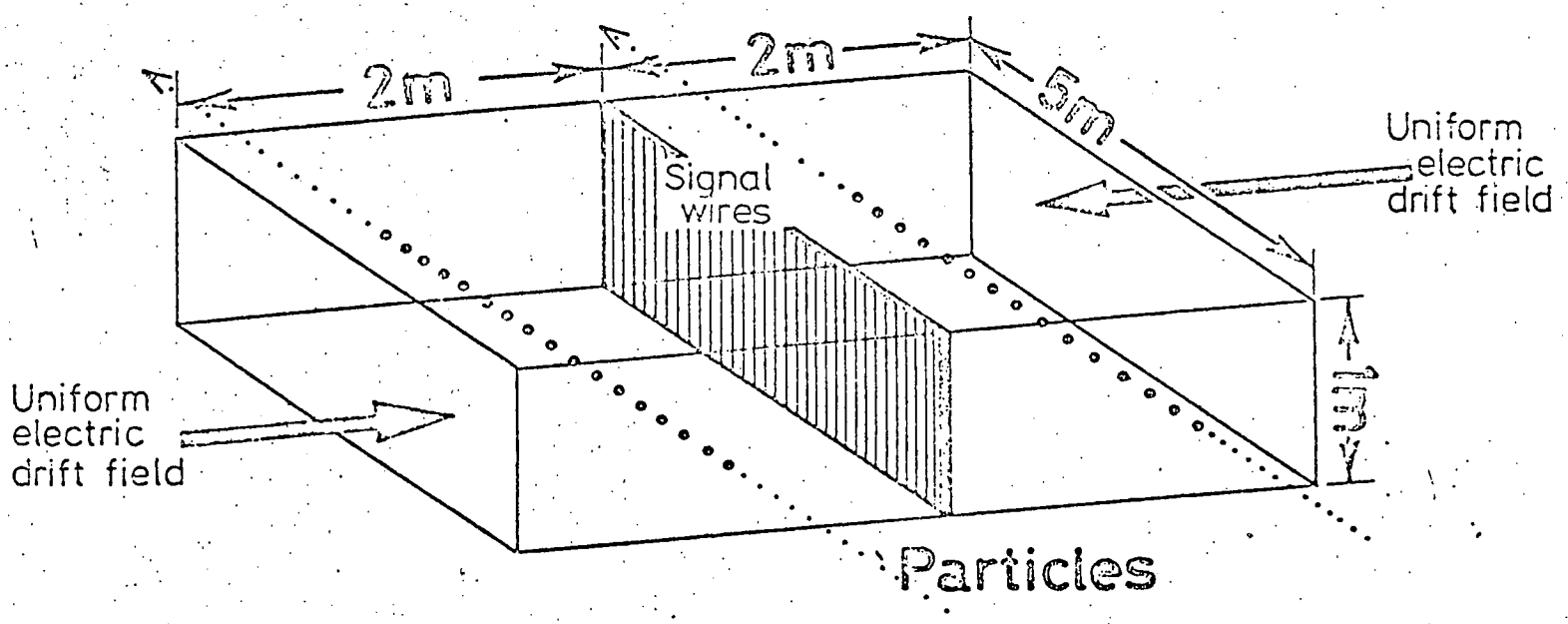

FIG 8.14 Proposed ISIS device

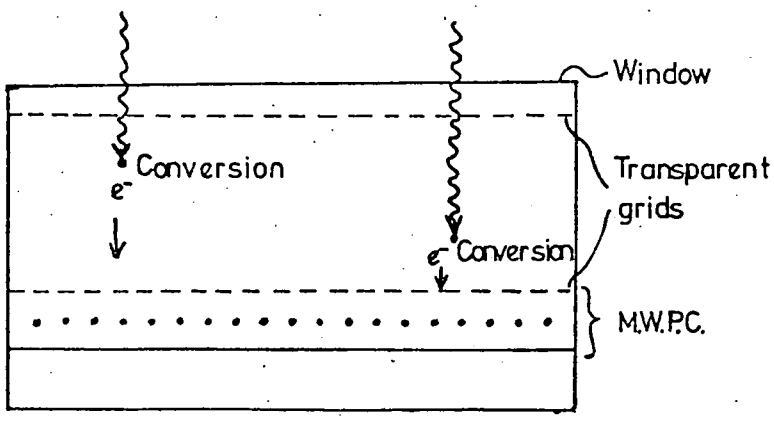

FIG 8.15 Principle of X-ray drift chamber

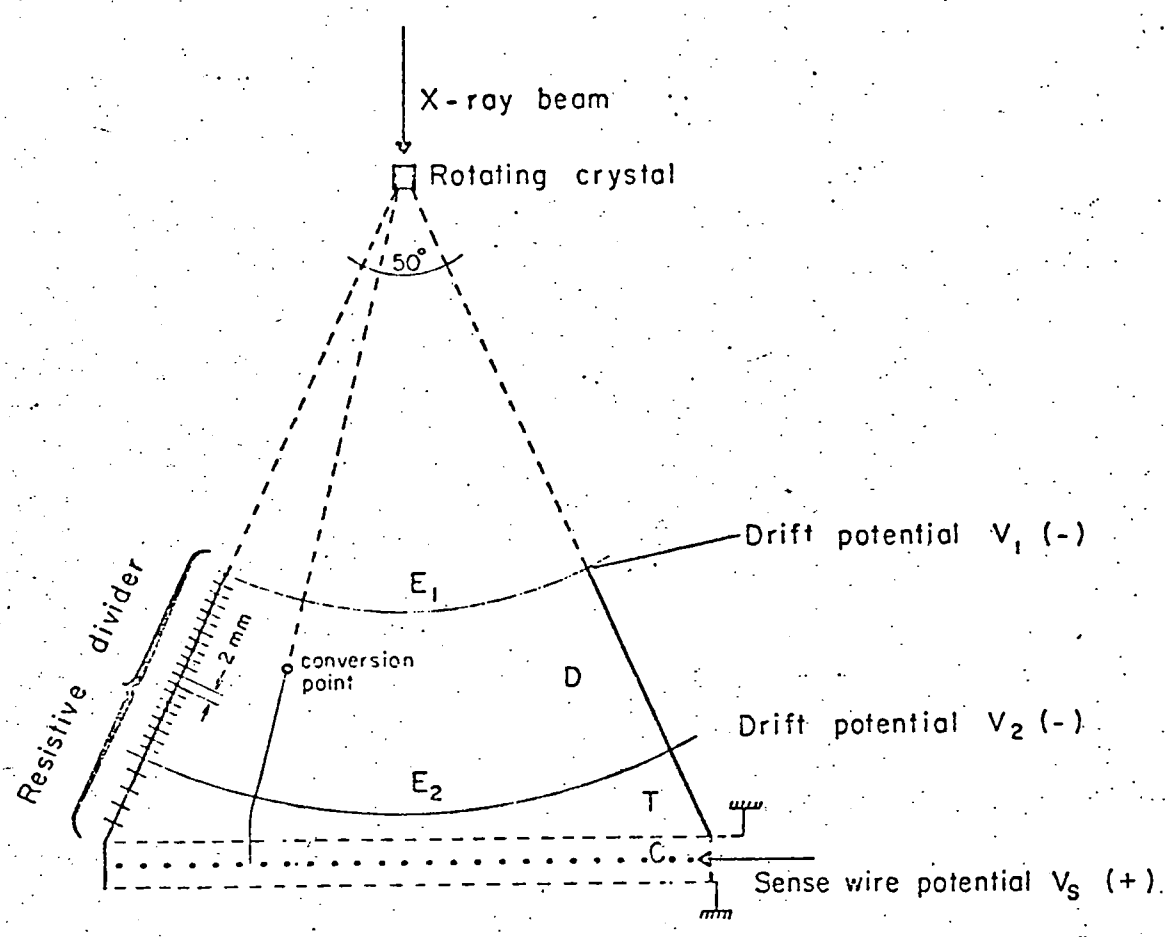

FIG 8.16 Principle of spherical drift chamber

8.3 The Left-Right Ambiguity

The fact that for a conventional multiwire drift chamber a recorded drift time does not indicate on which side of the sense wires the incident particle passed is a major drawback of such devices for experimental use, and as such will be discussed in this chapter on applications. Several methods exist to overcome the problem, as will be listed below.

If the chamber has drift space on one side of the sense wire only, as for instance in the Saclay chambers (10) then the problem does not exist.

Two superimposed chambers, displaced by half a cell width will resolve the ambiguity and also provide information on the possible inclination of the particle track. Some uncertainty will exist for angled tracks near to the cell boundaries. Rubbia et al (9) proposed 3 chambers rotated at 120° to each other which would produce an unambiguous 2 dimensional location for any particle.

For large drift distances a simpler form of detector (possibly the one providing the zero time pulse) could be used to indicate the general particle position (e.g. a separate scintillator over each half cell).

An internal solution involves the use of 2 closely spaced sense wires to deal separately with each half of the cell. The Heidelburg group (22) use a thick shielding wire between the pair, which have a separation of 1 mm, with some positional uncertainty in this region. Charpak and Sauli (23) have proposed a 2 wire system, separation 0.2 mm which is electronically more complex but reduces the area of uncertainty. Electrostatic repulsion of the sense wire pair however, produces some constructional problems, particularly for large wire lengths.

During laboratory tests at Durham the problem did not apply as the area of chamber being irradiated was either well known (radioactive source tests), or irrelevant (whole chamber tests). The method used during the g-2 runs (6) was to deal with the problem in the data analysis. Thus events in 3 chambers, produced 8 possible tracks, several of which could be rejected knowing roughly the shape of the track expected. Fitting the remaining tracks to drift times in a fourth chamber invariably produced an unambiguous 'correct' track.

8.4 Other practical considerations

The second coordinate of a particles trajectory through a single chamber (i.e. in the sense wire direction) can be determined by similar techniques to those developed for proportional counters or M.W.P.C's. For instance measurement of the pulse as received at each end of the sense wire can give information on where along the wire the avalanche occurred (15,16,17). The same information can be obtained from the induced pulses on the cathode wires, particularly if they are in the form of delay lines so that timing measurements can be obtained (18). Using the centre of gravity of the positive pulses induced on the cathode wires nearest to the avalanche (13) is only useful when the cathode wires run orthogonally to the sense wires (which does not apply in adjustable field drift chambers as described in this work). A separate orthogonal wire plane may be feasible, although distortion of the drift field may occur.

Multi-particle resolution is governed by two factors, the length of the pulse provided by the sense wire amplifier to the discrimination circuit, and the dispersion of the positive ion cloud from the region of the sense wire. The second point is only relevant for

two events very close together spatially. Experimentally it has been shown (19) that simultaneous events with drift distance separation of 2 mm (40 nsec) can be resolved, and with good efficiency (80%). Note that the localisation of two such events is only valid for two simultaneous particles, i.e. having the same zero-time pulse. For two unconnected events ambiguity is always possible if they are separated by less than the maximum drift time, so that the event which stops the timing system is not necessarily the one which started it. There would appear to be no way to avoid this effect and it will obviously limit acceptance rates for large drift distances.

High count rates will be precluded anyway due to a build up of positive ion space charge around the sense wire. It has been predicted by comparison with M.W.P.C's that rates of approximately $10^5/cm^2 sec$ should be acceptable without loss of efficiency, although the positive ion concentration will also depend on the gain of the chamber. Thus for high gains efficiency will fall off for lower rates. Experimentally rates of $10^4/mm$ of anode wire.sec have been shown to reduce the efficiency by only 1% (19). There is a related effect however in that for long sense wires a high rate will produce a significant current in the wire which will tend to modify the accelerating field.

CHAPTER 8 - References

1. B.E. Lautrup, A. Petersen and E. de Rafael, Phys.Reports 3C (1972) 193

2. J. Bailey and E. Picasso, Prog. Nucl. Phys 12 (1970) 43

3. J. Bailey, F.H. Combley and P.M. Hattersley 'Proposal to measure the anomolous magnetic moment of the muon at a level of 10-20 ppm' DNPL/SCP 77 (1972)

4. J. Bailey, F.J.M. Farley, H. Jostlein, G. Petrucci, E. Picasso and F. Wickens, CERN Proposal PH I/COM-69/20 (1969)

5. F.H. Combley and E. Picasso, Phys. Reports 14C (1974)1.

6. K.A. Short, Ph.D. Thesis, University of Durham (1976)

7. J.M. Breare, R. Browell and K.A. Short, Durham University Internal Report NI-74-6 (1974)

8. A.H. Walenta, Nuc. Inst. Meth. 3 (1973) 461

9. D.C. Cheng, W.A. Kozanecki, R.L. Piccioni, C. Rubbia, L.R. Sulak, H.J. Weedon and J.J. Whittaker Nuc. Inst. Meth. 117 (1975) 157

10. R. Chaminade, J.C. Duchazeaubeneix, C. Laspalles and J. Saudinos, Nuc. Inst. Meth 111 (1973) 77.

11. W.W.M. Allison, C.B. Brooks, J.H. Cobb, J.N. Bunch, J.L. Lloyd, and R.W. Plenning, 'The identification of secondary particles by ionisation sampling (1S1S) Oxford University Nuclear Physics Laboratory Report 17/74 (1974)

12. The European Muon Collaboration. Proposed experiments and equipment for a programme of muon physics at the S.P.S. CERN Report SPSC/74-78 (1974).

13. G. Charpak, D. Rahm and H. Steiner Nuc. Inst. Meth. 80 (1970) 13.

14. G. Charpak, Z. Hajduk, A. Jeavons, R. Kalm and R. Stubbs, Nuc. Inst. Meth. 122 (1974) 307.

15. G. Charpak, F. Sauli and W. Duinker, Nuc. Inst. Meth. 108 (1973) 413.

16. P. Christie, K.D. Evans, J. Griffiths, E. Mathieson, and P. Murphy, Nuc. Inst. Meth. 130 (1975) 279

17. H. Foeth, R. Hammarstrom and C. Rubbia, Nuc. Inst. Meth 109 (1973) 521.

18. A. Breskin, G. Charpak, F. Sauli and J.C. Santiard, Nuc. Inst. Meth, 119 (1974) 1.

19. A. Breskin, G. Charpak, F. Sauli, M. Atkinson and G. Schultz Nuc. Inst. Meth. 124 (1975) 189.

20. A.P. Jeavons, G. Charpak and R.J. Stubbs, Nuc. Inst. Meth 124 (1975) 491

21. C.B. Lim, D. Chu, L. Kaufman, V. Perez-Mendez and J. Sperinde, IEEE. Trans. Nuc. Sci. NS21 (1974) 85.

22. A.H. Walenta, J. Heintze and B. Schurlein, Nuc. Inst. Meth 92 (1971) 373.

23. G. Charpak and F. Sauli, Nuc. Inst. Meth. 107 (1973) 371

CHAPTER NINE

FUTURE DEVELOPMENTS AND CONCLUSION

9.1 Recent drift chamber developments

Many of the recent directions of drift chamber development were recently reviewed by Charpak (1), and are briefly presented here.

Much work is being done on improving the operating characteristics of the X-ray and γ-ray detecting chambers described in the previous chapter. Because of the fast response time of such detectors they may be used in X-ray crystallography to investigate rapid changes of structure, not detectable by conventional film techniques. The devices are also suitable for X-ray imaging systems, with possible medical applications.

By using drift chambers to accurately determine the trajectories of high energy protons scattered from an object, a three dimensional picture of the scattering sites can be determined. This will give a measure of the density distribution of nucleii within the object, and the technique has been used as an alternative to X-ray methods for examining internal structure.

The high spatial accuracy of drift chambers has enabled them to be used to detect the small variations in angular scattering for relativistic particles passing through cyrstals, due to lattice structure.

A basic change in detector technique is involved in the scintillating drift chamber, first developed in Portugal in 1972, and now studied at CERN. The CERN chamber comprises separate drift and detection regions, but in the detection region the electric field is not sufficient to cause avalanche. Significant atomic excitation does take place however, leading to many photons being emitted which are detected by

photomultiplier tubes. The main advantage of this technique is that because there is no avalanche, there are no clouds of positive ions to disperse and thus the maximum event rate is increased (by a factor of 100).

These examples only represent new developments under study at CERN, and simultaneously drift chambers are being developed in many places for the more conventional aspects of charged particle detection.

9.2 Drift chamber development at Durham

The experience gained in the construction, testing and operation of multiwire drift chambers during this study, and the existing expertise in M.W.P.C. techniques, has led the Nuclear Instrumentation group at Durham to become involved in several new drift chamber applications.

In conjunction with Durham University Astrophysics group and I.R.D. Co. Ltd., work has been carried out on an array of chambers for use in a balloon-borne experiment run by a Southampton University - E.S.T.E.C. collaboration.

Proposals have been made (2) for the design of drift chambers to be used in conjunction with a Rapid Cycling Vertex Detector (Bubble chamber) at the Rutherford Laboratory, in an experiment to investigate Λ - p interactions. Because of the very low signal to noise ratios in such experiments, a fast, efficient trigger is required to select events to be photographed, by analysis of interaction products. This trigger will be provided by layers of drift chambers which will also give spatial information on the interaction product trajectories. Operation in magnetic fields up to 20 kG will be required, and there may be many constructional innovations necessary, connected with surrounding the vertex dector by detectors.

Studies are also being made on X-ray detection with drift chambers, using devices containing perforated conversion material as described in the previous chapter. Topics of interest include optimisation of the geometry of the photon converter, to improve efficiency and spatial resolution.

A full array of 8 chambers (see section 8.1) is still in use on the g-2 experiment at CERN, and data is expected in the future from runs with μ^- rather than μ^+ particles.

9.3 Some possible extensions of general drift chamber studies

The analysis of data taken during this study has indicated areas where further investigations would be useful. For instance the experiments to test the effects of strong magnetic fields only gave an indirect measurement of the drift velocity and variation of efficiency with distance. Both these parameters are better measured by the simpler method of moving a narrow scintillator telescope across the drift region to give start pulse and observing the corresponding drift time distributions from one chamber (see section 5.2, figure 5.5). This will give a drift time versus position graph, and assuming the minimum to correspond to the sense wire position, this can be used to give time distance relationships regardless of any deviation of the beam in the magnetic field. Using a scintillator telescope which does not exceed the height of the chamber will, at the same time, enable actual efficiencies to be determined across the detecting region.

Another topic which appears to be worthy of study involves variations of chamber geometry. For instance the results of Sadoulet and Litke (3) indicate that wide gap, short drift distance chambers offer many advantages in simplicity of operation, particularly in magnetic fields. Investigations of long drift distances also has applications. A

combination of large drift spaces and a 'fast' gas (e.g. methane, which we have shown to be a practicable drift chamber gas) would enable large areas to be covered with a minimum of electronics, at the expense of some resolution and rate handling capacity. Such a device seems to embody one of the main advantages of drift chambers, and may find application for low count rate environments (e.g. cosmic rays studies, such as the Durham experiment to measure very high energy cosmic ray momentum, M.A.R.S.)

Constructional details which might be studied include the replacement of H.T. wires by supported metallic strips and the use of planes in place of field wires. Some progress in this context has already been made by Atac and Taylor (4).

9.4 A proposed new theoretical technique

The theoretical estimation of the various drift process parameters as performed in chapters 6 and 7 although useful, were hardly rigorous. Indeed many theoretical treatments of the process involve approximations and assumptions, probably the most notable being the estimation of the electron velocity distribution and the mean electron energy, and these can seriously affect the final results.

A much more basic approach is proposed which involves a Monte-Carlo simulation of the drift of an electron through a given gas. This requires only a knowledge of the cross-sections for the various types of collision possible and it will yield the electron energy distribution as one of its results. The technique is an extension of previously used simulations to study electron behaviour in single component gases in uniform electric fields (5,6).

The principle is as follows. An electron with initial energy ERG, velocity v is considered at the origin of a coordinate system, travelling at an angle θ to an electric field E in the x direction, and with a magnetic field B in the z direction. Data for the total cross section of the gas mixture constituents are supplied and added in the required proportions so that the overall mean free path λ for the mixture may be calculated for the particular value of ERG. The electron path is then analysed in steps of 0.1λ, the probability of a collision in this distance being given by $(1-\exp(-\lambda/10\lambda))$ which is approximately equal to 0.1. A random number A, between 0 and 1 is then called, and a collision is assumed if $A < 0.1$, with the distance travelled before collision given as $A\lambda$. For no collision, a straight path is assumed for 0.1λ and new system parameters (v_1, θ_1, coordinates X and Y, time t) are calculated from the following equations of motion (c.f. section 7.3) based on conservation of momentum and energy

$$mv_1 \cos\theta_1 = mv \cos\theta + eE\ t - Bev \sin\theta$$

$$mv_1 \sin\theta_1 = mv \sin\theta + Bev \cos\theta$$

$$\tfrac{1}{2}mv_1^2 = \tfrac{1}{2}mv^2 + eE\ X$$

where

$$X = 0.1\lambda \cos\theta$$

$$t = 0.1\lambda/v$$

If a collision is assumed then similar increments are made (except θ) for $A\lambda$. The gas component with which the electron has collided can be found using another random number and comparing the relative cross-sections. Then the type of collision is decided depending on the electron energy ERG and the probability of the various types of collisions (obtained from the appropriate cross-section data. Thus for argon, if ERG is less than 11.5eV then the collision must be elastic. Then the slight energy loss is calculated and a random number

determines the resulting angle after collision. For the ranges of ERG high enough to cause metastable, radiative or ionising collisions, the type is decided on the relative probabilities, with respect to the total cross section, using another random number B. If an inelastic collision is decided, the appropriate energy loss is subtracted from ERG (and randomly proportioned between the 2 products for ionisation). In this case the position of the ionisation is recorded so that the second electron can be dealt with later.

Having decided on the type of collision, if any, amended ERG and the coordinates, and introduced a new value of θ if required, the new coordinates can be tested to see if any predetermined value has been reached, causing the system parameters to be printed. Otherwise a new overall value of λ is found for the new ERG value, and the process is repeated starting with the collision-no collision decision.

A possible addition to the programme could be a sampling routine such that for instance ERG could be printed out at fixed intervals of t thus providing an effective energy distribution from a single drifting electron.

A simplified form of the flow diagram for such a process is shown in figure 9.1. Only the collision determination for argon is shown, for four possible types; elastic, metastable, radiative and ionising. The corresponding probabilities (PE,PM,PR,PI) are defined as the ratios of the appropriate cross-sections to the total cross-section at that energy.

Although the initial development of such a programme may take considerable work, its value and range of application to all aspects of drift chamber study would be great. For example running the programme for several electrons for a fixed distance d and crossed E and B, one could immediately determine the mean drift velocities W_L, W_T, W_A, the angle of drift, and the distribution of drift times for that distance.

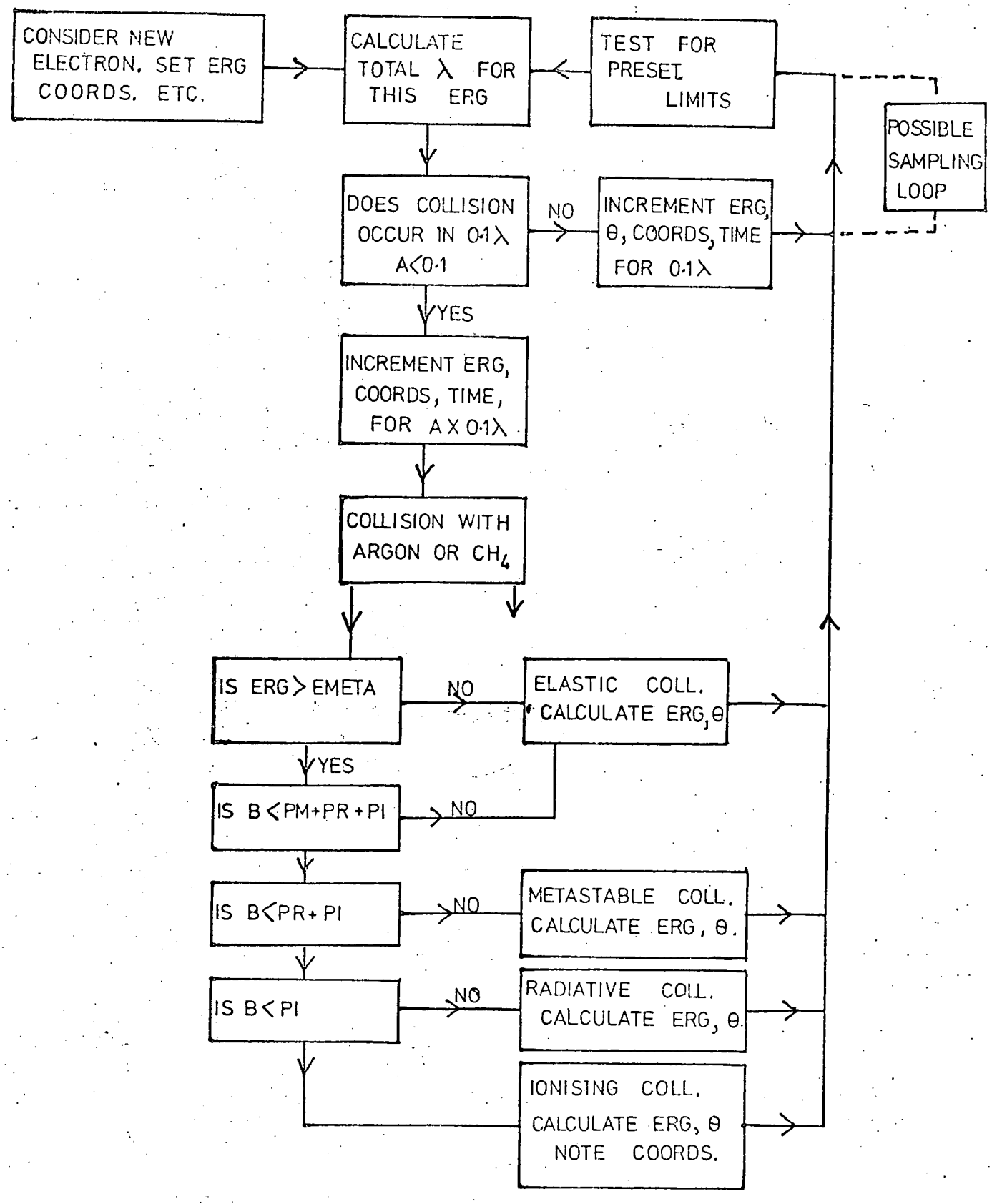

FIG 9.1 FLOW DIAGRAM FOR ELECTRON DRIFT SIMULATION PROGRAMME.

Electrons could be created at different coordinates to more properly simulate a charged particle path at any angle.

Values of E and B could be easily varied, or even made a function of position, in order to accurately predict chamber behaviour in non-uniform magnetic fields. The relative proportions of gases could be easily altered, and by feeding in new cross-section data, many gas mixtures could be studied.

Similar programmes do exist, that of Itoh and Musha (5) giving excellent agreement with experiment for drift velocity and other parameters in helium. The main new extensions of the programme for this work would be the inclusion of a second gas component, and the effect of a magnetic field.

9.5 Concluding remarks

At the outset of this work, although drift chambers were in use in one or two applications, they still represented a very new technique and there was little published data on the fundamental processes involved. Thus a major purpose of the study was to provide such data, predominantly for the one specific gas mixture, and simultaneously to investigate practical aspects of drift chamber operation. The main results of the work may be summarised as follows:

1) Many problems regarding design and construction of practical chambers have been met and overcome.

2) Experimental test procedures have been devised to ascertain basic drift chamber operating characteristics.

3) These operating characteristics have been systematically determined for a wide range of conditions, mainly using a gas mixture of argon + 10% methane.

4) From this data, details of the electron drift process for the gas mixture have been derived.

5) The behaviour of chambers in strong magnetic fields, and their applications to high energy physics have been demonstrated by tests on the Daresbury Laboratory e^+ beam.

6) Using the above results specialised chambers have been developed for use in an actual experiment and have functioned successfully.

Thus the study has established the suitablity of a new simple gas mixture for use in drift chambers, and constituted a basis for more specialised chamber development, a basis which should find considerable application, such is the potential of these devices in the present field of particle detection.

CHAPTER 2 - References

1. G. Charpak, CERN, Courier No. 6. Vol. 15. (June 1975)

2. J.M. Breare and J.V. Major, Draft Proposal, University of Durham (1975)

3. B. Sadoulet and A. Litke, Nuc. Inst. Meth.

4. M. Atac and W.E. Taylor, Nuc. Inst. Meth. 120 (1974) 147.

5. T. Itoh and T. Musha, J. Phys. Soc. Japan 15 (1960) 1675.

6. R.J. Stubbs, Private communication.

APPENDIX I

EFFECT OF ELECTRON VELOCITY DISTRIBUTION AND COLLISION CROSS SECTION ON TRANSPORT PARAMETERS

1. No magnetic fields

In the derivation of equation 6.12,

$$W_o = \frac{eE}{m}\left(\frac{\bar{\lambda}}{v}\right)$$

it was assumed that the mean free time T was independent of electron velocity v. A more rigorous derivation of the expression for W_o, for $\lambda = \lambda(v)$ and a distribution of velocities $f(v)$ has been made by several authors (1,2,3) and yields

$$W_o = \frac{4\pi}{3}\frac{eE}{m}\int_0^\infty v^2 \lambda \frac{df}{dv}\, dv \qquad (A.1)$$

This reduces by partial integration, and by assuming $v^2 \lambda f$ tends to zero for $v \to 0$ and $v \to \infty$, to

$$W_o = \frac{Ee}{3m}\left[\overline{v^{-2}\frac{d}{dv}\lambda v^2}\right] \qquad (A.2)$$

where the horizontal bar indicates that the mean value of the expression underneath must be used. Assuming λ to vary as v^r then equation A.2 may be written

$$W_o = k_\lambda \frac{eE}{m}\left(\frac{\bar{\lambda}}{v}\right) \qquad (A.3)$$

where for $r = 1$, $k_\lambda = 1$; $r = 0$, $k_\lambda = {}^2/_3$; $r = -1$, $k_\lambda = {}^1/_3$.

Expression A.3 should also include a constant factor k_D if the value of v used is anything other than $\bar{v}^{-1}$.

$$\text{i.e.} \qquad W_o = k_\lambda \, k_D \, \frac{eE}{m} \, \frac{\lambda}{v} \qquad \text{(A.4)}$$

The value of k_D depends on the form of f(v) and on the value of v which is used. The relationship between the various 'mean' values of v can be derived by writing the velocity distribution function as,

$$f(v) = A \exp - \left(\frac{v}{\alpha}\right)^S \qquad \text{(A.5)}$$

where S = 2 defines a Maxwell Distribution, S = 4 a Druyvesteyn Distribution, and A and α are functions of S. The value of A is chosen to satisfy

$$4\pi \int_0^\infty f(v) \, v^2 \, dv = 1 \qquad \text{(A.6)}$$

Substituting f(v) from equation A.5 gives A, and the mean value of v^x is given by

$$\bar{v}^x = 4\pi A \int_0^\infty v^{x+2} \left[\exp - \left(\frac{v}{\alpha}\right)^S\right] dv \qquad \text{(A.7)}$$

This can be evaluated using the value of A from A.6 and the standard integral

$$\int_0^\infty \left[\exp(-x^n)\right] \, x^m \, dx = \frac{1}{n} \Gamma\left(\frac{m+1}{n}\right) \qquad \text{(A.8)}$$

The final value is

$$\overline{v^x} = \left[\frac{\Gamma\left(\frac{x+3}{S}\right)}{\Gamma\left(\frac{3}{S}\right)} \right] \alpha^x \qquad (A.9)$$

As an example, for a Maxwell Distribution, S = 2

$$\bar{v}^{-1} = \frac{1.128}{\alpha}$$

and $$\bar{v}^{-2} = 1.5\,\alpha^2$$

therefore $$\bar{v}^{-1} = \frac{1.38}{\bar{v}^2}$$

Thus in equation A.4 if we use a value of v obtained from the mean electron energy (i.e. $\sqrt{\bar{v}^2}$) then k_D will have a value of 1.38 (1.24 for a Druyvesteyn Distribution). By combining appropriate values of k_D and k_λ we can determine the value of k in equation 6.14 for any conditions, as for example in table 6.1.

One way to define v is from measurements of the electron characteristic energy ϵ_k, defined as the ratio D/μ, and it is useful to determine the relationship between ϵ_k and the actual mean electron energy. Expressing D and μ in the same terms we have

$$D = \frac{1}{3}\,(\overline{\lambda v}) \qquad (A.10)$$

$$\mu = \frac{e}{3m}\left[\overline{v^{-2}\,\frac{d}{dv}\,\lambda v^2}\right] \qquad (A.11)$$

thus $\frac{D}{\mu}$ =

$$\left[\frac{2(\overline{\lambda v})}{\bar{v}^{2}\ \overline{v^{-2}\ \frac{d}{dv}\lambda v^{2}}}\right] \quad \frac{\frac{1}{2}m\bar{v}^{2}}{e}$$

i.e. = F $\mathscr{E}$

where $\mathscr{E}$ is the mean electron energy in electron volts. F may be evaluated as before if $\lambda(v)$ and $f(v)$ are known, using the useful factor,

$$\frac{\bar{v}}{\overline{v^{-1}}} = \frac{2}{3}\bar{v}^{2} \qquad \text{(Maxwell)}$$

$$= 0.76\,\bar{v}^{2} \qquad \text{(Druyvesteyn).}$$

Values of F calculated for various conditions are shown in table 6.2.

2. Magnetic fields

In the presence of a magnetic field B ($\omega = Be/m$) the expressions for drift velocity are modified. Using the nomenclature of Chapter 7 and assuming $\omega T \ll 1$ we have,

$$W_L = \frac{Ee}{3m}\left[\overline{v^{-2}\ \frac{d}{dv}\ \lambda\, v^{2}}\right] \qquad \text{(A.12)}$$

$$W_T = \frac{Ee}{3m}\left[\overline{v^{-2}\ \frac{d}{dv}\ \lambda^{2} v}\right] \qquad \text{(A.13)}$$

Thus to a first approximation $W_L = W_o$. The value of W_T however depends somewhat differently on $f(\lambda)$ and $f(v)$ than does W_o, so that W_T is given by $k_B W_o \omega T$, where k_B depends on $f(\lambda)$ and $f(v)$. Tan ϕ ($= W_T/W_L$) is then

given by $k_B \omega T$, although for argon + 10% methane, which is represented by $\lambda \propto v^{-1}$, k_B is found to be approximately 1.

In drift chamber applications ωT is not usually much less than 1 so that more precise expressions than A.12 and A.13 are required. Huxley (4) has given these as,

$$W_L = \frac{eE}{3m} \left[\overline{v^{-2} \frac{d}{dv} \left(\frac{v^3 \gamma}{\gamma^2 + \omega^2} \right)} \right] \qquad (A.14)$$

$$W_T = \frac{eE}{3m} \left[\overline{v^{-2} \frac{d}{dv} \left(\frac{\omega \gamma^3}{\gamma^2 + \omega^2} \right)} \right] \qquad (A.15)$$

for all T, where $\gamma = v/\lambda = 1/T$

Equation A.14 is equivalent to equation 7.12

It should be remembered that the preceding equations and value of various averaging constants are indications only, as in actual gas mixtures λ will not be a simple function of v, and the occurrence of inelastic collisions will seriously affect the electron velocity distribution.

References

1. L.G.H. Huxley and R.W. Crompton, The Diffusion and Drift of Electrons in gases, Wiley, New York (1974)

2. W.P. Allis, Handbuch der Physik, Vol 21, (ed S. Flugge), Springer-Verlag, Berlin, (1950)

3. V. Palladino and B. Sadoulet, Lawrence Berkeley Laboratory Internal Report, LBL 3013 (1974)

4. L.G.H. Huxley, Phil. Mag. 23 (1937) 210.

ACKNOWLEDGEMENTS

The author would like to thank Professor G.D. Rochester, F.R.S. and Professor A.W. Wolfendale for their support of this work, and the use of laboratory facilities. The S.R.C. is thanked for the provision of an award, additional expenses and the use of their laboratories at Daresbury.

The author is deeply indebted to his supervisor Dr. J.M. Breare for the encouragement, assistance and tolerance shown by him throughout this work.

He is also grateful to all the members, past and present, of the Nuclear Instrumentation group at Durham for their assistance and companionship, in particular Dr. K.A. Short for his collaboration on matters pertaining to the g-2 experiment. The technical support provided by Mr. J. Webster is gratefully acknowledged, as are the machining skills of Mr. R. McDermott.

Thanks are due to the staff of the S.R.C. laboratories at Daresbury for their interest and assistance, particularly Mr. M.D. Rousseau, Dr. J.M. Bailey, Dr. P.A. Ridley, and members of the NINA beam crews, and also to Professor E. Picasso at CERN for permission to work on the g-2 experiment.

Mrs. J. Johnston is thanked for the excellence of her typing, as is Mr. M. Lee for the photographs and Mrs. E. Johnson for some of the diagrams.

Finally the author would like to express his special thanks to his parents, and his wife Sylvia, who also helped with the diagrams, for all their invaluable support and encouragement.